UNIVERSIDADE DE SÃO PAULO
Instituto de Ciências Matemáticas e de Computação

Reliability analysis of repairable systems considering unobserved heterogeneity and competing risks

Éder Silva de Brito

Tese de Doutorado do Programa Interinstitucional de Pós-Graduação em Estatística (PIPGEs)

ICMC USP SÃO CARLOS

Éder Silva de Brito

Reliability analysis of repairable systems considering unobserved heterogeneity and competing risks

Thesis submitted to the Institute of Mathematics and Computer Science – ICMC-USP and to the Department of Statistics – DEs-UFSCar – in accordance with the requirements of the Statistics Interagency Graduate Program, for the degree of Doctor in Statistics. *FINAL VERSION*

Concentration Area: Statistics

Advisor: Prof. Dr. Francisco Louzada Neto
Co-advisor: Profa. Dra. Vera Lúcia Damasceno Tomazella

USP – São Carlos
December 2023

Ficha catalográfica elaborada pela Biblioteca Prof. Achille Bassi
e Seção Técnica de Informática, ICMC/USP,
com os dados inseridos pelo(a) autor(a)

BB862r

Brito, Éder Silva de
Reliability analysis of repairable systems considering unobserved heterogeneity and competing risks / Éder Silva de Brito; orientador Francisco Louzada Neto; coorientadora Vera Lúcia Damasceno Tomazella. -- São Carlos, 2023.
185 p.

Tese (Doutorado - Programa Interinstitucional de Pós-graduação em Estatística) -- Instituto de Ciências Matemáticas e de Computação, Universidade de São Paulo, 2023.

1. Repairable systems. 2. power law process. 3. frailty models. 4. unobserved heterogeneity. 5. competing risks. I. Louzada Neto, Francisco, orient. II. Tomazella, Vera Lúcia Damasceno, coorient. III. Título.

Bibliotecários responsáveis pela estrutura de catalogação da publicação de acordo com a AACR2:
Gláucia Maria Saia Cristianini - CRB - 8/4938
Juliana de Souza Moraes - CRB - 8/6176

Éder Silva de Brito

Análise de confiabilidade de sistemas reparáveis considerando heterogeneidade não observada e riscos competitivos

Tese apresentada ao Instituto de Ciências Matemáticas e de Computação – ICMC-USP e ao Departamento de Estatística – DEs-UFSCar, como parte dos requisitos para obtenção do título de Doutor em Estatística – Programa Interinstitucional de Pós-Graduação em Estatística. *VERSÃO REVISADA*

Área de Concentração: Estatística

Orientador: Prof. Dr. Francisco Louzada Neto
Coorientadora: Profa. Dra. Vera Lúcia Damasceno Tomazella

USP – São Carlos
Dezembro de 2023

UNIVERSIDADE FEDERAL DE SÃO CARLOS

Centro de Ciências Exatas e de Tecnologia
Programa Interinstitucional de Pós-Graduação em Estatística

Folha de Aprovação

Defesa de Tese de Doutorado do candidato Éder Silva de Brito, realizada em 09/10/2023.

Comissão Julgadora:

Prof. Dr. Francisco Louzada Neto (USP)

Prof. Dr. Enrico Antonio Colosimo (UFMG)

Prof. Dr. Paulo Henrique Ferreira da Silva (UFBA)

Profa. Dra. Maria Luiza Guerra de Toledo (ENCE)

Prof. Dr. Eder Angelo Milani (UFG)

O Relatório de Defesa assinado pelos membros da Comissão Julgadora encontra-se arquivado junto ao Programa Interinstitucional de Pós-Graduação em Estatística.

ACKNOWLEDGEMENTS

Quando decidi iniciar o Doutorado, redirecionando minha formação para a área da Estatística, já esperava um caminho naturalmente desafiador pela frente. Mal poderia imaginar que isso seria exponencialmente agravado pela pandemia de COVID-19. A incerteza e as adversidades que caracterizaram esse período tornaram esse processo ainda mais complexo. No entanto, neste trajeto repleto de desafios, se sobressaiu o apoio incansável e o carinho daqueles que estiveram ao meu lado. Neste contexto, gostaria de expressar minha profunda gratidão às pessoas que tornaram esta jornada possível e significativa, acadêmica e afetivamente.

À minha família, meu maior alicerce, que sempre me apoia a cada novo sonho que me aventuro a buscar. Em especial, ao meu companheiro Jorge por todo o suporte, (muita) paciência, carinho e compreensão nesses últimos anos.

À minha querida professora e orientadora Vera Tomazella que me acolheu desde a primeira conversa, me orientando antes mesmo de me conhecer. Nada que eu falar ou escrever será suficiente para expressar minha admiração pela sua atuação como professora e pesquisadora, seu cuidado com as pessoas, seu entendimento sobre as particularidades e dificuldades de cada um e a forma como extrai o melhor das nossas potencialidades. Sou muito grato por todas as orientações acadêmicas, profissionais e pessoais e por ter sido adotado como "filho" acadêmico, um filho feliz pela "mãe" que encontrou nesse processo.

Ao meu orientador Professor Francisco Louzada pelas orientações e constante incentivo às atividades de pesquisa e produção científica. Em particular, agradeço imensamente pelo convite para participar do projeto vinculado à Petrobras. Aprendi muito nesses últimos anos, no projeto, nas monitorias e nos eventos indicados, e, ter a oportunidade de vivenciar tudo isso me fez crescer bastante enquanto pesquisador.

Aos professores Paulo Henrique Ferreira (UFBA) e Oilson Gonzatto (USP) que me acompanharam por todo o processo de pesquisa e elaboração da tese, sempre solícitos a ajudar seja com códigos, com revisões ou discussões sobre os diversos problemas que surgiram. Sou profundamente grato à atenção e disponibilidade de vocês.

Aos professores Maria Luiza Toledo (ENCE), Enrico Colosimo (UFMG) e Eder Milani (UFG) pela participação na banca examinadora e pelas valiosas correções e sugestões dadas.

Aos professores, secretários e demais servidores vinculados ao PIPGEs pela constante disposição em nos auxiliar durante todo o processo formativo e, sobretudo, pelo cuidado e empenho que tiveram durante o período adverso de pandemia.

Aos meus queridos amigos do PIPGEs (Turma de 2019, Chile Vive e Pós-Pandemia) que estiveram presentes durante todos esse anos, em diferentes momentos, presencial ou virtualmente. Vocês fizeram com que o caminho fosse menos árduo, compartilhando dilemas, anseios, palavras de conforto, risos e comidinhas gostosas. Sou muito grato e honrado de ter feito amizades que certamente carregarei para o resto da vida. Desejo a todos vocês muito sucesso e toda felicidade do mundo!

Ao Instituto Federal de Educação, Ciência e Tecnologia de Goiás (IFG) pela concessão do meu afastamento do trabalho para me dedicar integralmente ao Doutorado. Em particular, agradeço aos colegas do Campus Anápolis pelo constante apoio e incentivo à minha formação.

Ao Centro de Ciências Matemáticas Aplicadas à Indústria (CeMEAI) pela disponibilização dos recursos computacionais (financiados pela FAPESP) utilizados durante o desenvolvimento desse trabalho.

À Petrobras pelo apoio financeiro.

RESUMO

BRITO, E. S. **Análise de confiabilidade de sistemas reparáveis considerando heterogeneidade não observada e riscos competitivos**. 2023. 185 p. Tese (Doutorado em Estatística – Programa Interinstitucional de Pós-Graduação em Estatística) – Instituto de Ciências Matemáticas e de Computação, Universidade de São Paulo, São Carlos – SP, 2023.

Em sistemas reparáveis, o processo de falhas definido pela função de intensidade de falhas pode ser impactado por três características importantes: o tipo de reparo realizado após a ocorrência das falhas, a causa que provocou a falha (riscos competitivos) e a existência de fatores não observáveis atuando sobre cada tempo de falha ou sobre o sistema de modo geral (heterogeneidade não observada). Em particular, a heterogeneidade não observada pode ser modelada por modelos de fragilidade, bem conhecidos na literatura de confiabilidade. No entanto, a grande maioria destes trabalhos assume apenas reparos mínimos após as falhas, uma suposição bastante restritiva e nem sempre aplicável. Há, portanto, uma lacuna teórica a ser explorada envolvendo modelos de fragilidade considerando sistemas submetidos a reparos perfeitos e imperfeitos e ainda sujeitos a riscos competitivos. Dessa forma, o principal objetivo deste trabalho é apresentar novos modelos paramétricos de fragilidade univariada e compartilhada para múltiplos sistemas reparáveis sob diferentes tipos de reparo e sob estrutura de riscos competitivos. Os modelos propostos são extensões e generalizações de outros existentes na literatura, pois consideram reparos perfeitos e todas as possíveis memórias de falha para ambas as classes ARA_m e ARI_m de reparo imperfeito. Nesse sentido, são modelos capazes de identificar simultaneamente o efeito dos reparos realizados e a existência de heterogeneidade não observada entre os tempos de falha ou entre os sistemas analisados. Essa característica é bastante relevante para situações do mundo real, pois com maiores informações sobre o processo de falhas de sistemas é possível aprimorar políticas de manutenção preventiva e diminuir custos referentes aos reparos realizados. Em todos os modelos propostos, admitimos que a intensidade inicial de falha segue um Processo de Lei de Potência e que os termos de fragilidade paramétrica associados aos tempos de falha ou aos sistemas seguem uma mesma distribuição Gama. A abordagem frequentista é utilizada para a construção da função de verossimilhança de cada modelo e métodos numéricos são sugeridos para a obtenção dos estimadores de máxima verossimilhança e seus respectivos intervalos de confiança assintóticos. Ainda propomos o uso de metodologias Bayesianas baseadas em algoritmo de Monte Carlo e Cadeias de Markov como alternativa ao método frequentista. Estudos de simulações são realizados para cada modelo proposto e, por fim, os métodos apresentados são sempre aplicados a conjuntos de dados reais.

Palavras-chave: Sistemas reparáveis, Processo de lei de potência, Modelos de fragilidade, Heterogeneidade não observada, Riscos competitivos.

ABSTRACT

BRITO, E. S. **Reliability analysis of repairable systems considering unobserved heterogeneity and competing risks**. 2023. 185 p. Tese (Doutorado em Estatística – Programa Interinstitucional de Pós-Graduação em Estatística) – Instituto de Ciências Matemáticas e de Computação, Universidade de São Paulo, São Carlos – SP, 2023.

In repairable systems, the failure process defined by the failure intensity function can be impacted by three crucial characteristics: the type of repair performed after the failures occur, the underlying cause of the failure (competing risks) and the presence of unobervable factors acting on each failure time or on the system as a whole (unobserved heterogeneity). In particular, unobserved heterogeneity can be modeled by frailty models, well known in the reliability literature. However, the majority of existing studies in this domain assume only minimal repairs after failures, which is a highly restrictive assumption and not always applicable. There is, therefore, a theoretical gap to be explored encompassing frailty models that consider systems subject to both perfect and imperfect repairs and still subject to competing risks. The primary objective of this work is to present new parametric univariate and shared frailty models for multiple repairable systems, considering different types of repairs and a competing risks framework. These proposed models extend and generalize those already existing in the literature, as they account for perfect repairs and all possible failure memories within both the ARA_m and ARI_m classes of imperfect repairs. In this sense, they are models capable of simultaneously identifying the effect of the repairs actions and the presence of unobserved heterogeneity among failure times or among the systems under analysis. This characteristic holds substantial relevance in real-world situations, as a deeper understanding of the system's failure process can lead to improved preventive maintenance policies and reduced repair-related costs. In all proposed models, we assume that the initial failure intensity follows a Power Law Process and that the parametric frailty terms associated with failure times or systems follow a Gamma distribution. We employ a frequentist approach to construct the likelihood function for each model and suggest numerical methods for obtaining maximum likelihood estimators and their corresponding asymptotic confidence intervals. Additionally, we propose the use of Bayesian methodologies based on Markov Chain Monte Carlo algorithms as an alternative to the frequentist method. Simulation studies are conducted for each proposed model, and, finally, the methods presented are applied to real datasets.

Keywords: Repairable systems, Power law process, Frailty models, Unobserved heterogeneity, Competing risks.

LIST OF FIGURES

LIST OF TABLES

LIST OF ABBREVIATIONS AND ACRONYMS

ABAO	As Bad As Old
AGAN	As Good As New
AIC	Akaike Information Criterion
ARA	Arithmetic Reduction of Age
ARI	Arithmetic Reduction of Intensity
BE	Bayes Estimator
BIC	Bayesian Information Criterion
CDF	Cumulative Distribution Function
CI	Confidence Intervals
CI_B	Credible Intervals
CP	Coverage Probability
DIC	Deviance Information Criterion
HPP	Homogeneous Poisson Process
IID	Independent and Identically Distributed
IR	Imperfect Repair
MCF	Mean Cumulative Failure
MCMC	Markov Chain Monte Carlo
MH	Metropolis-Hastings
MLE	Maximum Likelihood Estimators
MR	Minimal Repair
MRE	Mean Relative Estimate
NHPP	Non-Homogeneous Poisson Process
PLP	Power Law Process
PR	Perfect Repair
RMSE	Root of the Mean Squared Error
ROCOF	Rate of Occurrence of Failures

CONTENTS

CHAPTER

1

INTRODUCTION

In recent decades, reliability studies have gained increasing importance among the main and most competitive industries and manufacturers of various products. The reason is simple: among other possibilities, reliability studies provide support for reducing failures in systems and operations through both preventive and corrective maintenance policies. In particular, corrective maintenance leads us to systems known as *repairable systems* and the focus of this work is on data from these types of systems.

In the reliability literature, a system can be classified as either non-repairable or repairable and its distinction is totally natural. A system is considered non-repairable if it cannot be repaired after a failure has occurred. In contrast, a repairable system can undergo a repair procedure after the failure occurrence, which restores it to working condition, enabling it to perform its designated activity satisfactorily (ASCHER; FEINGOLD, 1984).

The difference between non-repairable and repairable systems also affects the methodological approach required for statistical modeling. Models for repairable systems must account for the occurrence of several failures over time, as well as the effect of the repair performed after each failure. In the literature, the theoretical framework used for repairable systems is naturally related to recurrent events, since successive failures can occur for the same system. Further details of the recurrent events theory can be found in Cook and Lawless (2007) and Nelson (2003).

In general, statistical modeling for recurrent events in repairable systems is achieved through counting processes. This kind of process is completely characterized by the system's failure intensity function, which provides the necessary tools to perform the inference and estimation of the model's parameters. In the literature of repairable systems, it is commonly assumed that recurrent failures follow a Non-Homogeneous Poisson Process (NHPP), and, in particular, one of its most important and widely used parametric forms is the Power Law Process (PLP). PLP was proposed by Crow (1975) and it is a convenient choice given its flexibility,

applicability, and the interpretability of its parameters. For a more detailed exploration of NHPP and PLP, see Rigdon and Basu (2000), Ross (1996) and Hamada *et al.* (2008).

The effect of the repair performed immediately after the failure is a critical characteristic in repairable system models and its definition is closely tied to the system's failure intensity function. In the majority of literature concerning repairable systems, it is assumed that the repair effect is minimal, that is, after performing a repair the system returns to the same condition as it was immediately before the failure. This type of repair is known as *minimal repair* and is closely associated with PLP, as these models share the exact same system failure intensity function. Among the various works with this approach, we can mention Barlow and Hunter (1960), Engelhardt and Bain (1986), Rigdon and Basu (1989), Park, Jung and Yum (2000) and Gilardoni and Colosimo (2007).

Barlow and Hunter (1960), in particular, presented a maintenance policy that considers, in addition to minimal repairs, another type of repair that accounts for more extreme situations where the system is repaired in order to restore it to the same condition as when it was new. This type of repair is referred to as *perfect repair* and can be classified as a renewal process. In this case, the system intensity function takes into account the previous failure times as it will be renewed after each occurrence.

While the assumptions of minimal repair or perfect repair can be suitable for certain scenarios, they may not always reflect reality accurately. Repair procedures can sometimes have an intermediate effect on a system, meaning that after a repair, the system returns to a better condition than before the failure but not as good as a new system. Repairs of this type are referred to as *imperfect repairs* and were originally introduced by Kijima, Morimura and Suzuki (1988). These authors introduced the concept of *virtual age*, which assigns a new age to the system after each repair is performed, distinct from the real age. In this virtual age model, a crucial parameter $\theta \in (0,1)$ is introduced to quantify the impact of the repair.

Subsequently, Doyen and Gaudoin (2004) explored the potential effects of the repair procedures on the intensity function of a system and defined two important classes for imperfect repair. The first considers an arithmetic reduction in age (ARA) of the system after repair, while the second considers an arithmetic reduction in the intensity function (ARI) of the system. According to the model proposed by the authors, both ARA and ARI classes have a memory m of failures that takes into account the time of the last m failures of the system, influencing the current failure intensity. Further details on this type of repair can also be found in Kijima (1989) and Toledo *et al.* (2015).

In addition to understanding the effects of repairs performed on a system after the occurrence of a failure, it is important to consider factors contributing to the failure event. Two significant aspects concerning the analysis of system failure times come to the forefront: the cause of the failure and the influence of internal or external factors that can impact the system's operation.

The first point is obvious: generally, a system can fail for multiple reasons. In the literature, this is commonly referred to as *competing risks*, where the system is exposed to various risks that compete with each other to be the cause of failure (CROWDER, 2001).

Methodologies dealing with competing risks have been well established in the reliability literature and have been addressed in several works. In particular, we can cite the works of Langseth and Lindqvist (2006) and Doyen and Gaudoin (2006), which addressed problems of competing risks in repairable systems whose repairs are imperfect. In the first work, the authors focused on datasets where preventive maintenance does not necessarily need to be perfect, so they used a version of the imperfect repair models. On the other hand, in the second work the authors presented a robust theoretical discussion on imperfect maintenance within a broader framework of generalized competing risks.

The second point mentioned above concerns to factors that can influence a system's failure process. From a statistical modeling perspective, these factors can be regarded as covariates and easily incorporated into existing models. However, in practice, it is often challenging to account for all relevant covariates, leading to what is known in the literature as *unobserved heterogeneity*. According to Tomazella (2003) and Wienke (2010), assuming the absence of unobserved heterogeneity between recurring failures in a system or even between systems within the same group may not be a realistic assumption. Therefore, it is pertinent to consider the unobserved heterogeneity when modeling the failure processes of repairable systems. This unobserved heterogeneity can be estimated using models known in the literature as *frailty models*. Further foundational theory on these models can be found in Andersen *et al.* (2012) and Hougaard (2012).

As highlighted by Tomazella (2003), the frailty terms can be introduced in an additive or multiplicative way into the failure intensity function, which can naturally influence the occurrence of failures over time. Therefore, some authors have explored unobserved heterogeneity in repairable systems under the assumption of minimal repair, including D'Andrea (2019), Almeida *et al.* (2020) and Somboonsavatdee and Sen (2015a). These latter two works also considered a competing risks framework. Regarding frailty models and imperfect repair, the literature is relatively sparse; except for the works of Liu *et al.* (2020) and Junior (2021), with the latter work also considering a competing risks framework.

By analyzing the timeline of publications concerning repairable systems, we can note that the development of new methodologies is closely tied to the quest for models capable of encompassing various data characteristics, whether quantifiable or not. In this context, a common approach in this type of research has been to analyze an existing model and try to adapt it to a situation where more information about the data is desired. This is the central idea of the main results presented in this work.

Based on existing theories about repairable systems under minimal repair, frailty models and competing risks framework, our proposed methodologies aim to construct models that

combine and extend these concepts into more general models. The core objective is to provide models with the capacity to simultaneously discern multiple attributes within the failure processes of repairable systems and to provide practical interpretations in real-world scenarios.

In essence, our aim is to analyze multiple repairable systems susceptible to failures stemming from various causes, influenced by unobserved heterogeneity, and that can undergo to any type of repair following a failure — be it minimal, perfect, or imperfect. In this sense, we propose models that are extensions and generalizations of existing models, especially when analyzing the general classes ARA_m and ARI_m of imperfect repair within the framework of frailty and competing risks. Below, we list and contextualize our main contributions.

1.1 Thesis Contributions

Although the use of frailty models to detect unobserved heterogeneity in repairable systems is well established in the reliability literature, there remains a dearth of research considering systems under repair scenarios beyond minimal repair. To the best of our knowledge, only the recent works of Liu *et al.* (2020) and Junior (2021) have initiated discussions on frailty models for systems undergoing imperfect repairs, as previously highlighted.

Specifically, Liu *et al.* (2020) presented a shared frailty model only for the classes ARA_1 and ARA_∞ of imperfect repair, while Junior (2021) introduced a univariate frailty model for the general ARA_m class. There is, therefore, a gap in the field of reliability when it comes to extending frailty models for perfect repairs and for any class and memory of imperfect repairs. This discussion is important because assuming only minimal repairs after failures is not realistic and, on the other hand, the lack of knowledge about the true repair effect on the system implies the need to evaluate as many possibilities as feasible to make inferences about this impact.

In this sense, the main contributions of this thesis are the proposal of some novel models that extend and generalize prior models with the goal of furnishing multiple insights related to the repair effect and the unobserved heterogeneity into observed systems based on their failure processes. In each of Chapters 3, 4 and 6, we present new models in this regard. These models have not yet been presented in the literature and have a high potential for applicability in real problems.

Initially, in Chapter 3, we propose a univariate frailty model for multiple systems undergoing perfect repair. This model is an extension of the frailty models applied to systems under minimal repair presented by D'Andrea (2019). Here, we assume that the initial intensity function of the systems is modeled by a PLP and the frailty variables associated with failure times have a Gamma distribution.

In Chapter 4, our objective is to generalize the shared frailty models presented by Liu *et al.* (2020) to encompass any failure memory of the ARA_m and ARI_m imperfect repair classes,

and also to extend the univariate frailty model proposed by Junior (2021) to encompass any failure memory within the ARA_m and ARI_m classes. Therefore, we propose here four generalized models: two univariate frailty models for multiple systems undergoing imperfect repairs, each model considering all possible m failure memories of the ARA_m or ARI_m class of imperfect repair; and two additional shared frailty models, again for multiple systems undergoing imperfect repairs, each encompassing all possible failure memories m within the ARA_m or ARI_m class. In all cases, we presuppose that the initial intensity function is modeled by a PLP and the frailty variables follow a Gamma distribution.

In the context of repairable systems subjected to competing risks, the research gaps concerning unobserved heterogeneity in systems undergoing imperfect repairs persist. To our knowledge, only Junior (2021) presented a framework of competing risks (hierarchical, in this case) combined with univariate frailty and imperfect repairs. In light of this, we propose novel models that diverges from the author's approach. Our model centers on shared frailty between multiple systems and their respective causes of failure, encompassing imperfect repairs in both ARA_m and ARI_m classes, and all their possible failure memories. Here, the PLP is also assumed as initial intensity function and the Gamma distribution as frailty distribution. These models are presented in Chapter 6 and represent extensions of previous research that has established competing risk frameworks with imperfect repairs, as well as models that have explored competing risk frameworks with unobserved heterogeneity considering only minimal repairs.

1.2 Chapters Organization

The next chapters of this thesis are organized as follows.

- In Chapter 2, an extensive bibliographical and content review is conducted to provide essential support for the development of the thesis. Section 2.1 introduces key definitions related to counting processes, particularly focusing on Poisson processes, with an emphasis on PLP as a significant parametric case of NHPP. Section 2.2 provides a detailed exploration of the minimal repair, perfect repair, and the both ARA_m and ARI_m classes of imperfect repair, and includes inferential procedures for obtaining the likelihood function for systems under each type of repair. Section 2.3 introduces fundamental concepts about frailty models and unobserved heterogeneity, and presents the main algebraic developments related to parametric Gamma frailty models. In Section 2.4, the competing risks framework is established, and some inferential constructs are presented to guide future developments.

- In Chapter 3, a parametric frailty model is proposed for multiple repairable systems under perfect repair within an intensity function parameterized by a PLP. Section 3.1 presents an existing model from the literature that considers unobserved heterogeneity in the context

of minimal repair. Section 3.2 presents the newly proposed model. Section 3.3 offers an extensive simulation study for the proposed model. Finally, in Section 3.4, the developed procedures are applied to fit two real datasets.

- In Chapter 4, we propose parametric frailty models for multiple repairable systems under imperfect repair with an intensity function parameterized by a PLP for both classes ARA_m and ARI_m. The discussion in this chapter has been divided into two parts, according to the type of frailty incorporated in the model. Initially, in Section 4.1, we present a univariate frailty model, where the frailty variables are associated with each failure time and the Laplace Transform is used to obtain the intensity functions of the model. In Section 4.2, we present a shared frailty model, where frailty variables are associated with each system and shared by failure times. In each of these sections, we develop frequentist inferential procedures, conduct comprehensive simulation studies, and employ a real dataset to illustrate the application of the proposed models.

- In Chapter 5, we present a Bayesian approach for estimating the parameters of shared frailty models for multiple repairable systems. In Section 5.1, we present our proposed Bayesian model framework, which assumes a reparameterization for the PLP and considers the possibility of individually estimating repair effects for each system. In Section 5.1.1, we define the prior distributions and outline a hierarchical Bayesian approach to the problem. In Section 5.1.2, we propose an iterative sampling method based on Markov Chain Monte Carlo (MCMC) techniques to obtain the posterior density distributions of the model parameters. In Sections 5.1.3 and 5.1.4, we establish criteria for model selection and verify chain convergence. Finally, in Section 5.2, we revisit the real datasets previously presented in this work to demonstrate the application of the Bayesian techniques.

- In Chapter 6, we propose parametric frailty models for multiple repairable systems subjected to competing risks under imperfect repair with an intensity function parameterized by a PLP for both classes ARA_m and ARI_m. In Section 6.1.1, we present the models formulation, defining their intensity functions within the framework of competing risks combined with imperfect repairs. In Section 6.1.2, we outline frequentist inferential methods for estimating the parameters of the proposed models. In Section 6.1.3, we discuss and define reliability prediction functions in the context of competing risks. Section 6.2 features a simulation study to verify the asymptotic properties of the proposed estimators. Finally, in Section 6.3, we present and utilize two real datasets to illustrate the practical applicability of the proposed models.

- In Chapter 7, we provide a summary of the main results present in this work. Some future proposals of our research are also listed.

1.3 Products of the Thesis

The process of preparing the thesis has yielded one published article, one article that has already been submitted for consideration, and additional three articles currently in the final stages of preparation, set to be submitted in the near future. The following is a list of elaborated texts:

- BRITO, É. S.; TOMAZELLA, V. L.; FERREIRA, P. H. **Statistical modeling and reliability analysis of multiple repairable systems with dependent failure times under perfect repair**. Reliability Engineering & System Safety, Elsevier, v. 222, p. 108375, 2022. *(Published article (BRITO; TOMAZELLA; FERREIRA, 2022)).*

- BRITO, É. S.; TOMAZELLA, V. L.; FERREIRA, P. H.; LOUZADA, F.; GONZATTO-JUNIOR, O. A. **Reliability analysis of multiple repairable systems under imperfect repair and unobserved heterogeneity**. *(This paper is under review in Quality and Reliability Engineering International.)*

- BRITO, É. S.; TOMAZELLA, V. L.; FERREIRA, P. H.; LOUZADA, F. **Shared frailty models for multiple repairable systems under imperfect repair**. *(Paper related to Section 4.2, under internal review by the authors.)*

- BRITO, É. S.; TOMAZELLA, V. L.; FERREIRA, P. H.; LOUZADA, F. **Bayes inference for repairable systems under imperfect repair and unobserved heterogeneity**. *(Paper related to Chapter 5, under internal review by the authors.)*

- BRITO, É. S.; TOMAZELLA, V. L.; FERREIRA, P. H.; LOUZADA, F. **Frailty models for general repairable systems in competing risks framework**. *(Paper related to Chapter 6, under internal review by the authors.)*

CHAPTER

2

BACKGROUND

In this chapter, we will present some basic ideas that will serve as support for further discussions. The objective here is to list and review the main concepts known in the literature, which will be used in the research.

2.1 Counting Process

According to Ross (1996), a *stochastic process* $\{N(t),\ t \in \mathscr{T}\}$ is a collection of random variables where, for each t in the index set $\mathscr{T}$, $N(t)$ is a random variable. A *point process* is defined by Rigdon and Basu (2000, p. 23) as a stochastic model that describes occurrence of events in time. Thus, in a point process, if events are occurring randomly in time, the variable $N(t)$ can represent the number of events that occur in $[0,t]$ and this is the idea of a *counting process*, formally defined bellow.

Definition 1. A *counting process* is a stochastic process $\{N(t),\ t \geq 0\}$ that satisfies the following conditions:

1. $N(t) \geq 0$ and $N(0) = 0$;
2. $N(t)$ is an integer value;
3. $t \mapsto N(t)$ is right-continuous;
4. $\lim_{h \to 0} [N(t+h) - N(t)] = 0$.

As a direct consequence of the definition, if $s < t$ then $N(s) \leq N(t)$. In addition, $N(s,t] = N(t) - N(s)$ is the number of events that occurred in the range $(s,t]$.

In the context of survival analysis and reliability, we are interested in the occurrence of events over time $[0,t]$, and we will consider that the random variable T represents the time until failure (occurrence of the event of interest) since the experiment started at $t = 0$.

A point process described by a non-decreasing sequence of positive random variables $0 < T_1 \leq T_2 \leq \cdots$ can also be described by the corresponding counting process $N(t) = N_t(\upsilon)$, with $t \in \mathbb{R}_+$, since the random variable $N_t(\upsilon)$ counts the number of points T_k that occur until the time t, written as

$$N_t(\upsilon) = \sum_{k \geq 1} \mathbb{I}(T_k(\upsilon) \leq t),$$

where $\mathbb{I}(\cdot)$ is the indicator function. Note that for each realization υ, the function $N_t(\cdot)$ is a non-decreasing right-continuous step function with size jump 1. Furthermore, if we consider the sequence of times between events $X_i = T_i - T_{i-1}$, with $i \geq 1$ and $T_0 = 0$, the three specifications $\{N(t)\}_{t \geq 0}$, $\{T_{N(t)}\}_{t \geq 0}$ and $\{X_i\}_{i \geq 1}$ are equivalent and carry the same information, as seen in Figure 1.

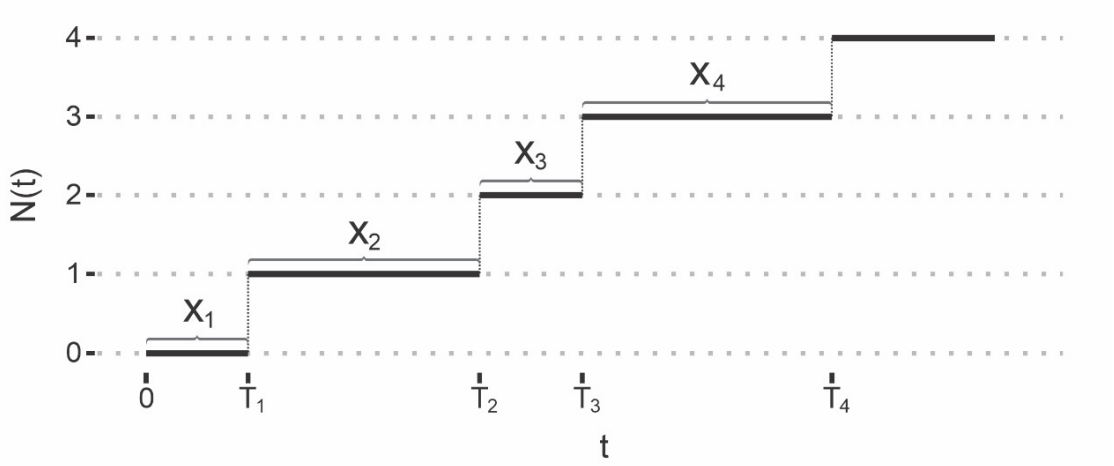

Figure 1 – Representation of the number of events $N(t)$, times to events T_i, and times between events X_i.

Definition 2. A point process has *independent increments* if for all n and for all $r_1 < s_1 \leq r_2 < s_2 \leq \cdots \leq r_n < s_n$, the random variables $N(r_1, s_1], N(r_2, s_2], \ldots, N(r_n, s_n]$ are independent, that is,

$$\mathbb{P}[N(r_1, s_1] = k_1, \ldots, N(r_n, s_n] = k_n] = \prod_{i=1}^{n} \mathbb{P}[N(r_i, s_i] = k_i].$$

In other words, a point process has independent increments if the number of events that occur in disjoint intervals are independent.

Definition 3. A point process has *stationary increments* if for all k, $\mathbb{P}[N(t, t+s] = k]$ is independent of t.

In other words, a point process has stationary increments if the distribution of the number of events occurring in any interval depends only on the length of the interval, that is, the random variable $N(t_1 + s, t_2 + s]$ has the same distribution as $N(t_1, t_2]$, for all t_1, t_2 and $s > 0$.

Other two important initial definitions are the mean function and the rate of occurrence of failures of a counting process, and they are presented below.

Definition 4. The *mean function* of a counting process is the expected number of failures through time t, that is

$$\Lambda(t) = \mathbb{E}[N(t)].$$

Definition 5. The Rate of Occurrence of Failures (ROCOF) of a counting process at time t is

$$\lambda(t) = \Lambda'(t) = \frac{d}{dt}\mathbb{E}[N(t)] = \lim_{\Delta t \to 0} \frac{\mathbb{E}[N(t+\Delta t) - N(t)]}{\Delta t}.$$

By the last expression of the definition above, the ROCOF represents the expected number of failures in the interval $(0,t]$. Moreover, according to Rigdon and Basu (2000, p. 24, 28), ROCOF can be interpreted as the instantaneous rate of change in the expected number of failures, and since the probability of instantaneous failures is zero, it will also be the *intensity function* of the counting process.

Definition 6. The *complete intensity function* of a point process is

$$\lambda(t) = \lim_{\Delta t \to 0} \frac{\mathbb{P}[N(t,t+\Delta t] \geq 1 \mid \mathscr{H}_t]}{\Delta t}, \tag{2.1}$$

where $\mathscr{H}_t$ is the history of the process at time t.

Note that the complete intensity function gives the instantaneous probability of an event occurring at t, conditional on the process history.

If the process is a counting process with independent increments, since the history of events does not interfere with the occurrence of the next event, we can rewritten the intensity function as

$$\lambda(t) = \lim_{\Delta t \to 0} \frac{\mathbb{P}[N(t,t+\Delta t] \geq 1]}{\Delta t}.$$

In this context, the mean function $\Lambda(t)$ can be reinterpreted as the *cumulative intensity function* of a counting process, and it is given by

$$\Lambda(t) = \int_0^t \lambda(u)du. \tag{2.2}$$

2.1.1 Poisson Process

The Poisson process is a particular case of the counting process that can be used to model occurrences (and counts) of events over a period of time, when they are not affected by past occurrences. It is a particular case of a Markov process in continuous time, where the only possibility of jumping is to the next state of the sequence.

Definition 7. A counting process $N(t)$ is a *Poisson Process* with intensity $\lambda(t) > 0$ if

1. $N(0) = 0$;

2. $N(t)$ has independent increments;

3. $\lim_{\Delta t \to 0} \dfrac{\mathbb{P}[N(t,t+\Delta]=1]}{\Delta t} = \lambda(t)$;

4. $\lim_{\Delta t \to 0} \dfrac{\mathbb{P}[N(t,t+\Delta] \geq 2]}{\Delta t} = 0$.

Note that the fourth property precludes the possibility of simultaneous failures.

As seen in Rigdon and Basu (2000, p. 36) and Hamada *et al.* (2008, p. 166), a consequence of these conditions is that

$$\mathbb{P}[N(t)=x] = \frac{\Lambda(t)^x e^{-\Lambda(t)}}{x!},$$

where $\Lambda(t) = \int_0^t \lambda(u)du$, and that means that the number of failures in an interval is a random variable having a Poisson distribution. In another words, if $N(t)$ is a Poisson process with intensity $\lambda(t)$, we have that

$$N(t) \sim \text{Poisson}\left(\Lambda(t) = \int_0^t \lambda(u)du\right)$$

and

$$N(a,b] \sim \text{Poisson}\left(\Lambda(b)-\Lambda(a) = \int_a^b \lambda(u)du\right).$$

Depending on the definition of $\lambda(t)$, we can have two types of Poisson Process: the Homogeneous Poisson Process (HPP) when $\lambda(t)$ is constant, and the Non-Homogeneous Poisson Process (NHPP) otherwise. To formalize these definitions, consider a function $o(h)$ such that $\lim_{h \to 0} \dfrac{o(h)}{h} = 0$.

Definition 8. A *homogeneous Poisson process* is a counting process $\{N(t); t \geq 0\}$ with intensity $\lambda(t)$ satisfying:

1. $N(0) = 0$;

2. $N(t)$ has independent increments;

3. $\mathbb{P}[N(t+h)-N(t)=1] = \lambda h + o(h)$;

4. $\mathbb{P}[N(t+h)-N(t) \geq 2] = o(h)$.

The third condition of the definition shows that the intensity function is constant over time, since it does not depend on t. This means that in a HPP, the intensity function $\lambda(t) = \lambda$ for all $t \geq 0$. As a direct consequence, since the number of failures $N(a,b]$ in a Poisson process

has a Poisson distribution with expected value $\int_a^b \lambda(u)du$, in a HPP the mean number and the variance of failures in an interval $(a,b]$ are given by

$$\mathbb{E}[N(a,b]] = Var[N(a,b]] = \int_a^b \lambda(u)du = \int_a^b \lambda du = \lambda(b-a),$$

a linear function of λ and the increments are stationary.

In addition, as can be seen in Hamada *et al.* (2008), in a HPP the times between failures X_i, $i \geq 1$, where $X_i = T_i - T_{i-1}$, are Independent and Identically Distributed (IID) with exponential distribution of mean λ^{-1}.

Definition 9. A *non-homogeneous Poisson process* is a counting process $\{N(t); t \geq 0\}$ with intensity $\lambda(t)$ satisfying:

1. $N(0) = 0$;
2. $N(t)$ has independent increments;
3. $\mathbb{P}[N(t+h) - N(t) = 1] = \lambda(t)h + o(h)$;
4. $\mathbb{P}[N(t+h) - N(t) \geq 2] = o(h)$.

The third condition establishes the difference between the HPP and the NHPP, since, in the latter case, the intensity function is not constant over time. In a NHPP, the stationary increments are not required and therein lies its importance and applicability. An important difference from HPP is that, in a NHPP, the times between failures are not necessarily independent or identically distributed.

According to Cook and Lawless (2007), Poisson process models may be nonparametric or parametric, and for the latter, the intensity function $\lambda(t)$ is specified as a function of a finite-dimensional parameter. These authors highlight some possibilities of models such as the exponential model whose intensity function is given by $\lambda(t \mid \alpha, \beta) = e^{\alpha+\beta t}$, and the power law process model which will be detailed in the next section and adopted for the development of this work.

2.1.2 Power Law Process

The Power Law Process (PLP) is a parametric model for the NHPP widely used in the literature. It is defined as follows.

Definition 10. A NHPP $N(t)$ follows a power law process if it has intensity function of the form

$$\lambda(t \mid \beta, \eta) = \frac{\beta}{\eta}\left(\frac{t}{\eta}\right)^{\beta-1}, \tag{2.3}$$

where $\beta > 0$ is the shape parameter and $\eta > 0$ is the scale parameter.

The PLP model was formally introduced and investigated by Crow (1975), where the author assigned the name "Weibull intensity function" to the intensity function. As pointed out by Hamada *et al.* (2008), this nomenclature can be confusing as it suggests that all recurrent failure times have a Weibull distribution, while in fact this is only the case for the first failure time. According to Rigdon and Basu (2000), the name PLP derives from the fact that the intensity function is proportional to the global time t raised to a power.

According to Oliveira, Colosimo and Gilardoni (2013), one of the reasons for the popularity of the PLP stems from the fact that the form of $\lambda(t)$ in (2.3) is flexible, as seen in Figure 2, where we fixed the scale parameter $\eta = 1$.

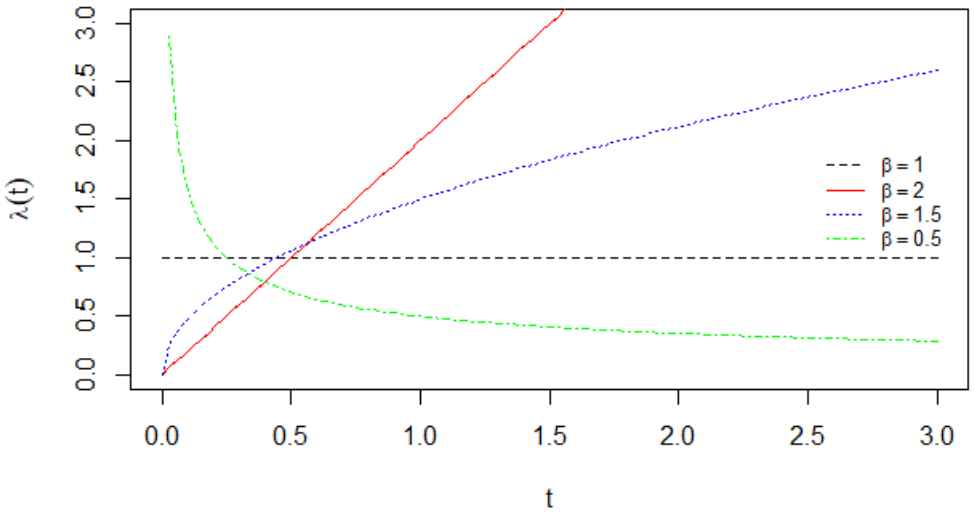

Figure 2 – Intensity function of the PLP with $\eta = 1$ and different β values.

Note that if $\beta > 1$, the intensity function is increasing, while if $\beta < 1$, it is decreasing, which indicates that the parameter β can be interpreted as a measure of elasticity of the expected number of failures. Specifically, if $\beta > 1$, the failure intensity increases over time, which indicates that the system is deteriorating, since the probability of failure increases with time. On the other hand, if $\beta < 1$, the failure intensity decreases over time, which indicates that the system is improving. In the special case that $\beta = 1$, the intensity function is constant and, hence, the PLP becomes an HPP. The scale parameter η, in turn, can be interpreted as the time in which exactly one failure is expected to occur, that is, $\mathbb{E}[N(\eta)] = \Lambda(\eta) = 1$.

As a direct consequence from Definition 10, the cumulative intensity function of a PLP is given by

$$\Lambda(t \mid \beta, \eta) = \left(\frac{t}{\eta}\right)^{\beta}, \tag{2.4}$$

and as seen by Definition 4, this function also represents the expected number of failures up to time t.

2.1.3 Renewal Process

In this section, we will discuss another type of counting process for recurring events, the *renewal processes*.

Definition 11. A counting process $\{N(t), t \geq 0\}$ is said a *renewal process* if the times between failures $X_1, X_2, \ldots$ are independent and identically distributed, where $X_i = T_i - T_{i-1}$, $i \geq 1$.

This process is called renewal because after the occurrence of each event or failure, the probability of recurrence of the failure restarts from zero, that is, the time until the occurrence of a new event is the same as the time until the occurrence of the first event. In this sense, it is as if the system were new after the occurrence of each event. Thus, according to Rigdon and Basu (2000) a renewal process cannot be used to model a system that is deteriorating, because each failure returns the system to a like-new condition.

The complete intensity function $\lambda(t)$ given by (2.1) depends only on the history $\mathscr{H}_t$ of the process only though the time since the most recent failure. Then, we can rewrite the intensity function as

$$\lambda(t \mid \mathscr{H}_t) = \lambda(t - T_{N(t^-)}), \tag{2.5}$$

where $N(t^-)$ is the number of failures before the time t, $T_{N(t^-)}$ is the time that the $N(t^-)$-th failure occurred and $t - T_{N(t^-)}$ is the elapsed time from the last failure to time t. In this case, the behavior of the intensity function can be illustrated by Figure 3, where it is clear that after the occurrence of each failure the intensity function returns to what it was at time $t = 0$.

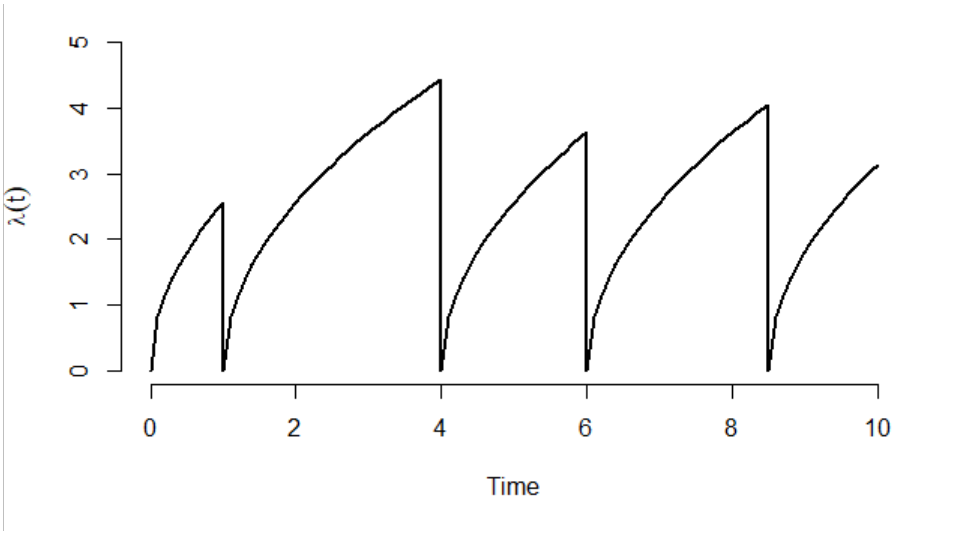

Figure 3 – Intensity function of a renewal process, conditioned on failures at times $t = 1, 4, 6$ and 8.5.

As said before, the times between the failures in a HPP are IID with exponential distribution, so this process is a particular case to the renewal process.

The study of renewal processes is justified by the fact that in some complex systems there is the possibility that the system returns to a state equivalent to the initial state, from the point of view of probability. In the next sections, we will discuss, for example, repair models on repairable systems that can be modeled by renewal processes since the repair will return the system to a new condition.

2.2 Repairable Systems

According to Rigdon and Basu (2000), a *repairable system* is a system that, when a failure occurs, can be restored to an operating condition by some repair process without having to replace the system as a whole. A *non-repairable system*, in turn, is a system that will be discarded after the occurrence of the first and only failure.

By the nature of this type of process, a non-decreasing sequence of failure times will be observed $0 < T_1 < T_2 < \cdots$, where T_i is the i-th failure time of the system, measured in a global time, that is, the time since the initial start up of the system. The sequence of failure times describe a stochastic point process, so we can consider a counting process $\{N(t); t \geq 0\}$, where $N(t)$ is the number of of failures in the interval $(0,t]$. As pointed out by Lindqvist *et al.* (2006), the implicit assumption is usually that the system is repaired and put into new operation immediately after the failure, so we can just ignore the possible repair times.

An important point to be considered in the analysis of a repairable system is the end of the study, that is, the moment when the observation of the system will be finished. This end of study can be determined in two ways: by a predetermined time or by a predetermined number of failures to be observed. When the system observation period ends at a predetermined time t^*, the data is said to be *time truncated* and can be represented by $0 < t_1 < t_2 < \ldots < t_n < t^*$, where t_n is the last observed failure time and n is the number of failures in $(0,t]$, that is, $N(t) = n$. On the other hand, the data is said to be *failure truncated* when the system observation window terminates after a predetermined number of failures n^*, and, in this case, it can be represented by $0 < t_1 < t_2 < \ldots < t_{n^*}$. It is important to highlight that in the case of time truncated system, the number of failures $N(t)$ is random and this should be taken into account.

When a failure occurs in a repairable system, different repair actions can be performed, interfering with the reliability of the system after its return to operation. These types of repair are defined according to the effect that the repair has on the system reliability. In the literature, we find three main types of repair: the Minimal Repair (MR), the Perfect Repair (PR) and the Imperfect Repair (IR). More details of each of these three types of repair will be covered below.

2.2.1 The Minimal Repair Model

The MR occurs when a repair action corrects only the root cause of the system failure, leaving it in the same operating conditions as the system was immediately before the failure, or as defined in the literature, As Bad As Old (ABAO).

According to Kijima (1989), the MR assumption seems plausible for systems consisting of many components each having its own failure mode. Using the MR concept, it is possible to describe in a simple way the fact that many repairs in real life bring the system to a condition that is basically the same before the failure.

In a MR model, the process associated with the occurrence of failure can be described by a NHPP, in which the probability of failure in a short time period does not depend on the history of failures, but only on the previous failure and thus, the intensity function will depend only on the age of the system. This means that the conditional intensity of the failure process immediately after a failure is the same as before the failure and, therefore, is exactly as it would be if no failure had occurred.

Thus, the MR model is a process whose intensity function is the NHPP intensity itself, that is, if we denote by $\lambda_{\text{MR}}(t)$ the intensity function of the MR process, we have that

$$\lambda_{\text{MR}}(t) = \lambda(t), \tag{2.6}$$

where $\lambda(t)$ is the intensity function of a NHPP. As a direct consequence, the cumulative intensity function of the MR process denoted by $\Lambda_{\text{MR}}(t)$ also will be equal to the cumulative intensity of a NHPP $\Lambda(t)$, that is,

$$\Lambda_{\text{MR}}(t) = \int_0^t \lambda_{\text{MR}}(u)du = \int_0^t \lambda(u)du = \Lambda(t).$$

Figure 4 shows a typical behavior of the intensity function of a MR model. The vertical dotted lines indicate the times where system failures and repairs occurred (assuming the repair occurred instantly after the failure). Note that there is no change in the intensity of failures after the occurrence of failures throughout the process, that is, the failure intensity of the system remains the same after the failure in a condition as bad as before the failure.

If the failure intensity function of a repairable system is parametric with a parameter vector $\boldsymbol{\mu}$, a natural issue is to perform inferential methods to obtain the estimates $\hat{\boldsymbol{\mu}}$ for the parameters. From here, we will focus on obtaining the general likelihood function for MR models with any $\lambda(t)$ parametric intensity function.

First of all, it is necessary to obtain the joint probability density function of failure times considering the time truncated and failure truncated cases. In the case of time truncated observation, it is still necessary to obtain the probability that a number n of failures occur on the system. All of these functions will be necessary to obtain the likelihood function and perform

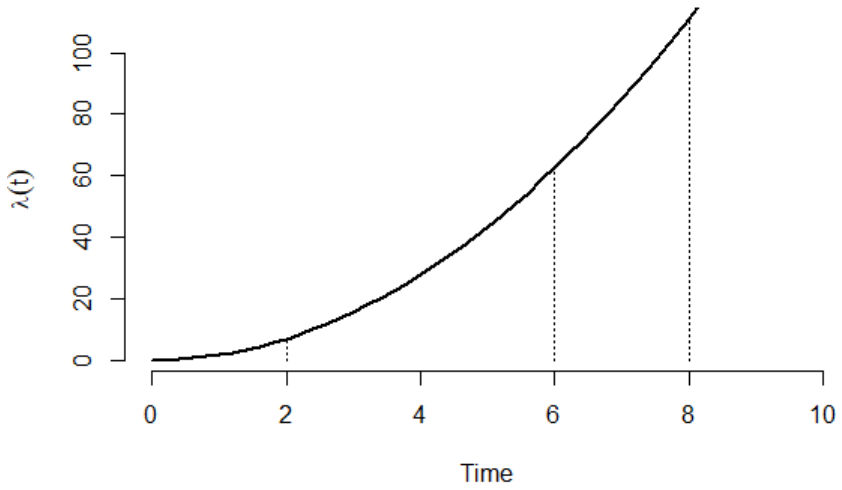

Figure 4 – Intensity function of a MR model, with failures at times $t = 2$, 6 and 8.

inference on the parameters of the intensity function of the system, both for the case of a single system and for the case of multiple systems.

Let t_j, $j = 1,\ldots,n$, be the observation of the random variable T, where each t_j represents the j-th failure time of the repairable system and n is the total number of observed failures.

Fist, we will consider the case of time truncated, being t^* the final observation time. As said before, the observed failure times and time of truncation are given by $0 < t_1 < t_2 < \ldots < t_n < t^*$, and, in this case, the number n of failures is random.

Due to the fact that the MR model is modeled by a NHPP, it has independent increments, that is, the failure times are conditioned only to the immediately previous failure times. Thus, the joint density function of the failure times $T_1,\ldots,T_n$ is given by

$$\begin{aligned} f(t_1,\ldots,t_n) &= f(t_1)f(t_2 \mid t_1)f(t_3 \mid t_1,t_2)\cdots f(t_n \mid t_1,t_2,\ldots,t_{n-1}) \\ &= f(t_1)f(t_2 \mid t_1)f(t_3 \mid t_2)\cdots f(t_n \mid t_{n-1}). \end{aligned}$$

Given the failure intensity function $\lambda_{\mathrm{MR}}(t) = \lambda(t)$, note that the conditional reliability function of T_j given the observation t_{j-1} is

$$\begin{aligned} R(t_j \mid t_{j-1}) &= \mathbb{P}[T_j > t_j \mid t_{j-1}] = \mathbb{P}[N(t_j) - N(t_{j-1}) = 0] \\ &= \exp\left(-\int_{t_{j-1}}^{t_j} \lambda(u)du\right) = \exp\left(-\Lambda(t_j) + \Lambda(t_{j-1})\right), \end{aligned}$$

since the fact that $N(t_j) - N(t_{j-1})$ has a Poisson distribution.

Therefore, it follows that

$$\begin{aligned} f(t_j \mid t_{j-1}) &= \frac{d}{dt_j}[1 - R(t_j \mid t_{j-1})] = \frac{d}{dt_j}[1 - e^{-\Lambda(t_j)+\Lambda(t_{j-1})}] \\ &= \lambda(t_j)e^{-\Lambda(t_j)+\Lambda(t_{j-1})}, \end{aligned}$$

and, in addition, $R(t_1) = \mathbb{P}[T_1 > t_1] = \mathbb{P}[N(t_1) = 0] = e^{-\Lambda(t_1)}$, whence it follows that

$$f(t_1) = \frac{d}{dt_1}[1 - e^{-\Lambda(t_1)}] = \lambda(t_1)e^{-\Lambda(t_1)}.$$

Then, we can rewrite the joint density function of the system failure times as

$$\begin{aligned} f(t_1,\ldots,t_n) &= f(t_1)\prod_{j=2}^{n} f(t_j \mid t_{j-1}) \\ &= \lambda(t_1)e^{-\Lambda(t_1)}\lambda(t_2)e^{-\Lambda(t_2)+\Lambda(t_1)}\cdots\lambda(t_n)e^{-\Lambda(t_n)+\Lambda(t_{n-1})} \\ &= \lambda(t_1)\lambda(t_2)\cdots\lambda(t_n)e^{-\Lambda(t_n)} \\ &= \left(\prod_{j=1}^{n}\lambda(t_j)\right)e^{-\Lambda(t_n)}. \end{aligned}$$

Since we are considering a time truncated process, we need to calculate the probability that up to the truncation time t^* there have been n failures in the system. This probability is given by

$$\begin{aligned} \mathbb{P}[N(t^*) = n \mid t_1,t_2,\ldots,t_n] &= \mathbb{P}[N(t^*) = n \mid t_n] \\ &= \mathbb{P}[N(t^*) - N(t_n) = 0] = e^{-\Lambda(t^*)+\Lambda(t_n)}. \end{aligned}$$

Finally, we can determine the likelihood function for the parameter vector $\boldsymbol{\mu}$ of the intensity function of a MR model time truncated, taking into account the randomness of the number n of failures occurring in the system until the time t^* and the observed failure times $t_1,\ldots,t_n$:

$$\begin{aligned} L_{\mathrm{MR}}(\boldsymbol{\mu} \mid t_j) &= f(t_1,\ldots,t_n,n) = f(t_1,\ldots,t_n) \times P[N(t^*) = n \mid t_1,t_2,\ldots,t_n] \\ &= \left(\prod_{j=1}^{n}\lambda(t_j)\right)e^{-\Lambda(t_n)}e^{-\Lambda(t^*)+\Lambda(t_n)} \\ &= \left(\prod_{j=1}^{n}\lambda(t_j)\right)e^{-\Lambda(t^*)}. \end{aligned} \tag{2.7}$$

Considering the case of failure truncated process, the development to obtain the likelihood function is exactly the same as that performed for the previous case, with the difference that now there is no randomness in the number of failures n, since this is a fixed and predetermined number n^*. Then, the likelihood function of the parameter vector $\boldsymbol{\theta}$ is given by

$$L_{\mathrm{MR}}(\boldsymbol{\mu} \mid t_j) = f(t_1,\ldots,t_{n^*}) = \left(\prod_{j=1}^{n^*}\lambda(t_j)\right)e^{-\Lambda(t_{n^*})}. \tag{2.8}$$

Note that the expression (2.8) obtained considering the failure truncated model can be directly obtained from the expression (2.7) of the time truncated process, just replacing the truncation time t^* with the time of the last observed failure t_n.

2.2.2 The Perfect Repair Model

The PR occurs when a repair action corrects an important component of the system, leaving it in conditions similar to those at the beginning of the experiment, that is, when the system had not yet worn out. In the literature, it is said that the system assumes a condition As Good As New (AGAN) after the repair.

According to Kijima (1989), in practice, the PR assumption may be reasonable for systems with one unit which is structurally simple. This makes sense since, in general, a PR occurs when an important component of the system is replaced after the failure, in order to leave the system as new again.

In this case, the failure process is modeled by a renewal process. As discussed in Section 2.1.3, the renewal process can be defined by the joint distribution of the counting process $N(t)$ and the probability of failure begins with each repair process. Furthermore, we pointed out that simplest characterization is through the intervals between times of failure occurrence being IID, and the intensity function depends on the last observed failure time, as defined by the equation (2.5).

Therefore, the failure intensity function of a PR model is given by

$$\lambda_{\mathrm{PR}}(t) = \lambda_0(t - T_{N(t)}), \tag{2.9}$$

where $\lambda_0(t)$ is the intensity function of a NHPP, $N(t)$ is the number of failures until the time t, $T_{N(t)}$ is the time until the $N(t)$-th failure, and $(t - T_{N(t)})$ is the time until t since the last failure strictly before t. Figure 5 shows an example of the behavior of the intensity function of a system under PR.

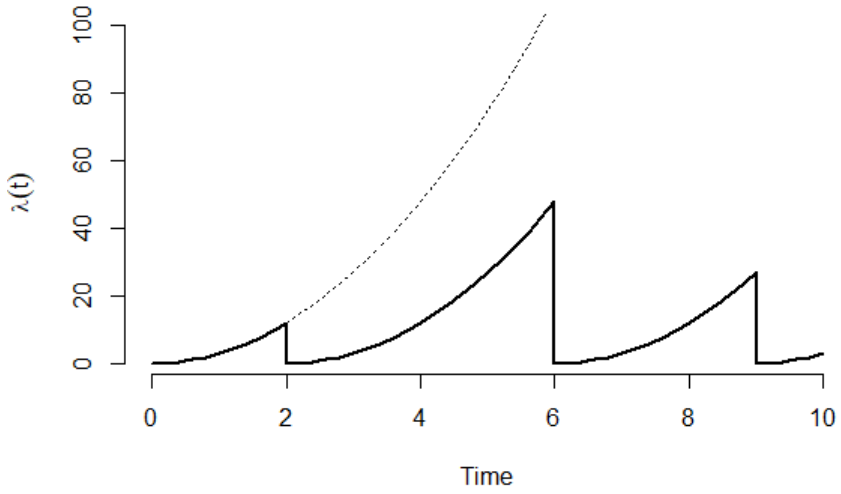

Figure 5 – Intensity function of a PR model, with failures at times $t = 2$, 6 and 9.

Figure 5 shows that after the occurrence of each failure, the intensity function returns to the initial value of zero, since the system assumes a like-new condition. In other words, after

each failure the intensity function behaves exactly as in the initial process time. Furthermore, the dotted curve is the curve referring to the MR model, that is, the intensity curve that would not change after the occurrence of failures and repairs. Note that the MR and PR curves are equal until the first failure, which allows us to say that $\lambda_0(t)$ is the *initial intensity function* of the system and it is exactly the MR intensity function.

From equation (2.9), we can obtain the cumulative intensity function for the PR model, since this is the integral of the intensity function as indicated in (2.2). But note that the change in behavior of the intensity function after each failure requires that its integral also be calculated separately in each of the intervals between two consecutive failure times. Finally, the cumulative intensity of failure at time t will take into account the cumulative intensity up to the last failure time prior to t, $T_{N(t)}$. By definition, we have:

$$\Lambda_{\text{PR}}(t) = \int_0^t \lambda_{\text{PR}}(u)du = \int_0^t \lambda_0(u - T_{N(t)})du = \Lambda_0(T_{N(t)}) + \Lambda_0(t - T_{N(t)}), \tag{2.10}$$

where $\Lambda_0(t)$ is the initial cumulative intensity function, that is, is the cumulative intensity function of the MR model.

As in the case of MR, the function $\lambda_{\text{PR}}(t)$ can be a parametric function with vector parameter $\boldsymbol{\mu}$ and we can obtain its parameter estimates. We will follow the same steps developed in Section 2.2.1 for the MR model to build the general likelihood function for the parameters of the PR model.

Let $T_1, \ldots, T_n$ be the failure times of a repairable system under PR process. By the analysis already carried out previously for the MR case, the joint density function of the failure times can be written by

$$f(t_1, \ldots, t_n) = f(t_1) f(t_2 \mid t_1) f(t_3 \mid t_2) \cdots f(t_n \mid t_{n-1}).$$

If the time $t \in [t_{j-1}, t_j)$, then $N(t) = j-1$, since there were $j-1$ failures up to time t, and consequently, $T_{N(t)} = t_{j-1}$. Thus, the conditional reliability function of t_j given the observed failure time t_{j-1} is given by

$$\begin{aligned} R(t_j \mid t_{j-1}) &= \mathbb{P}[T_j > t_j \mid t_{j-1}] = \mathbb{P}[N(t_j) - N(t_{j-1}) = 0] \\ &= \exp\left(-\int_{t_{j-1}}^{t_j} \lambda_{\text{PR}}(u)du\right) = \exp\left(-\int_{t_{j-1}}^{t_j} \lambda_0\left(u - t_{j-1}\right)du\right) \\ &= e^{-\Lambda_0\left(t_j - t_{j-1}\right) + \Lambda_0\left(t_{j-1} - t_{j-1}\right)} = e^{-\Lambda_0\left(t_j - t_{j-1}\right)}. \end{aligned} \tag{2.11}$$

We obtain the conditional density function of t_j given t_{j-1}, as follows:

$$\begin{aligned} f(t_j \mid t_{j-1}) &= \frac{d}{dt_j}[1 - R(t_j \mid t_{j-1})] = \frac{d}{dt_j}[1 - e^{-\Lambda_0\left(t_j - t_{j-1}\right)}] \\ &= \lambda_0\left(t_j - t_{j-1}\right) e^{-\Lambda_0\left(t_j - t_{j-1}\right)}, \end{aligned}$$

and then, the joint density function of the failure times is given by

$$f(t_1,\ldots,t_n) = \prod_{j=1}^{n} \lambda_0\left(t_j - t_{j-1}\right) e^{-\Lambda_0\left(t_j - t_{j-1}\right)}.$$

Considering the time truncated case, where t^* is the time of truncation, the number n of failures of the system is random and the probability of $N(t_n) = n$ should be taken into account in the likelihood function. Note that if $t \in [t_n, t^*)$ then $N(t) = n$, and the desired probability is given by

$$\begin{aligned}\mathbb{P}[N(t^*) = n \mid t_1,\ldots,t_n] &= \mathbb{P}[N(t^*) = n \mid t_n] = \mathbb{P}[N(t^*) - N(t_n) = 0] \\ &= e^{-\Lambda_0(t^* - t_n) + \Lambda_0(t_n - t_n)} = e^{-\Lambda_0(t^* - t_n)}.\end{aligned}$$

Thus, the likelihood function for the vector parameters $\boldsymbol{\mu}$ in the PR model time truncated is given by

$$L_{\mathrm{PR}}(\boldsymbol{\mu} \mid t_j) = \left(\prod_{j=1}^{n} \lambda_0\left(t_j - t_{j-1}\right) e^{-\Lambda_0\left(t_j - t_{j-1}\right)}\right) e^{-\Lambda_0(t^* - t_n)}. \tag{2.12}$$

By the definitions on (2.9) and (2.10), the general likelihood of the PR model can be written as

$$L_{\mathrm{PR}}(\boldsymbol{\mu} \mid t_j) = \left(\prod_{j=1}^{n} \lambda_{\mathrm{PR}}\left(t_j\right) e^{-\left[\Lambda_{\mathrm{PR}}\left(t_j\right) - \Lambda_{\mathrm{PR}}\left(t_{j-1}\right)\right]}\right) e^{-\left[\Lambda_{\mathrm{PR}}(t^*) - \Lambda_{\mathrm{PR}}(t_n)\right]}.$$

If we consider the failure truncated case with n^* fixed failure times in a system, we can obtain the likelihood function by just replacing the term t^* with t_{n^*} in the expression (2.12) obtained for the time truncated case, in a similar way to that observed for the MR model. Thus, the likelihood function, in this case, is given by

$$\begin{aligned}L_{\mathrm{PR}}(\boldsymbol{\mu} \mid t_j) &= \prod_{j=1}^{n} \lambda_{\mathrm{PR}}\left(t_j\right) e^{-\Lambda_{\mathrm{PR}}\left(t_j\right)} \\ &= \prod_{j=1}^{n} \lambda_0\left(t_j - t_{j-1}\right) e^{-\Lambda_0\left(t_j - t_{j-1}\right)}.\end{aligned}$$

2.2.3 The Imperfect Repair Model

In many situations, the repair actions leave the system at an intermediate level between AGAN and ABAO, characterizing a situation of IR. In other words, this type of repair does not return the system to the same conditions as the PR, but leaves it in a better condition than a MR. As placed by Kijima (1989), in this case the repair actions are more directed to the maintenance of the system as a whole than to the factor that causes the failure.

Kijima, Morimura and Suzuki (1988) introduced the concept of *virtual age* to model periodic maintenance issues without considering minimal or perfect repair. The main idea of

this concept is that after repair, the system will assume an unreal "new age" that describes the current condition of the system compared to a new system. The virtual age is a positive function of the real age and the history of system failures, that is, $V_t = V(t \mid N(t); T_1, \ldots, T_{N(t)})$, where V_t represents the virtual age at the time t. A system with virtual age $V_t = v_t$ at the time t behaves exactly like a new system that hasn't failed until time v_t (LINDQVIST *et al.*, 2006).

Definition 12. Let t be a failure time and denote by $V_{N(t)}$ the *virtual age* of the system at the time t, where $N(t)$ is the number of failures (and repairs) of the system at time t. If $V_{N(t)} = v$, the $(N(t)+1)$-th time between failures $X_{N(t)+1}$ of the system works according to

$$\mathbb{P}[X_{N(t)+1} = x \mid V_{N(t)} = v] = \frac{F(x+v) - F(v)}{1 - F(v)},$$

where $F(x)$ is the lifetime distribution of a new system.

Note that X_n can be interpreted as the additional age after the $(n-1)$-th failure. In the context of IR, after each repair performed some system malfunctions are alleviated in order to reduce the additional age X_n, that is, there is an efficiency in these repairs. The virtual age model inserts a measure a_n that represents the degree of the repair efficiency of the n-th repair. This term a_n must be a number in $(0,1)$ and acts so that after the n-th repair, the additional age X_n reduces to $a_n X_n$.

Of course, $T_n = \sum_{i=1}^{n} X_i$ is the real age of the system at the n-th failure and we also can say that the real age after the n-th failure is $T_n = T_{n-1} + X_n$. Similarly, the virtual age after the n-th failure (and repair) is $V_n = V_{n-1} + a_n X_n$, since the repair effect reduces the real age increment. If we assume that each repair produces the same effect, then the degree of repair is constant for all n, say $a_n = 1 - \theta$, with $0 \leq \theta \leq 1$. Thus, $V_n = \sum_{i=1}^{n} \theta X_i$, and it is clear that if $\theta = 1$ so $V_n = T_n$ and in this case the repair returns the system to an ABAO condition. On the other hand, if $\theta = 0$ then $V_n = 0$ and it means that the system is an AGAN condition.

In the literature, we find two classes of models for IR, the Arithmetic Reduction of Age (ARA) model and the Arithmetic Reduction of Intensity (ARI) model, defined by Doyen and Gaudoin (2004). We will describe each of these classes below, but first, we highlight that both classes are defined by a memory m, where m refers to the maximum number of previous failures that impact the effect of a repair and, consequently, the failure intensity function, suggesting a kind of Markovian property (DOYEN; GAUDOIN, 2004). Memory m indicates that each repair action reduces the system wear that occurs after the last m failures. If $m = 1$, for example, each repair action will reduce the wear that occurs only after the last system failure. In this way, the intensity function of the system will be recalculated after each failure, considering the most recent failure times.

2.2.3.1 The ARA_m Model

According to Doyen and Gaudoin (2004), the principle of the ARA_m class is to consider that repair rejuvenates the system such that its intensity at time t is equal to the initial intensity at time V_t, where $V_t < t$. In other words, the repair effect is expressed by a reduction in the virtual age of the system, so that the real age of the system will be t, while the virtual age will become V_t after the repair.

In this sense, the failure intensity of an ARA model can be written as a function of its virtual age, that is, $\lambda_{\text{ARA}m}(t) = \lambda_0(V_t)$, where $\lambda_0(t)$ is the initial intensity function (that is, the intensity function until the first failure). Considering the repair effect parameter θ and a memory m, the failure intensity function for a model of the ARA_m class is defined as

$$\lambda_{\text{ARA}m}(t) = \lambda_0\left(t - (1-\theta)\sum_{p=0}^{min(m-1,N(t)-1)}\theta^p T_{N(t)-p}\right). \tag{2.13}$$

The cumulative failure intensity function is again obtained by the integral of the intensity function and in this IR model, it is again necessary to calculate the integral in each interval between two consecutive failure times. Thus, this cumulative intensity function is given by

$$\begin{aligned}\Lambda_{\text{ARA}m}(t) &= \int_0^t \lambda_{\text{ARA}m}(u)du \\ &= \Lambda_{\text{ARA}m}(T_{N(t)}) + \Lambda_0\left(t-(1-\theta)S(T_{N(t)})\right) - \Lambda_0\left(T_{N(t)}-(1-\theta)S(T_{N(t)})\right),\end{aligned}$$

where $S(T_o) = \sum_{p=0}^{\min\{m-1,o-1\}}\theta^p T_{o-p}$.

Note that the expression in the functions argument in (2.13) represents the virtual age V_t of the system at time t, so that the second term is the reduction of the virtual age in relation to time t under the conditions of the repair effect θ and the history of m latest failures.

Two important particular (and extreme) cases of the ARA_m class are the ARA_1 and ARA_∞ models. If $m = 1$, the failure intensity function for the ARA_1 model is given by

$$\lambda_{ARA_1}(t) = \lambda_0\left(t-(1-\theta)T_{N(t)}\right),$$

once $min(m-1,N(t)-1) = min(0,N(t)-1) = 0$ and the only term of sum $\sum_{p=0}^{min(0,N(t)-1)}\theta^p T_{N(t)-p}$ is such that $p = 0$, by reducing the $\theta^0 T_{N(t)-0} = T_{N(t)}$. As stated before, in this case it is assumed that the repair effect is to reduce the age increase of the system considering only effect of the last failure.

On the other hand, in the class ARA_∞, it is assumed that each repair reduces the virtual age of the system by an amount proportional to its age immediately before the repair. In this case, the failure intensity function is given by

$$\lambda_{ARA_\infty}(t) = \lambda_0\left(t-(1-\theta)\sum_{p=0}^{N(t)-1}\theta^p T_{N(t)-p}\right).$$

The particular class ARA_1 corresponds to the virtual age model proposed by Kijima, Morimura and Suzuki (1988). In the introduction of Section 2.2.3, we said that if $\theta = 1$ or $\theta = 0$ in that virtual age model, the system assumes an ABAO or AGAN condition, respectively. As direct consequence, it is important to note that the MR and PR models are particular cases of the ARA_1 class models when $\theta = 1$ and $\theta = 0$, respectively, once that:

$$\text{if } \theta = 1, \text{ so } \lambda_{ARA_1}(t) = \lambda_0\left(t - (1-1)T_{N(t)}\right) = \lambda_0(t) = \lambda_{\text{MR}}(t);$$
$$\text{if } \theta = 0, \text{ so } \lambda_{ARA_1}(t) = \lambda_0\left(t - (1-0)T_{N(t)}\right) = \lambda_0\left(t - T_{N(t)}\right) = \lambda_{\text{PR}}(t).$$

In the ARA_m class, between two consecutive failures, its intensity is horizontally parallel to its initial intensity. This can be seen from the graph of Figure 6. In this graph, the dashed line is the graph of the initial intensity function (or MR intensity function), while the other curves are the graphs of the intensity function for each interval between two consecutive failures. Note that these graphs are horizontal displacements (and proportional to the size of the interval between consecutive failures) of the graph of the initial intensity function. In other words, the minimum point of each new curve starting at failure time t is $(t, \lambda_0(v_t))$, where v_t is the virtual age at time t given by $v_t = \theta^m t$ (DOYEN; GAUDOIN, 2004), and it is offset horizontally in $(1-\theta)S(T_{N(t)})$ to the right of the dotted curve.

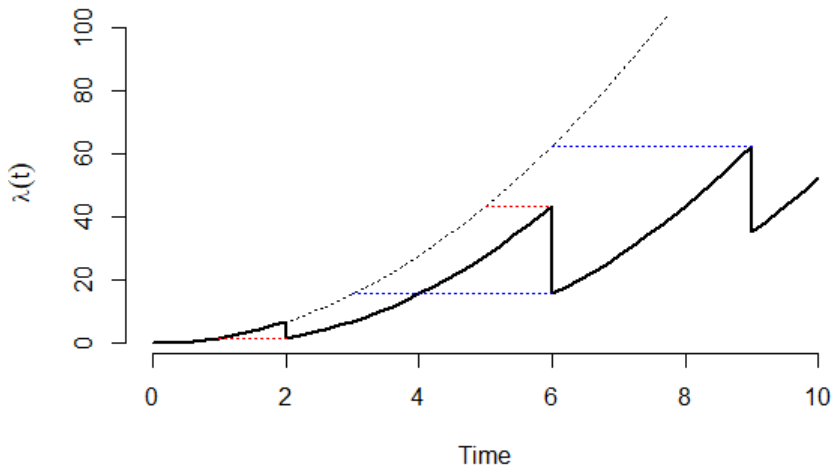

Figure 6 – Intensity function of an ARA_m model, with failures at times $t = 2$, 6 and 9.

Once again, the intensity function $\lambda_{\text{ARA}m}(t)$ can be a parametric function and, in this case, the parameter θ is necessarily in the vector parameter $\boldsymbol{\mu}$. Therefore, our goal in this section will be to obtain the likelihood function of the ARA_m model, following the same steps as in Sections 2.2.1 and 2.2.2.

Let $T_1, \ldots, T_n$ be the failure times of a repairable system and assume an IR model with arithmetic reduction of age and a failure memory m (ARA_m model). We will obtain the joint distribution function in the same way as in the previous MR and PR cases.

As previously discussed in Section 2.2.2, if $t \in [t_{j-1}, t_j)$ then $N(t) = j-1$ and $T_{N(t)} = t_{j-1}$. Thus, the conditional reliability function of t_j given the observed failure time t_{j-1} is

$$\begin{aligned} R(t_j \mid t_{j-1}) &= \mathbb{P}[T_j > t_j \mid t_{j-1}] = \mathbb{P}[N(t_j) - N(t_{j-1}) = 0] \\ &= \exp\left(- \int_{t_{j-1}}^{t_j} \lambda_{\mathrm{ARA}m}(u) du \right) = \\ &= \exp\left(- \int_{t_{j-1}}^{t_j} \lambda_0 \left(u - (1-\theta) \sum_{p=0}^{min(m-1,j-2)} \theta^p t_{j-1-p} \right) du \right) \\ &= e^{-\Lambda_0\left(t_j - (1-\theta) \sum_{p=0}^{min(m-1,j-2)} \theta^p t_{j-1-p} \right) + \Lambda_0\left(t_{j-1} - (1-\theta) \sum_{p=0}^{min(m-1,j-2)} \theta^p t_{j-1-p} \right)}. \end{aligned}$$

Thus, it follows that the conditional density function of t_j given t_{j-1} is given by

$$\begin{aligned} f(t_j \mid t_{j-1}) &= \frac{d}{dt_j}[1 - R(t_j \mid t_{j-1})] = \\ &= \lambda_0 \left(t_j - (1-\theta) \sum_{p=0}^{min(m-1,j-2)} \theta^p t_{j-1-p} \right) \times R(t_j \mid t_{j-1}), \end{aligned}$$

and then, the joint density function of the failure times is given by

$$\begin{aligned} f(t_1, \ldots, t_n) &= f(t_1) f(t_2 \mid t_1) f(t_3 \mid t_2) \cdots f(t_n \mid t_{n-1}) \\ &= \prod_{j=1}^{n} \lambda_0 \left(t_j - (1-\theta) \sum_{p=0}^{min(m-1,j-2)} \theta^p t_{j-1-p} \right) \times R(t_j \mid t_{j-1}). \end{aligned}$$

Considering the time truncated case at the time t^*, the number n of failures is random and the probability of $N(t^*) = n$ given all the observed failure times is given by

$$\begin{aligned} \mathbb{P}[N(t^*) = n \mid t_1, \ldots, t_n] &= \mathbb{P}[N(t^*) = n \mid t_n] = \mathbb{P}[N(t^*) - N(t_n) = 0] \\ &= e^{-\Lambda_0\left(t^* - (1-\theta) \sum_{p=0}^{min(m-1,n-1)} \theta^p t_{n-p} \right) + \Lambda_0\left(t_n - (1-\theta) \sum_{p=0}^{min(m-1,n-1)} \theta^p t_{n-p} \right)}. \end{aligned}$$

So we can write the likelihood function for vector parameter $\boldsymbol{\mu}$ of the ARA_m time truncated model as

$$\begin{aligned} L_{\mathrm{ARA}m}(\boldsymbol{\mu} \mid t_j) = \prod_{j=1}^{n} \Bigg[& \lambda_0 \left(t_j - (1-\theta) \sum_{p=0}^{min(m-1,j-2)} \theta^p t_{j-1-p} \right) \\ & \times e^{-\Lambda_0\left(t_j - (1-\theta) \sum_{p=0}^{min(m-1,j-2)} \theta^p t_{j-1-p} \right) + \Lambda_0\left(t_{j-1} - (1-\theta) \sum_{p=0}^{min(m-1,j-2)} \theta^p t_{j-1-p} \right)} \Bigg] \\ & \times e^{-\Lambda_0\left(t^* - (1-\theta) \sum_{p=0}^{min(m-1,n-1)} \theta^p t_{n-p} \right) + \Lambda_0\left(t_n - (1-\theta) \sum_{p=0}^{min(m-1,n-1)} \theta^p t_{n-p} \right)}, \end{aligned} \tag{2.14}$$

or more generally, (2.14) can be written as

$$L_{\mathrm{ARA}m}(\boldsymbol{\mu} \mid t_j) = \prod_{j=1}^{n} \left[\lambda_{\mathrm{ARA}m}\left(t_j\right) e^{-\left[\Lambda_{\mathrm{ARA}_m}\left(t_j\right)-\Lambda_{\mathrm{ARA}_m}\left(t_{j-1}\right)\right]}\right] e^{-\left[\Lambda_{\mathrm{ARA}_m}(t^*)-\Lambda_{\mathrm{ARA}_m}(t_n)\right]}. \quad (2.15)$$

From now on, to simplify these expressions, we will write $s(t_o) = \sum_{p=0}^{\min\{m-1,o-1\}} \theta^p t_{o-p}$, and the equation (2.14) can be written as

$$\begin{aligned} L_{\mathrm{ARA}m}(\boldsymbol{\mu} \mid t_j) = \prod_{j=1}^{n} & \left[\lambda_0\left(t_j-(1-\theta)s(t_{j-1})\right) e^{-\Lambda_0\left(t_j-(1-\theta)s(t_{j-1})\right)+\Lambda_0\left(t_{j-1}-(1-\theta)s(t_{j-1})\right)}\right] \\ & \times e^{-\Lambda_0(t^*-(1-\theta)s(t_n))+\Lambda_0(t_n-(1-\theta)s(t_n))}. \end{aligned}$$

If we consider the failure truncated case with n^* fixed number of failures to be observed, the likelihood function is also obtained just replacing t^* in time truncated case with t_n, getting

$$\begin{aligned} L_{\mathrm{ARA}m}(\boldsymbol{\mu} \mid t_j) &= \prod_{j=1}^{n} \lambda_{\mathrm{ARA}m}\left(t_j\right) e^{-\Lambda_{\mathrm{ARA}_m}\left(t_j\right)+\Lambda_{\mathrm{ARA}_m}\left(t_{j-1}\right)} \\ &= \left[\prod_{j=1}^{n} \lambda_0\left(t_j-(1-\theta)s(t_{j-1})\right) e^{-\Lambda_0\left(t_j-(1-\theta)s(t_{j-1})\right)+\Lambda_0\left(t_{j-1}-(1-\theta)s(t_{j-1})\right)}\right]. \end{aligned}$$

2.2.3.2 The ARI_m Model

The basic idea of the ARI class model is to consider that each repair reduces not only the virtual age, but also the intensity of failure, depending on the failure history of the process. In the ARI_m model, it is assumed that the repair reduces the intensity of the failure depending on the last m failures.

Thus, the failure intensity function of the ARI_m model, given the repair effect parameter θ and the history of the last m observed failures in the system, can be defined as

$$\lambda_{\mathrm{ARI}m}(t) = \lambda_0(t) - (1-\theta) \sum_{p=0}^{min(m-1,N(t)-1)} \theta^p \lambda_0(T_{N(t)-p}), \quad (2.16)$$

where $\lambda_0(t)$ is the initial failure intensity function of the process.

The cumulative intensity function for ARI_m class is given by

$$\begin{aligned} \Lambda_{\mathrm{ARI}m}(t) &= \int_0^t \lambda_{\mathrm{ARI}m}(u)du \\ &= \Lambda_{\mathrm{ARI}m}(T_{N(t)}) + \Lambda_0(t) - \Lambda_0(T_{N(t)}) - (t-T_{N(t)})(1-\theta)\underline{S}(T_{N(t)}), \end{aligned} \quad (2.17)$$

where $\underline{S}(T_o) = \sum_{p=0}^{\min\{m-1,o-1\}} \theta^p \lambda_0(T_{o-p})$ and $\Lambda(t)$ is the initial cumulative intensity function.

Analogous to the ARA class, in the ARI_m model we can consider the existence of two extreme cases, ARI_1 and ARI_∞. If $m = 1$, for the same reasons presented for the ARA_1 model, the failure intensity function for the ARI_1 model is given by

$$\lambda_{ARI_1}(t) = \lambda_0(t) - (1-\theta)\lambda_0(T_{N(t)}).$$

Chan and Shaw (1993) developed a model that assumes that each repair reduces the intensity of the failure by a proportional value to the intensity of the current failure, in a cumulative sense of intensity reduction since the first repair. Doyen and Gaudoin (2004) classified it as the ARI_∞ class, since the reduction in intensity after the occurrence of a failure takes into account all previous failures. In this case, the failure intensity function is given by

$$\lambda_{ARI_\infty}(t) = \lambda_0(t) - (1-\theta)\sum_{p=0}^{N(t)-1} \theta^p \lambda_0(T_{N(t)-p}).$$

In the ARI model class, between two consecutive failures, the failure intensity is vertically parallel to its initial intensity. It means that after failure, the wear-out speed is the same as before failure. This behavior can be observed in the graph of Figure 7, where the dashed line is the graph of the initial intensity function and the other curves are graphs of the intensity function between two consecutive failures. It is observed that these graphs are vertical displacements of the graph of the initial intensity function (dashed). In other words, the minimum point of each new curve starting at failure time t is $(t, \lambda_0(t))$, and it is offset vertically in $(1-\theta)\underline{S}(T_{N(t)})$ down of the dotted curve.

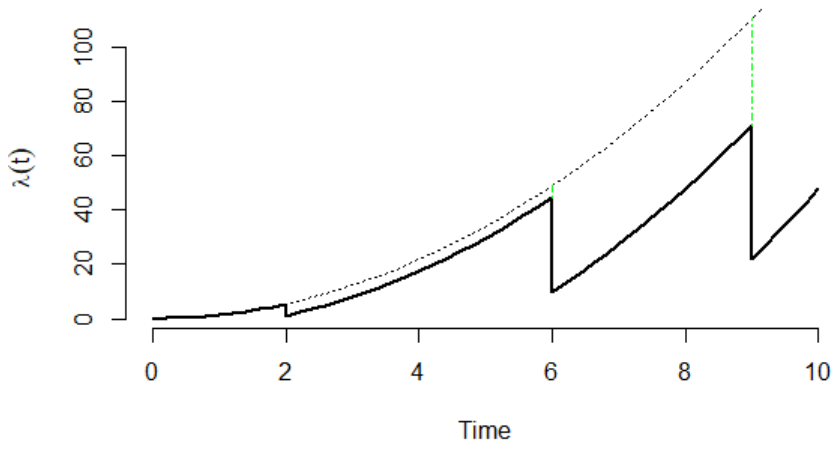

Figure 7 – Intensity function of an ARI_m model, with failures at times $t = 2$, 6 and 9.

Analogously to all the other cases, the intensity function λ_{ARI_m} can be a parametric function with vector parameter $\boldsymbol{\mu}$, so we can find the likelihood function to obtain the parameter estimates of this model. As in the ARA case, here the parameter θ is certainly in the vector parameter.

Let $T_1,\ldots,T_n$ be the failure times of a repairable system and assume an IR model with arithmetic reduction of intensity and a failure memory m (ARI$_m$ model). We have already concluded that the joint density function can be written in general by

$$f(t_1,\ldots,t_n) = f(t_1)f(t_2 \mid t_1)f(t_3 \mid t_2)\cdots f(t_n \mid t_{n-1}).$$

In a similar way to that discussed for the ARA$_m$ class in Section 2.2.3.2, if $t \in [t_{j-1},t_j)$ so $N(t) = j-1$ and $T_{N(t)} = t_{j-1}$. It follows that the conditional reliability function of t_j given the previous failure time t_{j-1} in the ARI$_m$ model is given by

$$\begin{aligned}
R(t_j \mid t_{j-1}) &= \mathbb{P}[T_j > t_j \mid t_{j-1}] = \mathbb{P}[N(t_j) - N(t_{j-1}) = 0] \\
&= \exp\left(-\int_{t_{j-1}}^{t_j} \lambda_{\text{ARI}m}(u)du\right) = \\
&= \exp\left(-\int_{t_{j-1}}^{t_j} \left[\lambda_0(u) - (1-\theta)\sum_{p=0}^{min(m-1,j-2)} \theta^p \lambda_0(t_{j-1-p})\right] du\right) \\
&= \exp\left(-\int_{t_{j-1}}^{t_j} \lambda_0(u)du + \int_{t_{j-1}}^{t_j} (1-\theta)\sum_{p=0}^{min(m-1,j-2)} \theta^p \lambda_0(t_{j-1-p})du\right) \\
&= e^{-\Lambda_0(t_j)+\Lambda_0(t_{j-1})+(t_j-t_{j-1})(1-\theta)\sum_{p=0}^{min(m-1,j-2)} \theta^p \lambda_0(t_{j-1-p})}
\end{aligned}$$

Thus, the conditional density function of t_j given t_{j-1} is given by

$$\begin{aligned}
f(t_j \mid t_{j-1}) &= \frac{d}{dt_j}[1 - R(t_j \mid t_{j-1})] = \\
&= \left[\lambda_0(t_j) + (1-\theta)\sum_{p=0}^{min(m-1,j-2)} \theta^p \lambda_0(t_{j-1-p})\right] \times R(t_j \mid t_{j-1}).
\end{aligned}$$

Considering a time truncated process at the time t^*, the number of failures n of the system is random and the probability that $N(t^*)$ is n given the observed failures is

$$\begin{aligned}
\mathbb{P}[N(t^*) = n \mid t_1,\ldots,t_n] &= \mathbb{P}[N(t^*) = n \mid t_n] = \mathbb{P}[N(t^*) - N(t_n) = 0] \\
&= e^{-\Lambda_0(t^*)+\Lambda_0(t_n)+(t^*-t_n)(1-\theta)\sum_{p=0}^{min(m-1,n-1)} \theta^p \lambda_0(t_{n-p})}.
\end{aligned}$$

We can write the likelihood function for the vector parameter $\boldsymbol{\mu}$ from ARI$_m$ model under

time truncated process as follows:

$$L_{\text{ARI}m}(\boldsymbol{\mu} \mid t_j) = \prod_{j=1}^{n} \left[\left(\lambda_0(t_j) + (1-\theta) \sum_{p=0}^{min(m-1,j-2)} \theta^p \lambda_0(t_{j-1-p}) \right) \right.$$
$$\left. \times e^{-\Lambda_0(t_j)+\Lambda_0(t_{j-1})+(t_j-t_{j-1})(1-\theta) \sum_{p=0}^{min(m-1,j-2)} \theta^p \lambda_0(t_{j-1-p})} \right] \tag{2.18}$$
$$\times e^{-\Lambda_0(t^*)+\Lambda_0(t_n)+(t^*-t_n)(1-\theta) \sum_{p=0}^{min(m-1,n-1)} \theta^p \lambda_0(t_{n-p})}.$$

Using the expressions (2.16) and (2.17), we can rewrite (2.18) more generally, reordering the terms and getting

$$L_{\text{ARI}m}(\boldsymbol{\mu} \mid t_j) = \prod_{j=1}^{n} \left[\lambda_{\text{ARI}m}(t_j) e^{-\left[\Lambda_{\text{ARI}m}(t_j)-\Lambda_{\text{ARI}m}(t_{j-1})\right]} \right] e^{-\left[\Lambda_{\text{ARI}m}(t^*)-\Lambda_{\text{ARI}m}(t_n)\right]}. \tag{2.19}$$

Once again, to simplify the expressions, we will write $\underline{s}(t_o) = \sum_{p=0}^{\min\{m-1,o-1\}} \theta^p \lambda_0(t_{o-p})$ from now on.The equation (2.18) can be written as

$$L_{\text{ARI}m}(\boldsymbol{\mu} \mid t_j) = \prod_{j=1}^{n} \left[\left(\lambda_0(t_j) + (1-\theta)\underline{s}(t_{j-1})\right) e^{-\Lambda_0(t_j)+\Lambda_0(t_{j-1})+(t_j-t_{j-1})(1-\theta)\underline{s}(t_{j-1})} \right]$$
$$\times e^{-\Lambda_0(t^*)+\Lambda_0(t_n)+(t^*-t_n)(1-\theta)\underline{s}(t_n)}.$$

Finally, if we consider a failure truncated process with n^* being the fixed number of failures to be observed, the likelihood and log-likelihood functions are also obtained, just replacing t^* with t_n, whence it follows that

$$L_{\text{ARI}m}(\boldsymbol{\mu} \mid t_j) = \prod_{j=1}^{n} \left[\lambda_{\text{ARI}m}(t_j) e^{-\Lambda_{\text{ARI}m}(t_j)+\Lambda_{\text{ARI}m}(t_{j-1})} \right]$$
$$= \prod_{j=1}^{n} \left[\left(\lambda_0(t_j) + (1-\theta)\underline{s}(t_{j-1})\right) e^{-\Lambda_0(t_j)+\Lambda_0(t_{j-1})+(t_j-t_{j-1})(1-\theta)\underline{s}(t_{j-1})} \right].$$

2.3 Frailty Models

In reliability studies, some assumptions about the observations or the absence of additional information can lead to analysis errors and distorted conclusions. For example, by assuming the failure times of individuals in the same group or cluster to be independent, or even by not observing significant covariates that affect the life behavior of these individuals or systems.

In the literature, models that consider the existence of this possible association between failure times or the existence of unquantified effects are called *frailty models* or models with *unobserved heterogeneity*. The idea of frailty models was introduced by Vaupel, Manton and Stallard (1979) as an extension of the traditional Cox model proposed by Cox (1972). In this work, the authors defined frailty (or fragility) as a multiplicative term that modifies the life expectancy function of individuals at the moment they are born. On the other hand, the authors also pointed out that there are several ways of thinking about the frailty in a study.

According to Wienke (2010), the basic idea of frailty (or unobserved heterogeneity) is an unobserved random proportionality factor that modifies the hazard function of an individual or related individuals. For univariate and independent lifetimes, the frailty can be used to adjust some unobserved risk factor in a hazard model. On the other hand, for multivariate and dependent lifetimes, the introduction of a common random effect (the frailty) is a way of modeling the dependence of event times. More details on these two approaches will be dealt with in Sections 2.3.1 and 2.3.2.

In studies involving repairable systems both approaches can be considered, with different interpretations. If the systems have the same default behavior and we assume the possibility of the existence of unobservable effects to which all systems are equally subject, we can think of univariate frailty models in which these effects directly affect the occurrence of each failure of these systems globally but that influence their failure behavior individually (JUNIOR, 2021). On the other hand, in a more classical perspective, the failure times of each system can be seen as observations of a cluster under the action of the same unobservable effect, taking place in a shared frailty model (WIENKE, 2010). Furthermore, in the latter case, considering that repairable systems naturally present recurrent failure events, it is reasonable to assume the absence of independence between these failure times and shared frailty models can be thought to verify and quantify this dependence.

In this work, we will consider the multiplicative frailty model, that is, we will introduce a random effect z that multiplies with the intensity function. This effect is a positive observation of a latent random variable Z and it can inflate, deflate or preserve the intensity function of the model on the cases that $z > 1$, $z < 1$ and $z = 1$, respectively.

The functions that characterize the frailty models are defined conditionally to the latent frailty variable Z. Considering the multiplicative frailty model and the absence of observed covariates, the failure intensity function of the frailty model is given by

$$\lambda(t \mid z) = z\underline{\lambda}(t), \tag{2.20}$$

where z is the frailty term and $\underline{\lambda}$ is the baseline hazard function.

Since the cumulative intensity function is given by (2.2), the cumulative failure intensity

function for the frailty model is given by

$$\Lambda(t \mid z) = \int_0^t \lambda(u \mid z)du = \int_0^t z\underline{\lambda}(u)du = z\int_0^t \underline{\lambda}(u)du = z\underline{\Lambda}(t), \tag{2.21}$$

where $\underline{\Lambda}(t)$ is the baseline cumulative failure intensity function related to the baseline failure intensity function $\underline{\lambda}(t)$.

Now, using the cumulative intensity function given in (2.21), we can obtain the reliability function for the frailty model

$$R(t \mid z) = e^{-\Lambda(t|z)} = e^{-z\underline{\Lambda}(t)} = [\underline{R}(t)]^z, \tag{2.22}$$

where $\underline{R}(t)$ is the baseline reliability function related to the baseline failure intensity $\underline{\lambda}$ of the model.

The random frailty effect z can be considered as an realization of a known probability distribution. This approach is found in several works in the literature, like Lancaster (1979), Hougaard (1984) and Tomazella (2003), among others, where the idea is to choose a positive, continuous and time-independent distribution that models the random effect of frailty. Some candidates with these characteristics present in the literature are the Gamma, log-normal, inverse Gaussian and Weibull distributions. In addition, frailty models may have identifiability problems, as shown in Elbers and Ridder (1982). In this work, the authors determine some necessary conditions so that the random effect of frailty is uniquely determined, where we highlight the condition that $\mathbb{E}[Z]$ must be equal to 1.

2.3.1 Univariate Frailty Models

Although traditionally in the literature repairable systems are analyzed by shared frailty models, there are recent works that use the univariate approach in this type of problem (JUNIOR, 2021; D'ANDREA *et al.*, 2019). In this case, the interpretation is that the frailty effect is not constant over time for a system, that is, at different times the probability of system failure can be impacted by different values of the unobservable effect of frailty. This makes sense when covariates are not observed and the frailty term has the role of identifying the existence of factors that act on the reliability of the system. In the context of perfect and imperfect repairs, this approach makes even more sense, since due to the very structure of models that assume this type of repair, the system's failure intensity function changes after each failure.

Let $t_1, \ldots, t_n$ be the observed failure times of a system and $z_1, \ldots, z_n$ the respective frailty terms associated with each failure time. The intensity function conditional on the system frailty term is $\lambda(t_j \mid z_j) = z_j\underline{\lambda}(t_j)$ and the z_j terms are i.i.d. observations of a random variable Z, where $j = 1, \cdots, n$. The likelihood function of the univariate frailty model for the failure times of this system is given by (here, just by simplicity, we will consider the MR model whose likelihood

function is defined on (2.8)):

$$L(\boldsymbol{\mu} \mid t_j, z_j) = \left(\prod_{j=1}^{n} \lambda(t_j \mid z_j) \right) e^{-\Lambda(t_n|z_n)} = \left(\prod_{j=1}^{n} z_j \underline{\lambda}(t_j) \right) e^{-z_n \underline{\Lambda}(t_n)}. \tag{2.23}$$

According to Wienke (2010), the random effect on frailty must be integrated out in (2.23) to get a likelihood function not depending on unobserved quantities. This same author shows that, for the univariate frailty model, this integration does not need to be done in the likelihood function. In this case, the construction of likelihood takes place from the intensity and cumulative intensity functions not conditional on the frailty term, which in turn are obtained as marginals of their respective functions conditional on the frailty term.

From the conditional intensity, cumulative intensity and reliability functions previous listed, our goal is to obtain these respective functions not conditioned to the frailty term z. The first of them is the reliability function not conditioned to the frailty term, obtained simply by integrating the expression (2.22) with respect to the term z, as follows:

$$R_f(t) = \int_0^\infty R(t \mid z) f(z) dz = \int_0^\infty e^{-z\underline{\Lambda}(t)} f(z) dz. \tag{2.24}$$

As pointed out by Wienke (2010), this reliability can be easily expressed using the Laplace transform, since the Laplace transform $Q(s)$ is given by

$$Q(s) = \int_0^\infty e^{-sx} f_X(x) dx. \tag{2.25}$$

Therefore, combining the equations (2.24) and (2.25), we can replace $s = \underline{\Lambda}(t)$ and $x = z$ to obtain the following expression for the reliability function not conditional on the frailty term z:

$$R_f(t) = Q(\underline{\Lambda}(t)).$$

As direct consequence, the cumulative intensity function unconditional on the frailty term is given by

$$\Lambda_f(t) = -\log(R(t)) = -\log Q(\underline{\Lambda}(t)), \tag{2.26}$$

and the failure intensity function unconditional on the frailty term is obtained by deriving the cumulative intensity function given by (2.26) in relation to time t, as follows:

$$\lambda_f(t) = \frac{d}{dt}\Lambda(t) = -\underline{\lambda}(t) \frac{Q'(\underline{\Lambda}(t))}{Q(\underline{\Lambda}(t))}. \tag{2.27}$$

With the non-conditional intensity and cumulative intensity functions obtained respectively in (2.27) and (2.26), the unconditional likelihood function to the frailty term is given by

simply replacing these two functions in (2.8). If we consider k independent systems with the same baseline intensity function being observed and let $t_{i,j}$ be the j-th failure time of the i-th system ($i = 1,\ldots,k$ and $j = 1,\ldots,n_i$), all the ideas discussed can be extended to construct the likelihood function for all these systems, as follows:

$$L_f(\boldsymbol{\mu} \mid t_{i,j}) = \prod_{i=1}^{k} \left(\prod_{j=1}^{n_i} \lambda_f(t_{i,j}) \right) e^{-\Lambda_f(t_{i,n_i})}. \tag{2.28}$$

Note that in the parametric context, in addition to the parameters of the baseline intensity function $\underline{\lambda}(t)$, now the likelihood function will also inherit the parameters of the distribution Z associated with the frailty term.

2.3.2 Shared Frailty Models

The shared frailty model is, in particular, suitable for repairable systems failure times, once here we can consider each system as a "group" and the recurrent failure times of a system as "individuals of the same group". In this context, the interpretation is that there are unobservable effects that act particularly on a system and are shared by failure times (seen here as individuals of a group). In addition, when considering multiple systems, shared frailty allows us to compare the level to which unobservable effects affect the systems, since it is possible to estimate which of these is more or less susceptible to failures resulting from these effects (WIENKE, 2010).

Consider k independent systems and let $t_{i,j}$ be the j-th observed failure times of the i-th system, with $i = 1,\ldots,k$ and $j = 1,\ldots,n_i$. Now, there is a unique frailty term z_i associated with each system i and shared by all this system's failure times. The intensity function of the system i conditional on its frailty term is $\lambda(t_{i,j} \mid z_i) = z_i \underline{\lambda}(t_{i,j})$, where z_i are i.i.d. observations of a random variable Z. The likelihood function of the shared frailty model for the systems and their failure times is given by (here again, by simplicity, we will also consider the MR model whose likelihood function is defined on (2.8) and we take into account that the systems are independent):

$$L(\boldsymbol{\mu} \mid t_{i,j}, z_i) = \prod_{i=1}^{k} \left(\prod_{j=1}^{n_i} \lambda(t_{i,j} \mid z_i) \right) e^{-\Lambda(t_{i,n_i}|z_i)} = \prod_{i=1}^{k} \left(\prod_{j=1}^{n_i} z_i \underline{\lambda}(t_{i,j}) \right) e^{-z_i \underline{\Lambda}(t_{i,n_i})}. \tag{2.29}$$

Again, to estimate the model parameters, it is necessary to obtain the non-conditional likelihood function to the z_i frailty terms. As all these terms are observations of the same distribution, according to Wienke (2010), it is enough to integrate the function (2.29) in relation to the frailty term z_i and obtain the marginal likelihood function:

$$\begin{aligned} L(\boldsymbol{\mu} \mid t_{i,j}) &= \prod_{i=1}^{k} \int_0^{\infty} \left(\prod_{j=1}^{n_i} z_i \underline{\lambda}(t_{i,j}) \right) e^{-z_i \underline{\Lambda}(t_{i,n_i})} f_{Z_i}(z_i) dz_i \\ &= \prod_{i=1}^{k} \left(\prod_{j=1}^{n_i} \underline{\lambda}(t_{i,j}) \right) \int_0^{\infty} z_i^{n_i} e^{-z_i \underline{\Lambda}(t_{i,n_i})} f_{Z_i}(z_i) dz_i \end{aligned} \tag{2.30}$$

It is clear that the choice of distribution for the frailty variable Z is essential for obtaining a closed and tractable form of the function (2.30). In this sense, again the Gamma distribution is a natural candidate. As we will see in the Section 2.3.3, the integral in equation (2.30) is easily solved when $Z \sim \text{Gamma}\left(\frac{1}{\alpha}, \frac{1}{\alpha}\right)$. However, other distributions could be considered, always paying attention to the necessary algebraic treatment in order not to make these models even more complex.

2.3.3 The Gamma Frailty Models

As stated before and pointed out by several authors in the reliability literature, such as Wienke (2010) and Tomazella (2003), choosing the distribution for the frailty term is not simple and needs to be done with caution. On the other hand, it is a latent variable, so it is not possible to deduce a distribution based on observations. In this sense, the guidelines for choosing this distribution are based on more general characteristics such as positive domain and easy algebraic treatment.

The Gamma distribution is particularly an attractive choice as the frailty term distribution as mentioned by Wienke (2010), especially for its algebraic convenience since it has closed-form expressions of unconditional intensity and reliability functions and closed Laplace Transform form. According to the author, from a computational and analytical point of view, this distribution fits reasonably well lifetime models. In Vaupel, Manton and Stallard (1979)'s pioneering work, for example, the Gamma distribution was chosen to model the frailty introduced by the authors.

Let Z be the random variable of the frailty effect and assume that it has a $\text{Gamma}\left(\frac{1}{\alpha}, \frac{1}{\alpha}\right)$ distribution, so that $\mathbb{E}[Z] = 1$, satisfying the identifiability condition stated above. The probability density function of Z is given by

$$f(z) = \frac{\left(\frac{1}{\alpha}\right)^{\frac{1}{\alpha}}}{\Gamma\left(\frac{1}{\alpha}\right)} z^{\frac{1}{\alpha}-1} e^{-\frac{z}{\alpha}},$$

and, in this case, $Var[Z] = \alpha$.

By assuming this Gamma distribution for the frailty variable Z, some developments are directly observed in the univariate and the shared models discussed in Sections 2.3.1 and 2.3.2. In Sections 2.3.3.1 and 2.3.3.2 that follow, we will present these results separately for each model since they will be the basis for the models that we propose in the next chapters of this work.

2.3.3.1 Univariate Gamma Frailty Model

The likelihood function for the univariate frailty model (2.28) was built with the intensity and cumulative intensity functions not conditional on the frailty term Z, which, in turn, were obtained from the Laplace Transform by the expressions (2.27) and (2.26), respectively.

Thus, assuming $Z \sim \text{Gamma}\left(\frac{1}{\alpha}, \frac{1}{\alpha}\right)$, we will initially obtain the form of its Laplace Transform by the equation (2.25), as follows:

$$Q(s) = \int_0^\infty e^{-sz} \frac{\left(\frac{1}{\alpha}\right)^{\frac{1}{\alpha}}}{\Gamma\left(\frac{1}{\alpha}\right)} z^{\frac{1}{\alpha}-1} e^{-\frac{z}{\alpha}} dz = \frac{\left(\frac{1}{\alpha}\right)^{\frac{1}{\alpha}}}{\left(\frac{1}{\alpha}+s\right)^{\frac{1}{\alpha}}} \int_0^\infty \frac{\left(\frac{1}{\alpha}+s\right)^{\frac{1}{\alpha}}}{\Gamma\left(\frac{1}{\alpha}\right)} z^{\frac{1}{\alpha}-1} e^{-\left(\frac{1}{\alpha}+s\right)z} dz$$
$$= \frac{\left(\frac{1}{\alpha}\right)^{\frac{1}{\alpha}}}{\left(\frac{1}{\alpha}+s\right)^{\frac{1}{\alpha}}} = (1+\alpha s)^{-\frac{1}{\alpha}}.$$

By the equation (2.26), cumulative intensity function unconditional on the frailty term is given by

$$\Lambda_f(t) = -\log\left(R_f(t)\right) = -\log\left(\left[1+\alpha\underline{\Lambda}(t)\right]^{-\frac{1}{\alpha}}\right), \tag{2.31}$$

and the failure intensity function unconditional on the frailty term by equation (2.27) is given by

$$\lambda_f(t) = -\underline{\lambda}(t)\frac{Q'(\underline{\Lambda}(t))}{Q(\underline{\Lambda}(t))} = \frac{\underline{\lambda}(t)}{\left[1+\alpha\underline{\Lambda}(t)\right]}, \tag{2.32}$$

where $\underline{\lambda}(t)$ and $\underline{\Lambda}(t)$ are the baselines intensity and cumulative intensity functions.

Finally, the likelihood function for k independent systems in (2.28), unconditional to the frailty terms $Z_{i,j} \sim \text{Gamma}\left(\frac{1}{\alpha}, \frac{1}{\alpha}\right)$ distributed can be rewritten as

$$L_f(\boldsymbol{\mu} \mid t_{i,j}) = \prod_{i=1}^{k}\left(\prod_{j=1}^{n_i}\lambda_f(t_{i,j})\right)e^{-\Lambda_f(t_{i,n_i})} = \prod_{i=i}^{k}\left(\prod_{j=1}^{n_i}\frac{\underline{\lambda}(t_{i,j})}{\left[1+\alpha\underline{\Lambda}(t_{i,j})\right]}\right)\left[1+\alpha\underline{\Lambda}(t_i^*)\right]^{-\frac{1}{\alpha}}.$$

Note that $\alpha \in \boldsymbol{\mu}$, that is, α is a new parameter to be estimated by the model. Remember that $\alpha = Var(Z)$, that is, α quantifies the variability of frailty effects related to system failure times. In the cases of univariate frailty, the term α indicates the existence of unobserved effects that can directly affect the intensity function at each failure time, which can cause the frequency of failures to be higher or lower in different time intervals.

Adapting the result presented in Wienke (2010) for the case where k systems are observed and $t_{i,j}$ are their failure times ($i = 1,\ldots,k$ and $j = 1,\ldots,n_i$), if $\hat{\alpha}$ is the estimate for the parameter α, the individual frailty $\hat{Z}_{i,j}$ related to each failure time $t_{i,j}$ is computed by the expression:

$$\hat{Z}_{i,j} = \frac{1/\hat{\alpha} + \delta_{i,j}}{1/\hat{\alpha} + \underline{\Lambda}(t_{i,j};\hat{\boldsymbol{\mu}})},$$

where $\delta_{i,j} = \mathbb{I}(i,j)$ is the indicator function of index i, j, $\underline{\Lambda}(T)$ is the baseline cumulative intensity function of the model and $\hat{\boldsymbol{\mu}}$ is the vector parameter estimates of this model.

2.3.3.2 Shared Gamma Frailty Model

Assuming that the frailty variables Z_i have a $\text{Gamma}\left(\frac{1}{\alpha}, \frac{1}{\alpha}\right)$ distribution ($i = 1,\ldots,k$), we can proceed with obtaining the likelihood function non-conditional to these Z_i given in (2.30).

$$
\begin{aligned}
L_f(\boldsymbol{\mu} \mid t_{i,j}) &= \prod_{i=1}^{k}\left(\prod_{j=1}^{n_i}\underline{\lambda}(t_{i,j})\right)\int_0^{\infty} z_i^{n_i} e^{-z_i\underline{\Lambda}(t_{i,n_i})} f_{Z_i}(z_i)dz_i \\
&= \prod_{i=1}^{k}\left(\prod_{j=1}^{n_i}\underline{\lambda}(t_{i,j})\right)\frac{\left(\frac{1}{\alpha}\right)^{\frac{1}{\alpha}}}{\Gamma\left(\frac{1}{\alpha}\right)}\int_0^{\infty} z_i^{n_i+\frac{1}{\alpha}-1} e^{-z_i\left[\frac{1}{\alpha}+\underline{\Lambda}(t_{i,n_i})\right]}dz_i \\
&= \prod_{i=1}^{k}\left(\prod_{j=1}^{n_i}\underline{\lambda}(t_{i,j})\right)\frac{\left(\frac{1}{\alpha}\right)^{\frac{1}{\alpha}}}{\Gamma\left(\frac{1}{\alpha}\right)}\frac{\Gamma\left(n_i+\frac{1}{\alpha}\right)}{\left(\frac{1}{\alpha}+\underline{\Lambda}(t_{i,j})\right)^{n_i+\frac{1}{\alpha}}} \\
&= \prod_{i=1}^{k}\frac{\alpha^{n_i}\Gamma\left(n_i+\frac{1}{\alpha}\right)\prod_{j=1}^{n_i}\underline{\lambda}(t_{i,j})}{\Gamma\left(\frac{1}{\alpha}\right)\left(1+\alpha\underline{\Lambda}(t_{i,j})\right)^{n_i+\frac{1}{\alpha}}},
\end{aligned}
$$

where $\underline{\lambda}(t)$ and $\underline{\Lambda}(t)$ are the baselines intensity and cumulative intensity functions.

Once again, $\alpha = Var[Z]$ is a parameter to be estimated by the model. In cases of shared frailty, the term α indicates the variability of unobservable effects among the failure times in the a system (in the sense of individuals in the same group). Thus, higher values of α indicate a strong relationship between the failure times of a system, but greater heterogeneity between different systems. In this sense, the parameter α can identify whether one system is more susceptible to failure than another.

Once again adapting the result presented in Wienke (2010) to the case where k systems are observed, $t_{i,j}$ are their failure times ($i = 1,\ldots,k$, and $j = 1,\ldots,n_i$), and Z_i are their associated frailty variables with Gamma$\left(\frac{1}{\alpha},\frac{1}{\alpha}\right)$ distribution, the shared frailty Z_i of the i-th system can be calculated by the expression:

$$
\hat{Z}_i = \frac{1/\hat{\alpha} + \sum_{j=1}^{n_i}\delta_{i,j}}{1/\hat{\alpha} + \sum_{j=1}^{n_i}\underline{\Lambda}(t_{i,j};\hat{\boldsymbol{\mu}})}, \tag{2.33}
$$

where n_i is the number of observed failures in the i-th system.

2.4 Competing Risks

Examining the process of system failure also involves delving into the underlying reasons behind these failures. It is reasonable to expect that complex systems are subject to failure due to different causes. Consequently, comprehending the root cause behind a failure can yield pertinent insights for future modeling endeavors. In the statistical literature, models that address the causes of failure of an individual or system are referred to as Competitive Risk Models.

According to Crowder (2001), the study of competing risks traces back to Daniel Bernoulli's pioneering work (BERNOULLI, 1760), where he dissected the risk of smallpox-related mortality from other concurrent risks. Subsequently, a number of competing risk works

emerged in various areas. Pintilie (2006) presents a brief history of the inception of competitive risk theory, contextualizing its first applications. However, according to Crowder (2001), it is currently in the field of reliability that the great applicability of competitive risks is found.

According to Pintilie (2006), there are two distinct methodologies prevalent in the literature for delineating competitive risks. The first approach involves bivariate random variables where each failure time will be associated with information on the cause of failure that caused it. Conversely, the second approach delves into latent failure times, where failure times relating to all causes are considered but only the first of these failures is observed. In the reliability literature, it is possible to find works under both approaches, such as the works of Somboonsavatdee and Sen (2015b) that use the first approach and the work of Lindqvist (2006) that uses the second. However, Pintilie (2006) points out that the approach of latent failures can generate identifiability issues in the models. Just as we avoided frailty-related identifiability problems in Section 2.3, here, we will define the use of competing risk models as bivariate random variables for the development of this work. In this context we assume that the competing risks are independent. Below we present more details about this approach.

Let us consider a repairable system susceptible to q distinct failure modes, or, in other words, the system has q competing risks that act to drive the system to failure. Let t be an observed failure time of the system, we define the indicator of the mode that caused this failure by $\delta(t) = r$, with $r = 1, \ldots, q$. Thus, let $t_1, \ldots, t_n$ be a sequence of n system failure times, then we can define the bivariate data $(t_1, \delta(t_1)), \ldots, (t_n, \delta(t_n))$ that represents the times and causes associated with each system failure. To simplify future usage, each element of this sequence will be written by (t_i, δ_i), where t_i represents the i-th time of failure ($i = 1, \ldots, n$) and $\delta_i = \delta(t_i) = r$ represents the cause of the i-th failure, for $r = 1, \ldots, q$.

Figure 8 below illustrates this failure process associated with competing risks in an example where n failures are observed up to time t^* and there are only two failure causes ($q = 2$ or $r = 1, 2$). This figure indicates, for example, that the first and second failures were caused by cause 2 while the third failure was caused by cause 1. In the terms previously defined, we could write the data $((t_1, 2), (t_2, 2), (t_3, 1), \ldots, (t_n, 1))$.

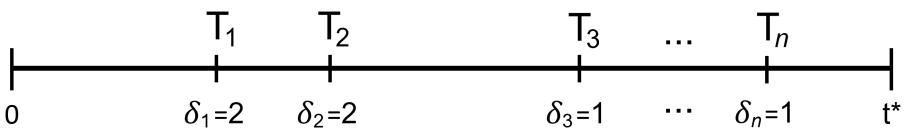

Figure 8 – Observable quantities from failure history of a repairable competing risks system with two recurrent causes of failure

Note that we can filter the data (t_i, δ_i) from a failure cause-specific r and this procedure can generate up to q failure processes, each one referring to a failure cause r, with $r = 1, \ldots, q$. Let $\{N_r(t),\ t \geq 0\}$ be the counting process relative to the cause-specific r, then by Definition 6,

the complete r cause-specific intensity function is given by

$$\lambda_r(t;\delta) = \lim_{\Delta t \to 0} \frac{\mathbb{P}[\delta(t) = r, N(t, t+\Delta t] \geq 1 \mid \mathscr{H}_{t,r}]}{\Delta t},$$

where $\mathscr{H}_{t,r}$ is the history of the process of the cause-specific r at time t.

Assume that $\{N_r(t),\ t \geq 0\}$ is a NHPP and let $N_r(t)$ be the number of observed failures related to the r-th cause up to time t, then the total number of failures observed in the system up to time t is then given by $N(t) = \sum_{r=1}^{q} N_r(t)$. As a direct consequence the global counting process $\{N(t),\ t \geq 0\}$ relative to all system failures can be considered as a superposition of NHPP whose intensity function is given by:

$$\lambda(t) = \sum_{r=1}^{q} \lim_{\Delta t \to 0} \frac{\mathbb{P}[\delta(t) = r, N(t, t+\Delta t] \geq 1 \mid \mathscr{H}_{t,r}]}{\Delta t} = \sum_{r=1}^{q} \lambda_r(t;\delta).$$

Finally, the r cause-specific and the global system cumulative intensity functions are respectively given by

$$\Lambda_r(t;\delta) = \int_0^t \lambda_r(u;\delta)du \quad \text{and} \quad \Lambda(t) = \sum_{r=1}^{q} \Lambda_r(t;\delta). \tag{2.34}$$

Let $(t_1, \delta_1), \ldots, (t_n, \delta_n)$ be the observed data of system failure times and its respective causes. The likelihood function of the competing risks model is given by (here again, just by simplicity, we will consider the time truncated MR truncated whose likelihood function is defined on (2.7)):

$$L(\boldsymbol{\mu} \mid t_j, \delta_j) = \left(\prod_{j=1}^{n} \lambda(t_j \delta_j) \right) e^{-\Lambda(t^*)}. \tag{2.35}$$

Note that t^* is the truncation time and it is not necessarily a failure time, so it is not related to any specific failure cause and is defined by its equation in (2.34).

Remember that the counting process $\{N(t)\}$ related to system failures can be partitioned into q processes $\{N_r(t)\}$ related to each cause of failure, with $r = 1, \ldots, q$. Let n_r be the total number of failures caused by cause r, then the contribution of cause-specific r is given by

$$L_r(\boldsymbol{\mu} \mid t_j, \delta_j = r) = \left(\prod_{j=1}^{n_r} \lambda_r(t_j, r) \right) e^{-\Lambda_r(t^*, r)}$$

or equivalently by

$$L_r(\boldsymbol{\mu} \mid t_j, \delta_j = r) = \left(\prod_{j=1}^{n} \left[\lambda_r(t_j, \delta_j)\right]^{\mathbb{I}(\delta_j = r)} \right) e^{-\Lambda_r(t^*, r)},$$

where $\mathbb{I}$ is the indicator function, for $r = 1, \ldots, q$.

Since the failure causes are independent by assumption, then the expression (2.35) can be re-expressed by $L = \prod_{r=1}^{q} L_r$ and the contribution of each failure time observed in the system will only be in relation to the cause of its occurrence (CROWDER, 2001). Therefore, the equation (2.35) can be rewritten as

$$L(\boldsymbol{\mu} \mid t_j, \delta_j) = \left(\prod_{r=1}^{q} \prod_{j=1}^{n_r} \lambda(t_j, r) \right) e^{-\sum_{r=1}^{q} \Lambda_r(t^*, r)}, \tag{2.36}$$

or equivalently by

$$L(\boldsymbol{\mu} \mid t_j, \delta_j) = \left(\prod_{r=1}^{q} \prod_{j=1}^{n} \left[\lambda(t_j, \delta_j) \right]^{\mathbb{I}(\delta_j = r)} \right) e^{-\sum_{r=1}^{q} \Lambda_r(t^*, r)}, \tag{2.37}$$

where t_i^* is the truncation time for the i-th system.

If k independent systems are observed, all under the same q causes of failure, the equation (2.36) can be extended as

$$L(\boldsymbol{\mu} \mid t_{i,j}, \delta_{i,j}) = \prod_{i=1}^{k} \left(\prod_{r=1}^{q} \prod_{j=1}^{n_{i,r}} \lambda(t_{i,j}, r) \right) e^{-\sum_{r=1}^{q} \Lambda_r(t_i^*, r)},$$

where $n_{i,r}$ is the total number of failures of cause r in the i-th system, for $i = 1, \ldots, k$, and $r = 1, \ldots, q$, and the equation (2.37) can be extended as

$$L(\boldsymbol{\mu} \mid t_{i,j}, \delta_{i,j}) = \prod_{i=1}^{k} \left(\prod_{r=1}^{q} \prod_{j=1}^{n_i} \left[\lambda(t_{i,j}, \delta_{i,j}) \right]^{\mathbb{I}(\delta_{i,j} = r)} \right) e^{-\sum_{r=1}^{q} \Lambda_r(t_i^*, r)},$$

where $t_{i,j}$ is the j-th failure time of the i-th system, for $i = 1, \ldots, k$ and $j = 1, \ldots, n_i$.

2.5 Concluding Remarks of the Chapter

In this chapter, we presented a bibliographic review necessary for the further development of the work, containing the main definitions and basic references that will be used.

Initially, in Section 2.1, we presented some basic concepts about Counting Process, including Non-Homogeneous Poisson Processes, from which we highlighted the Power Law Process as an important parametric particular case.

In Section 2.2 we presented the general ideas about repairable systems. Each type of repair was presented in detail, from the most basic conceptions to the development of inferential processes to obtain the parameter estimators for each model. The intensity and cumulative intensity functions for each type of repair were presented, as well as the joint probability density functions of the failure times and their respective reliability functions. Finally, the general form of the likelihood function was obtained for each type of repair, in order to obtain the MLEs for each model.

In Section 2.3 we presented the idea of frailty or unobserved heterogeneity in the context of repairable systems. We present general definitions for multiplicatively induced frailty in a risk model and discuss the two possibilities of representing the influence of unobservable effects on the systems failure time: univariate where the unobservable effects act globally on the systems but with particular influence at each failure time, or shared where the effects act particularly on each system and are shared across their failure times. In particular, we highlighted the parametric frailty considering that the unobserved heterogeneity of the repairable system can be modeled by a Gamma distribution. We present the basic likelihood functions for repairable systems considering Gamma frailty in each of the two approaches (univariate and shared), with the intention of extending them in our models proposed in the next chapters.

Finally, in Section 2.4 we presented the basic ideas of competitive risk models, where a single system can fail from more than one possible cause. We assume that each risk defines a function of related intensity and the sum of all of them defines the total failure intensity of a system. With these assumptions, we build the basic likelihood functions of these models, which will also be extended later.

CHAPTER

3

UNOBSERVED HETEROGENEITY FOR MULTIPLE REPAIRABLE SYSTEMS UNDER PERFECT REPAIR

As stated in Section 2.3, the failure times of a system can be impacted by unquantified effects, the so-called frailty effects. The failures of individuals in the same group or the recurrent failures of the same repairable system can be impacted to different extents by these effects, which may suggest the existence of an unobserved heterogeneity in the individuals or in the system's failure times. This information is latent and, in general, cannot be measured by covariates in a model or quantified in any way.

If we consider, for example, a set of several repairable systems produced by the same manufacturer under the same conditions and materials, we expect them to be hypothetically identical, in the sense of having similar failure histories. However, this does not always occur in practice, which suggests the existence of unobserved heterogeneity acting on the failure times of the observed systems. In this sense, we can try to extend the ideas presented in Section 2.3.1 to multiple repairable systems, assuming a frailty model not only between the failure times of each system, but between the failure times of all systems analyzed globally.

In the literature, we find some works that developed analysis for frailty models for multiple repairable systems, such as D'Andrea *et al.* (2019) and Asfaw and Lindqvist (2015) that consider a parametric Gamma distribution for the frailty model, and Slimacek and Lindqvist (2016) that consider a model with non-parametric frailty. All these works consider a minimal repair modeled by a NHPP process (in particular, a PLP process) to analyze the behavior of failure times and the existence of unobserved heterogeneity.

Our proposal in this chapter is to present a model capable of identifying frailty effects in multiple repairable systems submitted to perfect repair after each failure. The assumption we make is that systems are independent and their frailties related to their failure times are

parametric and identically distributed with Gamma$(\frac{1}{\alpha}, \frac{1}{\alpha})$ distribution. Furthermore, we consider that the initial intensity function follows a PLP.Our objective is, therefore, to perform classical inference through the likelihood method to obtain the Maximum Likelihood Estimators (MLE) for the parameters of the PLP model and the Gamma frailty distribution, and consequently, verify the existence of unobserved heterogeneity between the systems failure times and analyze the behavior of these failure times and the systems reliability after a new failure.

First of all, in Section 3.1, we review a literature work to analyze the unobserved heterogeneity of multiple repairable systems under MR modeled by a PLP. In Section 3.2, we present the proposed PR model which the initial failure intensity function follows a PLP process and that considers the possibility of unobserved univariate heterogeneity for multiple repairable systems. In Section 3.3, we carry out an extensive simulation study for the PR model with frailty to verify the suitability of the model. Finally, in Section 3.4, we present a real data set to illustrate the proposed methodology and calculate the model parameter estimates and the reliability for each system.

3.1 Unobserved Heterogeneity in MR Model

In this section, we will present a discussion about unobserved heterogeneity in multiple reparable systems under MR modeled by a PLP, as discussed by D'Andrea *et al.* (2019). In that work, the authors considered a parametric model to characterize the random effect of frailty and realized inferential procedures for estimation of the model parameters. This work will support us to future developments about PR considering unobserved heterogeneity for multiple repairable systems failure times.

First of all, let us recall what was discussed in Section 2.2 about the observation period of a repairable system. The observation can be time truncated by a time t^* or failure truncated by a number n^* of failures, but, on inferential procedures, the failure truncated is a particular case of a time truncated case when $t^* = t_{n^*}$. For this reason, we will adopt the time truncated observation for all our procedures as this is the most general case.

Suppose that k independent repairable systems are under observation, with $k = 1, 2, \ldots$ and let $0 < t_{i,1} < t_{i,2} < \cdots < t_{i,n_i}$ be the observed failure times of the i-th system, where n_i is the number of observed failures of the i-th system and $t_{i,j}$ represents the time of the j-th failure in the i-th system, with $i = 1, \ldots, k$ and $j = 1, \ldots, n_i$.

Since the study is time truncated, each system will be observed up to a predetermined fixed time t_i^*, $i = 1, \ldots, n_i$, which means that the truncation times for each system are not necessarily the same. Then, for each $i = 1, \ldots, k$, the observed failure times follow the relation $0 < t_{i,1} < \cdots < t_{i,n_i} < t_i^*$ and the number n_i of system failures is random. We will denote by N the total number of failures observed in k systems, that is, $N = \sum_{i=1}^{k} n_i$.

Considering that the systems undergo a MR process after the occurrence of each failure and that the time to carry out the repair is negligible, we are interested in verifying the existence of unobserved heterogeneity between the systems failure times. Thus, for each system the intensity function given in (2.20) can be written as

$$\lambda(t \mid z) = z\underline{\lambda}(t), \tag{3.1}$$

with $\underline{\lambda}(t)$ being the baseline intensity function of the MR model common to all systems and z being the observation of the frailty random variable Z.

Following the discussion in Section 2.3, we will assume that Z are independent and has a Gamma$\left(\frac{1}{\alpha}, \frac{1}{\alpha}\right)$ distribution, for all times of all systems. Thus, the failure intensity function not conditional on the systems' frailty term is given by

$$\lambda_f(t) = \frac{\underline{\lambda}(t)}{[1+\alpha\underline{\Lambda}(t)]}. \tag{3.2}$$

Now, remember that we consider a MR model under a PLP process. From the MR model, by the equation (2.6), the baseline intensity function $\underline{\lambda}(t) = \lambda_{\text{MR}}(t)$ and, because this model follows a PLP process, this intensity function can be directly defined by the equation (2.3) and the cumulative intensity function $\underline{\Lambda}(t)$ is defined by the equation (2.4). So we can rewrite (3.2) as the intensity function from MR model with frailty under PLP process:

$$\lambda_f(t) = \frac{\frac{\beta}{\eta}\left(\frac{t}{\eta}\right)^{\beta-1}}{\left[1+\alpha\left(\frac{t}{\eta}\right)^{\beta}\right]}, \tag{3.3}$$

and consequently, from the equation (2.26), obtain the cumulative intensity function:

$$\Lambda_f(t) = -\log\left(\left[1+\alpha\left(\frac{t}{\eta}\right)^{\beta}\right]^{-\frac{1}{\alpha}}\right), \tag{3.4}$$

and note that these functions are the same for all systems, since they are modeled by the same PLP model and their frailty variables are identically distributed.

Now that the intensity and cumulative intensity functions are defined for all systems, we are able to proceed with the inference to obtain estimates for the model parameters. Using the maximum likelihood method, we want to obtain the MLEs $\hat{\beta}$, $\hat{\eta}$ and $\hat{\alpha}$ of the corresponding parameters.

All the support procedures for inference on a MR model were presented in Section 2.2.1, where we obtained the likelihood function (2.7) for a system under minimal repair in a study truncated by a time t^*. So now, we can rewrite this expression for the i-th system, given by

$$L_{\text{MR}i}(\boldsymbol{\mu} \mid t_j) = \left(\prod_{j=1}^{n}\lambda_i(t_j)\right)e^{-\Lambda_i(t_i^*)},$$

where $\boldsymbol{\mu}$ represents the vector of parameters to be estimated and t_j the observed failure times. As we are now observing k independent repairable systems, the extension of this likelihood function happens naturally, just by adding a product relative to the systems, as follows:

$$L_{\mathrm{MR}}(\boldsymbol{\mu} \mid t_{i,j}) = \prod_{i=1}^{k} \left(\prod_{j=1}^{n_i} \lambda(t_{i,j}) \right) e^{-\Lambda(t_i^*)}. \tag{3.5}$$

Replacing the intensity function (3.3) and the cumulative intensity function (3.4) in (3.5) as discussed in Section 2.3.1, we obtain the likelihood function for the vector parameter $\boldsymbol{\mu} = (\beta, \eta, \alpha)$ of the frailty MR modeled by a PLP, as follows:

$$\begin{aligned} L_{f.\mathrm{MR}}(\boldsymbol{\mu} \mid t_{i,j}) &= \prod_{i=i}^{k} \left\{ \left(\prod_{j=1}^{n_i} \frac{\underline{\lambda}(t_{i,j})}{[1+\alpha\underline{\Lambda}(t_{i,j})]^{-1}} \right) [1+\alpha\underline{\Lambda}(t_i^*)]^{-\frac{1}{\alpha}} \right\} \\ &= \prod_{i=i}^{k} \left\{ \left(\prod_{j=1}^{n_i} \frac{\beta}{\eta^\beta} (t_{i,j})^{\beta-1} \left[1+\alpha \left(\frac{t_{i,j}}{\eta} \right)^\beta \right]^{-1} \right) \left[1+\alpha \left(\frac{t_i^*}{\eta} \right)^\beta \right]^{-\frac{1}{\alpha}} \right\}, \end{aligned} \tag{3.6}$$

and the log-likelihood function is easily obtained given by

$$\begin{aligned} l_{f.\mathrm{MR}}(\boldsymbol{\mu} \mid t_{i,j}) &= N[\log(\beta) - \beta\log(\eta)] + (\beta-1) \sum_{i=1}^{k} \sum_{j=1}^{n_i} \log(t_{i,j}) \\ &\quad - \sum_{i=1}^{k} \sum_{j=1}^{n_i} \log\left(1+\alpha \left(\frac{t_{i,j}}{\eta} \right)^\beta \right) - \frac{1}{\alpha} \sum_{i=1}^{k} \log\left(1+\alpha \left(\frac{t_i^*}{\eta} \right)^\beta \right). \end{aligned} \tag{3.7}$$

If the observation of the systems is failure truncated and for the i-th system the desired number of observed failures is n_i, we can proceed as in Section 2.2.1, just by replacing the truncation time t_i^* with the last observed failure time t_{i,n_i} of each of the i systems in equations (3.6) and (3.7) to obtain the likelihood and the log-likelihood for the failure truncated case, respectively.

It is evident that it is not possible to obtain the MLEs analytically, given the complexity of the log-likelihood function and the partial derivatives of the respective parameters. Thus, numerical methods will be needed to obtain the desired estimates, such as Nelder-Mead. Furthermore, we can use asymptotic theory based on the Normal distribution to construct Confidence Intervals (CI) for the model parameters.

3.2 Unobserved Heterogeneity in PR Model

In this section, we will construct a frailty model for multiple repairable systems under PR with the PLP initial intensity function. This frailty PR model construction is totally similar to the one made for the MR. Furthermore, we obtain the estimators for the reliability function after a failure observation, which allows us to predict the behavior of the failure process from the estimated model parameters.

3.2.1 The Frailty PR Model Definition

Under the same conditions listed in Section 3.1, we consider k independent repairable systems put on time truncated observation. Let $t_{i,j}$ be the j-th failure time of the i-th system and let t_i^* be the truncation time of the i-th system, with $i = 1,\ldots,k$ and $j = 1,\ldots,n_i$.

We will again assume that the frailty variables Z related to the systems' failure times are independent and identically distributed with Gamma$\left(\frac{1}{\alpha},\frac{1}{\alpha}\right)$ distribution, so that the intensity function for each system is given by (3.1).

The differences in relation to the MR model will be based on the baseline intensity function $\underline{\lambda}(t)$, since for the PR model this function is given by (2.9), which can be rewritten as $\lambda_{\text{PR}}(t) = \lambda_0(t - T_{N(t)})$. As we are assuming that the initial intensity function $\lambda_0(t)$ follows a PLP process, the intensity and cumulative intensity functions for the frailty PR model for a single system can be written, respectively, by

$$\lambda_f(t) = \frac{\frac{\beta}{\eta}\left(\frac{t-T_{N(t)}}{\eta}\right)^{\beta-1}}{\left[1+\alpha\left(\frac{t-T_{N(t)}}{\eta}\right)^{\beta}\right]} \tag{3.8}$$

and

$$\Lambda_f(t) = -\log\left(\left[1+\alpha\left(\frac{t-T_{N(t)}}{\eta}\right)^{\beta}\right]^{-\frac{1}{\alpha}}\right). \tag{3.9}$$

3.2.2 Inference for Multiple Systems

The objective now is to obtain the likelihood function of the frailty PR model and for this, we will use the results presented in Section 2.2.2 and follow the same ideas developed in Section 3.1.

Considering k independent repairable systems, $t_{i,j}$ the observed failure times and t_i^* the systems respective truncated time, we can again extend the likelihood function (2.12) to k systems, introducing a new product as follows:

$$L_{\text{PR}}(\boldsymbol{\mu} \mid t_{i,j}) = \prod_{i=i}^{k}\left\{\left(\prod_{j=1}^{n_i}\lambda\left(t_{i,j}-t_{i,j-1}\right)e^{-\Lambda\left(t_{i,j}-t_{i,j-1}\right)}\right)e^{-\Lambda\left(t_i^*-t_{i,n_i}\right)}\right\}, \tag{3.10}$$

where $\boldsymbol{\mu} = (\beta,\eta,\alpha)$ is the vector of parameters to be estimated. Considering the univariate frailty model discussed in Section 2.3.1, we can replace the equations of $\lambda(t)$ and $\Lambda(t)$ by (2.27)

and (2.26), respectively, and rewrite the function (3.10) as

$$\begin{aligned} L_{f.\mathrm{PR}}(\boldsymbol{\mu} \mid t_{i,j}) &= \prod_{i=i}^{k} \left\{ \left(\prod_{j=1}^{n_i} \frac{\lambda_0\left(t_{i,j}-t_{i,j-1}\right)}{1+\alpha\Lambda_0(t_{i,j}-t_{i,j-1})} [1+\alpha\Lambda_0(t_{i,j}-t_{i,j-1})]^{-\frac{1}{\alpha}} \right) \right. \\ &\quad \left. \times [1+\alpha\Lambda_0(t_i^*-t_{i,n_i})]^{-\frac{1}{\alpha}} \right\} \\ &= \prod_{i=i}^{k} \left\{ \left(\prod_{j=1}^{n_i} \lambda_0\left(t_{i,j}-t_{i,j-1}\right) [1+\alpha\Lambda_0(t_{i,j}-t_{i,j-1})]^{-\left(1+\frac{1}{\alpha}\right)} \right) \right. \\ &\quad \left. \times [1+\alpha\Lambda_0(t_i^*-t_{i,n_i})]^{-\frac{1}{\alpha}} \right\}. \end{aligned} \tag{3.11}$$

Finally, using the fact that the initial intensity function follows a PLP process, we replace the $\lambda_0(t)$ and $\Lambda_0(t)$ in (3.11) by (3.8) and (3.9), respectively, and we obtain the likelihood function for the vector parameter $\boldsymbol{\mu} = (\beta, \eta, \alpha)$ of the frailty PR model with k independent systems, given by

$$\begin{aligned} L_{f.\mathrm{PR}}(\boldsymbol{\mu} \mid t_{i,j}) = \prod_{i=i}^{k} \left\{ \left(\prod_{j=1}^{n_i} \frac{\beta}{\eta^\beta} \left(t_{i,j}-t_{i,j-1}\right)^{\beta-1} \left[1+\alpha\left(\frac{t_{i,j}-t_{i,j-1}}{\eta}\right)^\beta\right]^{-\left(1+\frac{1}{\alpha}\right)} \right) \right. \\ \left. \times \left[1+\alpha\left(\frac{t_i^*-t_{i,n_i}}{\eta}\right)^\beta\right]^{-\frac{1}{\alpha}} \right\}, \end{aligned} \tag{3.12}$$

and consequently, the log-likelihood function is given by

$$\begin{aligned} l_{f.\mathrm{PR}}(\boldsymbol{\mu} \mid t_{i,j}) &= N[\log(\beta) - \beta\log(\eta)] + (\beta-1)\sum_{i=1}^{k}\sum_{j=1}^{n_i} \log\left(t_{i,j}-t_{i,j-1}\right) \\ &\quad - \left(1+\frac{1}{\alpha}\right)\sum_{i=1}^{k}\sum_{j=1}^{n_i} \log\left(1+\alpha\left(\frac{t_{i,j}-t_{i,j-1}}{\eta}\right)^\beta\right) \\ &\quad - \frac{1}{\alpha}\sum_{i=1}^{k} \log\left(1+\alpha\left(\frac{t_i^*-t_{i,n_i}}{\eta}\right)^\beta\right). \end{aligned} \tag{3.13}$$

Once again, the likelihood function for the particular case of failure truncated observation can be easily obtained by replacing the truncation time t_i^* to the last observed failure time t_{i,n_i} in (3.12), for each system i.

The complexity of the log-likelihood function makes it again impossible to obtain closed-form expressions for the MLEs. Then again it will be necessary to use numerical methods, such as Nelder-Mead, to compute these estimates. As in the MR model, the confidence intervals can be obtained using the asymptotic theory based on Normal distribution.

3.2.3 Reliability Predictor

In order to estimate the future behavior of repairable systems, we can use the intensity function of the model to predict the reliability indicators. Assume that the last observed failure

time for a system is $T_n = t_n$, so our interest is to estimate the time t until the next failure, given the history up to time $T_n = t_n$. In other words, we want to predict the time $t = T_{n+1} - t_n$ until the next failure considering the history $\mathscr{H}_{t_n}$ until the last observed failure t_n.

In general, the reliability prediction function at time t is given by

$$\begin{aligned} R(t) &= \mathbb{P}[T_{n+1} - t_n > t \mid \mathscr{H}_{t_n}] = \mathbb{P}[N(t_n + t) - N(t_n) = 0 \mid \mathscr{H}_{t_n}] \\ &= \exp\left\{ - \int_{t_n}^{t_n + t} \lambda(u)\, du \right\}, \end{aligned}$$

where $\lambda(t)$ is the intensity function of the model and $t_n \leq u \leq t_n + t < T_{n+1}$. Considering, for example, the intensity function of the frailty model under MR presented in D'Andrea *et al.* (2019), where $\underline{\lambda}(t) = \lambda_0(t)$ is the PLP initial intensity function, we obtain the reliability prediction function given by

$$\begin{aligned} R_{f.\mathrm{MR}}(t) &= \exp\left\{ - \int_{t_n}^{t_n + t} \frac{\underline{\lambda}(u)}{1 + \alpha \underline{\Lambda}(u)}\, du \right\} = \exp\left\{ - \log[1 + \alpha \underline{\Lambda}(t_n + t)]^{\frac{1}{\alpha}} + \log[1 + \alpha \underline{\Lambda}(t_n)]^{\frac{1}{\alpha}} \right\} \\ &= [1 + \alpha \underline{\Lambda}(t_n + t)]^{-\frac{1}{\alpha}} [1 + \alpha \underline{\Lambda}(t_n)]^{\frac{1}{\alpha}} = \left[1 + \alpha \left(\frac{t_n + t}{\eta} \right)^{\beta} \right]^{-\frac{1}{\alpha}} \left[1 + \alpha \left(\frac{t_n}{\eta} \right)^{\beta} \right]^{\frac{1}{\alpha}}. \end{aligned} \tag{3.14}$$

To obtain the reliability prediction function for our proposed frailty model under PR, we replace the baseline intensity function $\underline{\lambda}(t)$ in (3.14) by the intensity function in (3.8). Since $u \in (t_n, t_n + t]$, $T_{N(u)} = t_n$, and using $\lambda_0(t)$ the PLP intensity function, we obtain the reliability prediction function as follows:

$$\begin{aligned} R_{f.\mathrm{PR}}(t) &= \exp\left\{ - \int_{t_n}^{t_n + t} \frac{\lambda_0(u - t_n)}{1 + \alpha \Lambda_0(u - t_n)}\, du \right\} = \exp\left\{ - \log[1 + \alpha \Lambda_0(t)]^{\frac{1}{\alpha}} \right\} \\ &= [1 + \alpha \Lambda_0(t)]^{-\frac{1}{\alpha}} = \left[1 + \alpha \left(\frac{t}{\eta} \right)^{\beta} \right]^{-\frac{1}{\alpha}}. \end{aligned} \tag{3.15}$$

Furthermore, from the reliability prediction function we can obtain the *mean time to failure* (MTTF) at the time $T_n = t_n$, that is, the expected time to the next failure occurring after a time t_n for a given system. The MTTF at the time t_n is given by

$$\mathrm{MTTF}_{t_n} = \mathbb{E}[T_{n+1} - t_n \mid \mathscr{H}_{t_n}] = \int_0^{\infty} R(t)\, dt, \tag{3.16}$$

where $R(t)$ in general is given by (3.14), and specifically for our frailty model under PR, it is given by (3.15).

3.3 Simulation Study

To evaluate the consistency and efficiency performance of the MLEs for the parameters of the frailty PR model with PLP initial intensity function for multiple repairable systems, we proceed with a large simulation study whose results will be discussed in this section.

Let t_j and t_{j+1} be two consecutive failures such that $t_{j+1} = t_j + x$, that is, x is the elapsed time from j-th to the $(j+1)$-th failure. So, the Cumulative Distribution Function (CDF) $F(x)$ for the variable X is given by $F(x) = \mathbb{P}[X \leq x] = 1 - \mathbb{P}[X > x]$, and the event $\{X > x\}$ is relative to no failures occurring between the j-th and $(j+1)$-th failures. Hence, we can rewrite $F(x) = 1 - \mathbb{P}[N(t_{j+1}) - N(t_j) = 0] = 1 - \mathbb{P}[N(t_j + x) - N(t_j) = 0]$, and by the equation (2.11) it follows that $F(x) = e^{-\Lambda_f(x)}$, where $\Lambda_f(t)$ is the cumulative intensity function of a frailty MR model (or frailty PLP process) given by (3.4).

Remember from discussed in Sections 2.1.3 and 2.2.2 that the times X between two consecutive failures of a repairable system under PR are independent and identically distributed. So, these earlier procedure to obtain $F(x)$, also provides a way to get the elapsed times between any two consecutive failures, just getting x as a solution to the equation $F(x) = u$, where u is an observation of the Uniform$(0,1)$ distribution.

Thus, to obtain a sample $\{t_j\}$ of n failure times of a system under PR, it is just necessary to generate a sample $\{u_j\}$ of size n from the Uniform$(0,1)$ distribution and solve n times the equation $F(x_j) = u_j$ to obtain a sample $\{x_j\}$ of n elapsed times between failures. The failure times are obtained recursively, that is, the first failure time is $t_1 = x_1$ and so, the j-th failure time is $t_j = t_{j-1} + x_j$.

Note that the construction described above refers to the failure truncated case. If we want to build a time truncated sample, we just define the truncation time t^* and generate the elapsed times as solution of the equation $F(x_j) = u_j$ until the first failure time obtained is greater than t^*, say t_{n+1}, and this last time will be excluded from the sample. In this study, we chose only the time truncated case, since the results of failure truncated case is as a particular case, as already discussed in Section 2.2. In addition, this process will be repeated for k times, where k is the number of systems we want to consider in the study.

Different parameter scenarios, truncation times and number of systems were considered in the simulation study. From the initial PLP intensity function, the chosen values for the parameter β were $(1.1, 1.5)$ while those chosen for the parameter η were $(5, 20)$. These values are chosen based on estimation without frailty effect for the real data applications that will be presented in the next section (these results are omitted here). Regarding the frailty terms $Z_{i,j}$, $i = 1, \ldots, k$ and $j = 1, \ldots, n_i$, we assume that they are independent and identically distributed with Gamma$(\frac{1}{\alpha}, \frac{1}{\alpha})$ distribution and given two values for the parameter α, $(0.05, 0.2)$. Two scenarios with different truncation times t^* were also considered, $(200, 1000)$, in which case we assume that all k systems will be observed for the same time. Finally, we consider five distinct possibilities for the amount k of observed systems, $(5, 15, 30, 50, 100)$, totaling 80 different scenarios.

For each combination of parameters, 1,000 samples were generated by Monte Carlo simulation using the R software (R Core Team, 2021). For each simulated sample, the MLEs for the parameters and their respective 95% CI were calculated. Some R packages can help us in the

process of obtaining these estimates and, in this work, we use the *optimr(·)* function from the `optimr` package (NASH, 2019). To summarize the data and evaluate the asymptotic performance of the estimators, three indicators were computed: the Bias via Mean Relative Estimate (MRE), the Root of the Mean Squared Error (RMSE) and the Coverage Probability (CP) of the 95% CI, calculated according to the following expressions:

$$\text{Bias}(\hat{\mu}) = \frac{1}{M}\sum_{m=1}^{M}(\hat{\mu}_m - \mu), \quad \text{RMSE}(\hat{\mu}) = \sqrt{\frac{1}{M}\sum_{m=1}^{M}(\hat{\mu}_m - \mu)^2}$$

and

$$\text{CP}(\hat{\mu}) = \frac{1}{M}\sum_{m=1}^{M}\mathbb{I}[\hat{\mu}_m \in (a_m, b_m)] \quad \text{with} \quad a_m = \hat{\mu}_m - 1.96\times\text{SE}(\hat{\mu}_m) \text{ and } b_m = \hat{\mu}_m + 1.96\times\text{SE}(\hat{\mu}_m),$$

where μ represents the parameter to be estimated, that is, $\mu \in (\beta, \eta, \alpha)$, M is the total of simulated samples, $\mathbb{I}$ is the indicator function, $\hat{\mu}_m$ is the estimated parameter of the $m-$th sample, $\text{SE}(\hat{\mu}_m)$ is the standard error of the m-th estimator $\hat{\mu}_m$ and, finally, a_m and b_m are the respective lower and upper bounds of the 95% CI of the m-th estimate.

We expect that with the increase in the number of systems - and consequently the increase in the number of observed failures - the MRE criterion will be close to one, in the sense that the estimated parameter value tends to approach the true value. For the same reason, we also expect the RMSE criterion to approach zero, indicating that the variability inherent in the estimation becomes less. Finally, since the CIs were produced using the MLE asymptotic normality, the CP criterion must be close to the nominal value of 0.95. Thus, if these three indicators present good results, the desired consistency and efficiency properties for the studied MLEs are attested.

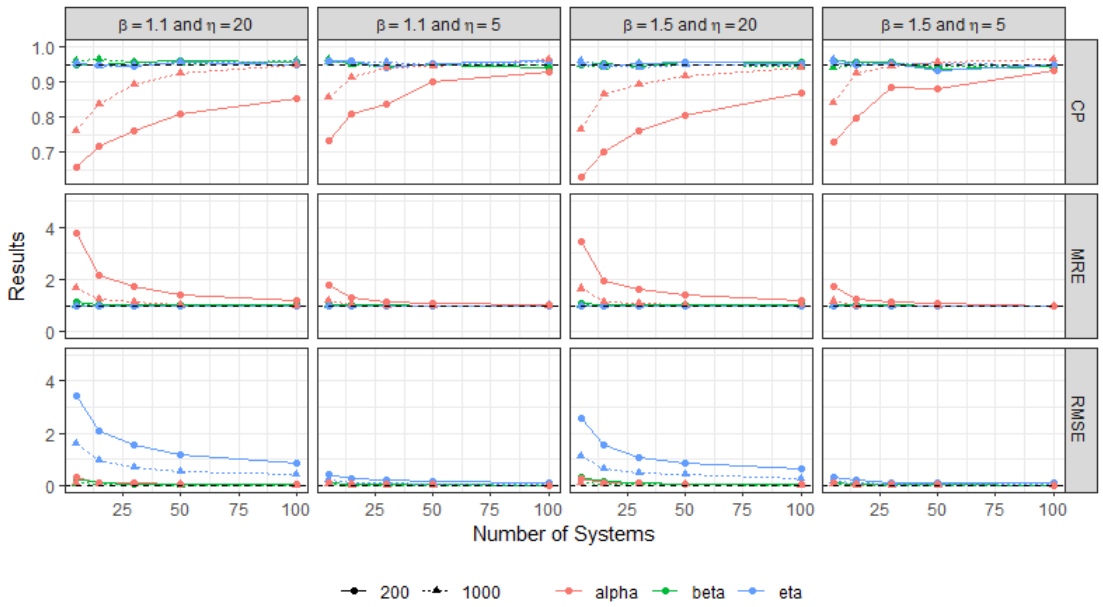

Figure 9 – Simulation results for the frailty PR model in scenarios with $\alpha = 0.05$.

Summaries of the results are shown in Figures 9 and 10. On all graphs, the solid and dotted lines indicate the truncation times $t^* = 200$ and $t^* = 1{,}000$, respectively. In Figure 9, the parameter α is set to 0.05, while in Figure 10 its value is set to 0.2.

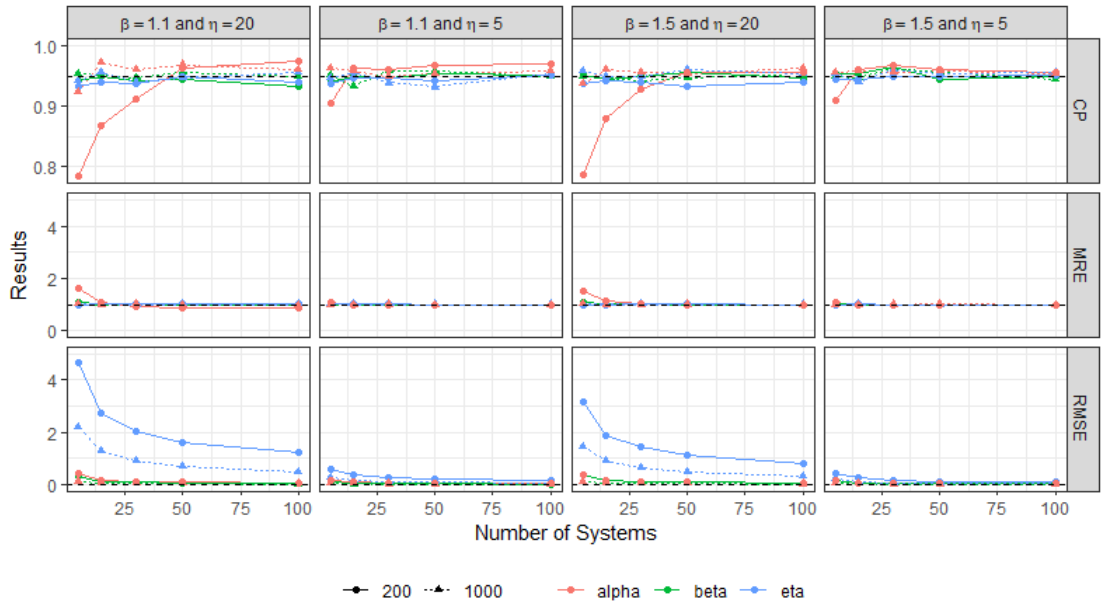

Figure 10 – Simulation results for the frailty PR model in scenarios with $\alpha = 0.2$.

The number of systems considered impacts the sample sizes, as the more systems are observed, the greater number of failure times will be obtained. Thus, it is expected that the behavior of the curves will approach the ideal as the number of units increases.

It is noticeable that the measures of MRE and RMSE present the expected asymptotic properties of MLEs for all scenarios, since their curves approach one and zero for a larger number of observed units, respectively. In cases where $\eta = 20$, the curves approach more slowly due to the magnitude and interpretation of this parameter, but still present the expected behavior.

Regarding the CP, we must highlight the difference in the behavior of the curves in relation to the values of α. In Figure 10, when the variance of the frailty term is $\alpha = 0.2$, the CPs of the nominally 95% CIs for all the estimates seem to be satisfactory and converge to the nominal value. On the other hand, when $\alpha = 0.05$ in Figure 9, the CP of the parameter α converges more slowly when $\eta = 20$ and $t^* = 200$, since in these scenarios the sample size of observed failure times is smaller.

In general, the simulation study presented the expected results. Exception cases particularly observed in CP will be better investigated in future works. For now, our conclusion is that the proposed model is adequate to estimate the desired parameters.

3.4 Real Data Applications

In this section, we use two real data sets to illustrate the methodology developed. The first example deals with a set of 9 sugarcane harvesters, observed during a fixed period of time, whose cutting blades failed several times in this interval. The second set deals with failure times recorded of 5 dump trucks in a mining company's fleet. Further details about these databases will be listed in the subsequent subsections.

For each data set, the MLEs for the parameters β, η and α of the frailty MR and frailty PR models were estimated, as well as their respective 95% confidence intervals. Our first objective is to verify which of the models best fits each data set and for that, we use the maximum of the estimated likelihood function, the Akaike Information Criterion (AIC) and the Bayesian Information Criterion (BIC) (for more details on these criteria, see, e.g., Burnham and Anderson (2004)). Furthermore, by choosing the best model, we are able to estimate the reliability prediction for the observed systems.

It is important to highlight that these two data sets differ in relation to the type of truncation, since the first was obtained from a time truncated observation, while the second was obtained from a failure truncated observation.

3.4.1 Sugarcane Harvester Data

In this subsection, we analyze the data set related to the failure times of sugarcane harvesters. More specifically, the data set consists of the failure times of a piece located in the sugarcane cutting system and the event of interest is the breakage of the *Chopper* blade component in the tractors.

The failure times were obtained during the 2014/2015 harvest in the Brazilian states of São Paulo and Paraná. The *Chopper* blade is responsible for cutting the cane into small pieces, which are later taken to the mill. When a blade failure occurs, the harvester needs to be repaired and the cane harvesting is impaired. Therefore, the failures of this system must be avoided in order to minimize financial losses for the company due to the harvest.

This data set describes the failure times, in days, of 9 sugarcane harvesters, each having a different number of repairs, ranging from 11 to 19 failures, totaling 127 blade *Chopper* failures. As soon as they fail, these machines are repaired in a short time, so they are up and running quickly. The observation ended in 200 days, featuring a time truncated case. The data set is represented in Figure 10, where each row describes a harvester and each point represents a failure time.

Figure 11 below represents the data set, where each row describes a harvester and each point represents a failure time.

Using the likelihood and log-likelihood functions (3.6) and (3.7) for the frailty MR

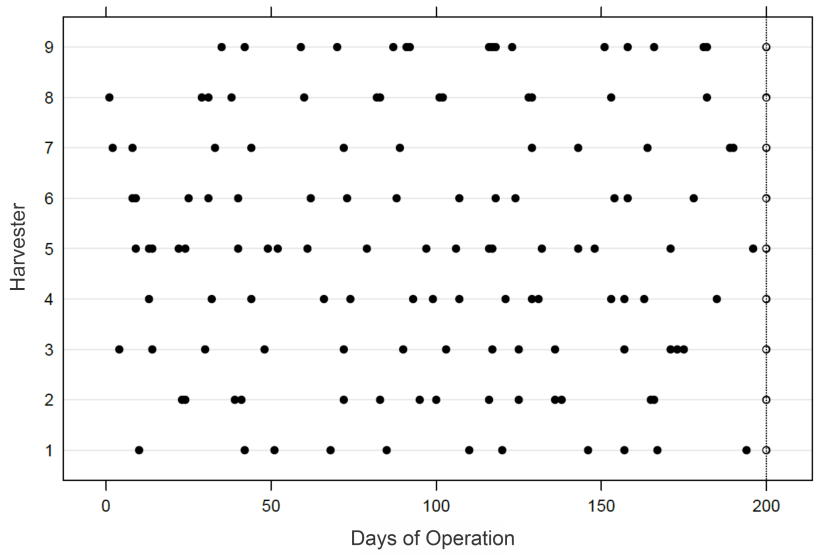

Figure 11 – Failure times, in days, for each sugarcane harvester.

model and (3.12) and (3.13) for the frailty PR model, we obtain the estimates $\hat{\beta}$ and $\hat{\eta}$ for the parameters β and η of the initial PLP intensity function, and the estimate $\hat{\alpha}$ for the parameter α of the frailty term. The MLEs for each parameter and their respective 95% CI are described in Table 1, as well as the maximum values of the log-likelihood function, the AIC and BIC criteria values.

Table 1 – Estimation results for frailty MR and frailty PR models applied to sugarcane harvesters data.

	$\hat{\beta}$ (95% $\text{CI}_{\hat{\beta}}$)	$\hat{\eta}$ (95% $\text{CI}_{\hat{\eta}}$)	$\hat{\alpha}$ (95% $\text{CI}_{\hat{\alpha}}$)
MR	1.11 (0.79, 1.55)	14.27 (8.75, 23.28)	0.038 (0.004, 0.364)
PR	1.32 (1.14, 1.53)	15.02 (13.11, 17.20)	5.6 (5.3, 5.9) $\times 10^{-7}$
	$\hat{l}$	AIC	BIC
MR	-463.26	932.53	941.06
PR	-457.36	920.72	929.25

From Table 1, we can see that the estimate $\hat{l}$ of the maximum log-likelihood function of the frailty PR model is greater than that of the frailty MR model and, accordingly, the AIC and BIC criteria have lower values for the frailty PR model than for the frailty MR model. Thus, we can conclude that the frailty PR model fit is better than the frailty MR model for the harvester failure time data set.

First of all, note that the estimate $\hat{\alpha}$ of a frailty PR model and its respective 95% CI are very close to zero, which indicates that the variance of the frailty random variable Z is practically null. In other words, it means that there is no evidence of the existence of unobserved heterogeneity among the failure times of the 9 tractors. In this case, for these systems, it can be thought that when considering that the repairs performed are perfect the frailty effects are potentially suppressed, not causing major impacts on their failure processes.

The parameters β and η of the initial intensity function can be interpreted as in the usual PLP model as discussed in Section 2.1.2. Since $\hat{\beta} > 1$, the harvesters' cutting systems are deteriorating over time. Furthermore, the estimate $\hat{\eta}$ indicates that the expected time for a single failure to occur on one of the systems is approximately 15 days.

In order to have a perception of the quality of the adjustment, we used the graphical procedures presented in Toledo *et al.* (2015) for the IR models, since the PR model is a particular case of the IR model. The idea of the procedure is to compare the empirical Mean Cumulative Failure (MCF) of the observed failure times with the average of all adjusted MCF, and so, the goodness-of-fit plot comparison is that the better the fit the closer the empirical MCF will be to that estimated by the model. The nonparametric estimation of the MCF is obtained based on the Nelson-Aalen procedure presented in Aalen (1978), while the estimated MCF of each system is given by the equation (3.9). In the latter case, the obtained parameter estimates and the system failure times will be plugged in (3.9) for each system, then, the MCF for the process at time t is the average of the MCF for each system at time t.

The empirical and estimated MCF are presented in Figure 12.

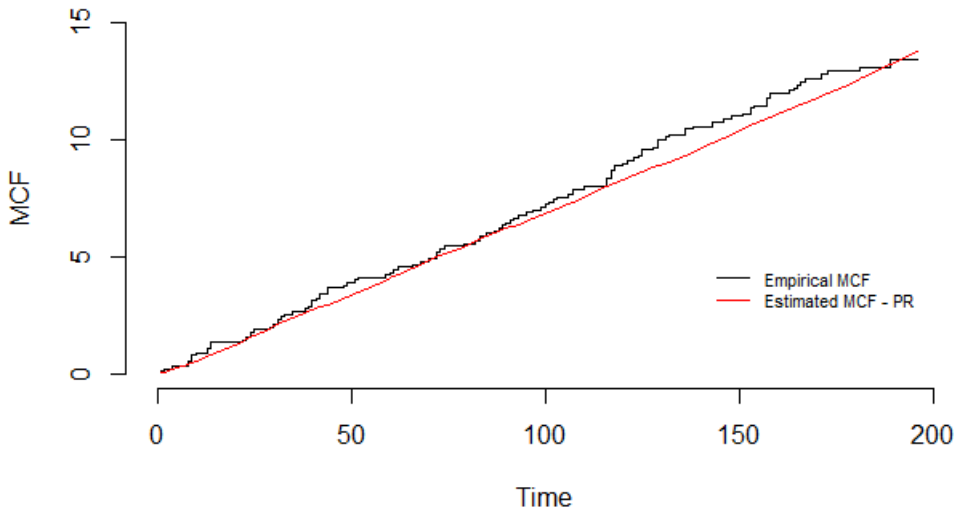

Figure 12 – Empirical and estimated MCF for the harvesters failure time in a frailty PR model.

We can conclude that the fit seems adequate, since the curve estimated for the average of MCF systems is close to the empirical MCF curve.

Using the equations (3.14) and (3.15), and replacing the respectively obtained estimates for the frailty models' parameters under MR and PR given in Table 1, we can obtain the reliability prediction function and the MTTF at the last observed time for each model, given a specific harvester. Taking the harvester #5, which had the highest number of failures during the observed time (19 failures), Figure 13 shows the reliability prediction function for the frailty models under MR and PR. We can see that the reliability probability for 40 days after the last failure is very

close to zero, given the entire history of the failure process. Furthermore, considering the PR model (the best frailty model fitted for the sugarcane harvesters data), we use the equation (3.16) to calculate the estimated MTTF after the last observed failure and obtain an estimate of 13.8 days for the selected harvester, which means that the expected time to the next failure of this harvester, after the last observed failure at the time $t_{19} = 196$ days, is approximately 14 days.

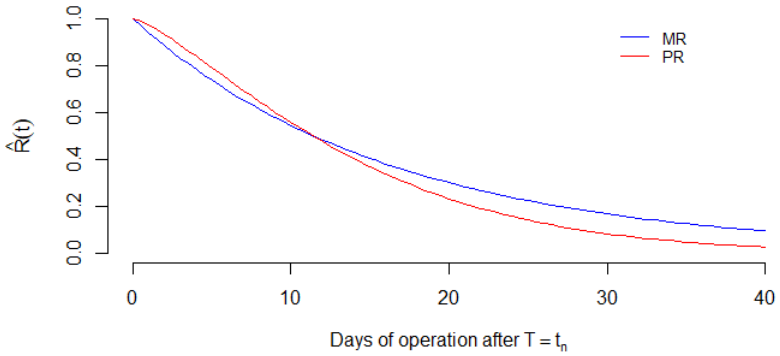

Figure 13 – Estimated reliability functions at time $t_{19} = 196$ days for a specific harvester in the data set, under the fitted MR and PR frailty models.

3.4.2 Dump Truck Data

The data set analyzed in this section refers to the failure times of 5 dump trucks in the fleet of a Brazilian mining company. These trucks aid in the mining process and are susceptible to several failures since they operate in extreme situations at mining sites.

The failure times were collected from July to October 2012, when 129 failures were observed, each followed by a repair. This observation was failure truncated, which means that the last observation for each truck corresponds to a failure time.

This data set was presented and studied by Toledo *et al.* (2015), who performed a complete inferential analysis considering the imperfect repair models to find the one that best fits the data.

Figure 14 represents the data set, where each line describes a truck and each point represents a failure time.

Using the likelihood and log-likelihood functions (3.6) and (3.7) for the frailty MR model and (3.12) and (3.13) for the frailty PR model adjusted to the failure truncated case, we get the estimates $\hat{\beta}$, $\hat{\eta}$ and $\hat{\alpha}$ for the respective parameters of both models. The MLEs for each parameter and their respective 95% CI are described in Table 2, as well as the estimate $\hat{l}$ and the AIC and BIC values.

From the results of $\hat{l}$ and the AIC and BIC criteria presented in Table 2, we can conclude that the frailty MR model fit is better than the frailty PR model for this data set.

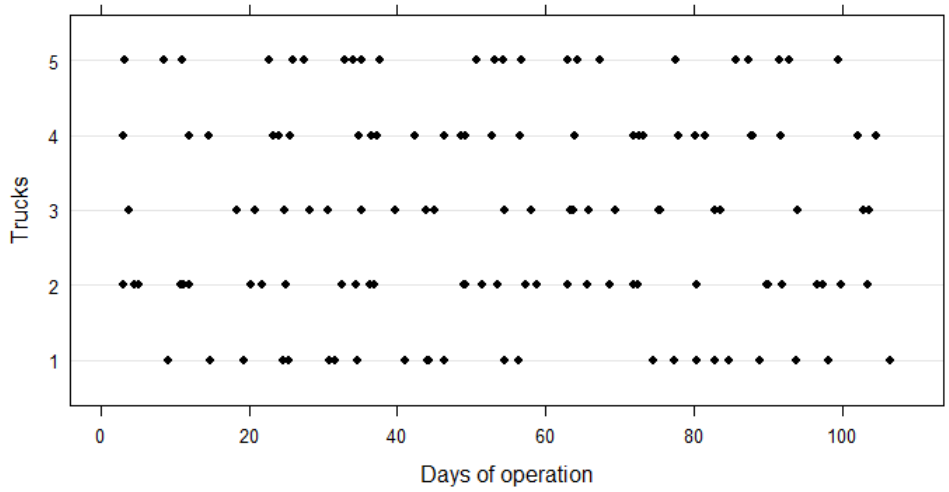

Figure 14 – Failure times, in days, for each dump truck.

Table 2 – Estimation results for frailty RM and frailty RP models applied to dump truck data.

	$\hat{\beta}$ (95% $CI_{\hat{\beta}}$)	$\hat{\eta}$ (95% $CI_{\hat{\eta}}$)	$\hat{\alpha}$ (95% $CI_{\hat{\alpha}}$)
MR	1.30 (0.91, 1.85)	6.79 (3.92, 11.76)	0.021 (0.002, 0.253)
PR	1.19 (1.04, 1.36)	4.41 (3.78, 5.12)	33×10^{-6} $(31, 37)\times10^{-6}$
	$\hat{l}$	AIC	BIC
MR	-306.85	619.71	628.28
PR	-310.67	627.35	635.93

Unlike the previous example, the estimate $\hat{\alpha}$ for the model chosen in this case cannot be considered to be zero (although the lower limit of the confidence interval is very close to zero). This value indicates that there is an unobserved heterogeneity related to the failure times of the analyzed trucks. This means that at certain times of observation, trucks are more likely to fail due to unobserved external factors. The intensity functions related to the failure times of the trucks undergo a change (very small, in this case) that describes this greater or lesser susceptibility to failures at different times.

Regarding the $\hat{\beta}$ and $\hat{\eta}$ parameter estimates, it is not advisable to use the same interpretation for the PLP process, since the existence of a multiplicative term for frailty impacts the failure intensity function, distorting the ideas of deterioration and expected time for a failure occurrence discussed in Section 2.1.2.

In order to have a perception of the quality of the adjustment, we used the same graphical procedures present in the last example to compare the empirical and estimated MCF of the process, shown in Figure 15.

We can again conclude that the fit is reasonable, since the empirical and estimated curves of the MCF are very close.

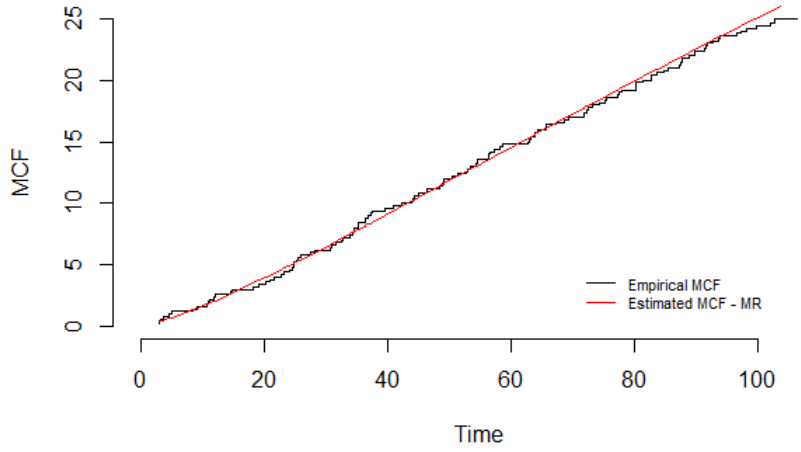

Figure 15 – Empirical and estimated MCF for the dump truck failure time in a frailty MR model.

Again using the equations (3.14) and (3.15), and replacing the respectively obtained estimates for the frailty models' parameters under MR and PR given in Table 2, we obtain the reliability prediction function and the MTTF at the last observed time for each model, given a specific truck. Taking the truck #2, which had the highest number of failures (32 failures), Figure 16 shows the reliability prediction function for the frailty models under MR and PR. It is noticeable that the reliability probability for more than 12 days after the last failure is close to zero, given all the history of the failure process. Considering the MR model (the best frailty model fitted for the dump truck data), we calculate the MTTF by integrating the reliability prediction function for the frailty model under MR, that is, $\int_0^\infty R_{\text{MR}}(t)\,dt$, where $R_{\text{MR}}(t)$ is given by (3.14). Thus, the estimated MTTF after the last observed failure is 4.00 days for the selected truck, which means that the expected time to the next failure of this truck, after the last observed failure at the time $t_{32} = 103.386$ days, is approximately 4 days.

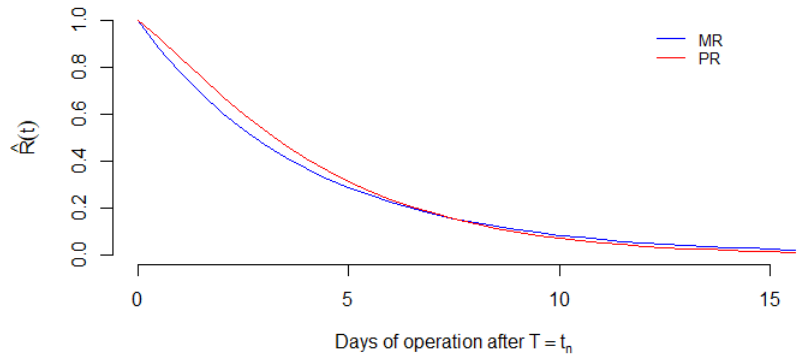

Figure 16 – Estimated reliability functions at time $t_{32} = 103.386$ days for a specific truck in the data set, under the fitted MR and PR frailty models.

3.5 Concluding Remarks of the Chapter

In this chapter, we proposed an extension of the perfect repair model to multiple independent repairable systems by introducing a multiplicative frailty term. In situations where it is known that the repair performed on a system returns it to an AGAN condition, the traditional PR model is unable to identify unobservable effects that can impact the time of system failures, that is, in these models the possibility of the existence of unobserved heterogeneity can be erroneously ignored.

In the proposed frailty PR model, the initial intensity function of the recurring failure times follows a PLP process and associated to each system failure time, it was assumed that the frailty terms are independent and have the same Gamma$(\frac{1}{\alpha}, \frac{1}{\alpha})$ distribution, where the parameter α indicates the variance of these random variables. Under a classical framework, we used the likelihood principle to obtain the model parameters' MLE and their respective 95% CI by using asymptotic theory.

An extensive Monte Carlo simulation study was carried out to check the quality of the estimators obtained and their behavior under different parameter scenarios, number of observed systems and time of observation. It was noted that results are in agreement with those expected for MLEs, since the obtained estimates approached the true parameters values with small dispersion as the number of simulated failures was greater.

As applications for the discussed procedures, we have brought two real data sets and the frailty PR and MR models were used to adjust each data set in order to verify the existence of unobserved heterogeneity and identify the most likely type of repair that was performed on the observed systems. In the first set, which deals with failure times in the cutting blades of sugarcane harvesters, it was identified that the repairs performed were PRs, but the existence of unobserved heterogeneity was not observed. In the second set, which deals with the failure times in dump truck engines, the fit with the MR assumption was superior to the fit with the PR, and, in this case, the evidence of the existence of non-observed heterogeneity between the trucks was significant.

The results obtained from theoretical discussions, simulation study and application show that the model proposed is relevant to the context of repairable systems. First, because it enables the modeling of failure times in situations where repairable systems are subjected to component replacement after failures occur, which characterizes a PR. At the same time, the model makes it possible to identify the existence of non-quantified factors that may interfere with the failure intensity function of the systems and, consequently, with their operating time.

CHAPTER

4

UNOBSERVED HETEROGENEITY FOR MULTIPLE REPAIRABLE SYSTEMS UNDER IMPERFECT REPAIR

In Chapter 3, we proposed a frailty model for multiple repairable systems considering the perfect repair as an alternative to the models previously presented in the literature, where only the minimal repair was considered. At this point, a natural question is the possibility of including a frailty term in the intensity failure functions of independent systems under imperfect repair, in a similar way to the other two types of repair discussed before.

In the literature, we find some recent works that deals with this problem, , from different perspectives. The first, Liu *et al.* (2020) investigate effects of unobserved heterogeneity in repairable system failures under imperfect repair, specifically for the ARA_1 and ARA_∞ classes. In this work, the authors considered the Gamma$(\frac{1}{\alpha}, \frac{1}{\alpha})$ distribution for the frailty term, the PLP as the initial intensity function of the model and considered the usual shared frailty model for multiple repairable systems. A second work is that of Junior (2021), who establishes frailty models for repairable systems hierarchically represented subject to competing risks. In this work the author also consider the frailty variables Gamma$(\frac{1}{\alpha}, \frac{1}{\alpha})$ distributed. ARA class of IR and PLP initial intensity function, but in this case, the frailty term is induced in the model in a univariate sense.

Our aim in this chapter is to insert the frailty term in the IR models in two different senses: considering univariate frailty and shared frailty. As discussed in Section 2.3, univariate frailty makes sense for imperfect repair models since the failure intensity function of these models changes after the occurrence of each failure and, in this case, we can consider the possibility of different random effects related to each of these failure times. In the shared frailty context, we pretend to extend some of the results presented by Liu *et al.* (2020), analyzing the effect of unobserved heterogeneity with Gamma distribution for independent systems under imperfect

repair of the general classes ARA_m and ARI_m of IR model.

In this sense, we use the imperfect repair models presented in Section 2.2.3 and include the parametric frailty term with Gamma distribution as discussed in Sections 2.3.1 and 2.3.2 The likelihood method will be adopted as a classical framework to estimate the PLP's β and η parameters, the efficiency parameter θ from IR models and the parameter α which is the variance of the Gamma distribution. Finally, for each model discussed and based on the estimates obtained, we define the reliability predictors after the occurrence of a new failure.

In Section 4.1, we present the first proposed models, the univariate frailty IR model, considering the both ARA_m and ARI_m classes for all possible memories m and assuming a PLP as initial intensity. In Section 4.2 we present the proposed shared frailty IR model, with the same PLP initial intensity and also considering the both ARA_m and ARI_m classes. In the two Sections 4.1.1 and 4.2.1 we define the functions models for both ARA_m and ARI_m classes of IR; in Sections 4.1.2 and 4.2.2 we present the inference procedures through the construction of the likelihood functions; and finally, in Sections 4.1.3 and 4.2.3 we present the reliability prediction functions. For each model, we carry out an extensive simulation study to verify the behavior of the model estimators that is described and discussed in Sections 4.1.4 and 4.2.4. In Sections 4.1.5 and 4.2.5 we use the same two data sets presented in Section 3.4 to illustrate the proposed methodologies and calculate the model parameter estimates and the reliability predictions.

4.1 Univariate Unobserved Heterogeneity in IR Models

In this Section we propose univariate frailty models for multiple repairable systems considering that IR are performed after each failure. In terms of type of repair, these models are generalizations of the PR frailty models presented in Section 3.2. The idea is to identify the existence of non-quantifiable effects that impact the occurrence of failures in identical systems and, at the same time, quantify the effect of repairs performed through the θ parameter of the IR models. The model's assumptions consider again that the time to carry out the repair is negligible.

In the next sections we will build the univariate frailty models for the imperfect repair classes ARA_m and ARI_m, as well as establish inferential methods for estimating parameters and predicting reliability for each of these models. As discussed in Sections 2.2.3.1 and 2.2.3.2 for the both ARA_m and ARI_m classes the failure intensity at a time t is defined in terms of the memory of the last m failures observed in the system and these failure memories are also taken into account in our models since they directly impact the reduction of the virtual age (in the ARA_m class) or the intensity (in the ARI_m class) of each system.

4.1.1 The Univariate Frailty ARA_m and ARI_m Models

Our models will again be defined for multiple repairable systems, now subjected to IR actions after each failure. Consider k independent repairable systems under observation,

$k = 1, 2, \ldots$, and let $0 < t_{i,1} < t_{i,2} < \cdots < t_{i,n_i}$ be the observed failure times of the i-th system, where n_i is the number of observed failures of the i-th system and $t_{i,j}$ is the time of the j-th failure in the i-th system, where $i = 1, \ldots, k$ and $j = 1, \ldots, n_i$. Assume that the study is time truncated for the same reasons listed in the previous sections, that is, each system will be observed up to a predetermined time t_i^*, so that for each $i = 1, \ldots, k$, the observed failure times follow the relation $0 < t_{i,1} < \cdots < t_{i,n_i} < t_i^*$ and the number of system failures n_i is random. Here again, N is the total number of failures observed on k systems, that is, $N = \sum_{i=1}^{k} n_i$.

As discussed in Section 3.1, if for each failure time $t_{i,j}$, $i = 1, \ldots, k$ and $j = 1, \ldots, n_i$, the frailty variables $Z_{i,j} = Z$ are independent and identically distributed with Gamma$\left(\frac{1}{\alpha}, \frac{1}{\alpha}\right)$ distribution, and the intensity function and cumulative intensity function related to each failure time are given by the equations (2.32) and (2.31), respectively. The difference for this case is given by the definition of the baseline intensity functions $\underline{\lambda}(t)$ and the cumulative intensity function $\underline{\Lambda}(t)$, since we must consider the functions related to each class of IR models.

For the ARA$_m$ class, the intensity functions are obtained by defining the baseline $\underline{\lambda}(t)$ and $\underline{\Lambda}(t)$ functions from the equations (2.32) and (2.31) by $\lambda_{\text{ARA}_m}(t)$ and $\Lambda_{\text{ARA}_m}(t)$ functions given by (2.13) and (2.14), respectively. Furthermore, assuming the initial failure process follows a PLP, we can use the PLP intensity functions $\lambda_0(t)$ and $\Lambda_0(t)$ defined by (2.3) and (2.4) to rewrite the univariate frailty ARA$_m$ intensity and cumulative intensity functions, respectively, as

$$\lambda_{f.\text{ARA}_m}(t) = \frac{\frac{\beta}{\eta^\beta}\left(t - (1-\theta)S(t_{N(t)})\right)^{\beta-1}}{1 + \alpha\Lambda^*{}_{\text{ARA}_m}(t)} \tag{4.1}$$

and

$$\Lambda_{f.\text{ARA}_m}(t) = -\log\left(\left[1 + \alpha\Lambda^*{}_{\text{ARA}_m}(t)\right]^{-\frac{1}{\alpha}}\right), \tag{4.2}$$

where

$$\Lambda^*{}_{\text{ARA}_m}(t) = \Lambda_{\text{ARA}_m}(T_{N(t)}) + \left(\frac{t - (1-\theta)S(t_{N(t)})}{\eta}\right)^\beta - \left(\frac{T_{N(t)} - (1-\theta)S(t_{N(t)})}{\eta}\right)^\beta.$$

In a completely analogous way, we obtain the intensity and cumulative intensity functions for the ARI$_m$ class. Now we define $\underline{\lambda}(t)$ and $\underline{\Lambda}$ of the equations (2.32) and (2.31) by $\lambda_{\text{ARI}_m}(t)$ and $\Lambda_{\text{ARI}_m}(t)$, given by (2.16) and (2.17), respectively. Considering again the PLP process as initial failure process, we can use the equations (2.3) and (2.4), and rewrite the intensity function and the cumulative intensity function of a univariate frailty ARI$_m$ as

$$\lambda_{f.\text{ARI}_m}(t) = \frac{\frac{\beta}{\eta^\beta}\left(t^{\beta-1} - (1-\theta)\underset{\sim}{S}(t_{N(t)})\right)}{1 + \alpha\Lambda^*{}_{\text{ARI}_m}(t)} \tag{4.3}$$

and

$$\Lambda_{f.\text{ARI}_m}(t) = -\log\left(\left[1 + \alpha\Lambda^*{}_{\text{ARI}_m}(t)\right]^{-\frac{1}{\alpha}}\right), \tag{4.4}$$

where

$$\Lambda^*{}_{\mathrm{ARI}m}(t) = \Lambda_{\mathrm{ARI}m}(T_{N(t)}) + \left(\frac{t}{\eta}\right)^{\beta} - \left(\frac{T_{N(t)}}{\eta}\right)^{\beta} - \frac{\beta}{\eta^{\beta}}(t - T_{N(t)})(1-\theta)\underset{\sim}{S}(t_{N(t)})$$

and $\underset{\sim}{S}(t_o) = \sum_{p=0}^{\min\{m-1,o-1\}} \theta^p T_{o-p}^{\beta-1}$.

4.1.2 Parameter Estimation for the Univariate Frailty ARA$_m$ and ARI$_m$ Models

Our interest now is to perform inference in a classical approach using the likelihood method, once we have obtained the failure intensity and cumulative failure intensity functions of the systems for both frailty ARA$_m$ and ARI$_m$ models.

First, for the frailty ARA$_m$ model, the general likelihood function given in (2.15) will be used, replacing the functions $\lambda_{\mathrm{ARA}m}(t)$ and $\Lambda_{\mathrm{ARA}m}(t)$ by the functions $\lambda_{f.\mathrm{ARA}m}(t)$ and $\lambda_{f.\mathrm{ARA}m}(t)$ obtained in (4.1) and (4.2) (for these last two functions, we will just write $\lambda(t)$ and $\Lambda(t)$, respectively, to simplify the notation). Thus, given the observed failure times $t_{i,j}$ from the k independent systems and considering the time of truncation t_i^* for each system, with $i = 1,\ldots,k$ and $j = 1,\ldots,n_i$, the likelihood function for the parameter vector $\boldsymbol{\mu} = (\beta,\eta,\theta,\alpha)$ of the univariate frailty ARA$_m$ model with PLP initial intensity is obtained as follows:

$$\begin{aligned} L_{f.\mathrm{ARA}m}(\boldsymbol{\mu} \mid t_{i,j}) &= \prod_{i=i}^{k}\left\{\prod_{j=1}^{n_i}\left(\lambda\left(t_{i,j}\right)e^{-\Lambda\left(t_{i,j}\right)+\Lambda\left(t_{i,j-1}\right)}\right)e^{-\Lambda\left(t_i^*\right)+\Lambda\left(t_{i,n_i}\right)}\right\} \\ &= \prod_{i=i}^{k}\left\{\prod_{j=1}^{n_i}\left(\frac{\beta}{\eta^{\beta}}\left(t_{i,j}-(1-\theta)s(t_{i,j-1})\right)^{\beta-1}\right.\right. \\ &\quad \left.\times\left[1+\alpha\Lambda^*{}_{\mathrm{ARA}m}(t_{i,j})\right]^{-\left(1+\frac{1}{\alpha}\right)}\left[1+\alpha\Lambda^*{}_{\mathrm{ARA}m}(t_{i,j-1})\right]^{\frac{1}{\alpha}}\right) \\ &\quad \left.\times\left[1+\alpha\Lambda^*{}_{\mathrm{ARA}m}(t_{i^*})\right]^{-\frac{1}{\alpha}}\left[1+\alpha\Lambda^*{}_{\mathrm{ARA}m}(t_{i,n_i})\right]^{\frac{1}{\alpha}}\right\}. \end{aligned} \tag{4.5}$$

Thus, the log-likelihood function for the frailty ARA$_m$ model is given, by

$$\begin{aligned} l_{f.\mathrm{ARA}m}(\boldsymbol{\mu} \mid t_{i,j}) &= N[\log(\beta) - \beta\log(\eta)] + (\beta-1)\sum_{i=1}^{k}\sum_{j=1}^{n_i}\log\left(t_{i,j}-(1-\theta)s(t_{i,j-1})\right) \\ &\quad -\left(1+\frac{1}{\alpha}\right)\sum_{i=1}^{k}\sum_{j=1}^{n_i}\log\left(1+\alpha\Lambda^*{}_{\mathrm{ARA}m}(t_{i,j})\right) \\ &\quad +\frac{1}{\alpha}\sum_{i=1}^{k}\sum_{j=1}^{n_i}\log\left(1+\alpha\Lambda^*{}_{\mathrm{ARA}m}(t_{i,j-1})\right) \\ &\quad -\frac{1}{\alpha}\sum_{i=1}^{k}\log\left(\frac{1+\alpha\Lambda^*{}_{\mathrm{ARA}m}(t_{i^*})}{1+\alpha\Lambda^*{}_{\mathrm{ARA}m}(t_{i,n_i})}\right) \end{aligned} \tag{4.6}$$

Analogously, for the ARI_m class, we use the general likelihood function given in (2.19) and replace the functions $\lambda_{\text{ARI}m}(t)$ and $\Lambda_{\text{ARI}m}(t)$ with the equations $\lambda_{f.\text{ARI}m}(t)$ (4.3) and $\Lambda_{f.\text{ARI}m}(t)$ (4.4) to obtain the desired likelihood function (we again will just write $\lambda(t)$ and $\Lambda(t)$ to simplify the notation). Hence, given the observed failure times $t_{i,j}$ from the k independent systems and considering the time of truncation t_i^* for each system, with $i = 1,\ldots,k$ and $j = 1,\ldots,n_i$, the likelihood function for the parameter vector $\boldsymbol{\mu} = (\beta,\eta,\theta,\alpha)$ of the frailty ARI_m model with PLP initial intensity is given by

$$\begin{aligned} L_{f.\text{ARI}m}(\boldsymbol{\mu} \mid t_{i,j}) &= \prod_{i=i}^{k}\left\{\prod_{j=1}^{n_i}\left(\lambda\left(t_{i,j}\right)e^{-\Lambda\left(t_{i,j}\right)+\Lambda\left(t_{i,j-1}\right)}\right)e^{-\Lambda\left(t_i^*\right)+\Lambda\left(t_{i,n_i}\right)}\right\} \\ &= \prod_{i=i}^{k}\left\{\prod_{j=1}^{n_i}\left(\frac{\beta}{\eta^\beta}\left(t_{i,j}^{\beta-1}-(1-\theta)\underset{\sim}{s}(t_{i,j-1})\right)\right.\right. \\ &\quad \times\left[1+\alpha\Lambda^*{}_{\text{ARI}m}(t_{i,j})\right]^{-\left(1+\frac{1}{\alpha}\right)}\left[1+\alpha\Lambda^*{}_{\text{ARI}m}(t_{i,j-1})\right]^{\frac{1}{\alpha}}\Bigg) \\ &\quad \left.\left.\times\left[1+\alpha\Lambda^*{}_{\text{ARI}m}(t_{i^*})\right]^{-\frac{1}{\alpha}}\left[1+\alpha\Lambda^*{}_{\text{ARI}m}(t_{i,n_i})\right]^{\frac{1}{\alpha}}\right\}, \end{aligned} \tag{4.7}$$

where $\underset{\sim}{s}(t_{i,o}) = \sum_{p=0}^{\min\{m-1,o-1\}}\theta^p t_{i,o-p}^{\beta-1}$.

The log-likelihood function for the frailty ARI_m class is given, by

$$\begin{aligned} l_{f.\text{ARI}m}(\boldsymbol{\mu} \mid t_{i,j}) &= N[\log(\beta)-\beta\log(\eta)]+\sum_{i=1}^{k}\sum_{j=1}^{n_i}\log\left(t_{i,j}^{\beta-1}-(1-\theta)\underset{\sim}{s}(t_{i,j-1})\right) \\ &\quad -\left(1+\frac{1}{\alpha}\right)\sum_{i=1}^{k}\sum_{j=1}^{n_i}\log\left(1+\alpha\Lambda^*{}_{\text{ARI}m}(t_{i,j})\right) \\ &\quad +\frac{1}{\alpha}\sum_{i=1}^{k}\sum_{j=1}^{n_i}\log\left(1+\alpha\Lambda^*{}_{\text{ARI}m}(t_{i,j-1})\right) \\ &\quad -\frac{1}{\alpha}\sum_{i=1}^{k}\log\left(\frac{1+\alpha\Lambda^*{}_{\text{ARI}m}(t_{i^*})}{1+\alpha\Lambda^*{}_{\text{ARI}m}(t_{i,n_i})}\right) \end{aligned} \tag{4.8}$$

All the results for failure-truncated systems are a particular case of the time-truncated scenario, and their respective likelihood and log-likelihood functions are obtained just by replacing t_i^* with the last observed failure time t_{i,n_i}, for each $i = 1,\ldots,k$.

The equations (4.6) and (4.8) are very complex and therefore, it is not possible to obtain the MLEs analytically. Thus, numerical methods, such as Nelder-Mead, can be used to obtain the desired estimates, and the asymptotic theory based on the normal distribution is used again to build CIs for the model's parameters.

4.1.3 Reliability Predictors for Univariate Frailty ARA$_m$ and ARI$_m$ Models

In this section we will define the reliability prediction functions for the proposed models, given the importance of this indicator for the real world of technology companies and factories for planning their maintenance policies and failure prevention. As discussed in Section 3.2.3, the idea is to estimate the probability of a new failure occurring in a system in a given time interval based on its failure history.

Let $T_n = t_n$ be the last observed failure time of a system and let t be the time until the next failure. Our interest is to estimate the time $t = T_{n+1} - t_n$ until the next failure considering the history $\mathscr{H}_{t_n}$ until the last observed failure t_n. In general, the reliability prediction function at time t is expressed as

$$R(t) = \mathbb{P}[T_{n+1} - t_n > t \mid \mathscr{H}_{t_n}] = \exp\left\{-\int_{t_n}^{t_n+t} \lambda(u)\,du\right\}, \tag{4.9}$$

where $\lambda(t)$ is the intensity function of the model and $t_n \leq u \leq t_n + t < T_{n+1}$. Then, we can simply use the intensity functions of the proposed frailty ARA$_m$ and ARI$_m$ models in equation (4.9) and obtain the desired reliability predictors for each model.

For the frailty ARA$_m$ model, taking the intensity function presented in (4.1) with the PLP initial intensity function, we obtain the reliability prediction function $R(t) = R_{f.\mathrm{ARA}m}(t)$ as follows:

$$\begin{aligned} R(t) = &\left[1 + \frac{\alpha}{\eta^\beta}\left(\eta^\beta \Lambda_{\mathrm{ARA}m}(t_n) + (t_n + t - (1-\theta)s(t_n))^\beta - (t_n - (1-\theta)s(t_n))^\beta\right)\right]^{-\frac{1}{\alpha}} \\ &\times \left[1 + \alpha\Lambda_{\mathrm{ARA}m}(t_n)\right]^{\frac{1}{\alpha}}. \end{aligned} \tag{4.10}$$

Using the same idea for the frailty ARI$_m$ model, replacing the intensity function (4.3) into (3.14), we obtain the reliability prediction function $R(t) = R_{f.\mathrm{ARI}m}(t)$ given by

$$\begin{aligned} R(t) = &\left[1 + \frac{\alpha}{\eta^\beta}\left(\eta^\beta \Lambda_{\mathrm{ARI}m}(t_n) + (t_n + t)^\beta - (t_n)^\beta - t\beta(1-\theta)\underset{\sim}{S}(t_n)\right)\right]^{-\frac{1}{\alpha}} \\ &\times \left[1 + \alpha\Lambda_{\mathrm{ARI}m}(t_n)\right]^{\frac{1}{\alpha}}. \end{aligned} \tag{4.11}$$

Moreover, the *mean time to failure* (MTTF) at time $T_n = t_n$ can be obtained from the reliability prediction functions as follows:

$$\mathrm{MTTF}_{t_n} = \mathbb{E}[T_{n+1} - t_n \mid \mathscr{H}_{t_n}] = \int_0^\infty R(t)\,dt, \tag{4.12}$$

where $R(t)$, in general, is given by (4.9), and specifically for our frailty ARA$_m$ and ARI$_m$ models, it is given, respectively, by (4.10) and (4.11). In other words, the MTTF is the expected time to the next failure occurring after a time t_n for a given system.

4.1.4 Simulation Study

In this section, we present the steps and the results of a large Monte Carlo simulation study, which was carried out in order to analyze the efficiency and consistency performances of the MLEs related to each of the frailty IR models proposed in the previous sections. We will analyze separately the proceeded simulation study for the two frailty ARA and ARI models and their respective results.

For each of the ARA and ARI classes, we used different procedures for data generation, which will be described apart in the next two subsections. In both cases, time truncation scenarios were considered, since this is the most general situation as discussed in Section 2.2. Different scenarios were defined for the simulation study, varying the parameter settings, the number of considered systems, the truncation times and the failure memories for both univariate frailty ARA and ARI models.

In both frailty model classes, for each defined scenario, the R software (R Core Team, 2021) was again used to generate 1,000 Monte Carlo samples. For each obtained sample, the function *optim* from the `stats` package was used to calculate the parameters MLEs and their respective 95% CIs. As in Section 3.3, three indicators were used to summarize the data and jointly evaluate the asymptotic performance of the proposed estimators: the RMSE, the MRE, and the CP of the 95% CIs, calculated as follows:

$$\text{RMSE}(\hat{\mu}) = \sqrt{\frac{1}{B}\sum_{b=1}^{B}(\hat{\mu}_b - \mu)^2}, \quad \text{MRE}(\hat{\mu}) = \frac{1}{B}\sum_{b=1}^{B}\frac{\hat{\mu}_b}{\mu}$$

and

$$\text{CP}(\hat{\mu}) = \frac{1}{B}\sum_{b=1}^{B}\mathbb{I}(\hat{\mu}_b \in (c_b, d_b)),$$

where $\mu \in \boldsymbol{\mu} = (\beta, \eta, \theta, \alpha)$ (is one of the four parameters), $\hat{\mu}_b$ is the estimate of the respective parameter μ of the b-th sample, $B = 1{,}000$ is the number of samples, $\mathbb{I}(\cdot)$ is the indicator function, $c_b = \hat{\mu}_b - 1.96 \times \text{SE}(\hat{\mu}_b)$ and $d_b = \hat{\mu}_b + 1.96 \times \text{SE}(\hat{\mu}_b)$, where $\text{SE}(\hat{\mu}_b)$ is the standard error of the b-th estimate $\hat{\mu}_b$.

It is expected that with the increasing number of systems and observation time (truncation), the asymptotic properties are achieved since the sample sizes of observed failure times also tend to increase. More specifically, it is expected that the RMSE criterion approaches zero, the MRE criterion approaches one, and the CP criterion is close to the nominal value 0.95 defined for the construction of the CIs. These indicators have been used in the reliability literature and their use is justified in several works (see, e.g., Junior (2021) and Brito, Tomazella and Ferreira (2022)).

4.1.4.1 Simulation Study for the Univariate Frailty ARA_m Model

Our interest is to generate, for k different and independent systems, a time-truncated sample $t_{i,1},\ldots,t_{i,n_i}$ of failure times so that $t_{i,n_i} \leq t_i^*$, where t_i^* is the truncation time of the system i, with $i = 1\ldots,k$. For the ARA_m class we will use the definition of virtual age itself to build a generator function of failure times. Remember that the virtual age is a function of the real age and it admits an inverse that is given by $V_t^{-1} = t + (1-\theta)S_t$. The idea is to use the inverse virtual age function and the inverse of the cumulative intensity function given in (4.2) to directly construct the desired sample of failure times.

Let $t_{i,j}$ be the j-th failure time of the i-th system and the elapsed time from j-th failure to the $(j+1)$-th failure be $x = t_{i,j+1} - t_{i,j}$. So the random variable X represents the time between two consecutive failures and the event $\{X > x\}$ refers to the non-occurrence of failures between the j-th and $(j+1)$-th failures. In this sense, $\mathbb{P}[X > x] = \mathbb{P}[N(t_{i,j}+x) - N(t_{i,j}) = 0]$, and therefore, the CDF $F(x)$ is given by $F(x) = 1 - e^{-\Lambda_{f.\text{ARA}_m}(t_{i,j}+x)+\Lambda_{f.\text{ARA}_m}(t_{i,j})}$, where $\Lambda_{f.\text{ARA}m}(t)$ is the cumulative intensity function for the frailty model in the ARA_m class, given by (4.2). As a direct consequence, we can rewrite

$$\Lambda_{f.\text{ARA}m}(t_{i,j}+x) = \Lambda_{f.\text{ARA}m}(t_{i,j}) - \log(1-F(x)), \tag{4.13}$$

where $0 \leq F(x) \leq 1$.

Let $V_{t_{i,j}}$ be the virtual age at time $t_{i,j}$ for the i-th system. By the equation (2.14), we can rewrite $\Lambda_{\text{ARA}_m}(t_{i,j})$ and $\Lambda_{\text{ARA}_m}(t_{i,j}+x)$ as $\Lambda(V_{t_{i,j}})$ and $\Lambda(V_{t_{i,j}+x})$, respectively. Hence, we can rewrite the equation (4.13) as $\Lambda(V_{t_{i,j}+x}) = \Lambda(V_{t_{i,j}}) - \log(1-F(x))$ and, as a direct result, we can write the time $t_{i,j+1} = (t_{i,j}+x)$ as

$$t_{i,j+1} = V^{-1}(\Lambda^{-1}(\Lambda(V_{t_{i,j}}) - \log(1-F(x)))). \tag{4.14}$$

Considering a failure-truncated process for each system i, with n_i observed points for the i-th system, a sample $\{u_{i,j}\}$ of size n_i from the Uniform$(0,1)$ distribution must be generated and $F(x)$ must be replaced by $u_{i,j}$ in the equation (4.14) for each j to obtain all the failure times $t_{i,j}$ of the i-th system under the frailty ARA_m class, for $j = 1,\ldots,n_i$. This procedure will be repeated k times to obtain the failure times sequences for the k independent systems.

Our interest in the simulation study is the time-truncated scenario and just as done in Section 3.3, it is necessary to make an adjustment so that the simulated times are lower than the predefined truncation time. We fix the truncation time t_i^* for each system i and repeat the previous process to generate times $t_{i,1}, t_{i,2},\ldots$ until the time t_i^* is exceeded. The time that exceeded the truncation time (say $t_{i,n+1}$) will be removed from the i-th sample.

Different parameter scenarios, truncation times, number of systems and failure memories were considered in this simulation study. We separated the presentation of the results based on the choice of three different memories of the failure process, considering memories $m = 1$,

$m = 10$ and $m = 20$. As the models' trend is a stability in relation to the increase of the failure memory, we opted for the memory $m = 20$ of failures as an approximation for the case $m = \infty$, without loss for comparison of obtained results in the simulation study.

With regard to the parameter of the PLP initial intensity function, we fixed the values: $\beta = 1.5$ and $\eta = 10$. For the repair effect parameter θ, we chose two intermediate values, $(0.4, 0.8)$, to try to avoid values close to the extremes 0 and 1, which would approximate the IR model to the PR model or the MR model. Regarding the frailty terms $Z_{i,j}$, for $i = 1, \ldots, k$ and $j = 1, \ldots, n_i$, we consider they are IID with Gamma$(1/\alpha, 1/\alpha)$ distribution, and assign the two values $(0.05, 0.2)$ for α. In order to verify the asymptotic properties of the MLEs, we considered four truncation times t^* for all systems, $(200, 1{,}000, 5{,}000, 10{,}000)$, since it is expected that more failures will be observed in longer observation periods, therefore, the generated samples will be larger. Finally, two amount of observed systems were considered, $k = (10, 30)$, totaling 32 different scenarios for each considered memory m. As said before, for each scenario we generate 1,000 Monte Carlo sample s and calculated the RMSE, MRE and CP. The results are summarized and shown in Figures 17, 18 and 19.

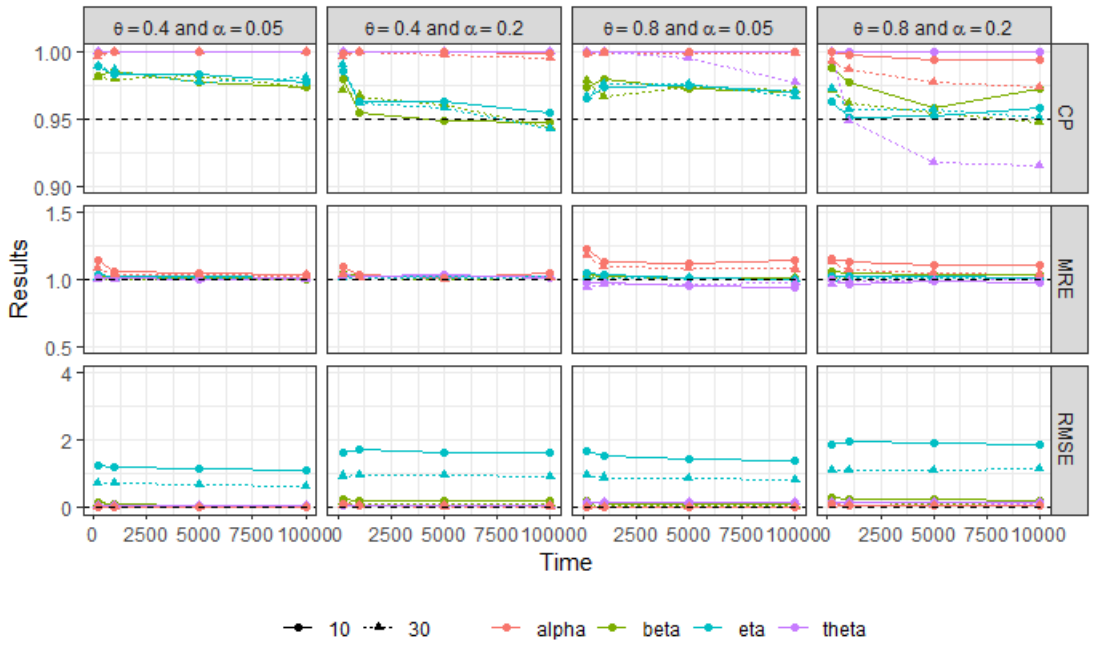

Figure 17 – Simulation results for the frailty ARA model in scenarios with memory $m = 1$.

On all graphs in Figures 17, 18 and 19, the solid lines indicate that 10 independent systems were considered, while the dotted lines indicate that 30 systems were considered. The number of systems impacts the sizes of the generated samples since the more systems are considered, the more recurrent failures will be observed and this difference is reflected in the observed results, especially for the RMSE. We can notice that for the three memories considered, the RMSE values for scenarios with 30 systems are always lower than those for scenarios with 10 systems. However, despite this difference, in both scenarios the expected convergence is

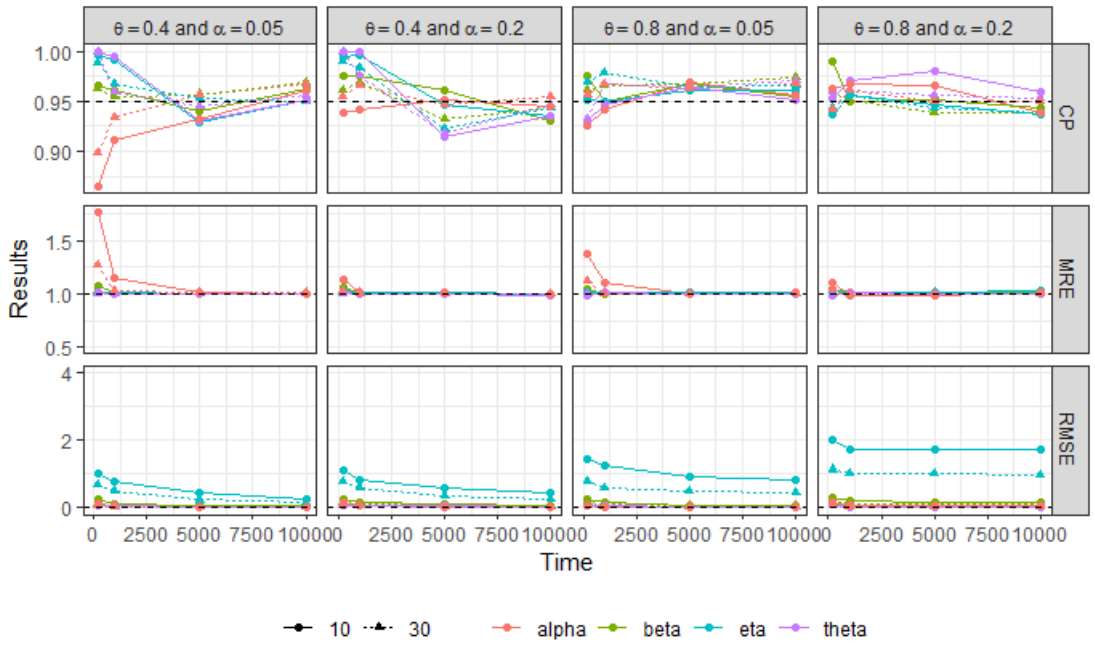

Figure 18 – Simulation results for the frailty ARA model in scenarios with memory $m = 10$.

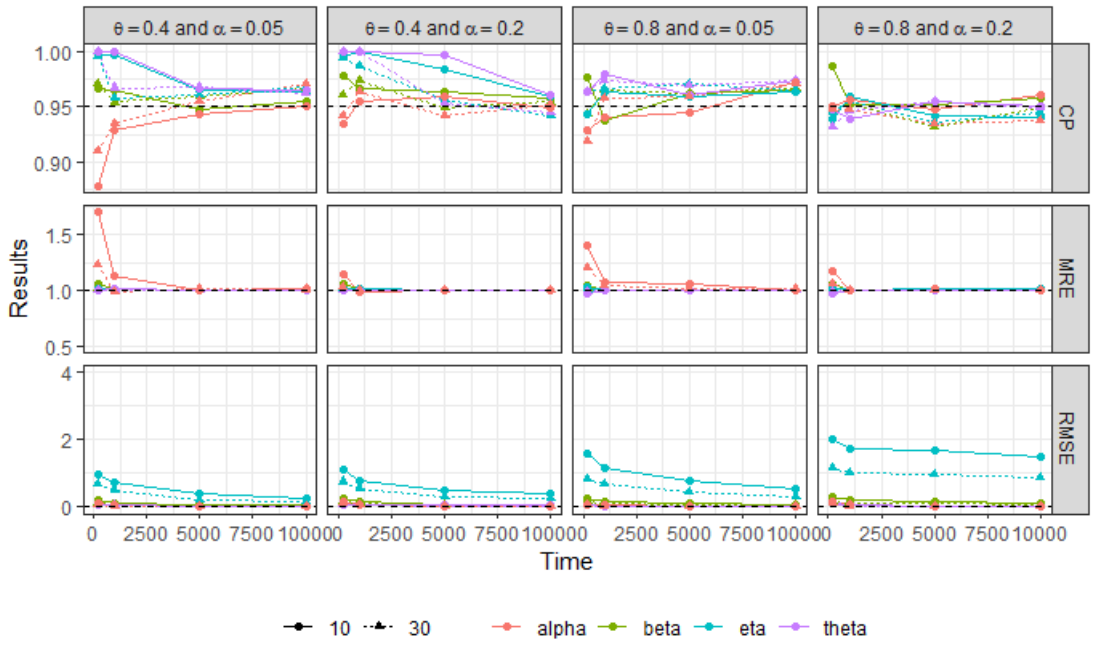

Figure 19 – Simulation results for the frailty ARA model in scenarios with memory $m = 20$.

observed as the truncated time increases (and, consequently, the size of the observed failure times samples). This convergence can also be observed for the other two indicators; although it occurs faster in the scenarios with 30 systems, it can also be clearly observed in the scenarios with 10 systems. These results indicate that the model works well asymptotically for different considered quantities of systems.

It is noticeable that the results referring to the MRE indicator are adequate since the

ratio between the estimated and the nominal values of the parameters are predominantly close to one for all scenarios, with some small differences occurring only when the samples are smaller (smaller truncation times and lower α values). Regarding the CP indicator, it is also noticeable that, in general, its estimates seem to be satisfactory since they are greater or converge to the nominal value of 0.95 or are very close to the expected value.

Comparing the results obtained by memory, we can see that the addition of memory impacts mainly on the convergence of RMSE indicators, since this convergence is faster for cases with memory $m = 20$. Furthermore, as the memory of the simulations was increased, the convergences of the indicators became more evident and the non-expected results decreased.

4.1.4.2 Simulation Study for the Univariate Frailty ARI_m Model

In order to generate the failure times sample of k independent systems under the univariate frailty ARI_m model discussed in Section 4.1.1, we followed the idea of the algorithm presented in Toledo (2014), where an approach to generate failure histories for systems under the ARA_1 class and PLP initial intensity function was proposed. We generalized that idea to any ARI_m class (considering the last m observed failure times) and adapted the intensity functions for our case with the univariate frailty model context.

Let $t_{i,j}$ be the j-th failure time of the i-th system and $x = t_{i,j+1} - t_{i,j}$ be the elapsed time from j-th to the $(j+1)$-th failure. For the same reasons discussed in Section 4.1.4.1, the CDF for the random variable X is given by

$$F(x) = 1 - e^{-\Lambda_{f.\text{ARI}_m}(t_{i,j}+x)+\Lambda_{f.\text{ARI}_m}(t_{i,j})}, \tag{4.15}$$

where $\Lambda_{f.\text{ARI}m}(t)$ is the cumulative intensity function for the frailty ARI_m model, given by (4.4).

For each system i a sample $\{u_{i,j}\}$ of size n_i from the Uniform$(0,1)$ distribution will be generated and $F(x)$ will be replaced by $u_{i,j}$ in the equation (4.15) for each j to obtain all the failure times $t_{i,j}$ of this system i, with $j = 1,\ldots,n_i$. This procedure will be repeated for all system i with $i = 1,\ldots,k$ to complete the failure time processes for the k simulated systems. As in the ARA_m case, for the time-truncated case a time of truncation t_i^* is defined for the system i and repeat the previous process to generate times $t_{i,1}, t_{i,1}, \ldots$ until to get the first failure time greater than t_i^* (say $t_{i,n+1}$).

All the parameters chosen for the sample simulations in the ARI case were the same as in the ARA case in the previous subsection. Once again, in order to verify the asymptotic properties of the MLEs, we considered four truncation times t^* for all systems, for the same reasons presented in the previous subsection. Summaries of the results are shown in Figures 20, 21 and 22.

As in the ARA case, here in the case of the frailty ARI models it is expected that in the scenarios observed for a longer period of time and with more systems under study, larger

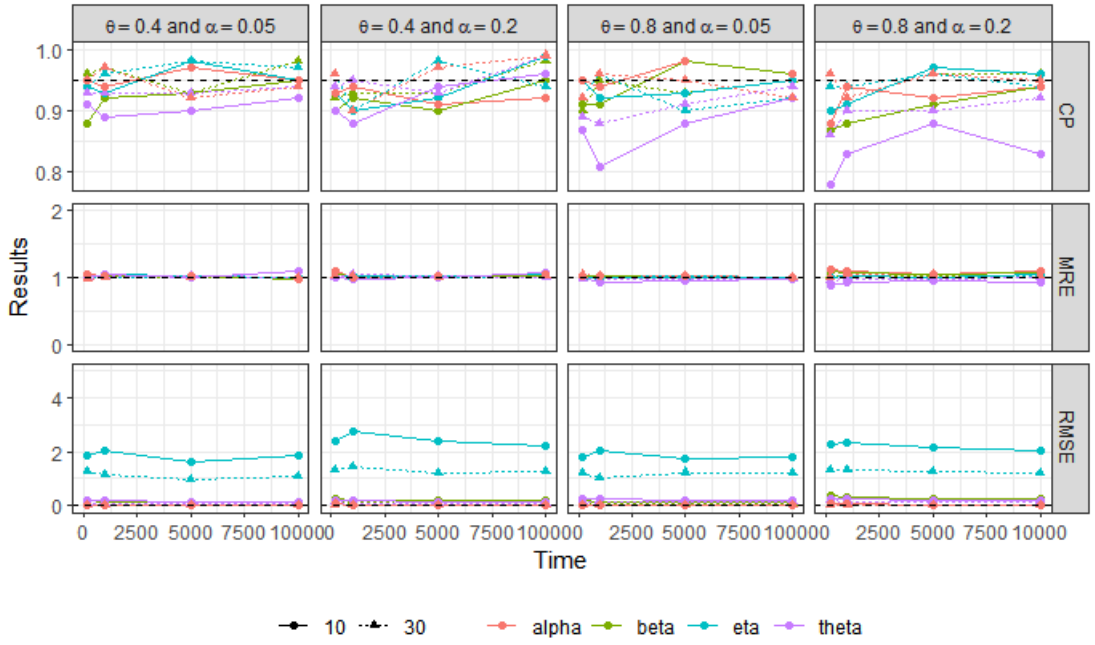

Figure 20 – Simulation results for the frailty ARI model in scenarios with memory $m = 1$.

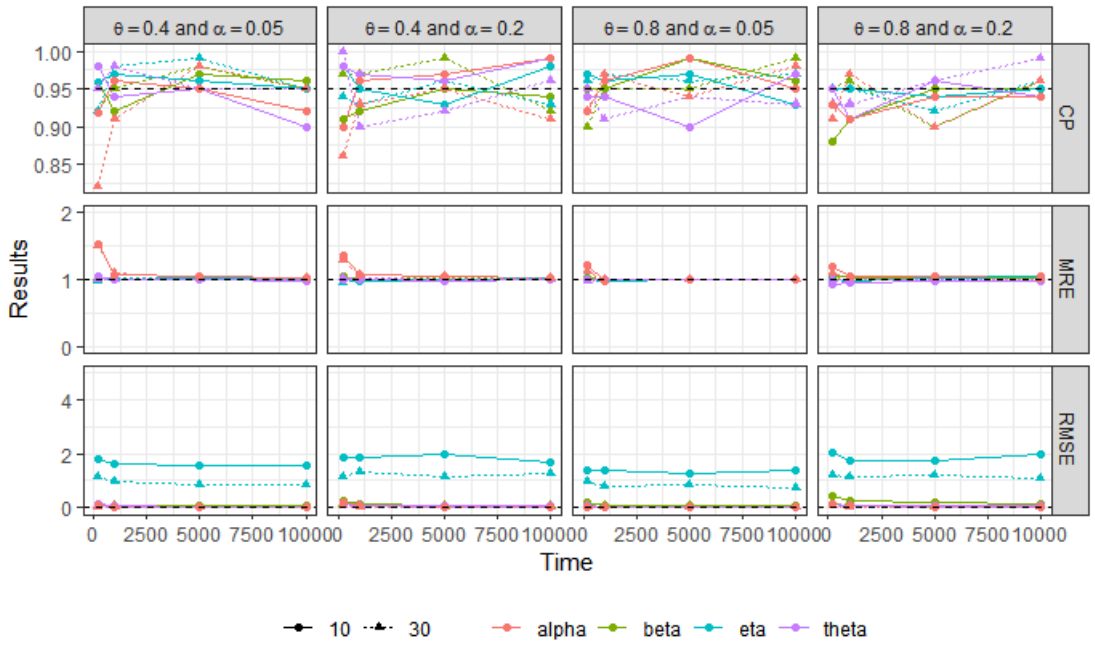

Figure 21 – Simulation results for the frailty ARI model in scenarios with memory $m = 10$.

samples of failure times will be generated and, consequently, will present better asymptotic results of consistency and efficiency. In general, we can see that this actually happens, since in all considered scenarios of parameters and memories, the RMSE of situations with 30 independent systems (dotted line) were always smaller than those of situations with 10 systems (solid line). Furthermore, in all scenarios the estimated RMSE approaches the expected value zero as the observation time increases for all parameters in both situations with 10 or 30 systems (in this

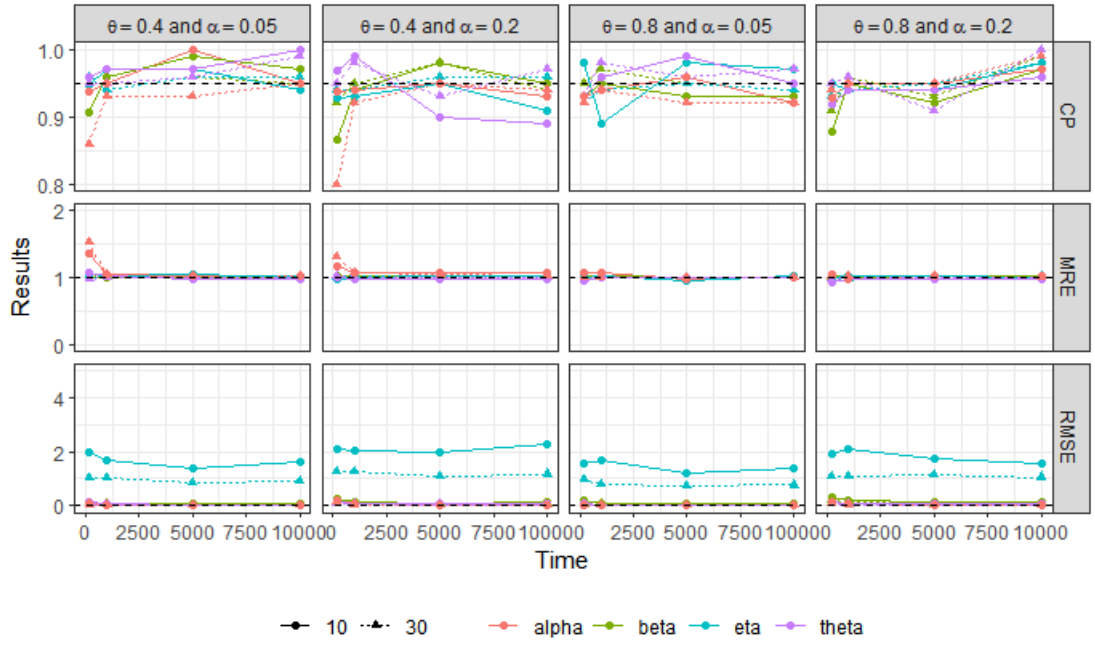

Figure 22 – Simulation results for the frailty ARI model in scenarios with memory $m = 20$.

case, with 30 systems approaching faster, as expected), although for parameter η a discrepancy is perceived due to the magnitude of the nominal value defined for this parameter.

Regarding the CP indicator, in general the nominal values of 0.95 were reached in almost all scenarios. The discrepancies are mostly perceived in situations with 10 systems and in combinations of θ and α parameters that result in the generation of small samples of observed failure times. However, it is noticeable that in most cases the desired coverage of the 95% CI is achieved for all parameters in longer observation times. The increase in memory for the ARI models showed good results in the simulation study for the CP indicator. It is noticeable that for the memory $m = 20$ (Figure 22), the nominal values were obtained more quickly than for the smaller memories (Figures 20 and 21) and without large fluctuations over time. These results attest to the quality of the asymptotic estimators defined for the model parameters, but it is still necessary to verify the relationship between the θ and α parameters and how it contributes to the variation in CP over time observed in some scenarios of Figures 20 and 21.

In all scenarios, the good behavior of the MRE indicator is remarkable, since the ratio between the estimated value and the nominal value for all parameters converged to the expected value of 1 without major problems, especially for larger samples.

4.1.5 Real Data Application - Sugarcane Harvester Data Revisited

In this section, we revisited the real data set presented in Section 3.4 to illustrate the procedures discussed for frailty IR models, that is, the data that describes the failure times of 9 sugarcane harvesters observed for 200 days (time-truncated case). The MLEs for the frailty

ARA_m and ARI_m classes were estimated and the estimation was performed considering, for both classes, all possible memories m, that is, $m = 1, \ldots, \max\{n_i\}$, where n_i is number of failures of the i-th system, for $i = 1, \ldots, k$.

As a criterion for model selection in each class with different memories, only the maximum estimated value of the log-likelihood function $\hat{l}$ was used, since in these cases all models have the same number of parameters. The best models of the frailty ARA_m and ARI_m classes were also compared with the frailty MR and frailty PR models studied in Section 3.4, and in this case, the AIC and BIC criteria were used to decide the best-fit model for the data set.

The likelihood function (4.5) and log-likelihood function (4.6) for the frailty ARA_m class, and the respective functions (4.7) and (4.8) for the frailty ARI_m class of IR models were maximized using numerical methods to obtain the estimates $\hat{\beta}$, $\hat{\eta}$, $\hat{\theta}$ and $\hat{\alpha}$ for the desired parameters considering each class and each memory m.

As the highest number of failures observed among the harvesters was 19 failures, the estimation was performed for all possible values of m, that is, from 1 to 19. The maximum estimated value of the log-likelihood function $\hat{l}$ was used to verify which of these 19 models best fits the data, since all these models have the same number of parameters. The summary of these values for both ARA_m and ARI_m classes is presented in Figure 23.

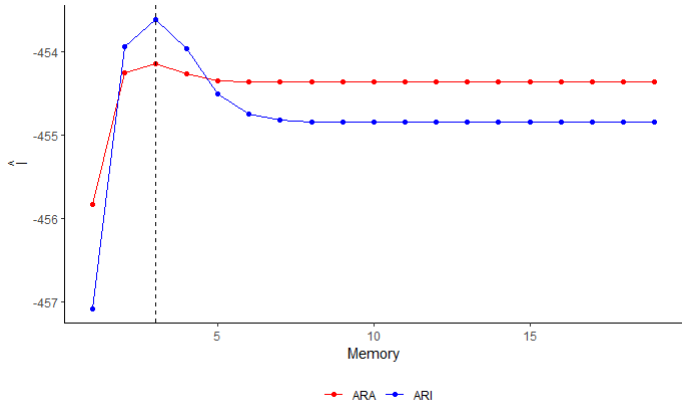

Figure 23 – Estimated maximum log-likelihood values $\hat{l}$ per memory m, for the sugarcane harvester data.

By these results, we can conclude that the models that best fit the harvester data set, among the possible ARA_m and ARI_m classes, are the models with memory $m = 3$, for both ARA and ARI classes, since they have the highest estimate for the maximum of the log-likelihood function in each context. Note that from memory $m = 7$ onwards, the log-likelihood of the models stabilizes for both classes, which was expected since the contribution of information from very old failures gradually approaches zero, becoming irrelevant for the estimation process.

The MLE results for each parameter of the frailty ARA_3 and frailty ARI_3 classes and their respective 95% CI are described in Table 3. For comparison purposes, the results presented

in Table 1 are also listed in this table for the parameter estimates of the frailty MR and frailty PR models for this same data set.

Table 3 – MLE results for the frailty MR, PR, ARA_9 and ARI_3 models applied to sugarcane harvester data.

	$\hat{\beta}$ (95% $CI_{\hat{\beta}}$)	$\hat{\eta}$ (95% $CI_{\hat{\eta}}$)	$\hat{\theta}$ (95% $CI_{\hat{\theta}}$)	$\hat{\alpha}$ (95% $CI_{\hat{\alpha}}$)
MR	1.11 (0.79, 1.55)	14.27 (8.75, 23.28)	-	0.038 (0.004, 0.364)
PR	1.32 (1.14, 1.53)	15.02 (13.11, 17.20)	-	$5.6\ (5.3, 5.9)\times 10^{-7}$
ARA_3	1.71 (1.31, 2.21)	15.44 (11.96, 19.90)	0.25 (0.10, 0.49)	0.047 (0.015, 0.155)
ARI_3	1.73 (1.45, 2.07)	13.82 (10.03, 19.04)	0.33 (0.21, 0.47)	0.016 (0.011, 0.024)

As stated before, to choose the model that best fits this data set, the AIC and BIC criteria of the frailty ARA_3 and ARI_3 models were calculated and also compared to the obtained values presented in Section 3.4 referring to the frailty MR and PR models. The results of the information criteria for the four compared models are shown in Table 4.

Table 4 – AIC and BIC results for the frailty MR, PR, ARA_3 and ARI_3 models applied to the sugarcane harvester data.

	$\hat{l}$	AIC	BIC
MR	-463.26	932.53	941.06
PR	-457.36	920.72	929.25
ARA_3	-454.15	916.30	927.68
ARI_3	-453.61	915.24	926.61

From Table 4, we can conclude that the ARI_3 model is the most parsimonious, since its related AIC and BIC have lower values than the respective values for the frailty MR, PR and ARA_3 models. Therefore, the ARI_3 model is the one chosen to adjust the harvesters' failure times.

Initially interpreting the results obtained for the parameter α, it can be concluded that the estimate $\hat{\alpha}$ and its respective 95% CI are significantly different from zero, since the lower limit of the CI is minimally distant from zero. Such results indicate that the model captured the existence of unobserved heterogeneity between the failure times of the observed systems, since the estimate of the variance of the frailty effect (parameter α) is non-zero. In practice, this indicates that there are non-quantifiable factors that interfere in the failure process of all sugarcane harvesters and specifically on each observed failure time.

The existence of unobserved heterogeneity excludes the original interpretability of the parameter η for models under PLP, since the individual frailties have a multiplicative impact on the baseline intensity function of the frailty model as described in equation (2.20). On the other hand, for the parameter β, the original interpretation remains and, in this case, as the estimate $\hat{\beta}$ is greater than 1 (as well as its respective 95% CI does not contain the value 1), it can be concluded that the machines under study are deteriorating over time.

Regarding parameter θ, the estimate $\hat{\theta}$ and its respective 95% CI obtained by the frailty ARI_3 model did not approach 1 or 0, which would indicate the particular cases of MR or PR. This means that the proposed model identified the existence of effects of the repairs performed and, in addition, it was able to quantify the reduction in the intensity of failures resulting from these repairs. Note that in Section 3.4 we concluded that the frailty PR model was superior to the fit of these data compared to the MR model, but here we concluded that both IR models were superior to the previous two. This result indicates evidence that the repairs carried out on these harvesters caused some impact, leaving them in an intermediate operating condition between ABAO and AGAN, as discussed in Section 2.2.3.

As proposed in Section 3.4, the graphical procedure presented in Toledo *et al.* (2015) was used to verify the quality of adjustment for the best frailty ARA and ARI class models, but now, by comparing the empirical MCF of the observed failure times with the average of the MCFs estimated by the frailty ARA_3 and ARI_3 models (equations (4.2) and (4.4), respectively) from each system. The goodness-of-fit plot comparison is shown in Figure 24 with the empirical and estimated (from frailty ARA_3 and ARI_3 models) MCFs. It is notable that the curves of the empirical MCF and the average of systems' MCFs are close for both the ARA and ARI models and this behavior attests to the quality of both adjustments.

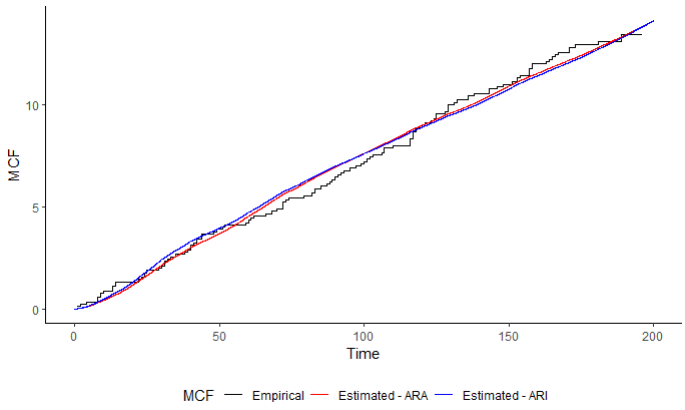

Figure 24 – Empirical and estimated MCFs for the harvesters' failure times, in the frailty ARA_3 and ARI_3 models.

As the fits are reasonable, we are finally able to estimate the predicted reliability for each sugarcane harvester from its last observed failure, according to the two proposed frailty models. The reliability curves related to both frailty ARA_3 and ARI_3 models are drawn from their corresponding obtained estimates, that is, they are obtained replacing the respective estimates $\hat{\beta}$, $\hat{\eta}$, $\hat{\theta}$ and $\hat{\alpha}$ from each frailty ARA_3 and ARI_3 models in the equations (4.10) and (4.11). Using the estimates obtained by the frailty ARI_3 model (best fitted model), it is also possible to calculate the MTTF after the last observed failure of each system, in this case, replacing the parameter estimates in equation (4.12). The resulting predicted reliability graphs and MTTFs are shown in Figure 25.

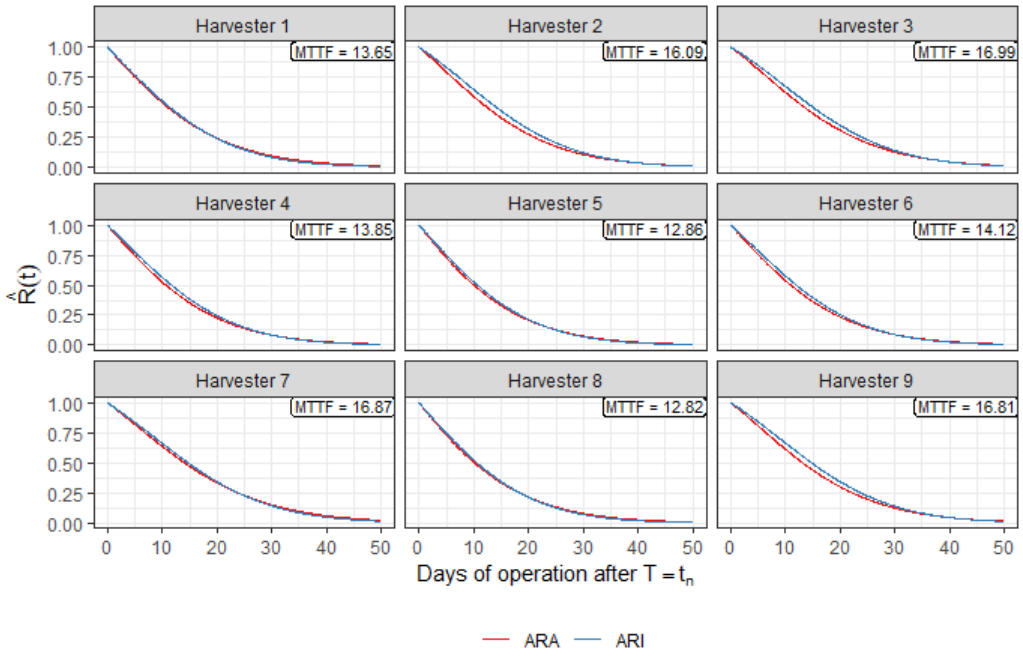

Figure 25 – Estimated reliability functions and MTTFs$_{ARI_3}$ at last failure time t_n, for each harvester in the data set, under the fitted frailty ARA$_3$ and ARI$_3$ models.

By Figure 25, it can be seen that for all the sugarcane harvesters, given the entire history of each failure process, the reliability probability is very close to zero for 40 days onward after the last failure. Moreover, the harvesters' MTTFs (from their last observed failure) range from approximately 13 to 17 days. This information is extremely relevant for the producers who own these machines, as it allows them to establish preventive and/or corrective maintenance strategies in order to reduce the financial losses caused by the failures of these machines, especially in high harvest periods.

4.2 Shared Unobserved Heterogeneity in IR Model

In this section we propose shared frailty models for multiple repairable systems subjected to IR after each failure. In the reliability literature, shared frailty models are well established for the analysis of failure times of repairable systems. However, there is still not much attention paid to models that consider IR even though this type of repair is more plausible than MR and PR in the real world. As previously mentioned, in his recent work, Liu *et al.* (2020) presented a shared frailty model with Gamma distribution for the ARA$_1$ and ARA$_\infty$ classes of IR. In this sense, our objective is to propose a shared frailty model that generalizes the one presented by the authors, considering a general ARA$_m$ class of repairs and similarly establishing the shared frailty model for the general ARI$_m$ class.

The idea of this section is very similar to Section 4.1, that is, we will propose general shared Gamma frailty models for systems under IR considering both ARA$_m$ and ARI$_m$ classes

and all their possible memories m. Here, we will again assume that the frailty variables Z_i are IID with a Gamma$\left(\frac{1}{\alpha},\frac{1}{\alpha}\right)$ distribution, just like in the previous models.

4.2.1 The Shared Frailty ARA$_m$ and ARI$_m$ Models

In our shared frailty models, the assumptions about the systems are the same defined in the previous sections: k systems observed for a time t_i^* (truncation scenario by time), where $t_{i,j}$ is the j-th failure time of the i-th system, with $i=1,\ldots,k$, $j=1,\ldots,n_i$ and n_i being the number of observed failures of the i-th system. As discussed in Section 2.3.2, in the context of shared frailty a random variable Z_i is multiplicatively associated with the baseline intensity function of each system and, so that the failure times of a system share this same effect. Just to recall, the intensity function conditional on the frailty term is given by $\lambda_f(t_{i,j}\mid z_i)=z_i\underline{\lambda}(t_{i,j})$, where $\underline{\lambda}(t)$ is the baseline function.

Thus, the shared frailty model considering the ARA$_m$ class is obtained by simply assuming that the baseline function $\underline{\lambda}(t)$ is given by the intensity function of the ARA$_m$ class defined by (2.13), obtaining the expression

$$\lambda_{f.\mathrm{ARA}m}(t_{i,j}\mid z_i)=z_i\lambda_{\mathrm{ARA}m}(t_{i,j})=z_i\lambda_0\left(t_{i,j}-(1-\theta)\sum_{p=0}^{\min(m-1,j-2)}\theta^p t_{i,j-1-p}\right), \qquad (4.16)$$

where $\lambda_0(t)$ is the initial intensity function. The cumulative intensity function is obtained in analogous way.

Considering again that the initial function follows a PLP, function (4.16) can be rewritten as

$$\lambda_{f.\mathrm{ARA}m}(t_{i,j}\mid z_i)=z_i\frac{\beta}{\eta^\beta}\left(t_{i,j}-(1-\theta)\sum_{p=0}^{\min(m-1,j-2)}\theta^p t_{i,j-1-p}\right)^{\beta-1}.$$

The construction of the shared frailty model for the ARI$_m$ class is completely similar to the construction for the ARA$_m$ class above, now, using the ARI$_m$ intensity function defined by (2.16) as baseline function. The conditional failure intensity function in the shared frailty ARI$_m$ class context is given by

$$\lambda_{f.\mathrm{ARI}m}(t_{i,j}\mid z_i)=z_i\lambda_{\mathrm{ARI}m}(t_{i,j})=z_i\left[\lambda_0\left(t_{i,j}\right)-(1-\theta)\sum_{p=0}^{\min(m-1,j-2)}\theta^p\lambda_0\left(t_{i,j-1-p}\right)\right], \qquad (4.17)$$

where $\lambda_0(t)$ is the initial intensity function. The cumulative intensity function is obtained in analogous way.

Once again considering that the initial intensity function follows a PLP process, the function (4.17) can be rewritten as

$$\lambda_{f.\mathrm{ARI}m}(t_{i,j}\mid z_i)=z_i\frac{\beta}{\eta^\beta}\left[t_{i,j}^{\beta-1}-(1-\theta)\sum_{p=0}^{\min(m-1,j-2)}\theta^p t_{i,j-1-p}^{\beta-1}\right].$$

4.2.2 Parameter Estimation for the Shared Frailty ARA$_m$ and ARI$_m$ Models

As in Section 4.1.2, our interest now is to obtain the parameter estimates in a classical approach. Once again, the likelihood method will be adopted and, in this case, it will be necessary to follow the same steps discussed in Section 2.3.2 to obtain the expression (2.30) of the likelihood unconditional on the frailty term for both shared frailty ARA$_m$ and ARI$_m$ models. The difference will occur in the choice of the general likelihood function, according to the analyzed model as we will see below.

For the shared frailty ARA$_m$ model we use the general likelihood function of the ARA$_m$ model given by (2.15), and then proceed with obtaining the marginal likelihood, as follows:

$$\begin{aligned}
L_{f.\mathrm{ARA}m}(\boldsymbol{\mu} \mid t_{i,j}) &= \prod_{i=1}^{k} \int_0^{\infty} \left(\prod_{j=1}^{n_i} z_i \lambda_{\mathrm{ARA}m}\left(t_{i,j}\right) e^{-z_i\left[\Lambda_{\mathrm{ARA}_m}\left(t_{i,j}\right)-\Lambda_{\mathrm{ARA}_m}\left(t_{i,j-1}\right)\right]} \right) \\
&\quad \times e^{-z_i\left[\Lambda_{\mathrm{ARA}_m}\left(t_i^*\right)-\Lambda_{\mathrm{ARA}_m}\left(t_{i,n_i}\right)\right]} f_{Z_i}(z_i) dz_i \\
&= \prod_{i=1}^{k} \left(\prod_{j=1}^{n_i} \lambda_{\mathrm{ARA}m}(t_{i,j}) \right) \int_0^{\infty} z_i^{n_i} \exp\left(-z_i \sum_{j=1}^{n_i} \left[\Lambda_{\mathrm{ARA}m}\left(t_{i,j}\right) - \Lambda_{\mathrm{ARA}m}\left(t_{i,j-1}\right) \right] \right) \\
&\quad \times \exp\left(-z_i \left[\Lambda_{\mathrm{ARA}m}\left(t_i^*\right) - \Lambda_{\mathrm{ARA}m}\left(t_{i,n_i}\right) \right] \right) f_{Z_i}(z_i) dz_i \\
&= \prod_{i=1}^{k} \left(\prod_{j=1}^{n_i} \lambda_0(t_{i,j} - (1-\theta) s(t_{i,j-1})) \right) \int_0^{\infty} z_i^{n_i} \exp\left(-z_i W_{\mathrm{ARA}m} \right) f_{Z_i}(z_i) dz_i,
\end{aligned}$$

where

$$\begin{aligned}
W_{\mathrm{ARA}m} = \sum_{j=1}^{n_i} &\left[\Lambda_0\left(t_{i,j} - (1-\theta) s(t_{i,j-1})\right) - \Lambda_0\left(t_{i,j-1} - (1-\theta) s(t_{i,j-1})\right) \right] \\
&+ \left[\Lambda_0\left(t_i^* - (1-\theta) s(t_{i,n_i})\right) - \Lambda_0\left(t_{i,n_i} - (1-\theta) s(t_{i,n_i})\right) \right]
\end{aligned}$$

where $\lambda_0(t)$ and $\Lambda_0(t)$ are, respectively, the initial intensity and cumulative intensity functions.

Now, assuming that the frailty variables Z_i have a common Gamma$\left(\frac{1}{\alpha}, \frac{1}{\alpha}\right)$ distribution $(i = 1, \ldots, k)$, similarly to what we did to obtain the equation (2.30), we obtain the following likelihood function unconditional to the Gamma frailty term:

$$L_{f.\mathrm{ARA}m}(\boldsymbol{\mu} \mid t_{i,j}) = \prod_{i=1}^{k} \frac{\alpha^{n_i} \Gamma\left(n_i + \frac{1}{\alpha}\right) \prod_{j=1}^{n_i} \lambda_0(t_{i,j} - (1-\theta) s(t_{i,j-1}))}{\Gamma\left(\frac{1}{\alpha}\right) \left(1 + \alpha W_{\mathrm{ARA}m}\right)^{n_i + \frac{1}{\alpha}}}. \tag{4.18}$$

The equation (4.18) can be rewritten by replacing the initial functions $\lambda_0(t)$ and $\Lambda_0(t)$ with the PLP model functions given by (2.3) and (2.4), respectively, as done for the models discussed in the previous sections, obtaining:

$$L_{f.\mathrm{ARA}m}(\boldsymbol{\mu} \mid t_{i,j}) = \prod_{i=1}^{k} \frac{\left(\frac{\beta\alpha}{\eta^{\beta}}\right)^{n_i} \Gamma\left(n_i + \frac{1}{\alpha}\right) \prod_{j=1}^{n_i} \left(t_{i,j} - (1-\theta) s(t_{i,j-1})\right)^{\beta-1}}{\Gamma\left(\frac{1}{\alpha}\right) \left(1 + \frac{\alpha}{\eta^{\beta}} W^*_{\mathrm{ARA}m}\right)^{n_i + \frac{1}{\alpha}}}, \tag{4.19}$$

where

$$W^*_{\text{ARA}m} = \sum_{j=1}^{n_i} \left[\left(t_{i,j} - (1-\theta)s(t_{i,j-1}) \right)^{\beta} \right) - \left(t_{i,j-1} - (1-\theta)s(t_{i,j-1}) \right) \right)^{\beta} \Big] + \left[(t_i^* - (1-\theta)s(t_{i,n_i}) \right))^{\beta} - (t_{i,n_i} - (1-\theta)s(t_{i,n_i})))^{\beta} \right].$$

The log-likelihood function is given by

$$\begin{aligned} l_{f.\text{ARA}m}(\boldsymbol{\mu} \mid t_{i,j}) = {} & N[\log(\beta) + \log(\alpha) - \beta \log(\eta)] + \sum_{i=1}^{k} \log\Gamma\left(n_i + \frac{1}{\alpha} \right) \\ & + (\beta - 1) \sum_{i=1}^{k} \sum_{j=1}^{n_i} \log\left(t_{i,j} - (1-\theta)s(t_{i,j-1}) \right) - \sum_{i=1}^{k} \log\Gamma\left(\frac{1}{\alpha} \right) \\ & - \sum_{i=1}^{k} \left(n_i + \frac{1}{\alpha} \right) \log\left(1 + \frac{\alpha}{\eta^{\beta}} W^*_{\text{ARA}m} \right). \end{aligned} \tag{4.20}$$

For the shared frailty ARI_m model, the likelihood function for the shared frailty ARI_m model is given by replacing equation (2.19) into the equation of unconditional likelihood (2.30), obtaining:

$$\begin{aligned} L_{f.\text{ARI}m}(\boldsymbol{\mu} \mid t_{i,j}) = {} & \prod_{i=1}^{k} \int_0^{\infty} \left(\prod_{j=1}^{n_i} z_i \lambda_{\text{ARI}m}\left(t_{i,j} \right) e^{-z_i \left[\Lambda_{\text{ARI}_m}\left(t_{i,j} \right) - \Lambda_{\text{ARI}_m}\left(t_{i,j-1} \right) \right]} \right) \\ & \times e^{-z_i \left[\Lambda_{\text{ARI}_m}\left(t_i^* \right) - \Lambda_{\text{ARI}_m}\left(t_{i,n_i} \right) \right]} f_{Z_i}(z_i) dz_i \\ = {} & \prod_{i=1}^{k} \left(\prod_{j=1}^{n_i} \lambda_{\text{ARI}m}(t_{i,j}) \right) \int_0^{\infty} z_i^{n_i} \exp\left(- z_i \sum_{j=1}^{n_i} \left[\Lambda_{\text{ARI}m}\left(t_{i,j} \right) - \Lambda_{\text{ARI}m}\left(t_{i,j-1} \right) \right] \right) \\ & \times \exp\left(- z_i \left[\Lambda_{\text{ARI}m}\left(t_i^* \right) - \Lambda_{\text{ARI}m}\left(t_{i,n_i} \right) \right] \right) f_{Z_i}(z_i) dz_i \\ = {} & \prod_{i=1}^{k} \left(\prod_{j=1}^{n_i} \left[\lambda_0(t_{i,j}) - (1-\theta)\underline{s}(t_{i,j-1}) \right] \right) \int_0^{\infty} z_i^{n_i} \exp\left(- z_i W_{\text{ARI}m} \right) f_{Z_i}(z_i) dz_i, \end{aligned}$$

where

$$W_{\text{ARI}m} = \sum_{j=1}^{n_i} \left[\Lambda_0(t_{i,j}) + \Lambda_0(t_{i,j-1}) + (t_{i,j} - t_{i,j-1})(1-\theta)\underline{s}(t_{i,j-1}) \right] + \left[\Lambda_0(t_{i^*}) + \Lambda_0(t_{i,n_i}) + (t_{i^*} - t_{i,n_i})(1-\theta)\underline{s}(t_{i,n_i}) \right]$$

and $\lambda_0(t)$ and $\Lambda_0(t)$ are, respectively, the initial intensity and cumulative intensity functions.

Assuming that the frailty variables Z_i have a common $\text{Gamma}\left(\frac{1}{\alpha}, \frac{1}{\alpha} \right)$ distribution ($i = 1, \ldots, k$), the likelihood function unconditional to the Gamma frailty term is given by

$$L_{f.\text{ARI}m}(\boldsymbol{\mu} \mid t_{i,j}) = \prod_{i=1}^{k} \frac{\alpha^{n_i} \Gamma\left(n_i + \frac{1}{\alpha} \right) \prod_{j=1}^{n_i} \left[\lambda_0(t_{i,j}) - (1-\theta)\underline{s}(t_{i,j-1}) \right) \right]}{\Gamma\left(\frac{1}{\alpha} \right) \left(1 + \alpha W_{\text{ARI}m} \right)^{n_i + \frac{1}{\alpha}}}.$$

Finally, replacing the initial functions $\lambda_0(t)$ and $\Lambda_0(t)$ with the PLP model functions given by (2.3) and (2.4), respectively, the equation (4.18) can be rewritten as

$$L_{f.\mathrm{ARI}m}(\boldsymbol{\mu} \mid t_{i,j}) = \prod_{i=1}^{k} \frac{\left(\frac{\beta\alpha}{\eta^{\beta}}\right)^{n_i} \Gamma\left(n_i + \frac{1}{\alpha}\right) \prod_{j=1}^{n_i} \left[t_{i,j}^{\beta-1} - (1-\theta)\underset{\sim}{s}(t_{i,j-1})\right]}{\Gamma\left(\frac{1}{\alpha}\right) \left(1 + \frac{\alpha}{\eta^{\beta}} W^{*}{}_{\mathrm{ARI}m}\right)^{n_i + \frac{1}{\alpha}}}, \tag{4.21}$$

where

$$W^{*}{}_{\mathrm{ARI}m} = \sum_{j=1}^{n_i} \left[t_{i,j}^{\beta-1} + t_{i,j-1}^{\beta-1} + \beta(t_{i,j} - t_{i,j-1})(1-\theta)\underset{\sim}{s}(t_{i,j-1})\right] + \left[t_{i^*}^{\beta-1} + t_{i,n_i}^{\beta-1} + \beta(t_{i^*} - t_{i,n_i})(1-\theta)\underset{\sim}{s}(t_{i,n_i})\right].$$

The log-likelihood function is given by

$$\begin{aligned} l_{f.\mathrm{ARI}m}(\boldsymbol{\mu} \mid t_{i,j}) = {} & N[\log(\beta) + \log(\alpha) - \beta\log(\eta)] + \sum_{i=1}^{k} \log\Gamma\left(n_i + \frac{1}{\alpha}\right) \\ & + \sum_{i=1}^{k}\sum_{j=1}^{n_i} \log\left(t_{i,j}^{\beta-1} - (1-\theta)\underset{\sim}{s}(t_{i,j-1})\right) - \sum_{i=1}^{k} \log\Gamma\left(\frac{1}{\alpha}\right) \\ & - \sum_{i=1}^{k} \left(n_i + \frac{1}{\alpha}\right) \log\left(1 + \frac{\alpha}{\eta^{\beta}} W^{*}{}_{\mathrm{ARI}m}\right). \end{aligned} \tag{4.22}$$

Note that again, for both ARA_m and ARI_m classes we construct the likelihood and log-likelihood functions for the more general case with time truncation. The particular functions for the failure truncation case are again obtained just by replacing t_i^* in equations (4.19), (4.20), (4.21) and (4.22) by the last observed failure time t_{i,n_i} for each system i.

Estimates of the parameters $\boldsymbol{\mu} = (\beta, \eta, \theta, \alpha)$ are obtained by maximizing the log-likelihood functions (4.20) and (4.22) for the ARA_m and ARI_m models, respectively. Note that, once again, we obtained very complex functions with equally complex derivatives, which makes it impossible to obtain an analytical solution to these optimization problems. Therefore, numerical methods aided by the *R statistics* software will again be used to obtain the MLEs. Finally, the interval estimates for the both models parameters will be built using the asymptotic theory based on the Normal distribution as a direct consequence of MLEs properties.

4.2.3 Reliability Predictors for Shared Frailty ARA_m and ARI_m Models

In this section, as is Section 4.1.3, we will define the reliability prediction functions for the proposed shared frailty models. The idea is again to estimate the probability of a new failure occurring in a system in a given time interval based on its failure history.

Given a system i, let $T_{i,n_i} = t_{i,n_i}$ be its last observed failure time and let t be the time until the next failure. Given the estimate of the frailty term $\hat{z}_i$ fo the system i and its failure history

$\mathscr{H}_{t_{i,n_i}}$ until the last observed failure t_{i,n_i}, our interest is to estimate the time $t = T_{i,n_i+1} - t_{i,n_i}$ until the next failure. Remember that the general reliability prediction function at time t is given by (4.9), which, in this case, can be rewritten as

$$R(t) = \mathbb{P}[T_{i,n_i+1} - t_{i,n_i} > t \mid \mathscr{H}_{t_{i,n_i}}] = \exp\left\{-\hat{z}_i \int_{t_{i,n_i}}^{t_{i,n_i}+t} \underline{\lambda}(u)\, du\right\}, \tag{4.23}$$

where $\underline{\lambda}(t)$ is the baseline intensity function of the shared frailty model, and $t_{i,n_i} \leq u \leq t_{i,n_i} + t < T_{i,n_i+1}$. Due the fact that the frailty variables Z_i are assumed to be IID with a Gamma$\left(\frac{1}{\alpha}, \frac{1}{\alpha}\right)$ distribution, the estimates $\hat{z}_i$ are obtained by the equation (2.33) as presented in Section 2.3.3. As discussed in Section 4.2.1, we can simply use the intensity functions of the ARA$_m$ and ARI$_m$ classes as the baseline function in equation (4.23) to obtain the desired reliability predictors for each shared frailty model.

For the shared frailty ARA$_m$ model, taking the ARA$_m$ intensity function presented in (2.13) and assuming the PLP as initial intensity function (2.3), we obtain the reliability prediction function $R(t) = R_{f.\mathrm{ARA}m}(t)$ as follows:

$$\begin{aligned} R(t) &= \exp\left\{-\hat{z}_i \int_{t_{i,n_i}}^{t_{i,n_i}+t} \lambda_{\mathrm{ARA}m}(u)\, du\right\} \\ &= \exp\left\{-\frac{\hat{z}_i}{\eta^\beta}\left[(t_{i,n_i} + t - (1-\theta)s(t_{i,n_i}))^\beta - (t_{i,n_i} - (1-\theta)s(t_{i,n_i}))^\beta\right]\right\}. \end{aligned} \tag{4.24}$$

Using the same idea for the shared frailty ARI$_m$ model, replacing the intensity function (2.16) as the baseline intensity function into (4.23) and again assuming the PLP as initial intensity function, we obtain the reliability prediction function $R(t) = R_{f.\mathrm{ARI}m}(t)$ given by

$$\begin{aligned} R(t) &= \exp\left\{-\hat{z}_i \int_{t_{i,n_i}}^{t_{i,n_i}+t} \lambda_{\mathrm{ARI}m}(u)\, du\right\} \\ &= \exp\left\{-\frac{\hat{z}_i}{\eta^\beta}\left[(t_{i,n_i} + t)^\beta - (t_{i,n_i})^\beta - t\beta(1-\theta)\underset{\sim}{s}(t_{i,n_i})\right]\right\}. \end{aligned} \tag{4.25}$$

Finally, the MTTF at time $T_{i,n_i} = t_{i,n_i}$ is obtained in the same way as discussed in Section 4.1.3, that is, by equation (4.12). Obviously, for the shared frailty ARA$_m$ and ARI$_m$ models, the reliability functions to be substituted in the equation (4.12) are (4.24) and (4.25), respectively. Thus, we obtain the expected time for the next failure to occur in system i after the last failure occurred at time t_{i,n_i}.

4.2.4 Simulation Study

In this section, we proceed with another large Monte Carlo simulation study with the objective of verifying the consistency and efficiency performances of the MLEs defined for the shared frailty IR models. As in Section 4.1.4, the procedures and analyses of the simulations

referring to each of the shared frailty ARA_m and ARI_m models will be done differently and presented separately in Sections 4.2.4.1 and 4.2.4.2, respectively. The definitions for this simulation study are the same as presented in Section 4.1.4.

The three indicators used to summarize the results obtained were again the RMSE, the MRE and the CP of the 95% CIs, the same ones defined and used in Section 4.1.4. In this simulation study for the shared frailty IR models, the increase in the sample of generated failure times will be given by the increase in the number of observed systems, that is, the more observed systems, the more total failure times will be generated. As in the other simulation studies presented so far, it is expected that with the increasing number of systems, the asymptotic properties are achieved since the sample sizes of observed failure times also tend to increase.

4.2.4.1 Simulation Study for the Shared Frailty ARA_m Model

We begin this section by describing the algorithm for generating the failure times $t_{i,j}$, with $i = 1,\ldots,k$ and $j = 1,\ldots,n_i$, for k independent systems, assuming that each system i has a frailty variable Z_i associated with it. First of all, for each system i we generate the related frailty term z_i as an observation of the $\text{Gamma}\left(\frac{1}{\alpha},\frac{1}{\alpha}\right)$ distribution, as defined at the beginning of Section 4.2. As already discussed, this generated value z_i impacts all failure occurrences of system i, therefore, it will also impact the generation of all the system's failure times.

Let $t_{i,j}$ be the j-th failure time of the i-th system, and the elapsed time from j-th failure to the $(j+1)$-th failure be $x = t_{i,j+1} - t_{i,j}$. Based on the discussion already carried out in Section 4.1.4.1, given z_i, x is an observation of a random variable X that represents the time between two consecutive failures, whose conditional CDF is given by $F(x \mid z_i) = 1 - e^{-\Lambda_{f.\text{ARA}_m}(t_{i,j}+x|z_i)+\Lambda_{f.\text{ARA}_m}(t_{i,j}|z_i)}$, where, in this case, $\Lambda_{f.\text{ARA}_m}(t \mid z_i)$ is the cumulative intensity function for the shared frailty ARA_m model conditional on z_i. From the equation (2.21) we know that $\Lambda_{f.\text{ARA}_m}(t \mid z_i) = z_i\Lambda_{f.\text{ARA}_m}(t)$ and using the definition of $\Lambda_{\text{ARA}_m}(t)$ in (2.14), it follows that

$$\begin{aligned}
\log(1-F(x)) &= -z_i\left[\Lambda_{\text{ARA}_m}(t_{i,j}+x)+\Lambda_{\text{ARA}_m}(t_{i,j})\right]\\
\Lambda_{\text{ARA}_m}(t_{i,j}+x) &= \Lambda_{\text{ARA}_m}(t_{i,j}) - \frac{\log(1-F(x))}{z_i}\\
\Lambda_0(t_{i,j}+x-(1-\theta)s(t_{i,j-1})) &= \Lambda_0(t_{i,j}-(1-\theta)s(t_{i,j-1})) - \frac{\log(1-F(x))}{z_i},
\end{aligned}$$

so

$$t_{i,j+1} = (1-\theta)s(t_{i,j-1}) + \lambda_0^{-1}\left(\Lambda_0(t_{i,j}-(1-\theta)s(t_{i,j-1})) - \frac{\log(1-F(x))}{z_i}\right), \tag{4.26}$$

where $\Lambda_0(t)$ is the initial cumulative intensity function (in this case, a PLP cumulative intensity function), Λ_0^{-1} is its inverse function and $0 \leq F(x) \leq 1$. Note that $t_{i,j+1} = t_{i,j} + x$ is the $(j+1)$-th failure time of system i, generated directly by expression (4.26).

The process for generating the failure times $t_{i,j}$ of all i systems, with $i = 1,\ldots,k$ and $j = 1,\ldots,n_i$, such that $t_{i,n_i} \leq t_i^*$ where t_i^* is the truncation time for system i, is exactly the same as that described in Section 4.1.4.1 and will therefore be omitted here.

Different parameter scenarios, truncation times, number of systems and failure memories were considered in this simulation study. We separated the presentation of the results based on the choice of three different memories of the failure process, considering memories $m = 1$, $m = 5$ and $m = 15$. Again, memory $m = 15$ was chosen as an approximation for memory $m = \infty$ based on the stability of the model for larger memories, as was done in Section 4.2.4.1.

The parameter settings chosen for this simulation study were: $\beta = 1.5$ and $\eta = 10$ for the PLP initial functions; $\theta = (0.4, 0.8)$ for the imperfect repair effect parameter; $\alpha = (0.2, 2)$ to generate the z_i as observations of a Gamma$(1/\alpha, 1/\alpha)$ distributed Z_i variable; $t^* = (200, 500)$ as truncation time for all systems; and the number k of systems ranging from 5 to 40 (from 5 to 5). Remember that the asymptotic properties of the estimators will be observed by increasing the failure time samples due to the increase in the number of systems. For each scenario we generated 1,000 Monte Carlo samples and calculated the RMSE, MRE and CP. The results are summarized and shown in Figures 26, 27 and 28.

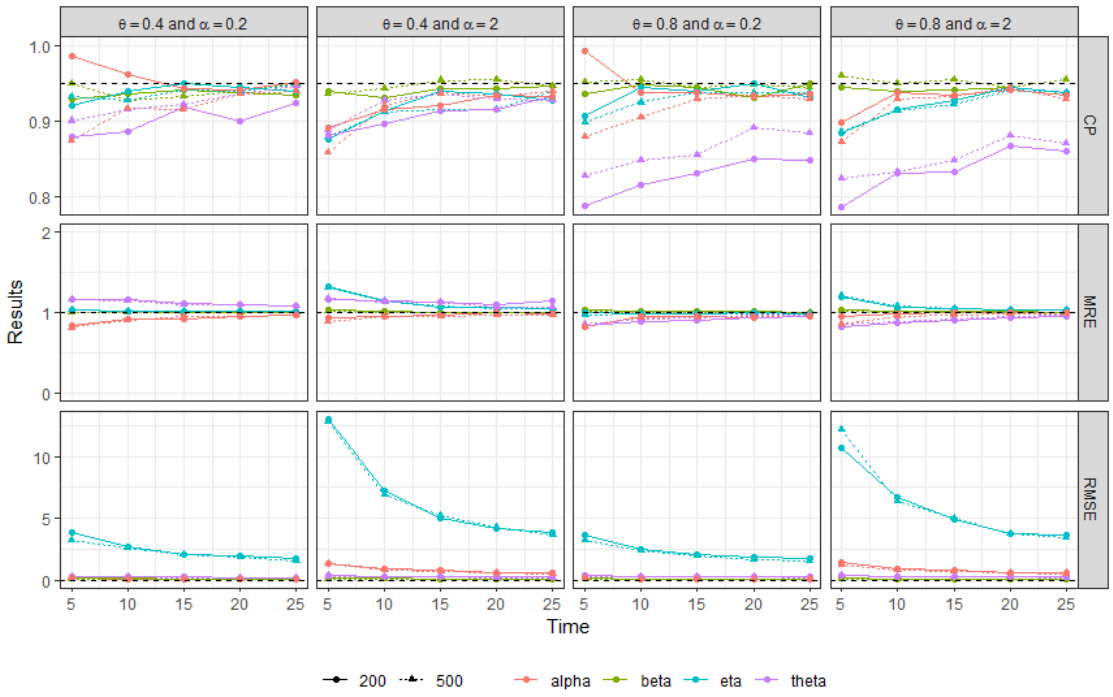

Figure 26 – Simulation results for the shared frailty ARA model in scenarios with memory $m = 1$.

As seen in Figures 26, 27 and 28, the estimators show, in general, the expected behaviors. The greatest discrepancies occur with the RMSE of the parameter η in the particular cases of small samples and greater frailty variance ($\alpha = 2$). This behavior is expected and justified in these scenarios, even more so due to the magnitude of the nominal value of the parameter η. Except for the observation about the magnitude of the parameter η, the MRE and RMSE

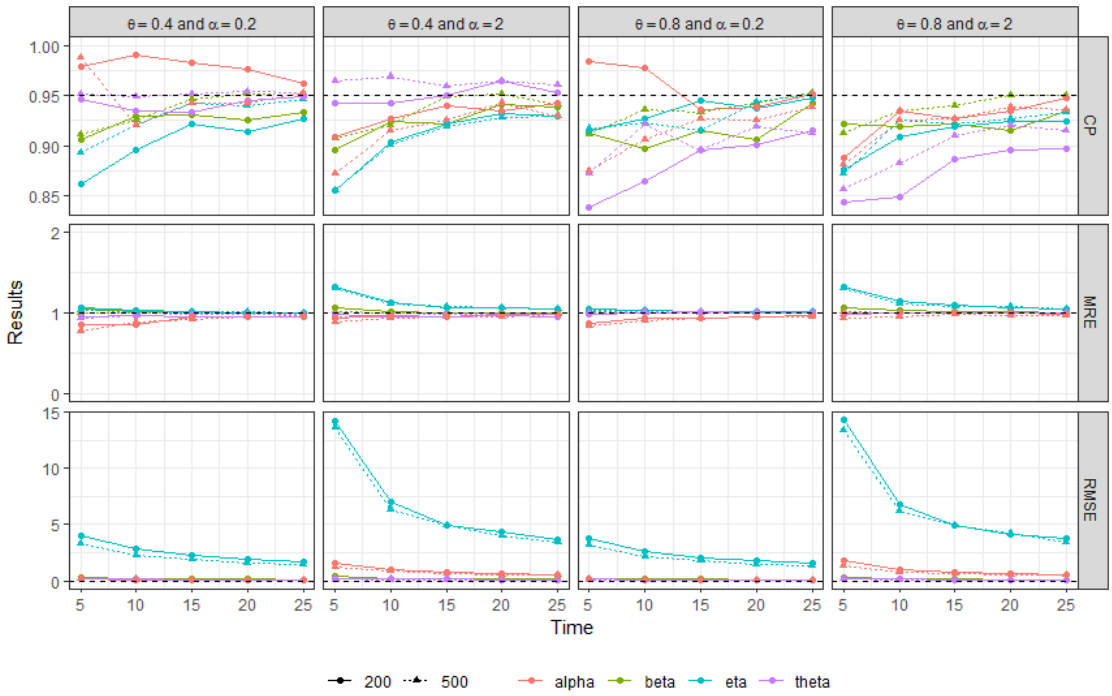

Figure 27 – Simulation results for the shared frailty ARA model in scenarios with memory $m = 5$.

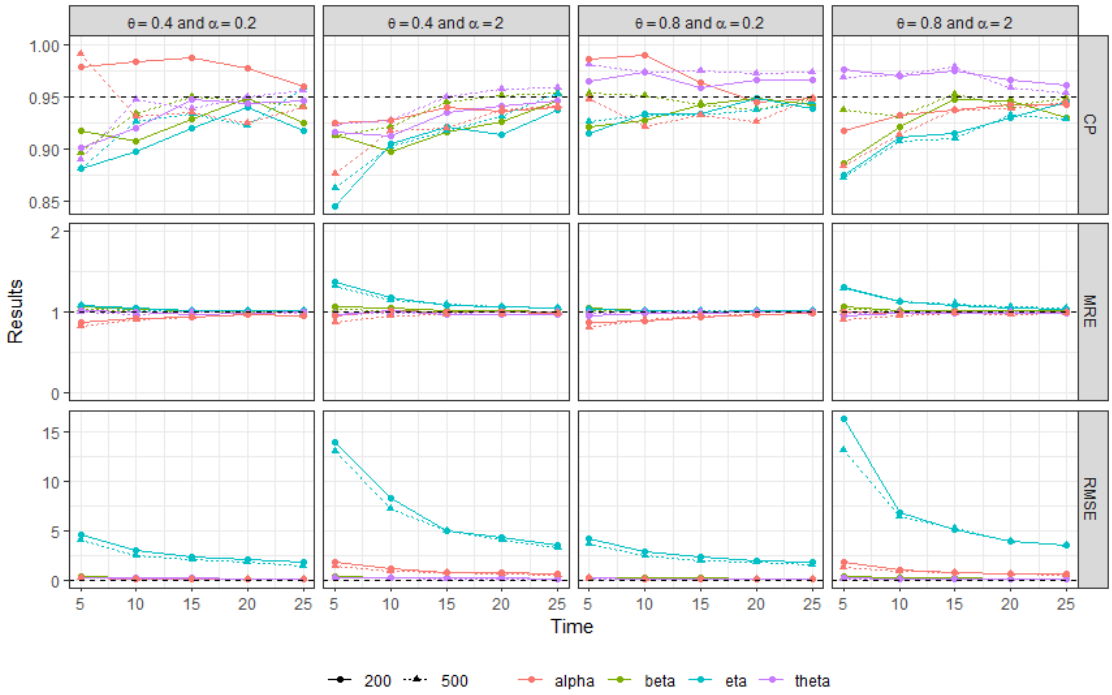

Figure 28 – Simulation results for the shared frailty ARA model in scenarios with memory $m = 15$.

of all parameters in all scenarios converge asymptotically to the expected values of 1 and 0, respectively. In addition, convergences are a little faster in cases where the truncation time is longer ($t^* = 500$), which is expected since in this scenario the generated failure time samples are larger.

Regarding the CP, it is also possible to verify that the nominal values are, in general, reached or approximated. It is possible to identify some scenarios where the nominal value of CP is not reached, especially in scenarios where $\alpha = 2$, which is expected since these scenarios consider precisely greater variance of the frailty variable. In the scenarios where we consider models with greater memories of the failure history ($m = 5$ and $m = 15$), the convergence of the CP measurements to the nominal value is faster and more evident, which indicates that models with greater information of the failure history are more stable in relation to the asymptotic estimator properties.

4.2.4.2 Simulation Study for the Shared Frailty ARI$_m$ Model

The generation of failure times for the shared frailty ARI$_m$ model will basically be done by repeating the procedures previously presented. After generating the frailty terms z_i for each system i, the procedures are the same as those presented in Section 4.1.4.2, as follows. Let $t_{i,j}$ be the j-th failure time of the i-th system and $x = t_{i,j+1} - t_{i,j}$ be the elapsed time from j-th to the $(j+1)$-th failure. The CDF for the random variable X is given by $F(x \mid z_i) = 1 - e^{-\Lambda_{f.\text{ARI}_m}(t_{i,j}+x|z_i)+\Lambda_{f.\text{ARI}_m}(t_{i,j}|z_i)}$, where $\Lambda_{f.\text{ARI}_m}(t)$ is the cumulative intensity function for the shared frailty ARI$_m$ model. Using the equation (2.21) and ARI$_m$ cumulative intensity function given by (2.17), we can rewrite the non-conditional CDF as

$$\begin{aligned} F(x) &= 1 - \exp\left\{-z_i\left[\Lambda_{\text{ARI}m}(t_{i,j}+x) + \Lambda_{\text{ARI}m}(t_{i,j})\right]\right\} \\ &= 1 - \exp\left\{-z_i\left[\Lambda_0(t_{i,j}+x) - \Lambda_0(t_{i,j}) - x(1-\theta)\underline{s}(t_{i,j-1})\right]\right\}, \end{aligned} \tag{4.27}$$

where $\Lambda_{\text{ARI}m}(t)$ is the ARI$_m$ cumulative intensity function given by (2.17) and $\Lambda_0(t)$ is the initial cumulative intensity function, again a PLP cumulative intensity function.

Note that it is not possible to solve the equation (4.27) analytically in terms of the elapsed time x as done for the ARA$_m$ model in Section 4.2.4.1. As discussed is Section 4.1.4.2, given a time $t_{i,j}$, the elapsed time x until the next failure time $t_{i,j+1}$ will be obtained by solving the equation (4.27) using computational numerical methods, after substituting $F(X)$ by an observation u of the Uniform$(0,1)$ distribution. The process for generating the failure times $t_{i,j}$ of all i systems, with $i = 1,\ldots,k$ and $j = 1,\ldots,n_i$, such that $t_{i,n_i} \leq t_i^*$ where t_i^* is the truncation time for system i, is exactly the same as that described in Section 4.1.4.2.

All the parameters chosen for the sample simulations in the shared frailty ARI$_m$ model were the same as in the shared frailty ARA$_m$ model in Section 4.2.4.1. We again considered three distinct memories ($m = 1$, $m = 5$ and $m = 15$) for the same reasons justified for the previous case, and the other nominal parameters values are: $\beta = 1.5$, $\eta = 10$, $\theta = (0.4, 0.8)$ and $\alpha = (0.2, 2)$. The truncation times are also the same $t^* = (200, 500)$ and the number k of systems are also ranging from 5 to 40 (from 5 to 5) for the same reasons presented in the previous section. For each scenario we generated 1,000 Monte Carlo samples and calculated the RMSE, MRE and CP. The results are summarized and shown in Figures 29, 30 and 31.

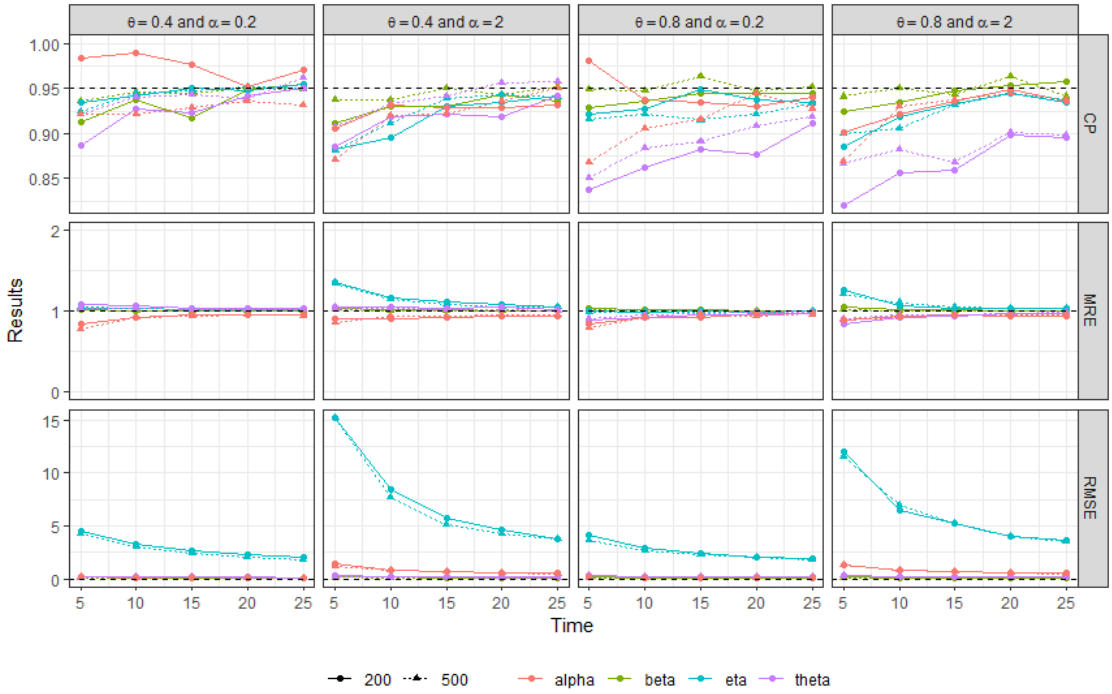

Figure 29 – Simulation results for the shared frailty ARI model in scenarios with memory $m = 1$.

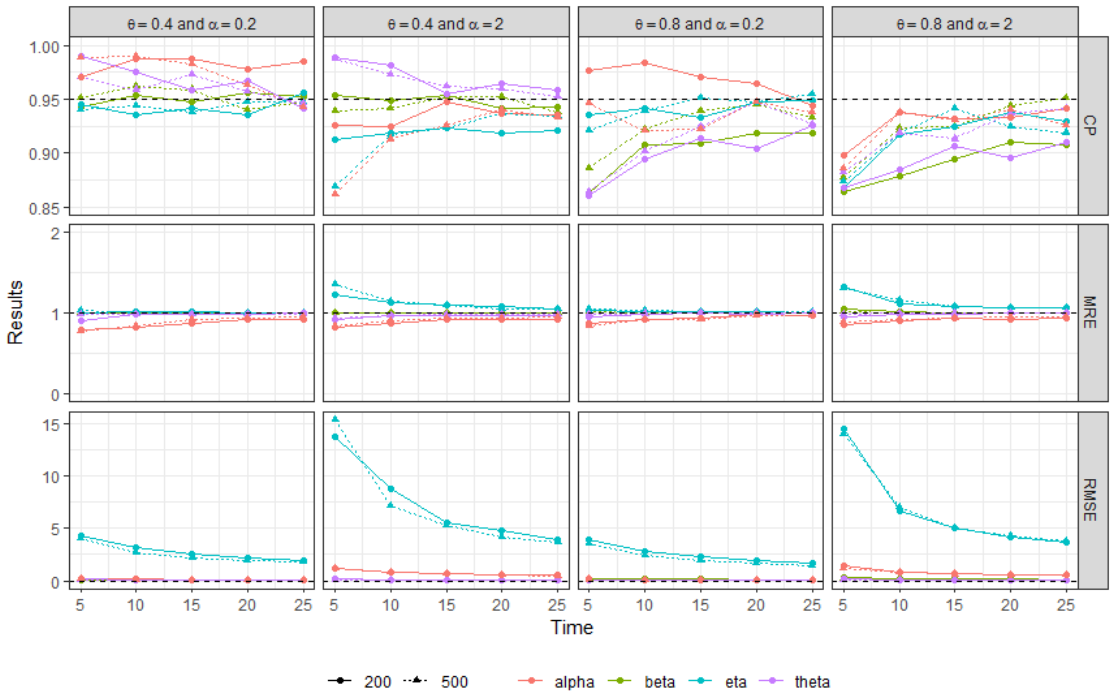

Figure 30 – Simulation results for the shared frailty ARI model in scenarios with memory $m = 5$.

As in the simulation study of Section 4.2.4, Figures 29, 30 and 31 show that the estimators behave asymptotically as expected. Observations on discrepancies in the RMSE value of the parameter η are the same as discussed in the previous study. Again, it is possible to see that the results and convergences are better for larger failure history memories ($m = 5$ and $m = 15$) and for longer truncation time ($t^* = 500$).

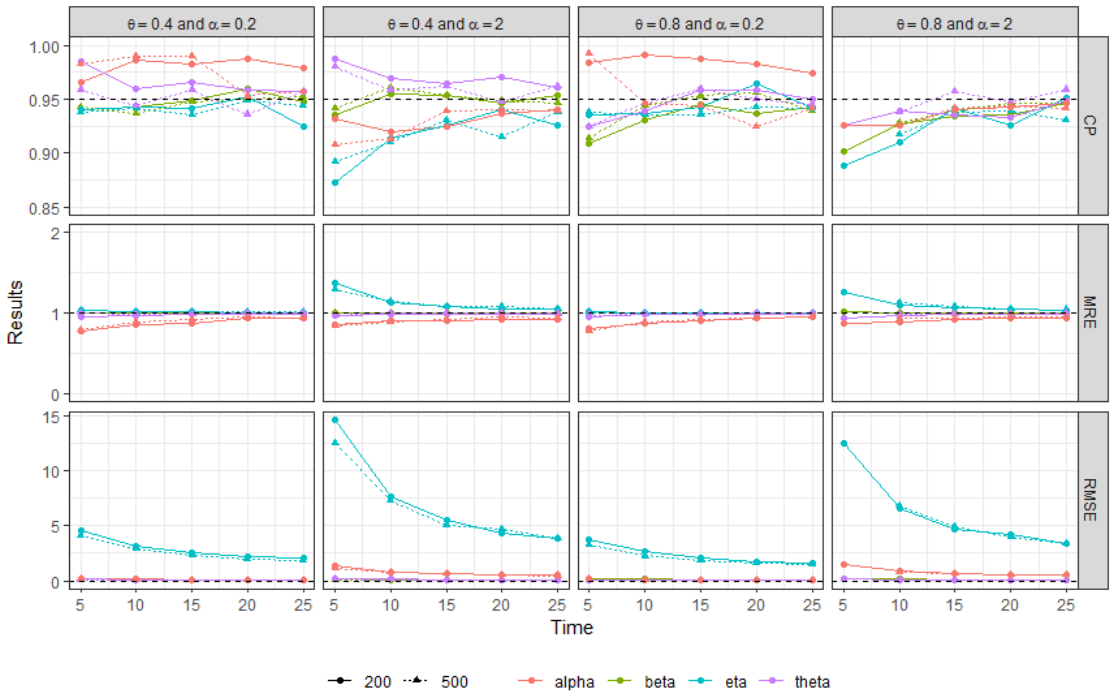

Figure 31 – Simulation results for the shared frailty ARI model in scenarios with memory $m = 15$.

In scenarios where the frailty variance is smaller, all estimators show excellent results. However, in scenarios with greater frailty variance ($\alpha = 2$), we noticed some deviations in the MRE and CP estimates of parameter α. This is somewhat to be expected, since frailty variability can generate uncontrolled samples for individual system frailties during the sampling process.

4.2.5 Real Data Application - Dump Truck Data Revisited

In this section we revisit the real dataset presented in Section 3.4.2 to illustrate the methodology of the shared frailty ARA_m and ARI_m models presented. Our goal is to fit the both models to the dataset, obtaining the MLEs for the parameters β, η, θ and α, as well as their respective 95% CIs. For this, the procedures discussed in Section 4.2.2 will be used for each of the models. The AIC and BIC criteria will be used to select the best models to fit the data in terms of the failure memory m. After obtaining the MLEs of the best model and their respective estimates for the frailty terms z_i, it will be possible to estimate the reliability prediction for each system as discussed is Section 4.2.3. All these procedures are very similar to what was done in Section 4.1.5.

As previously stated, this database was presented by Toledo *et al.* (2015), who performed a complete inferential analysis considering the IR models to find the one that best fits the data. Here, we will do the same analysis considering the two classes ARA_m and ARI_m and all their possible failure memories m. The difference in our work is that here we consider the possibility of non-quantifiable effects acting on truck failure times. In this sense, in addition to identifying the efficiency of the repairs carried out through the best model as done by the authors, our model

allows, at the same time, to capture the existence of unobserved heterogeneity shared between the trucks.

By maximizing the log-likelihood functions (4.19) and (4.21) for the shared frailty ARA_m and ARI_m models, respectively, we obtain the parameter estimates $\hat{\beta}$, $\hat{\eta}$, $\hat{\theta}$ and $\hat{\alpha}$ for both models, and this procedure was performed for all possible memories m. As the highest number of failures among the trucks was 32, the estimation was performed for both ARA_m and ARI_m classes considering memories $m = 1, \ldots, 32$, where memory $m = 32$ is equivalent to memory $m = \infty$. The maximum estimated value of the log-likelihood function $\hat{l}$ was used to verify which of these 32 models best fits the data for the both classes, since all these models have the same number of parameters. The summary of these values for both shared frailty ARA_m and ARI_m models is presented in Figure 32.

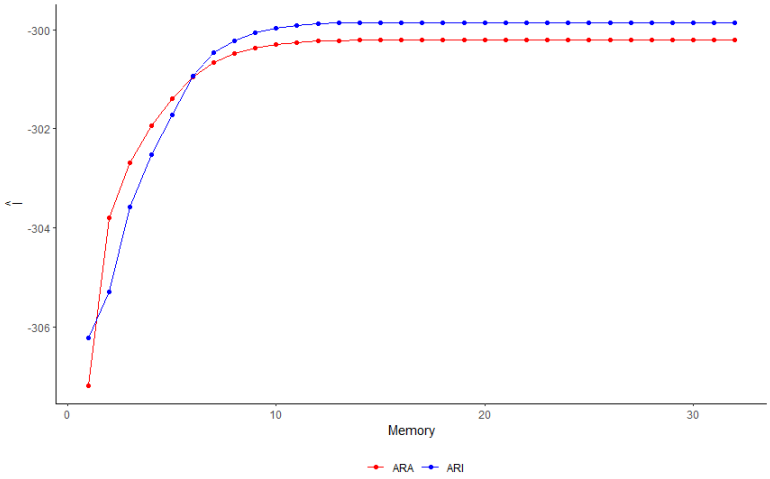

Figure 32 – Estimated maximum log-likelihood values $\hat{l}$ per memory m, for the dump truck data.

Note that for both models there is a stability in the log-likelihood estimates from a certain memory, specifically the memory $m = 10$. This means that considering any shared frailty ARA_m (or ARI_m, analogously) models with $m \geq 10$, the estimates for the parameters do not differ. Furthermore, the maximum log-likelihood values for these memories are the highest for the two models, so we will adopt the shared ARA_∞ and ARI_∞ models as the best models for the ARA and ARI classes for this dataset, respectively.

The MLE results for each parameter of the shared frailty ARA_∞ and ARI_∞ models, and their respective 95% CIs, are described in Table 5. For comparison, we also estimated the parameters of the shared frailty MR and PR models (particular cases of ARA_1, with $\theta = 1$ and $\theta = 0$, respectively) and also displayed their results in Table 5.

Quickly, in Table 5, it is possible to see that the shared MR and PR frailty models did not identify the presence of unobserved heterogeneity between the systems. This result differs significantly from the other two models, which, in addition to capturing the existence of unobserved heterogeneity, also captures the effect of the repairs performed. To decide for the

Table 5 – MLE results for the shared frailty MR, PR, ARA_∞ and ARI_∞ models applied to dump truck data.

	$\hat{\beta}$ (95% $CI_{\hat{\beta}}$)	$\hat{\eta}$ (95% $CI_{\hat{\eta}}$)	$\hat{\theta}$ (95% $CI_{\hat{\theta}}$)	$\hat{\alpha}$ (95% $CI_{\hat{\alpha}}$)
MR	1.13 (0.96, 1.35)	5.92 (3.53, 9.93)	-	7.23 (7.21, 7.24) $\times 10^{-8}$
PR	1.18 (1.03, 1.36)	4.25 (3.64, 4.95)	-	7.84 (7.83, 7.85) $\times 10^{-8}$
ARA_∞	1.85 (1.40, 2.43)	7.72 (5.43, 10.99)	0.60 (0.40, 0.77)	0.014 (0.009, 0.019)
ARI_∞	1.90 (1.71, 2.11)	7.65 (5.63, 10.16)	0.67 (0.48, 0.81)	0.020 (0.013, 0.029)

best of the four presented models, we will again use the estimated maximum log-likelihood, the AIC and the BIC criteria, whose results are listed in Table 6.

Table 6 – AIC and BIC results for the shared frailty MR, PR, ARA_∞ and ARI_∞ models applied to the dump truck data.

	$\hat{l}$	AIC	BIC
MR	-307.18	620.36	628.94
PR	-305.36	616.72	625.30
ARA_∞	-300.21	608.42	619.86
ARI_∞	-299.87	607.74	619.18

From Table 6, it is possible to conclude that the ARI_∞ model is the one that best fits the dataset, since it was superior by all three comparison criteria (greater maximum log-likelihood and smaller AIC and BIC). This will therefore be our chosen model and we will discuss a little more about its results.

Initially, let us analyze the estimates of the parameters β and η of the initial PLP. As in the example in Section 4.1.5, here the $\hat{\beta}$ parameter estimate indicates that the trucks are deteriorating over time, since $\hat{\beta}$ and its 95% CI limits are greater than 1. In this shared frailty model, we can perform the usual interpretation of the parameter η, since it is expected that the average of the individual frailty estimates be equal to 1. In fact, this occurs (as we will discuss later) and the estimate $\hat{\eta}$, therefore, tells us that the expected time that only one failure occurs on a truck is approximately 7 days.

An important result rests on the estimation of the parameter θ. In this case, it is possible to state that there is an effect of the repairs performed on the trucks and, in this case, this effect proportionally reduces the failure intensity function of these systems by $\hat{\theta} = 0.67$ after each repair. Furthermore, the 95% CI obtained indicates a significant difference from the extreme models of MR or PR.

Finally, as mentioned briefly earlier, the shared frailty ARI_∞ model captured the existence of unobserved heterogeneity through the parameter α. Despite being only slightly greater than zero, the estimate $\hat{\alpha}$ obtained can be considered significant since its 95% CI limits are also slightly greater than zero. This indicates that there are non-quantifiable effects that impact the failure process of trucks, making some more or less fragile than others. As discussed in Section

2.3.3, once the estimate $\hat{\alpha} > 0$, it is possible to use equation (2.33) to calculate the individual frailties of each of the systems. These results are listed in Table 7.

Table 7 – Individual frailty for each dump truck, in the shared frailty ARI_∞ model.

Frailty	Estimate
$\hat{z}_1$	0.919
$\hat{z}_2$	1.142
$\hat{z}_3$	0.934
$\hat{z}_4$	1.050
$\hat{z}_5$	0.955

From Table 27 we see that trucks #2 and #4 can be considered more fragile than the others. As their estimated individual frailties are greater than 1, their failure intensity functions are greater than the intensity function of a system operating in a hypothetical situation of non-existence of non-quantifiable effects. The direct mathematical consequence of this is that, with greater failure intensity, these systems are expected to fail more times in less time. Finally, just for the record, the average of the 5 estimated individual weaknesses is approximately 1, as expected by the theoretical model and confirming its applicability.

Once again, we employed the graphical procedure of goodness-of-fit to compare the empirical and estimated MCFs in the example. The idea is to have a perception of the quality of the adjustment by the shared frailty ARA_∞ and ARI_∞ models. The goodness-of-fit plot comparison is shown in Figure 33. Once again the empirical and estimated curves of the MCFs (from each frailty ARA_∞ and ARI_∞ models) are very close to each other, which leads us to conclude that the both fits are reasonable. But it is still possible to verify a slight superiority of the ARI_∞ model, especially in the interval of 40 to 70 days, where the fit of this model is closer to the empirical fit than the ARA_∞ model.

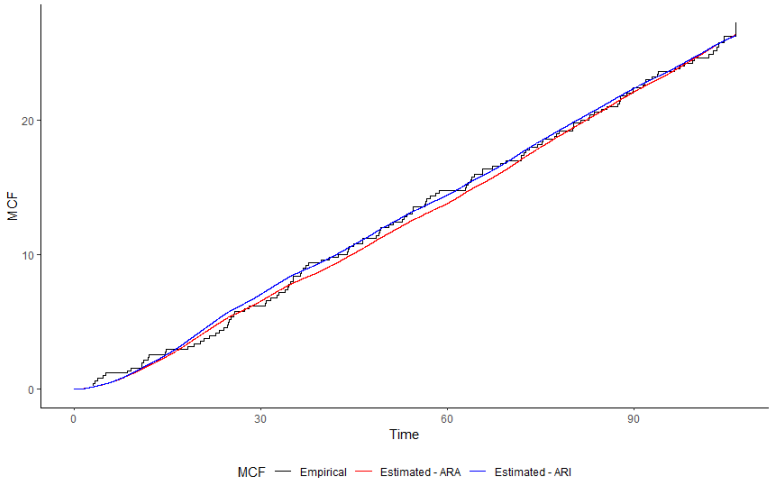

Figure 33 – Empirical and estimated MCFs for the truck's failure times, in the shared frailty ARA_∞ and ARI_∞ models.

Finally, the predicted reliability for each dump truck and their respective MTTFs from their last observed failures were estimated and the results are shown in Figure 34. For the reliability curves, we considered the respective estimates $\hat{\beta}$, $\hat{\eta}$ and $\hat{\theta}$ obtained from each frailty ARA_∞ and ARI_∞ models, as well as the individual frailty estimates for all the trucks. The estimates are replaced in the equations (4.24) and (4.25), respectively. For the MTTFs, we again only considered the estimates obtained from the best fitted model, in this case the shared frailty ARI_∞ model, and replaced them in equation (3.16).

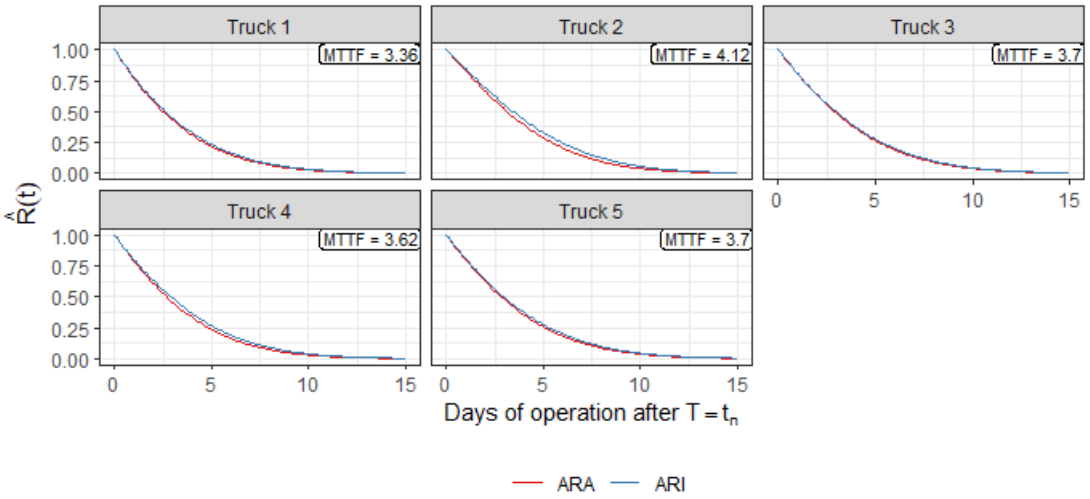

Figure 34 – Estimated reliability functions and MTTFs (only for the ARI_∞ model) at last failure time t_n, for each truck in the data set, under the fitted frailty ARA_∞ and ARI_∞ models.

The reliability curves presented in Figure 34 reveal that the probability that the trucks will operate without failure for more than 10 days after their last observed failures is practically zero. The reliability curves estimated from the frailty ARA_∞ and ARI_∞ models are quite close in this case, which was expected due to the proximity of the fit estimates obtained for these two models, and this attests that either of them could be used to infer about the dataset.

Regarding the MTTFs estimated and presented in Figure 34, given the history of the dump truck failure process, their mean times to the next failure vary from approximately 3 to 4 days operating in the mine. This result is related to the estimate of the parameter η (in this case where the individual frailties approach 1 for all systems), since the obtained $\hat{\eta}$ close to 7 indicates that a single failure is expected by the model in an average of 7 days.

The information on expected failure times and predicted reliability are important for the mining company in the sense that they contribute to the proposition of cost reduction strategies involving repairs of these machines and/or losses resulting from their failures.

4.3 Concluding Remarks of the Chapter

In this chapter, we proposed an extension of the IR model to multiple independent repairable systems by introducing a multiplicative term of frailty. In another words, we considered cases where repairable systems are subjected to an IR whereas there may be unobserved heterogeneity related to the system failure times or between systems.

As stated for the frailty PR model, ignoring the existence of unobserved heterogeneity in models that consider multiple systems can lead to the wrong estimation of parameters and, consequently, to a wrong conclusion about the observed systems, and this justifies the importance of the model proposed in this chapter.

In the proposed frailty IR models, the initial intensity function of the recurring failure times follows a PLP process and for each system, it was assumed that the frailty terms are independent and have the same Gamma$(\frac{1}{\alpha}, \frac{1}{\alpha})$ distribution, where the parameter α indicates the variance of these random variables. Furthermore, our proposed models maintains the ability to identify and quantify the repair effect through the original θ parameter of the IR models.

We present frailty models from two different perspectives: considering univariate and shared frailty for repairable systems. This distinction was necessary due to the approaches present in the literature and the different interpretations and applications that these two scenarios contemplate. In the first case, our models allow verifying the existence of global effects that act individually on each failure time of each system, while in the second case, the models verify the existence of effects that act differently on each system but equally in their respective failure times.

Under a classical framework, we used the likelihood principle to obtain the model parameters' MLEs and their respective 95% CIs by using asymptotic theory. Furthermore, we established reliability prediction functions for each proposed model.

A simulation study was carried out to check the quality of the estimators obtained and their behavior under different parameter scenarios, times of the observation truncation, number of observed systems and failure memories for the univariate and shared ARA$_m$ and ARI$_m$ models. We concluded that, in general, the estimates present good asymptotic behavior in terms of Bias and RMSE, as well as good CP measures.

Finally, we revisited the applications presented in Section 3.4 to use the proposed univariate and shared frailty IR models, with the both classes ARA and ARI, to adjust each of the two real datasets. In the first example we used the proposed univariate frailty IR models and checked the existence of unobserved heterogeneity related to the systems failure times and the possible repair effect on the virtual age or on the failure intensity function after the occurrence of each repair. In the second example, we used the proposed shared frailty IR models and also checked for the existence of a repair effect and, in this case, the existence of unobserved heterogeneity between the systems. In each example, we have identified the most likely type

of repair that may have been performed on the systems, as well as the most likely memory of failures that impact their intensity functions. Finally, we calculated the reliability of each system from the last observed failure.

CHAPTER

5

BAYESIAN APPROACH TO FRAILTY IMPERFECT REPAIR MODELS

In this chapter we present Bayesian methods for the shared frailty models presented in Chapter 4. The idea is to revisit these models, which were exclusively analyzed using a frequentist approach, and now explore Bayesian methodologies as an alternative. Furthermore, we employ hierarchical Bayesian models to capture variations in repair effect parameters across distinct systems.

As widely recognized in the statistical literature, the Bayesian approach involves assuming a probability distribution for the model parameters (see, for example, Gelman *et al.* (1995)). In this context, the primary objective of inference is to characterize this distribution, allowing us to gain insights into the parameters' characteristics. Obtaining this distribution, known as the *posterior distribution*, relies on prior knowledge about the parameters, incorporated into the model through another probability distribution called the *prior distribution*. Additionally, it incorporates data related to the studied phenomenon through the model's likelihood function. Consequently, the general idea is that the collected data contribute to updating and refining the prior distribution of each parameter.

In our context of reliability and repairable systems, the Bayesian approach proves to be practical. As discussed in previous chapters, the failure processes of repairable systems can be modeled as NHPP with parametric initial intensity functions. The parametric form assumed for the initial intensity function can be chosen so that the parameters make physical meaning, as discussed earlier in the case of the PLP. In this regard, experts and technicians familiar with the repairable systems in question can provide valuable technical knowledge, guiding the definition of consistent priors for problems within this context.

In the reliability literature, we have come across some papers that analyze repairable systems using a Bayesian approach. As we mentioned earlier, the assumption of MR after an occurrence of failure, while not ideal, is more commonly found in the repairable systems

literature. Pievatolo and Ruggeri (2004) proposed Bayesian models to describe the failure process of repairable systems, considering an NHPP and only minimal repairs after the occurrence of failures. Oliveira, Colosimo and Gilardoni (2012) also presented Bayesian models in this context, considering minimal repairs following failures and modeling the intensity function with a PLP. Additionally, these last authors extended the analysis to encompass multiple systems, each characterized by different realizations of the same PLP.

A proposal of Bayesian models for repairable systems subjected to IR can be found in Pan and Rigdon (2009). In this work, the authors explored the ARA and ARI classes of IR defined by Doyen and Gaudoin (2004) and proposed a hierarchical Bayesian model to analyze multiple systems sharing the same initial intensity function (modeled by a PLP), but that potentially can have different repair effects. This work serves as a main reference for our chapter's studies, and our aim is to extend it to a frailty models context.

In this regard, we are proposing hierarchical Bayesian models for estimating the parameters of the shared frailty IR models defined in Section 4.2. Once again, we consider all possible memories m of the two IR classes ARA_m and ARI_m. As suggested by Pan and Rigdon (2009), we assume that the repair effects of the systems may vary, but are modeled by random variables sharing the same probability distribution. The parameters of these random variables are also treated as random variables themselves, characterizing the hierarchical nature of the model. Our contribution to this chapter is twofold: we extend the work of Pan and Rigdon (2009) by introducing the frailty idea, and we present Bayesian modeling as an alternative approach to the methods detailed in Section 4.2.

This chapter is structured as follows. In Section 5.1, we introduce the comprehensive model framework, beginning with the reparameterization of the shared frailty models discussed in Section 4.2 and incorporating multiple repair effects within this context. In Section 5.1.1, we present the prior distributions for each model parameter and introduce the idea of a hierarchical Bayesian approach. In Section 5.1.2, we detail the sampling methodology based on Markov Chain Monte Carlo (MCMC) techniques for obtaining the posterior density distributions of each parameter and their respective point estimates. In Section 5.1.3, we discuss a criterion for selecting models, while in Section 5.1.4 we present some criteria for assessing the convergence of the chains generated by the MCMC procedures. Finally, in Section 5.2, we revisit the two datasets previously presented in this work to illustrate and verify the applicability of the Bayesian procedures discussed.

5.1 Bayesian Model Framework

In this section, we introduce our proposed Bayesian approach for conducting inference in shared frailty IR models with a PLP initial intensity. First of all, for Bayesian models, we reparameterize the PLP intensity and cumulative intensity functions presented in (2.3) and (2.4),

respectively, by

$$\lambda(t \mid \beta, \omega) = \omega\beta t^{\beta-1} \qquad \text{and} \qquad \Lambda(t \mid \beta, \omega) = \omega t^{\beta}.$$

This parameterization is also usual in the literature and, in particular, is used in works with Bayesian methodologies, as seen in Pan and Rigdon (2009) and Somboonsavatdee and Sen (2015b). The parameter β maintains the same interpretation as in the previous parameterization, while the parameter ω is the scale parameter and can be called the intrinsic failure ratio (obtained when $\beta = 1$) (PAN; RIGDON, 2009). The algebraic effect of this reparameterization on the functions involving the PLP in Chapter 4 is just by replacing $\omega = 1/\eta^{\beta}$.

Furthermore, as discussed in the introduction to this chapter, we are assuming that the systems share the same failure process initial intensity function, but may be subjected to post failure repair with different effects. In this way, each system i will be associated with a particular θ_i, $i = 1, \ldots, k$, where k is the total number of systems. Therefore, the new vector of parameters to be estimated is given by $\boldsymbol{\mu} = (\beta, \omega, \alpha, \theta_i)$.

Let $t_{i,j}$ be the failure times observed in k independent systems, with $i = 1, \ldots, k$ and $j = 1, \ldots, n_i$, and let t_i^* be the truncation times of each system observation, with $t_{i,n_i} \leq t_i^*$ for all i. Rewritten the equations (4.19) and (4.21), the likelihood functions for the parameter vector $\boldsymbol{\mu} = (\beta, \omega, \alpha, \theta_i)$ of the shared frailty ARA_m and ARI_m models with reparameterized initial PLP are, respectively, given by

$$L_{f.\text{ARA}m}(\boldsymbol{\mu} \mid t_{i,j}) = \frac{(\beta\omega\alpha)^N}{\Gamma\left(\frac{1}{\alpha}\right)^k} \prod_{i=1}^{k} \frac{\Gamma\left(n_i + \frac{1}{\alpha}\right) \prod_{j=1}^{n_i} \left(t_{i,j} - (1-\theta_i)s(t_{i,j-1})\right)^{\beta-1}}{\left(1 + \alpha\omega W^*_{\text{ARA}m}\right)^{n_i + \frac{1}{\alpha}}} \tag{5.1}$$

and

$$L_{f.\text{ARI}m}(\boldsymbol{\mu} \mid t_{i,j}) = \frac{(\beta\omega\alpha)^N}{\Gamma\left(\frac{1}{\alpha}\right)^k} \prod_{i=1}^{k} \frac{\Gamma\left(n_i + \frac{1}{\alpha}\right) \prod_{j=1}^{n_i} \left[t_{i,j}^{\beta-1} - (1-\theta_i)\underset{\sim}{s}(t_{i,j-1})\right]}{\left(1 + \alpha\omega W^*_{\text{ARI}m}\right)^{n_i + \frac{1}{\alpha}}}, \tag{5.2}$$

where

$$\begin{aligned} W^*_{\text{ARA}m} = \sum_{j=1}^{n_i} &\left[\left(t_{i,j} - (1-\theta_i)s(t_{i,j-1})\right)^{\beta} - \left(t_{i,j-1} - (1-\theta_i)s(t_{i,j-1})\right)^{\beta}\right] \\ &+ \left[\left(t_i^* - (1-\theta_i)s(t_{i,n_i})\right)^{\beta} - \left(t_{i,n_i} - (1-\theta_i)s(t_{i,n_i})\right)^{\beta}\right] \end{aligned}$$

and

$$\begin{aligned} W^*_{\text{ARI}m} = \sum_{j=1}^{n_i} &\left[t_{i,j}^{\beta-1} + t_{i,j-1}^{\beta-1} + \beta(t_{i,j} - t_{i,j-1})(1-\theta_i)\underset{\sim}{s}(t_{i,j-1})\right] + \\ &\left[t_{i^*}^{\beta-1} + t_{i,n_i}^{\beta-1} + \beta(t_{i^*} - t_{i,n_i})(1-\theta_i)\underset{\sim}{s}(t_{i,n_i})\right], \end{aligned}$$

with $N = \sum_{i=1}^{k} n_i$ being the total number of observed failures across the systems.

5.1.1 Bayesian Hierarchical Approach and Prior Distributions

As commented at the beginning of this chapter and pointed out by Gelman *et al.* (1995), in the Bayesian approach, the results of fitting a model to a given dataset are summarized by a probability distribution over the model parameters. This means that within the Bayesian framework, the model parameters are treated as random variables and their respective parameters are called *hyperparameters*. The goal of Bayesian inference is to obtain the parameter probability distribution, called the *posterior distribution*.

The posterior distribution of the parameter of interest is derived by combining the information gleaned from the data with prior knowledge about this parameter, utilizing Bayes Theorem. The data's contribution to this information is conveyed through the model's likelihood function, while the prior information about the parameter is incorporated by assuming a prior distribution that reflects this existing knowledge. In this sense, an important stage of the analysis in the Bayesian context is the definition of the parameters' priors.

A relatively simple choice, from an algebraic perspective, is the use of conjugate priors, where both the prior and posterior distributions belong to the same class of distributions. Thus, updating the knowledge about the parameter involves only changes in the hyperparameters. Another possible choice is the objective (or non-informative) priors, which aim to minimize the impact of prior knowledge on parameter estimation and are obtained using Fisher's information measure.

Unfortunately, due to the complexity of the likelihood functions described in equations (5.1) and (5.2), neither of these two prior choices is applicable to our models. Note that our likelihood functions cannot be reformulated as density functions of known probability distributions, making it impossible to choose conjugate priors. On the other hand, as previously highlighted in Chapter 4, the derivatives of these functions concerning each parameter are quite complex, which poses challenges in calculating Fisher's information measure and, consequently, makes it impractical to opt for objective priors. In this context, the choice of priors will draw from similar works in the literature. These priors will be selected to effectively encompass prior knowledge about the parameters, while maintaining flexibility in cases where prior knowledge is limited or uncertain.

As previously discussed, we are assuming that the k systems share the same reparameterized initial PLP function, with the same parameters β and ω for all of them. Furthermore, we presume that these systems deteriorate over time, implying that $\beta > 1$. Based on Pan and Rigdon (2009), we will adopt a Uniform(a,b) prior for the parameter β and a Gamma(c,d) prior for the parameter ω. In terms of frailty, our models assume that the frailty variables Z_i are IID with Gamma$(1/\alpha, 1/\alpha)$ distribution for all systems $i = 1,\ldots,k$. Consequently, the parameter α is the same for all systems and here we assume a Gamma(e,f) prior for it. Note that the hyperparameters a, b, c, d, e and f can be chosen in order to reflect the knowledge (or not) about

each of the respective parameters according to the defined prior distribution.

Regarding imperfect repair effects, we will follow the same ideas presented by Pan and Rigdon (2009). We assume that the parameters $\theta_1,\ldots,\theta_k$ have a common prior distribution, characterized by hyperparameters g and h. In this case, we assume that g and h are also random variables and have an hyperprior distribution $p(g,h)$, thus establishing a *hierarchical Bayesian model*. For the $\theta_1,\ldots,\theta_k$ parameters we assume a Beta(g,h) prior, and for each hyperparameter g and h we assume a shifted exponential prior with location and scale parameters being 1.

The prior PDFs for all the model parameters are given by

$$\pi_1(\beta \mid a,b) = \mathbb{I}_{(a,b)}(\beta), \quad \pi_2(\omega \mid c,d) = \frac{d^c}{\Gamma(c)}\omega^{c-1}e^{-d\omega}, \quad \pi_3(\alpha \mid e,f) = \frac{f^e}{\Gamma(e)}\alpha^{e-1}e^{-f\alpha},$$

$$\pi_{4,i}(\theta_i \mid g,h) = \frac{\Gamma(g+h)}{\Gamma(g)\Gamma(h)}\theta_i^{g-1}(1-\theta_i)^{f-1}, \quad \pi_5(g) = e^{-(g-1)} \quad \text{and} \quad \pi_6(h) = e^{-(h-1)},$$

where $\mathbb{I}(\cdot)$ is the indicator function, $a,b,g,h > 1$ and $c,d,e,f > 0$.

Assuming that the model parameters are independent and considering the hierarchy of the parameter θ and the hyperparameters g and h, the joint prior density is given by

$$\pi(\beta,\omega,\alpha,\theta_i,g,h) = \pi_1(\beta \mid a,b)\pi_2(\omega \mid c,d)\pi_3(\alpha \mid e,f)\prod_{i=1}^{k}\pi_{4,i}(\theta_i \mid g,h)\pi_5(g)\pi_6(h). \quad (5.3)$$

5.1.2 MCMC Solution

Given the joint prior density in (5.3) and the failure times $\boldsymbol{t} = \{t_{i,j}, i = 1,\ldots,k;\ j = 1,\ldots,n_i\}$ of the k systems, the joint posterior density of the model parameters is given by

$$\pi_{post}(\beta,\omega,\alpha,\theta_i,g,h \mid \boldsymbol{t}) = \frac{L(\beta,\omega,\alpha,\theta_i)\pi(\beta,\omega,\alpha,\theta_i,g,h)}{\int\cdots\int L(\beta,\omega,\alpha,\theta_i)\pi(\beta,\omega,\alpha,\theta_i,g,h)d\beta\ d\omega\ d\alpha\ d\theta_i\ dg\ dh},$$

where L represents a likelihood function given by (5.1) or (5.2).

Obviously, this is an analytically intractable expression and iterative computational methods need to be used to estimate the posterior distribution. In this case, a simulation using MCMC will be used to obtain the posterior distribution of interest.

According to Gelman *et al.* (1995), the MCMC simulation is a general method based on drawing values of the parameters from approximate distributions and then correcting those draws to better approximate the target posterior distribution. MCMC is an iterative simulation process where the distribution of the sampled draws (or state) depends on the previous drawn. The idea is to obtain a sample of the posterior distribution and calculate sample estimates of characteristics of this distribution.

For multidimensional problems, a particular MCMC algorithm is the *Gibbs sampler*, where the transitions between states are performed according to the complete conditional distributions. The complete conditional distribution is just the conditional posterior distribution of

each parameter given the data (the failure times $\boldsymbol{t}$) and all of the other parameters. Next, we will present the complete conditional distribution of each parameter based on the previously defined prior distributions and on the likelihood functions of the shared frailty ARA_m and ARI_m models.

Shared frailty ARA_m model

For the shared frailty ARA_m model, the likelihood function is given by (5.1). The complete conditional distribution of each parameter is obtained as follows:

$$\begin{aligned}\pi(\beta \mid \omega,\alpha,\theta_i,g,h,\boldsymbol{t}) &\propto L_{f.\text{ARA}m}(\boldsymbol{\mu} \mid t_{i,j})\pi_1(\beta \mid a,b)\\ &\propto \beta^N \prod_{i=1}^{k} \frac{\prod_{j=1}^{n_i}(t_{i,j}-(1-\theta_i)s(t_{i,j-1}))^{\beta-1}}{(1+\alpha\omega W^*_{\text{ARA}m})^{n_i+\frac{1}{\alpha}}}\mathbb{I}_{(a,b)}(\beta),\end{aligned}$$

$$\begin{aligned}\pi(\omega \mid \beta,\alpha,\theta_i,g,h,\boldsymbol{t}) &\propto L_{f.\text{ARA}m}(\boldsymbol{\mu} \mid t_{i,j})\pi_2(\omega \mid c,d)\\ &\propto \omega^N \prod_{i=1}^{k} \frac{\prod_{j=1}^{n_i}(t_{i,j}-(1-\theta_i)s(t_{i,j-1}))^{\beta-1}}{(1+\alpha\omega W^*_{\text{ARA}m})^{n_i+\frac{1}{\alpha}}}\omega^{c-1}e^{-d\omega},\end{aligned}$$

$$\begin{aligned}\pi(\alpha \mid \beta,\omega,\theta_i,g,h,\boldsymbol{t}) &\propto L_{f.\text{ARA}m}(\boldsymbol{\mu} \mid t_{i,j})\pi_3(\alpha \mid e,f)\\ &\propto \frac{\alpha^N}{\Gamma\left(\frac{1}{\alpha}\right)^k} \prod_{i=1}^{k} \frac{\Gamma\left(n_i+\frac{1}{\alpha}\right)}{(1+\alpha\omega W^*_{\text{ARA}m})^{n_i+\frac{1}{\alpha}}}\alpha^{e-1}e^{-f\alpha},\end{aligned}$$

$$\begin{aligned}\pi(\theta_i \mid \beta,\omega,\alpha,g,h,\boldsymbol{t}) &\propto L_{f.\text{ARA}m}(\boldsymbol{\mu} \mid t_{i,j})\pi_{4,i}(\theta_i \mid g,h)\\ &\propto \prod_{i=1}^{k} \frac{\prod_{j=1}^{n_i}(t_{i,j}-(1-\theta_i)s(t_{i,j-1}))^{\beta-1}}{(1+\alpha\omega W^*_{\text{ARA}m})^{n_i+\frac{1}{\alpha}}}\theta_i^{g-1}(1-\theta_i)^{h-1},\end{aligned}$$

$$\pi(g \mid \beta,\omega,\alpha,\theta_i,h,\boldsymbol{t}) \propto L_{f_u.\text{ARA}m}(\boldsymbol{\mu} \mid t_{i,j})\pi_{4,i}(\theta_i \mid g,h)\pi_5(g) \propto \prod_{i=i}^{k}\left(\theta_i^{g-1}\right)e^{-(g-1)},$$

$$\pi(h \mid \beta,\omega,\alpha,\theta_i,g,\boldsymbol{t}) \propto L_{f_u.\text{ARA}m}(\boldsymbol{\mu} \mid t_{i,j})\pi_{4,i}(\theta_i \mid g,h)\pi_6(h) \propto \prod_{i=i}^{k}\left((1-\theta_i)^{h-1}\right)e^{-(h-1)}.$$

Shared frailty ARI_m model

For the shared frailty ARI_m model, the likelihood function is given by (5.2) and the complete conditional distribution of each parameter are defined as follows:

$$\pi(\beta \mid \omega,\alpha,\theta_i,g,h,\boldsymbol{t}) \propto L_{f.\mathrm{ARI}m}(\boldsymbol{\mu} \mid t_{i,j})\pi_1(\beta \mid a,b)$$
$$\propto \beta^N \prod_{i=1}^{k} \frac{\prod_{j=1}^{n_i}\left[t_{i,j}^{\beta-1} - (1-\theta_i)\underset{\sim}{s}(t_{i,j-1}))\right]}{(1+\alpha\omega W^*_{\mathrm{ARI}m})^{n_i+\frac{1}{\alpha}}} \mathbb{I}_{(a,b)}(\beta),$$

$$\pi(\omega \mid \beta,\alpha,\theta_i,g,h,\boldsymbol{t}) \propto L_{f.\mathrm{ARI}m}(\boldsymbol{\mu} \mid t_{i,j})\pi_2(\omega \mid c,d)$$
$$\propto \omega^N \prod_{i=1}^{k} \frac{\prod_{j=1}^{n_i}\left[t_{i,j}^{\beta-1} - (1-\theta_i)\underset{\sim}{s}(t_{i,j-1}))\right]}{(1+\alpha\omega W^*_{\mathrm{ARI}m})^{n_i+\frac{1}{\alpha}}} \omega^{c-1}e^{-d\omega},$$

$$\pi(\alpha \mid \beta,\omega,\theta_i,g,h,\boldsymbol{t}) \propto L_{f.\mathrm{ARI}m}(\boldsymbol{\mu} \mid t_{i,j})\pi_3(\alpha \mid e,f)$$
$$\propto \frac{\alpha^N}{\Gamma\left(\frac{1}{\alpha}\right)^k} \prod_{i=1}^{k} \frac{\Gamma\left(n_i+\frac{1}{\alpha}\right)}{(1+\alpha\omega W^*_{\mathrm{ARI}m})^{n_i+\frac{1}{\alpha}}} \alpha^{e-1}e^{-f\alpha},$$

$$\pi(\theta_i \mid \beta,\omega,\alpha,g,h,\boldsymbol{t}) \propto L_{f.\mathrm{ARI}m}(\boldsymbol{\mu} \mid t_{i,j})\pi_{4,i}(\theta_i \mid g,h)$$
$$\propto \prod_{i=1}^{k} \frac{\prod_{j=1}^{n_i}\left[t_{i,j}^{\beta-1} - (1-\theta_i)\underset{\sim}{s}(t_{i,j-1}))\right]}{(1+\alpha\omega W^*_{\mathrm{ARI}m})^{n_i+\frac{1}{\alpha}}} \theta_i^{g-1}(1-\theta_i)^{h-1},$$

$$\pi(g \mid \beta,\omega,\alpha,\theta_i,h,\boldsymbol{t}) \propto L_{f_u.\mathrm{ARI}m}(\boldsymbol{\mu} \mid t_{i,j})\pi_{4,i}(\theta_i \mid g,h)\pi_5(g) \propto \prod_{i=i}^{k}\left(\theta_i^{g-1}\right)e^{-(g-1)},$$

$$\pi(h \mid \beta,\omega,\alpha,\theta_i,g,\boldsymbol{t}) \propto L_{f_u.\mathrm{ARI}m}(\boldsymbol{\mu} \mid t_{i,j})\pi_{4,i}(\theta_i \mid g,h)\pi_6(h) \propto \prod_{i=i}^{k}\left((1-\theta_i)^{h-1}\right)e^{-(h-1)}.$$

Note that none of the complete conditional distributions of the both considered models can be simplified into a known probability distribution. Consequently, direct parameter sampling from these conditional posteriors is not feasible. In this case, to obtain a sample from the posterior distribution of the parameters, we will use the Metropolis-Hastings (MH) algorithm, an useful simulation method for sampling from Bayesian posterior distributions (GELMAN *et al.*, 1995).

Basically, the MH algorithm is an iterative simulation algorithm that uses acceptance/rejection rules for each new value generated. In other words, a value is drawn from an auxiliary distribution and accepted with a given probability. This acceptance/rejection mechanism acts as a way of correcting the generated values and guarantees the convergence of the chain to the equilibrium distribution, which in this case is the parameter posterior distribution.

More specifically, suppose that the chain of simulated values of a parameter μ is in state l, that is, the last generated value was $\mu^{(l)}$. A new μ' value is drawn from an auxiliary distribution, called *jumping* or *proposal distribution*, say $q(\mu' \mid \mu^{(l)})$, which depends on the last $\mu^{(l)}$ generated value in the chain. The new value μ' is accepted with probability

$$R(\mu^{(l)}, \mu') = \min\left(1, \frac{\pi(\mu')q(\mu^{(l)} \mid \mu')}{\pi(\mu^{(l)})q(\mu' \mid \mu^{(l)})}\right),$$

where $\pi(\mu)$ is the target distribution. If μ' is accepted, then $\mu^{(l+1)} = \mu'$ and we say that the chain moves. Otherwise $\mu^{(l+1)} = \mu^{(l)}$, the chain does not move but this still counts as an iteration in the algorithm. As said before, with this procedure, the sequence of draws converges to the posterior distribution of the parameter μ.

In this work, for executing the MH algorithm that will be detailed later, and to derive the complete conditional distributions for all parameters across the both proposed models, we consider a Normal distribution centered on the last value generated by the chain as the proposal distribution $q(\cdot \mid \cdot)$ (with truncation when necessary). As the Normal distribution is symmetric, this is considered a Metropolis algorithm and the acceptance probability can be succinctly expressed as follows:

$$R(\mu^{(l)}, \mu') = \min\left(1, \frac{\pi(\mu')}{\pi(\mu^{(l)})}\right).$$

By combining the Gibbs sampler with the Metropolis algorithm, the algorithm for generating a MCMC sample from the posterior distribution of the parameters for the both models discussed in this chapter is described below. Note that the algorithm is the same for the two models and for this reason we will present it only once. The adaptation to a specific model is accomplished by selecting the appropriate complete conditional distributions referring to that model.

(1) Set values to the hyperparameters a, b, c, d, e and f that reflect the prior knowledge about the parameters.

(2) Start the algorithm with initial values $\beta = \beta^{(0)}$, $\omega = \omega^{(0)}$, $\alpha = \alpha^{(0)}$, $\theta_i = \theta_i^{(0)}$ $(i = 1, \ldots, k)$, $g = g^{(0)}$ and $h = h^{(0)}$ and set $l = 0$.

(3) In the $(l+1)$-th iteration, for each $i = 1 \ldots, k$, generate a θ_i' from the proposal Normal distribution centered on the previous $\theta_i^{(l)}$ and compute the acceptance ratio:

$$R_{\theta_i} = \min\left(1, \frac{\pi(\theta_i' \mid \beta^{(l)}, \omega^{(l)}, \alpha^{(l)}, g^{(l)}, h^{(l)}, \boldsymbol{t})}{\pi(\theta_i^{(l+1)} \mid \beta^{(l)}, \omega^{(l)}, \alpha^{(l)}, g^{(l)}, h^{(l)}, \boldsymbol{t})}\right).$$

(4) Generate random numbers u_{θ_i} from the Uniform$(0,1)$ distribution, for $i = 1, \ldots, k$. For each i, if $u_{\theta_i} < R_{\theta_i}$, so $\theta_i^{(l+1)} = \theta_i'$, otherwise $\theta_i^{(l+1)} = \theta_i^{(l)}$.

(5) Generate β' from the proposal Normal distribution centered on the previous $\beta^{(l)}$ and compute the acceptance ratio:

$$R_\beta = \min\left(1, \frac{\pi(\beta' \mid \omega^{(l)}, \alpha^{(l)}, \theta_i^{(l+1)}, g^{(l)}, h^{(l)}, \boldsymbol{t})}{\pi(\beta^{(l+1)} \mid \omega^{(l)}, \alpha^{(l)}, \theta_i^{(l+1)}, g^{(l)}, h^{(l)}, \boldsymbol{t})}\right).$$

(6) Generate a random number u_β from the Uniform$(0,1)$ distribution. If $u_\beta < R_\beta$, so $\beta^{(l+1)} = \beta'$, otherwise $\beta^{(l+1)} = \beta^{(l)}$.

(7) Generate ω' from the proposal Normal distribution centered on the previous $\omega^{(l)}$ and compute the acceptance ratio:

$$R_\omega = \min\left(1, \frac{\pi(\omega' \mid \beta^{(l+1)}, \alpha^{(l)}, \theta_i^{(l+1)}, g^{(l)}, h^{(l)}, \boldsymbol{t})}{\pi(\omega^{(l+1)} \mid \beta^{(l+1)}, \alpha^{(l)}, \theta_i^{(l+1)}, g^{(l)}, h^{(l)}, \boldsymbol{t})}\right).$$

(8) Generate a random number u_ω from the Uniform$(0,1)$ distribution. If $u_\omega < R_\omega$, so $\omega^{(l+1)} = \omega'$, otherwise $\omega^{(l+1)} = \omega^{(l)}$.

(9) Generate α' from the proposal Normal distribution centered on the previous $\alpha^{(l)}$ and compute the acceptance ratio:

$$R_\alpha = \min\left(1, \frac{\pi(\alpha' \mid \beta^{(l+1)}, \omega^{(l+1)}, \theta_i^{(l+1)}, g^{(l)}, h^{(l)}, \boldsymbol{t})}{\pi(\alpha^{(l+1)} \mid \beta^{(l+1)}, \omega^{(l+1)}, \theta_i^{(l+1)}, g^{(l)}, h^{(l)}, \boldsymbol{t})}\right).$$

(10) Generate a random number u_α from the Uniform$(0,1)$ distribution. If $u_\alpha < R_\alpha$, so $\alpha^{(l+1)} = \alpha'$, otherwise $\alpha^{(l+1)} = \alpha^{(l)}$.

(11) Generate g' from the proposal Normal distribution centered on the previous $g^{(l)}$ and compute the acceptance ratio:

$$R_g = \min\left(1, \frac{\pi(g' \mid \beta^{(l+1)}, \omega^{(l+1)}, \alpha^{(l+1)}, \theta_i^{(l+1)}, h^{(l)}, \boldsymbol{t})}{\pi(g^{(l+1)} \mid \beta^{(l+1)}, \omega^{(l+1)}, \alpha^{(l+1)}, \theta_i^{(l+1)}, h^{(l)}, \boldsymbol{t})}\right).$$

(12) Generate a random number u_g from the Uniform$(0,1)$ distribution. If $u_g < R_g$, so $g^{(l+1)} = g'$, otherwise $g^{(l+1)} = g^{(l)}$.

(13) Generate a h' from the proposal Normal distribution centered on the previous $h^{(l)}$ and compute the acceptance ratio

$$R_h = \min\left(1, \frac{\pi(h' \mid \beta^{(l+1)}, \omega^{(l+1)}, \alpha^{(l+1)}, \theta_i^{(l+1)}, g^{(l+1)}, \boldsymbol{t})}{\pi(h^{(l+1)} \mid \beta^{(l+1)}, \omega^{(l+1)}, \alpha^{(l+1)}, \theta_i^{(l+1)}, g^{(l+1)}, \boldsymbol{t})}\right).$$

(14) Generate a random number u_h from the Uniform$(0,1)$ distribution. If $u_h < R_h$, so $h^{(l+1)} = h'$, otherwise $h^{(l+1)} = h^{(l)}$.

(15) Set $l = l + 1$.

(16) Repeat the steps (3) to (15) N times and obtain a MCMC sample $\{(\beta_l, \omega_l, \alpha_l, \theta_{i,l}, g_l, h_l),\ l = 1\ldots,N\}$.

If N is sufficiently large, the generated chains $(\beta_l, \omega_l, \alpha_l, \theta_{i,l}, g_l, h_l)$ will stabilize and be approximately distributed from the joint posterior of the models' parameters. Finally, adopting the *squared error loss* for the Bayesian approach, the Bayes Estimator (BE) $\hat{\mu}$ for each parameter μ is obtained by the mean of the MCMC sample obtained by the previous algorithm (or the posterior mean), that is,

$$\hat{\mu} = \frac{1}{N}\sum_{l=1}^{N} \mu_l.$$

To compute the Credible Intervals (CI_B) of the parameter μ, the sample $\mu_1, \ldots, \mu_N$ is ordered as $\mu_{(1)} < \cdots < \mu_{(N)}$ and the $100(1-\gamma)\%$ CI_B of μ is given by

$$\left(\mu_{(\lfloor \frac{N\gamma}{2} \rfloor)}, \mu_{(\lfloor N(1-\frac{\gamma}{2}) \rfloor)}\right),$$

where $\lfloor x \rfloor$ is the *greatest integer function*, that is, the greatest integer that is less than or equal to x. Finally, it is also possible to define the *posterior median* of the ordered sample generated for each parameter, as $\mu_{Md} = \mu_{\left(\lfloor \frac{N}{2} \rfloor + 1\right)}$.

5.1.3 Model Selection

In our study, we are introducing Bayesian methodologies for frailty models, taking into account both IR classes, ARA and ARI, and considering all potential memories for each class. So, it is necessary to establish a selection criterion to determine the best-fitting model for each dataset. This is crucial because information by increasing the failure memory can lead to better or worse models, as observed in the applications of Sections 4.1.5 and 4.2.5.

The model selection criterion used in this work will be the Deviance Information Criterion (DIC). This measure is related to model predictive accuracy, and, as an information criteria, it estimates the predictive error of a fitted model (GELMAN *et al.*, 1995). Thus, when used to compare models, smaller values of DIC indicate better model fitting.

The DIC is an extension of the AIC criterion already used in this work. As they are information criteria, these two measures are defined based on the bias correction on the predictive accuracy. While the AIC makes this correction using the number of model parameters, the DIC uses the effective number of parameters (the average of the parameter estimate over its posterior distribution). The DIC is especially suitable in complex, hierarchical Bayesian models or whose posterior distributions are obtained via MCMC, as is totally our case.

Let $\{\hat{\boldsymbol{\mu}}^{(v)},\ v = 1,\ldots,N\}$ be the posterior sample of parameter vectors, obtained by the MCMC procedure discussed, $\bar{\boldsymbol{\mu}}$ be the average of the posterior sample (or the BE) and $L(\cdot)$ be the model likelihood function. The DIC criterion is defined as (PAN; RIGDON, 2009):

$$DIC = -2(2\bar{l} - \hat{l}),$$

where

$$\bar{l} = \frac{1}{N}\sum_{v=1}^{N} \log L(\hat{\boldsymbol{\mu}}^{(v)}) \qquad \text{and} \qquad \hat{l} = \log L(\bar{\boldsymbol{\mu}}).$$

5.1.4 Diagnostic Checking

After obtaining an MCMC sample, it is essential to verify if it represents the desired posterior distribution. This is a well-recognized issue in the literature, and several established solutions exist. In this section, we will list and comment on some convergence diagnostic criteria that will be employed in our future applications.

The most direct and intuitive methods for assessing convergence include trace, density, autocorrelation, and cumulative quantile plots. Here is how each of these methods contributes to convergence diagnostics: trace plots display how the mean of the chain evolves with each iteration; stable behavior in a trace plot can indicate the chain's stability. The posterior density plots indicate whether the sample aligns with the expected distribution. The cumulative quantile plots indicate whether the quantiles of the obtained chain converge as iterations progress, which is the expected behavior. Finally, the autocorrelation plots show the decline in autocorrelation among sample elements generated over iterations; a rapid decrease in autocorrelation is expected.

All these first procedures are analyzed graphically and plots can be easily obtained using specific packages available for statistical software. In our study, we used the `coda` package of the R software (PLUMMER *et al.*, 2006). However, it is necessary to establish statistical measures that quantify the diagnosis of convergence, in addition to graphical analyses.

The first formal criterion presented here is the Geweke's diagnostic criteria (GEWEKE, 1991), which verifies the stationarity of the chain by comparing the mean of elements at the beginning and at the end of the chain. The final part of the chain is subdivided into smaller segments and, for each of them, a z-test is performed to compare it with the initial segment. If the null hypothesis of no difference between the means of these segments is not rejected, it indicates the stationarity of the chain. When conducting this test with the `coda` package, the z-scores are provided, and assuming a significance level of 5%, the absolute values of these z-scores are expected to be less than 1.96 for the test to pass.

Another criterion presented here is the Heidelberger-Welch diagnostic criterion (HEIDELBERGER; WELCH, 1983). This is a convergence test with null hypothesis that the sample values are derived from a stationary distribution. The test is applied progressively, first to the whole chain, and then discarding portions of the chain sequentially until either the null hypothesis

is accepted or it discards 50% of the chain, at which point the null hypothesis is rejected. This test can also be performed using the `coda` package and, in this case, the p-value of the test is returned and the diagnosis whether the convergence passed or failed.

The last criterion we employ is the Gelman-Rubin's diagnostic criteria (GELMAN; RUBIN, 1992). This criterion involves observing the behavior of multiple parallel chains, each starting from different initial values. If the MCMC sampling procedures yield a sample from the target posterior distribution, then all these chains should eventually reach a steady state, becoming indistinguishable when compared. The Gelman-Rubin criterion calculates a statistic called "potential scale reduction" based on the variance of these chains. The `coda` package also provides this statistic. If this statistic is close to 1, around 1.1 or even 1.2, there is a good indication that the chains are converging to a steady state.

5.2 Real Data Applications

In this section, we revisit the two real datasets introduced in Section 3.4 to illustrate the hierarchical Bayesian methodologies for the shared frailty ARA_m and ARI_m models, as discussed in Section 5.1. The goal here is to compute BEs for the parameters of these models and their respective 95% credible intervals. This is achieved by using the MCMC samples from the posterior distributions, obtained through a combination of the Gibbs sampler and the MH algorithm as discussed earlier. The priors used are those defined in the Section 5.1.1, and the hyperparameters associated with each prior will be determined later.

Each dataset undergoes analysis using the shared frailty model considering both ARA and ARI classes, as well as different failure memory possibilities. The selection criteria for the optimal model in each case are based on the DIC, as discussed in Section 5.1.3. Subsequently, once the best model is selected, we conduct a study on the convergence of the MCMC samples, using the diagnostic criteria presented in Section 5.1.4 and additional sample characteristics, which will be elaborated upon.

Before starting the study of each dataset, let us establish some conditions that will be similar in both cases, according to the definition of our model. Being in the context of shared frailty, remember that a frailty variable Z_i is associated with the intensity function of each system i, so that Z_i are IID with $\text{Gamma}(1/\alpha, 1/\alpha)$ distribution, where α is the variance of the random variables Z_i, $i = 1, \ldots, k$, as discussed in Section 4.2. Consequently, the parameter α to be estimated in the model is the same for all systems.

As discussed at the outset of Section 5.1 and in line with the parametric approach adopted throughout this work, we assume that the initial failure intensity functions of the systems in each application are the same for all of them, that is, they are all modeled by a PLP with equal parameters β and ω for each system. However, within the Bayesian framework, we are considering the possibility that the effects of the repair performed after each failure are unique to

each system. In essence, we can have k different parameters θ_i ($i = 1,\ldots,k$) that represent the repair effect on each system. Hence, the vector of parameters to be estimated in these applications is $\boldsymbol{\mu} = (\beta, \omega, \alpha, \theta_i)$, for $i = 1,\ldots,k$.

Finally, regarding the choice of prior distributions, for both examples the adopted priors will be the same defined in Section 5.1.1 and, in line with the hierarchical approach discussed across this chapter, the hierarchy over the θ_i parameters will be considered. The hyperparameters used in both examples will be the same, intending to establish vague priors. Specifically, their values are as follows: $a = 1$, $b = 3$, $c = 0.01$, $d = 1$, $e = 1$, $f = 1$, $g = 1$ and $h = 1$.

5.2.1 Sugarcane Harvester Data Revisited

In this section, we will analyze again the dataset of the failure times of the cutting blades of the sugar cane harvesters presented in Section 3.4.1, but now, under a hierarchical Bayesian approach of shared frailty ARA_m and ARI_m models. As this dataset is composed by the failure times of 9 sugarcane harvesters, the vector of parameters to be estimated is $\boldsymbol{\mu} = (\beta, \omega, \alpha, \theta_1, \ldots, \theta_9)$.

As established in the introduction to this section, we analyzed the dataset using all possible failure memories m for the both shared frailty ARA_m and ARI_m models. For each analyzed model, we performed the MCMC methods with 50,000 replications with a *burn-in* of the first 5,000 and jumps of 10 for each chain, generating a sample of size $N = 4{,}500$ for each parameter. The *burn-in* of initial values and the jump between elements of the generated chains are techniques to ensure the stability state and to avoid high autocorrelation in the chain (more details about these procedures can be seen in Gelman *et al.* (1995)).

For each parameter, the corresponding BE was obtained as an average of the chain elements after the *burn-in* and jump procedures, as indicated in Section 5.1.2. Furthermore, the DIC value was calculated after each adjustment to select the best class and memory from among the possible models. Table 8 displays the DIC results for a selection of the analyzed models (note that although we conducted the analysis for all possible memories, we will omit some of those results here).

Table 8 – Estimated DIC values for different memories of the ARA and ARI classes.

	ARA_m	ARI_m
$m = 1$	931.76	938.08
$m = 10$	923.80	927.87
$m = 19$	919.07	925.66

Based on the values shown in Table 8, we chose the ARA_∞ model (corresponding to the ARA_{19}) due to its lowest DIC score. Now, we need to check the effectiveness of the proposed MCMC for this model. For each parameter, the trace, density, autocorrelation, and cumulative quantile plots of the simulated MCMC samples were obtained using the `coda`

package, as discussed in Section 5.1.4. These plots are available in Appendix A.1, in Figures 51-62. Analyzing these plots, it is noticed that the chains of all model parameters converged to the marginal posterior distribution. To improve the analysis and certify the convergence of the chains, the formal diagnostic criteria presented in Section 5.1.4 were used and the results are presented in Table 9.

Table 9 – Diagnostic criteria results for the shared frailty ARA_∞ model.

	Geweke ($\|z$-scores$\|$)	Heidelberger-Welch (p-values)	Gelman-Rubin (point estimation)
β	0.242	0.554	1.001
ω	0.448	0.497	1.003
α	0.375	0.333	1.014
θ_1	1.665	0.070	1.001
θ_2	0.753	0.819	1.004
θ_3	1.111	0.590	1.001
θ_4	0.978	0.645	1.001
θ_5	0.528	0.081	1.010
θ_6	1.874	0.583	1.002
θ_7	1.656	0.390	1.001
θ_8	1.952	0.629	1.001
θ_9	0.777	0.739	1.000

Based on the findings presented in Table 9 and recalling what was discussed in Section 5.1.4, we can assert that the sample generated through our MCMC procedures has successfully converged to the desired posterior distribution and reached a stable state. All test statistics of the three criteria used were favorable to the conclusion of convergence for all model parameters. Note that for the Geweke's criterion the absolute z-score values for all parameters were consistently below 1.96, which indicates the non-rejection of the chain's stationarity hypothesis at a 5% significance level.

Furthermore, the Heidelberger-Welch's criterion results, available in Table 9, provide p-values for the stationarity tests of the generated sample. Once again, all parameters pass this test at a 5% significance level, as all p-values exceed 0.05.

Finally, considering the Gelman-Rubin's criterion, we generated another sample with different initial values and the estimated potential scale reduction statistic is reported in Table 9. Note that this statistic was close to 1 for all parameters, reinforcing the conclusion of stationarity of the chain. In Figure 63 of Appendix A.1, we present the plots of the Gelman-Rubin test, which demonstrate that the test statistics remain below 1.2 for almost all iterations of the process.

After concluding that the iterative process has led to the convergence of the sampled chain to the posterior distribution, we can obtain the BE for each parameter of the model as an average of the elements of their respective chains. Furthermore, by analyzing this sorted sample, it is possible to obtain the estimates of the median and the 95% CI for each parameter, as

discussed in Section 5.1.2. All of these results for data fitting by the shared frailty ARA_∞ model are shown in Table 10.

Table 10 – Estimation results for the hierarchical Bayesian shared frailty ARA_∞ model applied to dump truck data.

$\hat{\mu}$	BE (Posterior Mean)	Posterior Median	95% CI_B
$\hat{\beta}$	1.613	1.613	(1.248, 1.962)
$\hat{\omega}$	0.010	0.008	(0.002, 0.028)
$\hat{\alpha}$	0.092	0.057	(0.002, 0.425)
$\hat{\theta}_1$	0.209	0.173	(0.008, 0.603)
$\hat{\theta}_2$	0.455	0.452	(0.124, 0.796)
$\hat{\theta}_3$	0.300	0.280	(0.019, 0.708)
$\hat{\theta}_4$	0.354	0.336	(0.031, 0.765)
$\hat{\theta}_5$	0.416	0.425	(0.059, 0.777)
$\hat{\theta}_6$	0.290	0.272	(0.028, 0.664)
$\hat{\theta}_7$	0.214	0.183	(0.014, 0.576)
$\hat{\theta}_8$	0.375	0.364	(0.084, 0.734)
$\hat{\theta}_9$	0.582	0.593	(0.216, 0.879)

Analyzing the estimates presented in Table 10, in a global way, it is possible to verify that the model identified the existence of unobserved heterogeneity affecting the systems failure process ($\hat{\alpha} > 0$) and repair effect in all systems. The estimates of the PLP parameters β and ω (from the reparameterization of the originally adopted η parameter) are in line with expectations and similar to those obtained in Section 4.1.5, where a similar analysis was performed with the same dataset.

Focusing specifically on the estimates obtained for the parameters θ_i, $i = 1, \ldots, 9$, we reinforce that there is evidence of a repair effect for all observed systems. However, note that the lower bounds of the 95% CI_B are in close proximity to zero. An effective way to improve this interpretation is to analyze the posterior density distribution of these parameters, which represents a key advantage of the Bayesian approach we have employed. By analyzing Figures 54-62 of Appendix A.1, it is noticeable that some of the parameters θ_i are more inclined to approach zero, such as θ_1 and θ_7. This suggests that, while the presence of a repair effect is identified, in these systems, repair tends to approach to PR. Conversely, systems #2 and #9 exhibit a different pattern; for these two systems, the posterior density is concentrated at a certain distance from zero.

This difference in repair effect posterior density distribution suggests a potential classification scheme for systems based on their repair characteristics. Systems with higher θ values are more poorly maintained, and as a consequence have higher failure rates than other units. Insights of this type can be very well used in policies for preventing failures and preventive maintenance politics for complex systems. This shows a clear advantage of using the hierarchical Bayesian approach within the context of multiple repairable systems.

Finally, with regard to the estimate for the parameter α, the estimate $\hat{\alpha}$ enables the calculation of individual frailty for each system, as discussed in Section 4.2.2. The results of individual frailty are shown in Table 11 and were obtained using equation (2.33) incorporating the observed failure times of the system and the obtained estimates.

Table 11 – Individual frailty for each dump truck, in the hierarchical Bayesian shared frailty ARA_∞ model.

Frailty	Estimate	Frailty	Estimate
$\hat{z}_1$	0.823	$\hat{z}_6$	1.022
$\hat{z}_2$	0.972	$\hat{z}_7$	0.779
$\hat{z}_3$	1.005	$\hat{z}_8$	0.872
$\hat{z}_4$	1.026	$\hat{z}_9$	0.900
$\hat{z}_5$	1.132		

It is worth noting that the z_i estimates are closely clustered around 1, which is to be expected, given that the estimate $\hat{\alpha}$ is not significantly greater than zero. It is important to point out that the calculation of individual frailties took into account the unique estimation of the parameters θ_i for each system i, which makes the failure process of each system even more specific. In summary, while these systems share their initial characteristics (modeled by a common PLP), they diverge as the wear and tear of their own functioning and the influence of external factors take effect within each of them.

In this sense, to perform the graphical goodness-of-fit analysis in this case, we will use two approaches: the first, analyzing the MCF of the global failure process of all systems, and the second, also analyzing the individual fit of each system. As discussed before, in a global way, the graphical procedure consists in comparing the empirical MCF of the observed failure times with the average of the MCFs estimated by the shared frailty ARA_∞ model from each system. The general goodness-of-fit plot comparison is shown in Figure 35 and it is notable that the curves of the empirical MCF and the average of the systems' MCFs exhibit a close alignment.

Finally, when comparing the individual accumulated failures of each system with the failures predicted by the proposed model, we can employ the same graphical approach used for the global analysis to verify the quality of the fit. The graphs resulting from this comparison are shown in Figure 36 and illustrate that, in general, the model effectively captures the failure times of the systems. However, there are two discrepant cases with systems #5 and #9: in the former case, the model underestimates the number of failures, while in the latter, it overestimates them. These outliers can be attributed to the influence of the parameters β and ω on the fit, since these parameters are shared by all systems, and the optimization process seeks to balance their contributions. In conclusion, by combining the analysis of the graphs displayed in Figures 35 and 36, we can conclude that the model offers a good fit to the failure times of the harvesters. This underscores its suitability for analyzing this dataset and, consequently, for deriving meaningful interpretations and guiding actions based on this analysis.

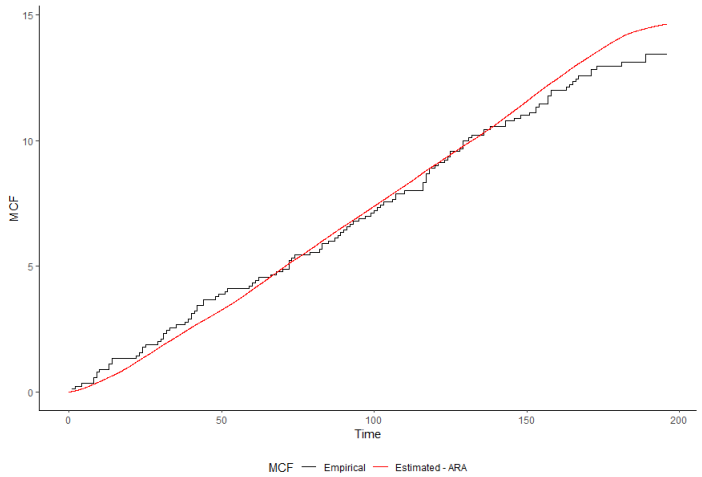

Figure 35 – Empirical and estimated MCF average for the sugarcane harvester data under hierarchical Baysean analysis for the shared frailty ARA_∞ model.

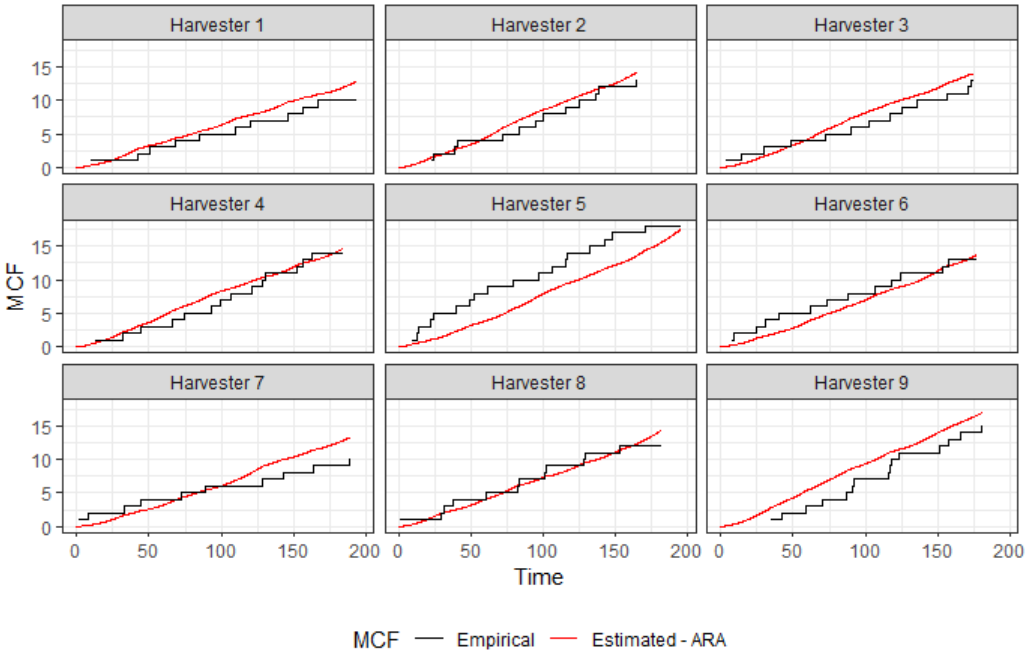

Figure 36 – Empirical and estimated MCF for each sugarcane harvester under hierarchical Bayesian analysis for the shared frailty ARA_∞ model.

5.2.2 Dump Truck Data Revisited

The dump truck failure times dataset presented in Section 3.4.2 will be revisited in this section. As previously done in the preceding section, our objective here is to illustrate the methodologies of the hierarchical Bayesian approach applied within our proposed shared frailty ARA_m and ARI_m models for modeling this dataset. Remember that this dataset consists of the failure times of 5 trucks, and therefore, the vector of parameters to be estimated is $\boldsymbol{\mu} = (\beta, \omega, \alpha, \theta_1, \ldots, \theta_5)$.

The procedures for this analysis are exactly the same as those performed in Section 5.2.1. Therefore, we will skip redundant details already discussed and concentrate only on the results obtained.

To select the optimal model among those observed, the DIC criterion was used again. Table 12 displays the results of the DIC estimates for some of these models. In this case, the selected model is again ARA_∞, since it has the lowest DIC. Note that here, the ARA_∞ class corresponds to ARA_{32}, since the highest number of failures observed in a single truck was 32 failures.

Table 12 – Estimated DIC values for different memories of the ARA and ARI classes.

	ARA_m	ARI_m
$m = 1$	619.51	669.69
$m = 10$	611.91	662.28
$m = 32$	611.46	661.92

To verify the efficiency of the proposed MCMC methods in terms of chain convergence, we conducted graphical analyses and utilized the formal criteria discussed in Section 5.1.4. The trace, density, autocorrelation, and cumulative quantile plots related to each parameter of this example can be found in Figures 64-71 of Appendix A.2, and their initial analysis indicates the convergence of all chains. To complete this analysis, the results of the formal convergence criteria are shown in Table 13.

Table 13 – Diagnostic criteria results for the shared frailty ARA_∞ model.

	Geweke (|z-scores|)	Heidelberger-Welch (p-values)	Gelman-Rubin (point estimation)
β	0.240	0.910	1.020
ω	0.531	0.797	1.028
α	0.477	0.203	1.005
θ_1	0.922	0.623	1.024
θ_2	0.297	0.739	1.019
θ_3	1.743	0.242	1.012
θ_4	0.244	0.874	1.002
θ_5	1.277	0.663	1.022

The results of the estimates presented in Table 13 indicate that the MCMC samples for all model parameters successfully converged to a stationary state in the target posterior density distribution. The plots of Gelman-Rubin test for this application are displayed in Figure 72 of Appendix A.2.

Table 14 shows the estimates obtained from fitting the shared frailty ARA_∞ model to the truck failure data, using the proposed hierarchical Bayesian methodology.

Upon a brief analysis of the results in Table 14, it is possible to conclude about the existence of unobserved heterogeneity between the systems and the effect of the repair performed

Table 14 – Estimation results for the hierarchical Bayesian shared frailty ARA_∞ model applied to dump truck data.

	BE (Posterior Mean)	Posterior Median	95% CI_B
$\hat{\mu}$	1.683	1.671	(1.300, 2.159)
$\hat{\beta}$	0.050	0.043	(0.001, 0.128)
$\hat{\omega}$	0.212	0.117	(0.004, 0.936)
$\hat{\alpha}$	0.459	0.466	(0.088, 0.797)
$\hat{\theta}_1$	0.564	0.579	(0.236, 0.816)
$\hat{\theta}_2$	0.464	0.466	(0.112, 0.805)
$\hat{\theta}_3$	0.591	0.605	(0.247, 0.859)
$\hat{\theta}_4$	0.447	0.457	(0.080, 0.790)
$\hat{\theta}_5$			

after each failure on their failure process. Notably, the estimated value $\hat{\alpha}$ is significantly higher than the estimate obtained in the example presented in Section 4.2.5 (which involves the same dataset), suggesting a substantial impact of observing multiple repair effect parameters θ_i on its estimation.

Analyzing the estimates of the parameters θ_i and their posterior density distributions presented in Figures 67-71 of Appendix A.2, it is possible to consistently conclude that all systems are subjected to IR. It is noteworthy that neither the 95% CI_B of these parameters nor their posterior density distributions approach the extremes of the interval $(0, 1)$, indicating that these repairs do not tend towards PR or MR. Furthermore, the BEs of each θ_i allow for the categorization of the trucks into two groups with highly similar repair effects: the first group comprises trucks #1, #3 and #5 (better maintained), while the second consists of trucks #2 and #4 (poorly maintained).

Utilizing the parameter estimates and the observed failure times, the individual frailty of each truck are calculated and these results are presented in Table 15. Note that the value of the estimate $\hat{\alpha}$ is significantly greater than zero, indicating greater variability in the individual frailties of these systems compared to the previous example. This suggests that certain systems are more prone to failure in shorter timeframes due to external and not quantifiable factors affecting them.

Table 15 – Individual frailty for each dump truck, in the hierarchical Bayesian shared frailty ARA_∞ model.

Frailty	Estimate	Frailty	Estimate
$\hat{z}_1$	0.749	$\hat{z}_4$	0.851
$\hat{z}_2$	1.060	$\hat{z}_5$	0.830
$\hat{z}_3$	0.773		

Finally, we examine the MCF graph for all systems and the cumulative number of failures graphs for each system to assess the model's goodness-of-fit. The results are presented in Figures 37 and 38, respectively.

In Figure 37, it is evident that the average curve of the MCF estimated by the model is

very close to the empirical MCF graph, indicating a reasonable overall model fit. Additionally, individual assessments in Figure 38 show that the model provides good fits for each system, as the empirical number of failures for each one are very close to the individual curve estimated by the model.

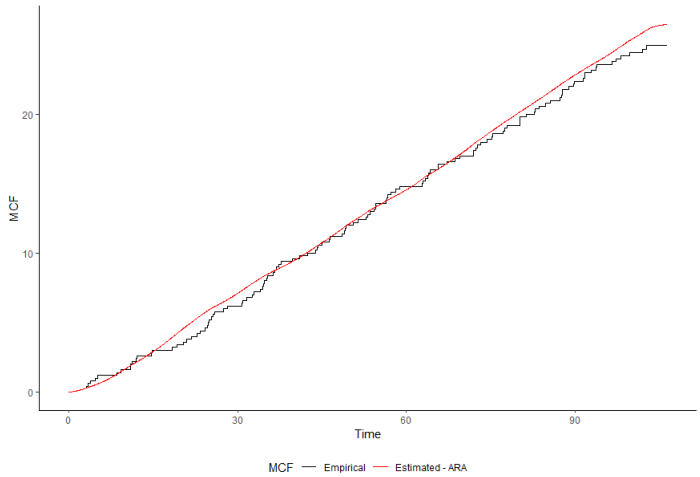

Figure 37 – Empirical and estimated MCF average for the dump truck data under hierarchical Bayesian analysis for the shared frailty ARA_∞ model.

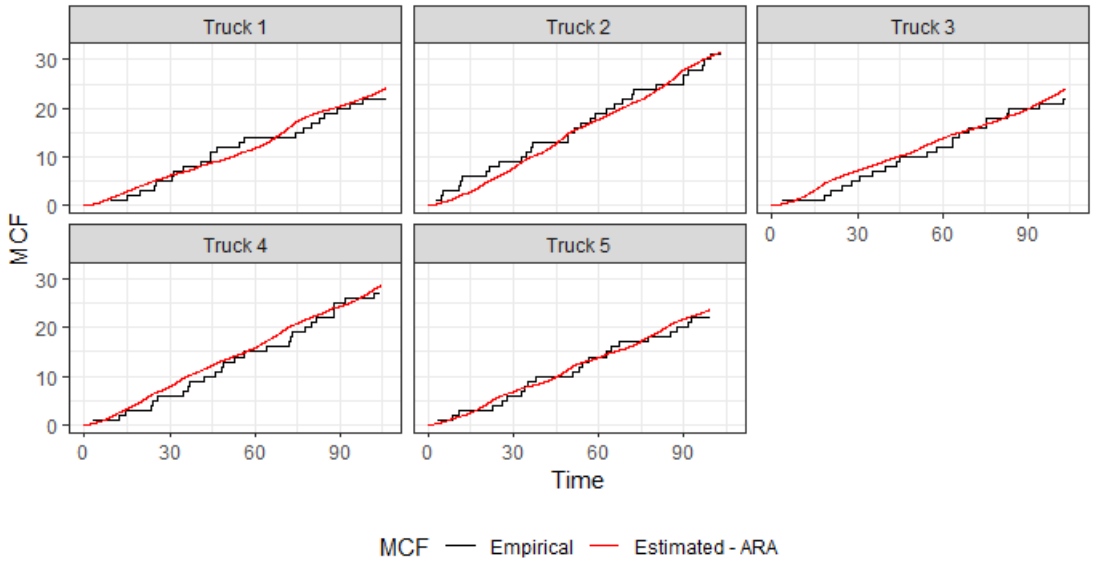

Figure 38 – Empirical and estimated MCF for each dump truck under hierarchical Bayesian analysis for the shared frailty ARA_∞ model.

5.3 Concluding Remarks of the Chapter

In this chapter we proposed Bayesian inference for estimating parameters of our proposed shared frailty models considering repairable systems subjected to IR. This approach offers an

alternative to the frequentist estimation methods discussed in previous chapters and provides new avenues for interpreting and applying parameter estimates, as they are now treated as random variables.

Unlike previous chapters, in this chapter we proposed that each system can have its individual repair effect, which expands the scope of our previous discussions. As this measure is often not precisely quantified by those overseeing repairs, it is feasible to assume that each system can have its individual measure, since the effect of the repair on each system can cause impacts of different magnitudes on their respective failure processes.

We introduced a hierarchical Bayesian framework to relate the multiple repair effect parameters and employed MCMC sampling methods, including the Gibbs sampler and the MH algorithm. In addition, criteria for selecting models and verifying the convergence of the generated chains were presented. In this sense, we provided a comprehensive summary of all the techniques and theories used to implement our Bayesian approach.

Finally, we revisited the two datasets previously presented in this work to illustrate our proposed methodologies. In both applications, our Bayesian estimation approach proves its adequacy. The chains generated for each parameter converge to the desired posterior distribution, and the point estimates obtained yield a good fit for each dataset.

In conclusion, the suggested Bayesian inferential methods are suitable for our proposed shared frailty models. These methods offer more accurate interpretations of individual system failure process, including the individual repair effects and individual frailty estimation, while also identifying common characteristics shared across the entire system set. This kind of information can be extremely relevant when applied to real situations in industries and sectors that operate complex machines and need to manage maintenance policies for their equipment.

CHAPTER

6

UNOBSERVED HETEROGENEITY FOR MULTIPLE REPAIRABLE SYSTEMS SUBJECTED TO COMPETING RISKS UNDER IMPERFECT REPAIR

In this chapter we introduce competing risks in the models studied in the previous chapters. More specifically, the idea is to take into account the fact that a repairable system can fail due to different causes by adding the possibility that repairs related to these causes may have distinct effects on the system's lifetime. Additionally, all these processes of failures and repairs are subjected to potential influences from unobservable effects. In this sense, our objective is to propose shared frailty models for multiple repairable systems subjected to competing risks and whose repairs performed after each failure are considered IR. These models are generalizations of the models presented in the previous chapters in the sense of extending the previously discussed models to a context of competing risks. In addition, they are also generalizations of other works in the literature that present competing risks for systems under IR (such as Lindqvist (2006)) or frailty models for systems under competing risks but considering only MR after each failure (such as Almeida *et al.* (2020) and Somboonsavatdee and Sen (2015b)).

These models stand out from others in the existing literature due to their capacity to facilitate a comprehensive analysis of various inherent characteristics within a system's failure process. The more answers about a dataset a model is able to provide, the more insights and applicability it can provide to stakeholders about the dataset in question. In the context of repairable systems, collecting the most information about a dataset of times and causes of failure holds significant relevance. It enables a profound comprehension of the failure processes for each cause, subsequently facilitating the formulation of maintenance and scrapping strategies for systems.

The assumptions for these new models are based on the same ones previously presented. In this case, each failure cause r corresponds to a distinct failure process, characterized by an initial failure intensity governed by a PLP whose parameters are (β_r, η_r). The repairs after the failure occurrence are considered IR with repair effect denoted by θ_r. Once again, the two classes ARA_m and ARI_m proposed by Doyen and Gaudoin (2004) will be considered as candidates for modeling failure processes with IR. Furthermore, we introduce a random variable Z_i with $\text{Gamma}\left(\frac{1}{\alpha}, \frac{1}{\alpha}\right)$ distribution associated with the system i and shared by its times and causes of failure, which is able to capture and quantify unobservable effects that act on the system.

This chapter is organized as follows. In Section 6.1, we present the models and all their theoretical aspects through its subsections. In Subsection 6.1.1, we define the failure intensity functions of the models while considering ARA and ARI as potential approaches for an IR model. In Subsection 6.1.2, we propose inferential procedures and suggest the maximum likelihood estimation as a parameter estimation method. In Subsection 6.1.3, we present procedures to obtaining the individual frailties for each system, as well as the formulation of their respective reliability prediction functions. In Section 6.2, we proceed with a simulation study to verify the asymptotic properties of the proposed models' MLEs. Finally, in Section 6.3, we apply two real data tests to exemplify the discussed theoretical procedures.

6.1 Unobserved Heterogeneity in Competing Risks under IR Models

In this section, we present our proposed shared frailty models for multiple repairable systems subjected to competing risks and IR models, and the theory involved in their definition and parameter estimation. As discussed in Section 2.4, we assume that the competing risks are independent and each of them defines a failure process with its own intensity function. In this way, each competing risk r will be associated with an repair effect θ_r that will act in the proportional reduction of the virtual age (in the case of the ARA class) or the failure intensity (in the case of the ARI class) of the cause-specific failure process. Furthermore, when defining a parametric form for each cause-specific failure intensity function, we will also have a parameter vector associated with each one of them. On the other hand, given the shared aspect of the assumed frailty model, the parameter related to the distribution of frailty variables will be the only parameter shared by all cause-specific failures. These features will be discussed in detail below.

6.1.1 Model Formulation

Suppose that k independent repairable systems are observed, each one for a time t_i^*, for $k = 1, 2, \ldots$ and $i = 1, \ldots, k$. Each of these systems can fail for q distinct and independent causes and each system failure is caused by a single cause r, with $r = 1, \ldots, q$. In this way, we

define the data $\{(t_{i,j}, \delta_{i,j}), i = 1,\ldots,k; j = 1,\ldots,n_i\}$ of the pairs of times and causes of each failure, where $t_{i,j}$ is the j-th failure time of the i-th system, $\delta_{i,j}$ is the corresponding failure cause and n_i is the number of failures of system i. Furthermore, for every pair (i,j), $\delta_{i,j} = r$ for some $r = 1,\ldots,q$. As discussed in Section 2.4, for each specific cause r we can define the data $\{(t_{i,j}, \delta_{i,j} = r), i = 1,\ldots,k; j = 1,\ldots,n_{i,r}\}$, where, for all i, the sequences correspond to counting processes (here, NHPP) fully characterized by an intensity function $\lambda_r(t)$, called r cause-specific intensity function.

Continuing with the assumptions, assume that there may be unobservable factors that impact the failure times of the systems, but that can interfere in a specific way in the failure process of each system. As discussed in Section 2.3, these factors can be modeled via frailty models by inserting a frailty variable Z associated with systems or failure times. In this case, we will assume that the effects act specifically on each system and are shared by their respective failure times, that is, we are assuming that the unobserved heterogeneity is shared by the failure times of each system. Thus, for each system i, we associate a shared frailty variable Z_i that will be multiplied by the baseline intensity function of the system, as discussed in Section 2.3.2. But note that now systems are subjected to q causes of failure and per the previous discussion, there are q related intensity functions for each system. Mathematically summarizing this scenario that aggregates the ideas of competing risks models with frailty models, we can define the intensity function of the system i conditional on its associated frailty variable Z_i, and considering its q causes of failure, as:

$$\lambda_f(t_{i,j}, \delta_{i,j} \mid z_i) = z_i \underline{\lambda}(t_{i,j}, \delta_{i,j}) = z_i \sum_{r=1}^{q} \underline{\lambda}_r(t_{i,j}, \delta_{i,j} = r). \tag{6.1}$$

In equation (6.1), it is explicit that the frailty variable Z_i affects all q intensity functions related to failure causes. In other words, we can say that the causes of failure also share the same frailty, or even that they share the same unobserved heterogeneity by system.

Finally, suppose that for each failure cause r, after an occurrence of a related failure, the repair performed is an IR. So the functions λ_{0_r} in (6.1) can still be rewritten by the intensity functions of the ARA$_m$ and ARI$_m$ classes of IR defined in (2.13) and (2.16), respectively. But note that neither the repair effect nor the assumed failure memory for each cause-specific need to be the same for different causes, which naturally expands the number of parameters in these models and also the number of possible models as a consequence of combining the failure memories for the causes. In this case, we will denote by θ_r the repair effect related to the specific cause r and by m_r the failure memory assumed for this cause, with $r = 1,\ldots,q$. Making explicit the intensity functions for this model of shared frailty and competing risks for the ARA$_m$ and ARI$_m$ classes of IR, we can rewrite the expression (6.1), respectively, as:

$$\lambda_{f.\mathrm{ARA}m}(t_{i,j}, \delta_{i,j} \mid z_i) = z_i \sum_{r=1}^{q} \lambda_{0,r}\left(t_{i,j} - (1-\theta_r) \sum_{p=0}^{\min(m_r-1, j-2)} \theta_r^p t_{i,j-1-p}, \delta_{i,j} = r\right) \tag{6.2}$$

and

$$\lambda_{f.\mathrm{ARI}m}(t_{i,j},\delta_{i,j}\mid z_i)=z_i\sum_{r=1}^{q}\left[\lambda_{0,r}(t_{i,j},r)-(1-\theta_r)\sum_{p=0}^{\min(m_r-1,j-2)}\theta_r^p\lambda_{0,r}(t_{i,j-1-p},r)\right], \quad (6.3)$$

where $\lambda_{0,r}(t)$ is the r cause-specific initial intensity function and $j=1,\ldots,n_{i,r}$, where $n_{i,r}$ is the number of failures of system i due to cause r.

As in the models presented in the previous chapters, here we also assume that the initial intensity function $\lambda_{0,r}(t)$ follows a PLP defined by equation (2.3) and, therefore, we will deal with a completely parametric model. But in this case, due to the existence of q intensity functions, there are also q initial intensity functions with different parameters related to each of the q failure causes. We will denote by β_r and η_r the parameters of the r cause-specific PLP, for $r=1,\ldots,q$. In this way, we can rewrite the expressions (6.2) and (6.3) considering now the PLP as the initial intensity, as follows:

$$\lambda_{f.\mathrm{ARA}m}(t_{i,j},\delta_{i,j}\mid z_i)=z_i\sum_{r=1}^{q}\frac{\beta_r}{\eta_r^{\beta_r}}\left(t_{i,j_r}-(1-\theta_r)\sum_{p=0}^{\min(m_r-1,j-2)}\theta_r^p t_{i,(j-1-p)_r}\right)^{\beta_r-1} \quad (6.4)$$

and

$$\lambda_{f.\mathrm{ARI}m}(t_{i,j},\delta_{i,j}\mid z_i)=z_i\sum_{r=1}^{q}\frac{\beta_r}{\eta_r^{\beta_r}}\left[t_{i,j_r}^{\beta_r-1}-(1-\theta_r)\sum_{p=0}^{\min(m_r-1,j-2)}\theta_r^p t_{i,(j-1-p)_r}^{\beta_r-1}\right], \quad (6.5)$$

and here we use the notation t_{i,j_r} to refer to the observed failure times of system i resulting from cause r so that $j_r=1,\ldots,n_{i,r}$, or even, mathematically expressed, $\lambda(t_{i,j},\delta_{i,j})=t_{i,j_r}$ if $\delta_{i,j}=r$ or 0 otherwise.

Note that in these models, each specific cause r is associated with a vector of parameters $\boldsymbol{\mu}_r=(\beta_r,\eta_r,\theta_r)$ referring to the PLP and IR failure effect referring to that cause. As previously stated, we are again assuming that the frailty variables have Gamma$(1/\alpha,1/\alpha)$ distribution, so that parameter α is shared across all systems and failure causes. Thus, globally these models are defined by $3q+1$ parameters, with the parameter vector given by $\boldsymbol{\mu}=(\alpha,\boldsymbol{\beta},\boldsymbol{\eta},\boldsymbol{\theta})$, where α is the variance of the assumed frailty variable and the other vectors are $\boldsymbol{\beta}=(\beta_1,\ldots,\beta_r)$, $\boldsymbol{\eta}=(\eta_1,\ldots,\eta_r)$ and $\boldsymbol{\theta}=(\theta_1,\ldots,\theta_r)$, where $(\beta_r,\eta_r,\theta_r)$ refers to the r cause-specific parameters, with $r=1,\ldots,q$.

6.1.2 Inference

Let $\{(t_{i,j},\delta_{i,j}),i=1,\ldots,k;j=1,\ldots,n_i\}$ be the observed data of failure times and their respective causes for k independent repairable systems and let t_i^* be the i-th system truncation time of observation. In order to perform inference and obtain estimates for the vector of parameters $\boldsymbol{\mu}=(\alpha,\boldsymbol{\beta},\boldsymbol{\eta},\boldsymbol{\theta})$ for the shared frailty models under competing risks and IR defined by the intensity functions (6.4) and (6.5) in a classical approach, we will construct the respective

likelihood functions following all the assumptions previously discussed in Section 6.1.1. To carry out this construction more generally and without repetition, let us write $\lambda_{\text{IR}}(t)$ and $\Lambda_{\text{IR}}(t)$ to refer to the intensity and cumulative intensity functions relative to any of the ARA_m and ARI_m classes of IR. After defining the general likelihood function, we will separately write the functions referring to each class.

As discussed in Section 2.2.3, the general likelihood function for the failure times of a system subjected to IR after each failure (or, equivalently for its failure process $\{N(t_j), j = 1,\ldots,n\}$) is defined by

$$L_{\text{IR}}(\boldsymbol{\mu} \mid t_j) = \prod_{j=1}^{n} \left[\lambda_{\text{IR}}\left(t_j\right) e^{-\left[\Lambda_{\text{IR}}\left(t_j\right)-\Lambda_{\text{IR}}\left(t_{j-1}\right)\right]}\right] e^{-\left[\Lambda_{\text{IR}}(t^*)-\Lambda_{\text{IR}}(t_n)\right]},$$

so that is going to be the structure of our likelihood function.

Fixing a system i subjected to q failure causes and the action of the frailty variable Z_i, the likelihood contribution of the r-th cause-specific conditioned to z_i in the IR structure is given by

$$L_{i,r} = \left(\prod_{j=1}^{n_{i,r}} z_i \lambda_{\text{IR}r}\left(t_{i,j},r\right) e^{-z_i\left[\Lambda_{\text{IR}r}\left(t_{i,j},r\right)-\Lambda_{\text{IR}r}\left(t_{i,j-1},r\right)\right]}\right) e^{-z_i\left[\Lambda_{\text{IR}r}\left(t_i^*,r\right)-\Lambda_{\text{IR}r}\left(t_{i,n_{i,r}},r\right)\right]},$$

where $L_{i,r} = L_{i,r}(\boldsymbol{\mu} \mid t_{i,j}, \delta_{i,j} = r, z_i)$, $\lambda_{\text{IR}r}(t,r)$ and $\Lambda_{\text{IR}r}(t,r)$ indicate the intensity functions of a failure process related to cause-specific r and subjected to IR (with effect θ_r) after each failure, and $n_{i,r}$ is the number of failures of system i due to cause r.

As the failure causes are assumed to be independent, the likelihood contribution of a specific system i conditional to z_i is given by

$$\begin{aligned}
L_i &= \prod_{r=1}^{q}\left[\left(\prod_{j=1}^{n_{i,r}} z_i \lambda_{\text{IR}r}\left(t_{i,j},r\right) e^{-z_i\left[\Lambda_{\text{IR}r}\left(t_{i,j},r\right)-\Lambda_{\text{IR}r}\left(t_{i,j-1},r\right)\right]}\right) e^{-z_i\left[\Lambda_{\text{IR}r}\left(t_i^*,r\right)-\Lambda_{\text{IR}r}\left(t_{i,n_{i,r}},r\right)\right]}\right] \\
&= \prod_{r=1}^{q}\left(\prod_{j=1}^{n_{i,r}} \lambda_{\text{IR}r}\left(t_{i,j},r\right)\right) z_i^{n_{i,r}} e^{-z_i\sum_{j=1}^{n_{i,r}}\left[\Lambda_{\text{IR}r}\left(t_{i,j},r\right)-\Lambda_{\text{IR}r}\left(t_{i,j-1},r\right)\right]} e^{-z_i\left[\Lambda_{\text{IR}r}\left(t_i^*,r\right)-\Lambda_{\text{IR}r}\left(t_{i,n_{i,r}},r\right)\right]} \\
&= \left(\prod_{r=1}^{q}\prod_{j=1}^{n_{i,r}} \lambda_{\text{IR}r}\left(t_{i,j},r\right)\right) z_i^{n_i} e^{-z_i\sum_{r=1}^{q}\left[\sum_{j=1}^{n_{i,r}}\left[\Lambda_{\text{IR}r}\left(t_{i,j},r\right)-\Lambda_{\text{IR}r}\left(t_{i,j-1},r\right)\right]+\left[\Lambda_{\text{IR}r}\left(t_i^*,r\right)-\Lambda_{\text{IR}r}\left(t_{i,n_{i,r}},r\right)\right]\right]},
\end{aligned}$$

where $L_i = L_i(\boldsymbol{\mu} \mid t_{i,j}, \delta_{i,j}, z_i)$ and n_i is the total number of failures of system i.

Given that the k systems are independent, the conditional likelihood function on the frailty z_i is given by

$$L(\boldsymbol{\mu} \mid z_i) = \prod_{i=1}^{k}\left(\prod_{r=1}^{q}\prod_{j=1}^{n_{i,r}} \lambda_{\text{IR}r}\left(t_{i,j},r\right)\right) z_i^{n_i} e^{-z_i W_{\text{IR}}},$$

where

$$W_{\text{IR}} = \sum_{r=1}^{q}\left[\sum_{j=1}^{n_{i,r}}\left[\Lambda_{\text{IR}r}\left(t_{i,j},r\right)-\Lambda_{\text{IR}r}\left(t_{i,j-1},r\right)\right]+\left[\Lambda_{\text{IR}r}\left(t_i^*,r\right)-\Lambda_{\text{IR}r}\left(t_{i,n_{i,r}},r\right)\right]\right].$$

To perform the estimation of the model parameters it is necessary to obtain the non-conditional likelihood function to the frailty variable z_i. To do this, as done in previous chapters, we just calculate the marginal likelihood function with respect to z_i:

$$L(\boldsymbol{\mu}) = \prod_{i=1}^{k} \left(\prod_{r=1}^{q} \prod_{j=1}^{n_{i,r}} \lambda_{\mathrm{IR}r}\left(t_{i,j}, r\right) \right) \int_0^{\infty} z_i^{n_i} e^{-z_i W} f_{Z_i}(z_i) dz_i. \tag{6.6}$$

Now, using the fact that the random variables Z_i are IID with Gamma$(1/\alpha, 1/\alpha)$ distribution, for $i = 1, \ldots, k$, and following the same ideas presented in Section 2.3.3, the likelihood function (6.6) can be rewritten as:

$$L(\boldsymbol{\mu}) = \prod_{i=1}^{k} \frac{\alpha^{n_i} \Gamma\left(n_i + \frac{1}{\alpha}\right) \prod_{r=1}^{q} \prod_{j=1}^{n_{i,r}} \lambda_{\mathrm{IR}r}\left(t_{i,j}, r\right)}{\Gamma\left(\frac{1}{\alpha}\right) (1 + \alpha W)^{n_i + \frac{1}{\alpha}}},$$

and consequently, the unconditional log-likelihood function is given by

$$\begin{aligned} l(\boldsymbol{\mu}) = \sum_{i=1}^{k} \Bigg[& \sum_{r=1}^{q} \sum_{j=1}^{n_{i,r}} \log \lambda_{\mathrm{IR}r}\left(t_{i,j}, r\right) + n_i \log(\alpha) + \log \Gamma\left(n_i + \frac{1}{\alpha}\right) \\ & - \log \Gamma\left(\frac{1}{\alpha}\right) - \left(n_i + \frac{1}{\alpha}\right) \log\left(1 + \alpha W_{\mathrm{IR}}\right) \Bigg]. \end{aligned} \tag{6.7}$$

Finally, we use the expressions (2.13) and (2.14) that define the intensity and cumulative intensity functions of the ARA class to replace the functions $\lambda_{\mathrm{IR}r}(t)$ and $\Lambda_{\mathrm{IR}r}(t)$ in equation (6.7), respectively. Furthermore, we also use the assumption that the initial intensity follows a PLP, whose intensity and cumulative intensity functions are given by (2.3) and (2.4). Note that here we write ARA instead of ARA$_m$ since the failure memories are related to each of the failure causes and are not necessarily all equal to a single value m. In this way, the explicit log-likelihood function for the shared frailty model for competing risks under ARA repair effects and initial PLP is given by

$$\begin{aligned} l_{f.\mathrm{ARA}}(\boldsymbol{\mu}) = {} & N \log(\alpha) + \sum_{i=1}^{k} \log \Gamma\left(n_i + \frac{1}{\alpha}\right) + \sum_{i=1}^{k} \sum_{r=1}^{q} n_{i,r} \left[\log(\beta_r) - \beta_r \log(\eta_r)\right] \\ & + \sum_{i=1}^{k} \sum_{r=1}^{q} \sum_{j=1}^{n_{i,r}} (\beta_r - 1) \log\left(t_{i,j_r} - (1 - \theta_r) s(t_{i,(j-1)_r})\right) - \sum_{i=1}^{k} \log \Gamma\left(\frac{1}{\alpha}\right) \\ & - \sum_{i=1}^{k} \left(n_i + \frac{1}{\alpha}\right) \log\left(1 + \alpha W_{\mathrm{ARA}}\right), \end{aligned} \tag{6.8}$$

with

$$\begin{aligned} W_{\mathrm{ARA}} = \sum_{r=1}^{q} \frac{1}{\eta_r^{\beta_r}} \Bigg[& \sum_{j=1}^{n_{i,r}} \left[\left(t_{i,j_r} - (1 - \theta_r) s(t_{i,(j-1)_r})\right)^{\beta_r} - \left(t_{i,(j-1)_r} - (1 - \theta_r) s(t_{i,(j-1)_r})\right)^{\beta_r} \right] \\ & + \left[\left(t_{i^*} - (1 - \theta_r) s(t_{i,n_{i,r}})\right)^{\beta_r} - \left(t_{i,n_{i,r}} - (1 - \theta_r) s(t_{i,n_{i,r}})\right)^{\beta_r} \right] \Bigg], \end{aligned}$$

where $N = \sum_{i=1}^{k} n_{i,r}$ is the total number of failures observed across all systems, j_r denotes the j-th failure occurred by cause r.

In a completely analogous way to ARA class, now using the intensity and cumulative intensity functions (2.16) and (2.17) of the ARI class, we obtain the explicit log-likelihood function for the shared frailty model for competing risks under ARI repair effects and initial PLP as:

$$\begin{aligned} l_{f.\mathrm{ARI}}(\boldsymbol{\mu}) = {} & N\log(\alpha) + \sum_{i=1}^{k} \log\Gamma\left(n_i + \frac{1}{\alpha}\right) + \sum_{i=1}^{k}\sum_{r=1}^{q} n_{i,r}\left[\log(\beta_r) - \beta_r \log(\eta_r)\right] \\ & + \sum_{i=1}^{k}\sum_{r=1}^{q}\sum_{j=1}^{n_{i,r}} \log\left[t_{i,j_r}^{\beta_r - 1} - (1-\theta_r)\underset{\sim}{s}(t_{i,(j-1)_r})\right] - \sum_{i=1}^{k}\log\Gamma\left(\frac{1}{\alpha}\right) \\ & - \sum_{i=1}^{k}\left(n_i + \frac{1}{\alpha}\right)\log(1+\alpha W_{\mathrm{ARI}}), \end{aligned} \tag{6.9}$$

where

$$\begin{aligned} W_{\mathrm{ARI}} = {} & \sum_{r=1}^{q}\frac{1}{\eta_r^{\beta_r}}\left[\sum_{j=1}^{n_{i,r}}\left[t_{i,j_r}^{\beta_r} - t_{i,(j-1)_r}^{\beta_r} - \beta_r(t_{i,j_r} - t_{i,(j-1)_r})(1-\theta_r)\underset{\sim}{s}(t_{i,(j-1)_r})\right]\right. \\ & \left. + \left[t_{i^*}^{\beta_r} - t_{i,n_{i,r}}^{\beta_r} - \beta_r(t_i^* - t_{i,n_{i,r}})(1-\theta_r)\underset{\sim}{s}(t_{i,n_{i,r}})\right]\right]. \end{aligned}$$

As in the other chapters, the equations (6.8) and (6.9) were constructed for a time truncation scenario, but can be adapted for the failure truncation scenario again by substituting the truncation time t_i^* for the time of the last observed failure $t_{i,n_{i,r}}$ for all systems $i = 1,\ldots,k$ and failure causes $r = 1,\ldots,q$.

And once again, the estimate $\hat{\boldsymbol{\mu}} = (\hat{\alpha}, \hat{\boldsymbol{\beta}}, \hat{\boldsymbol{\eta}}, \hat{\boldsymbol{\theta}})$ of the vector of parameters $\boldsymbol{\mu} = (\alpha, \boldsymbol{\beta}, \boldsymbol{\eta}, \boldsymbol{\theta})$ is obtained by maximizing the the equations (6.8) and (6.9) through numerical methods and with the aid of computational tools, since there is no analytical solution for this optimization problem. Following the analogies to the previous models, here we also suggest the construction of the CI according to the asymptotic theory of the Normal distribution.

6.1.3 Reliability Prediction

In this section we proceed with obtaining the reliability prediction functions for the two models proposed in Section 6.1.1. The reliability prediction is performed after estimating the parameters according to the inferential methods discussed in Section 6.1.2.

As discussed in Section 4.2.3, the first step in predicting reliability in shared frailty models is estimating the frailty terms for each system. Remember that we are assuming that the frailty variables Z_i are IID with Gamma$(1/\alpha, 1/\alpha)$ distribution and, therefore, an estimate for each expected value $\hat{z}_i$ can be obtained. For this, we use the ideas in Nielsen *et al.* (1992) to

adapt the equation (2.33), which can be rewritten as:

$$\hat{Z}_i = \frac{1/\hat{\alpha} + \sum_{r=1}^{q} n_{i,r}}{1/\hat{\alpha} + \sum_{r=1}^{q} \sum_{j=1}^{n_{i,r}} \left(\Lambda_{\mathrm{IR}r}(t_{i,j_r}, r) - \Lambda_{\mathrm{IR}r}(t_{i,(j-1)_r}, r) \right)}, \tag{6.10}$$

where $n_{i,r}$ is the number of observed failures in the i-th system due to the cause-specific r, for any system $i = 1, \ldots, k$.

With the estimated $\hat{z}_i$ and knowing the history $\mathscr{H}_{t_{i,n_i}}$ of failure processes and their respective causes for any system i with n_i observed failures, it is possible to estimate the reliability prediction of the system from a last observed failure at time t_{i,n_i}. The general reliability prediction function used in this case is the same given in (4.23), but we can rewrite it with adaptations for our new context using the intensity function with competing risks under shared frailty (6.1), as follows:

$$R(t) = \mathbb{P}[T_{i,n_i+1} - t_{i,n_i} > t \mid \mathscr{H}_{t_{i,n_i}}] = \exp\left\{ -\hat{z}_i \int_{t_{i,n_i}}^{t_{i,n_i}+t} \sum_{r=1}^{q} \lambda_{\mathrm{IR}r}(u, r)\, du \right\}, \tag{6.11}$$

where $\lambda_{\mathrm{IR}r}$ refers to the intensity function of one of the two IR classes ARA or ARI related to the failure cause r.

Some interesting discussions need to be established in this context where we take competing risks. Note that in equation (6.11) we purposely denote the last observed failure time by t_{i,n_i}, referring to the last failure time of the system globally, taking into account all possible causes of failure and not any specific one. This means that, regardless of what was the reason that caused the last system failure, all risks continue to compete to cause the next failure and, therefore, all interfere with the reliability prediction. This is obvious from the very definition of the intensity function of a system under competing risks by equation (6.1) as the sum of the risks referring to each specific one.

In our context of IR, after the occurrence of a failure due to a certain cause r and its repair, the reduction of intensity or virtual age occurs only in r cause-specific intensity function. That is, only the speed of increase in the r cause-specific accumulated intensity decreases, while that of the others causes continues to increase. This means that after the failure and the repair in time t_{i,n_i}, there is already an accumulation of failure intensity from the accumulated intensities of other causes that directly impacts the global system reliability. This information is mathematically explicit in equations (6.12) and (6.12), where it is possible to verify that, when resorting to the r cause-specific failure history, we look at the times $t_{i,n_{i,r}}$ referring to the last failure caused by the specific cause r.

Explicitly rewriting the reliability prediction function (6.11) for competing risks model under shared frailty with initial intensity PLP and ARA class of IR, we obtain the following

function:

$$\begin{aligned} R(t) &= \exp\left\{-\hat{z}_i \int_{t_{i,n_i}}^{t_{i,n_i}+t} \sum_{r=1}^{q} \lambda_{\mathrm{ARA,r}}(u)\, du\right\} \\ &= \exp\left\{-\hat{z}_i \sum_{r=1}^{q} \int_{t_{i,n_i}}^{t_{i,n_i}+t} \frac{\beta_r}{\eta_r^{\beta_r}} \left(u-(1-\theta_r)s(t_{i,n_{i,r}})\right)^{\beta_r-1} du\right\} \\ &= \exp\left\{-\hat{z}_i \sum_{r=1}^{q} \frac{1}{\eta_r^{\beta_r}} \left[\left(t_{i,n_i}+t-(1-\theta_r)s(t_{i,n_{i,r}})\right)^{\beta_r} - \left(t_{i,n_i}-(1-\theta_r)s(t_{i,n_{i,r}})\right)^{\beta_r}\right]\right\}. \end{aligned} \tag{6.12}$$

Using the same idea for the competing risks model under shared frailty with initial intensity PLP and ARI class of IR, we obtain the following function:

$$\begin{aligned} R(t) &= \exp\left\{-\hat{z}_i \int_{t_{i,n_i}}^{t_{i,n_i}+t} \sum_{r=1}^{q} \lambda_{\mathrm{ARI,r}}(u)\, du\right\} \\ &= \exp\left\{-\hat{z}_i \sum_{r=1}^{q} \int_{t_{i,n_i}}^{t_{i,n_i}+t} \frac{1}{\eta_r^{\beta_r}} \left[u^{\beta_r-1} - (1-\theta_r)\underset{\sim}{s}(t_{i,n_{i,r}})\right] du\right\} \\ &= \exp\left\{-\hat{z}_i \sum_{r=1}^{q} \frac{1}{\eta_r^{\beta_r}} \left[(t_{i,n_i}+t)^{\beta_r} - (t_{i,n_i})^{\beta_r} - t\beta_r(1-\theta_r)\underset{\sim}{s}(t_{i,n_{i,r}})\right]\right\}. \end{aligned} \tag{6.13}$$

Finally, the MTTF at time $T_{i,n_i} = t_{i,n_i}$ is given by

$$\mathrm{MTTF}_{t_n} = \int_0^{\infty} R(t)\, dt, \tag{6.14}$$

where $R(t)$ is given by (6.12) or (6.13) for calculation referred to ARA or ARI class, respectively. Note that expression (6.14) does not establish any specific cause of failure, which indicates that all causes are considered in this calculation.

6.2 Simulation Study

In this section, we carry out an extensive Monte Carlo simulation study to validate the properties of the MLEs within the proposed models. Our objective remains centered on assessing the efficiency and consistency performance of these estimators. The procedures conducted in this section are derived from previous simulation studies, particularly of the Section 4.2.4. Consequently, redundant details will be omitted. The key evaluation metrics for this analysis will again include the MRE, the RMSE and CP of the 95% CI, all of which have been previously defined.

The specificity of the failure time sample generation process in this case is that now we generate failure times referring to each specified cause of failure, departing from the earlier approach of considering the entire system. However, since the failure causes are assumed to be independent, it suffices to generate a sample of time failures corresponding to each cause.

Subsequently, these subsamples compose the failure sample per system, in line with the method outlined by Somboonsavatdee and Sen (2015a).

Let us consider the scenario where the simulated systems are susceptible to failure due to q distinct causes. For each system, q independent failure processes will be generated, each following the procedures elucidated in Sections 4.2.4.1 and 4.2.4.2 for the ARA and ARI classes, respectively. The ensuing algorithms outline the process of generating samples of failure times within the framework of competing risks.

Algorithm 1: Algorithm to generate ARA model failure times sample

Data: The nominal values: β_r, η_r, θ_r, m_r with $r = 1, \ldots, q$; α, k and t_i^* with $i = 1, \ldots, k$.
Result: The k ssamples failure times and causes: $(\boldsymbol{t}; \boldsymbol{r})$.
while $i \leq k$ **do**
  $z_i \sim$Gamma$\left(\frac{1}{\alpha}, \frac{1}{\alpha}\right)$
  while $r \leq q$ **do**
    $t_{i,j_r} \leftarrow 0$
    $j_r \leftarrow 1$
    while $t_{i,j_r} \leq t_i^*$ **do**
      $u \sim$Uniform$(0, 1)$
      Obtain t_{i,j_r} by Eq (4.26) with $F(x) = u$
      $j_r \leftarrow j_r + 1$
    end
    $(\boldsymbol{t}_{i,j_r}; r) = (t_{i,1}, \ldots, t_{i,j_r}; r)$; /* failures for the cause r */
  end
  $(\boldsymbol{t}_i; \boldsymbol{r}) = [(\boldsymbol{t}_{i,j_1}; 1), \ldots, (\boldsymbol{t}_{i,j_q}; q)]$; /* failures and causes of system i */
end
$(\boldsymbol{t}, \boldsymbol{r}) = [(\boldsymbol{t}_1; \boldsymbol{r}), \ldots, (\boldsymbol{t}_k; \boldsymbol{r})]$; /* complete failure times sample */

Algorithm 2: Algorithm to generate ARI model failure times sample

Data: The nominal values: β_r, η_r, θ_r, m_r with $r = 1, \ldots, q$; α, k and t_i^* with $i = 1, \ldots, k$.
Result: The k ssamples failure times and causes: $(\boldsymbol{t}; \boldsymbol{r})$.
while $i \leq k$ **do**
  $z_i \sim$Gamma$\left(\frac{1}{\alpha}, \frac{1}{\alpha}\right)$
  while $r \leq q$ **do**
    $t_{i,j_r} \leftarrow 0$
    $j_r \leftarrow 1$
    while $t_{i,j_r} \leq t_i^*$ **do**
      $u \sim$Uniform$(0, 1)$
      Solve the equation given by Eq (4.27) with $F(x) = u$
      $t_{i,j_r} = t_{i,j_r - 1} + x$
      $j_r \leftarrow j_r + 1$
    end
    $(\boldsymbol{t}_{i,j_r}; r) = (t_{i,1}, \ldots, t_{i,j_r}; r)$; /* failures for the cause r */
  end
  $(\boldsymbol{t}_i; \boldsymbol{r}) = [(\boldsymbol{t}_{i,j_1}; 1), \ldots, (\boldsymbol{t}_{i,j_q}; q)]$; /* failures and causes of system i */
end
$(\boldsymbol{t}, \boldsymbol{r}) = [(\boldsymbol{t}_1; \boldsymbol{r}), \ldots, (\boldsymbol{t}_k; \boldsymbol{r})]$; /* complete failure times sample */

For each scenario of parameters, truncation time and number of systems, 100 Monte Carlo samples were generated. The R software (R Core Team, 2021) was used for the generation process and all parameter and metric estimations. For simplicity, for both ARA and ARI classes, only two failure causes were considered for this study, denoted by causes A and B. The fixed nominal values for the parameters are:

- For cause A, fixed values: $\beta_A = 1.5$, $\eta_A = 15$ and $\theta_A = 0.3$;
- For cause B, fixed values: $\beta_B = 1.2$, $\eta_B - 20$ and $\theta_B = 0.7$;
- For the frailty variables variance, three values: $\alpha = (0.2, 1, 2)$;
- For the truncation time, two values for all systems: $t^* = (200, 500)$;
- For the memories related to causes A e B, three combinations: $m_A = m_B = (1, 5, 15)$;
- For the number of systems, five increasing values: $k = (5, 10, 15, 20, 25)$.

The results of the MRE, RMSE and CP estimates for the proposed competing risks under shared frailty ARA model are summarized in Figures 39, 40 and 41, while those for the respective ARI model are summarized in Figures 42, 43 and 44.

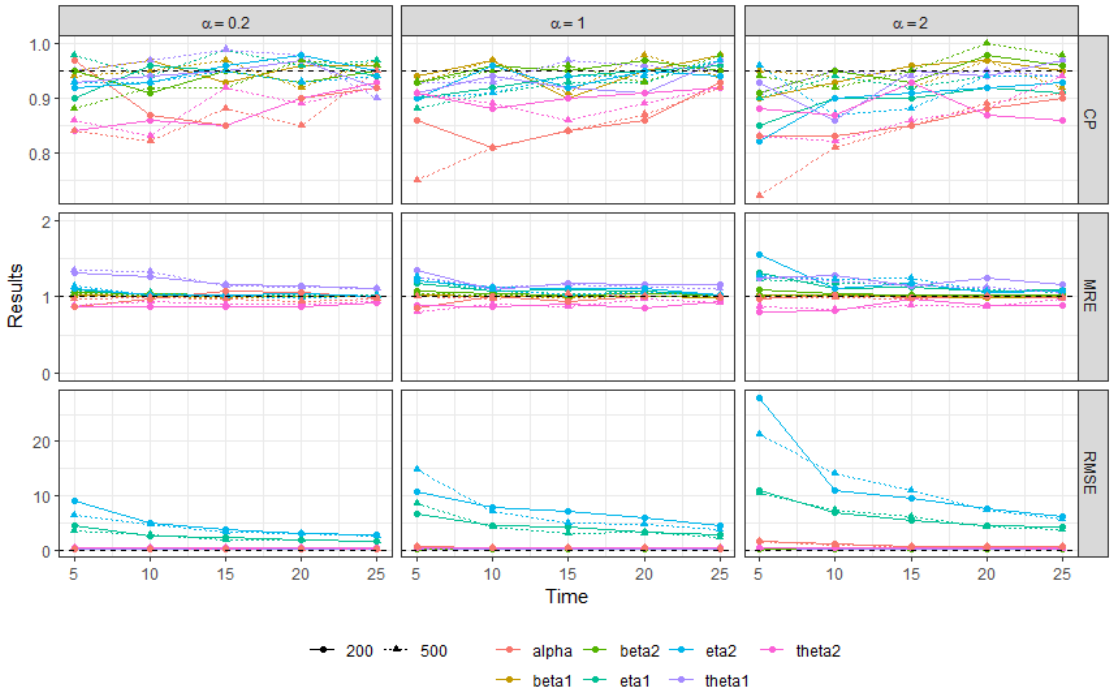

Figure 39 – Simulation results for the competing risks under shared frailty ARA model in scenarios with memory $m_A = m_B = 1$.

Note that the increase in the sample is due to the increase in the number of systems. As the number of systems increases, we expect the overall number of observed failures and their respective causes also increase. With the increasing of sample sizes, it is expected the

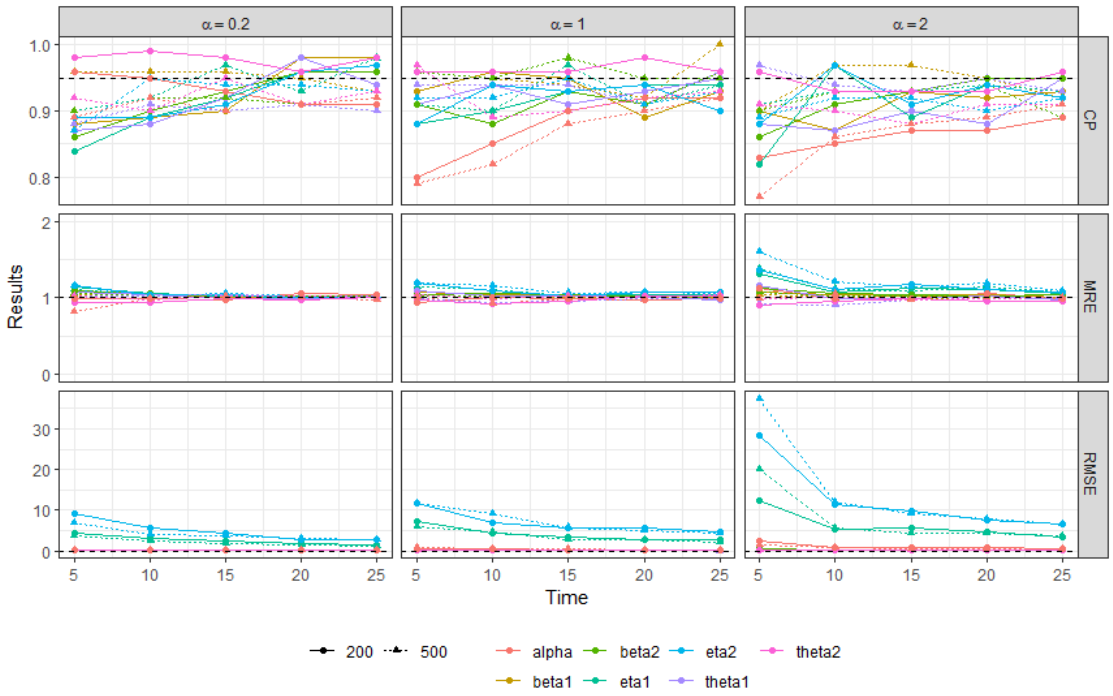

Figure 40 – Simulation results for the competing risks under shared frailty ARA model in scenarios with memory $m_A = m_B = 5$.

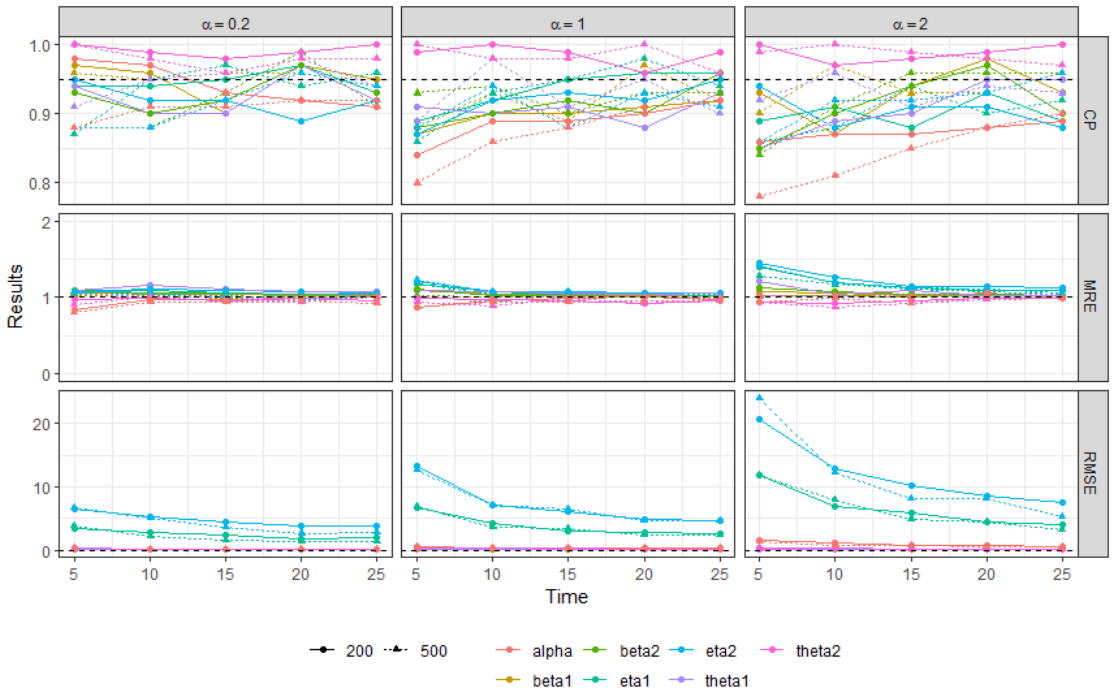

Figure 41 – Simulation results for the competing risks under shared frailty ARA model in scenarios with memory $m_A = m_B = 15$.

convergence of the MRE and RMSE criteria values to 1 and 0, respectively. Additionally, we expect the CP values to closely approach the nominal value of 0.95. As can be seen in Figures 39-44, the behavior of each criterion's measures occurs as expected for the both proposed ARA

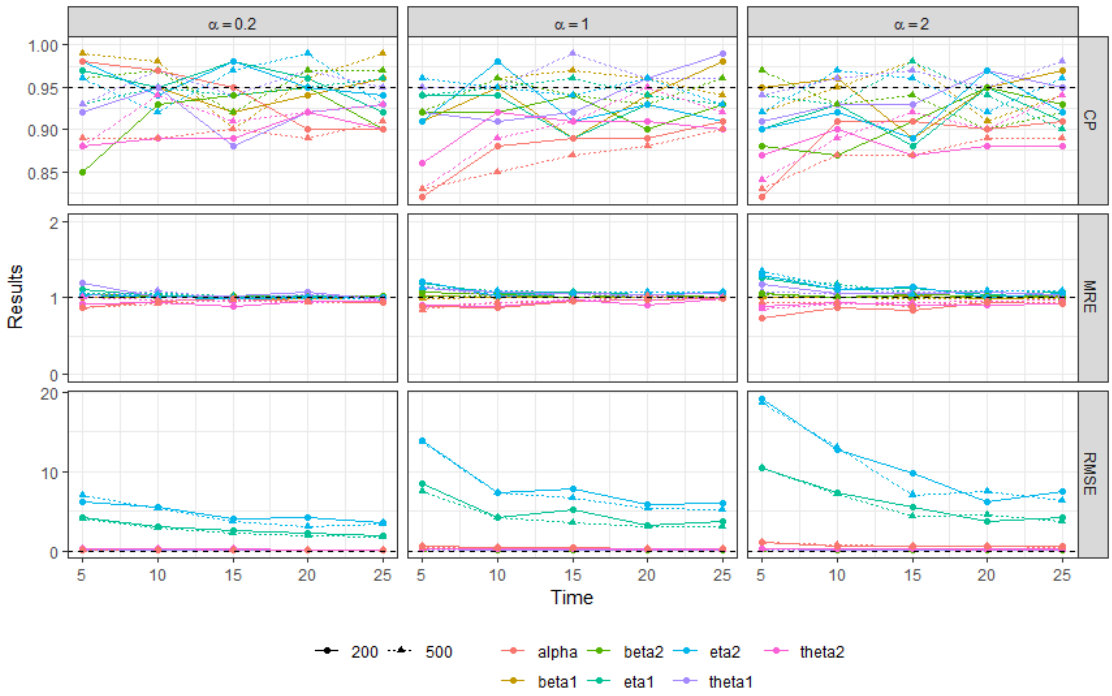

Figure 42 – Simulation results for the competing risks under shared frailty ARI model in scenarios with memory $m_A = m_B = 1$.

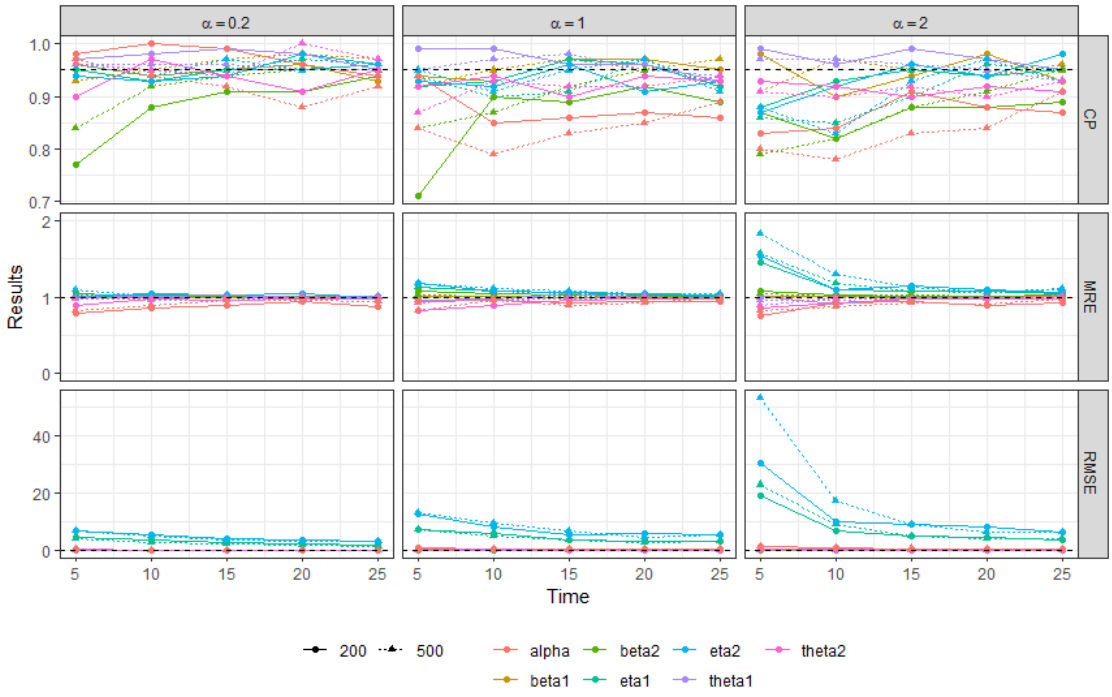

Figure 43 – Simulation results for the competing risks under shared frailty ARI model in scenarios with memory $m_A = m_B = 5$.

and ARI models.

In scenarios with higher values for the parameter α the convergence is slightly slower, particularly for the CP measure. This stems from the heightened variability of Gamma frailty,

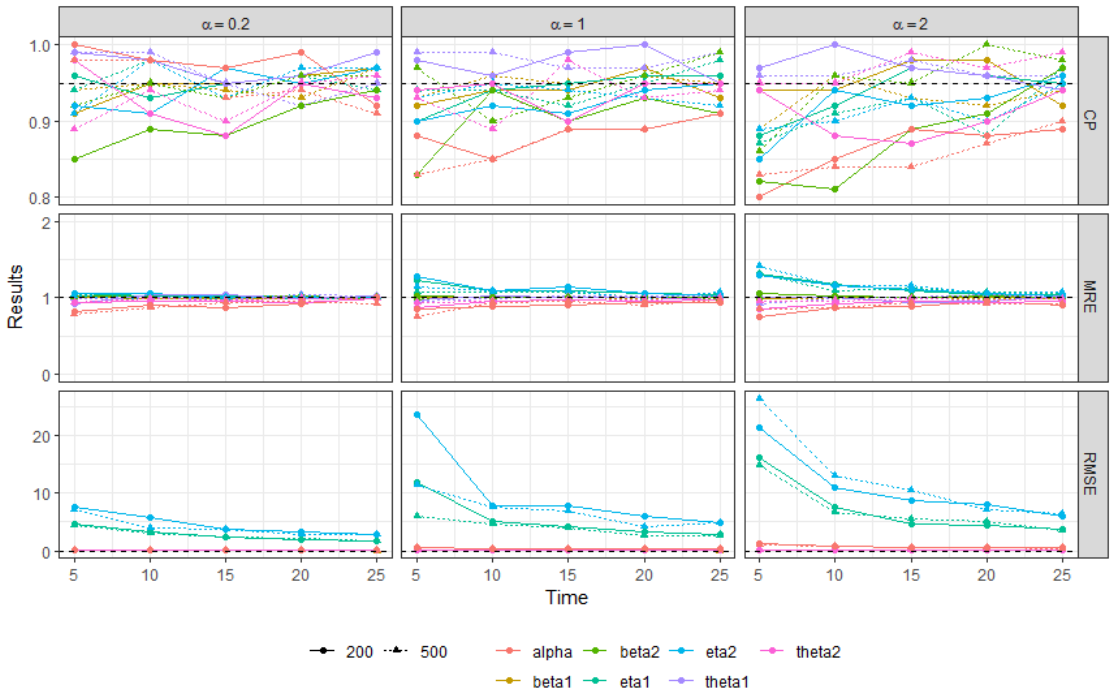

Figure 44 – Simulation results for the competing risks under shared frailty ARI model in scenarios with memory $m_A = m_B = 15$.

therefore it is an expected behavior. The graphs highlight the prominence of RMSE values for the parameter η in comparison to others, a result consistent with their high nominal magnitudes.

Comparing the performance of estimated measures in relation to the assumed failure memory for each failure cause, we have observed that scenarios with larger memories yield better results, since their estimates closely aligning with the expected values and displaying a quicker convergence. This fact is explained by the increase in information regarding the history of failures added to the modeling, both in the process of generating samples and estimating the parameters.

In conclusion, the simulation studies provide compelling evidence for the asymptotic properties of the MLEs outlined in the proposed models. As a result, these models can be reliably employed to derive estimates for the failure processes proposed in this work.

6.3 Real Data Applications

To illustrate the proposed models, we consider two sets of real data with failure times of multiple repairable systems caused by different causes. The first set refers to failure times of locomotive components of a Brazilian logistics company and the second, already known in the literature, deals with the failure history of a fleet of cars.

The competing risk models under shared frailty and IR discussed in the previous sections were used to model the both datasets, considering the PLP as initial intensity, the ARA and

ARI classes as IR models and all their possible failure memories for each cause-specific. The objective here is to estimate the model parameters, estimate the individual frailty of each system and its reliability predictions. As in the other applications previously discussed in this work, the AIC and BIC criteria were used to select the best models for each application.

The assumptions about the dataset are the same as those discussed in the previous sections, namely: the failure causes are independent, each failure occurs for a specific cause and each cause defines a counting process for its related failures. Details of each dataset and the estimation procedures will be presented and discussed in the follow sections.

6.3.1 Locomotive Components Data

In this section, we analyze a dataset of locomotive components from a Brazilian logistics company. Specifically, this dataset contains failure times and causes of message boards panels installed on the locomotives, which are susceptible to failures stemming from various factors. When these panels fail, the locomotive's operations must come to a halt until the component is either repaired or replaced. In this sense, it is crucial to establish reasonable reliability predictions based on the panels' failure history in order to minimize the financial losses incurred as a result of these operational disruptions.

The failure times were collected between 2014 and 2021. Subsequent to a failure, the affected item is sent to the restoration laboratory where proficient technicians document the information about the failure. These failure causes have been categorized into two groups: "Material" (cause A) and "Unidentified" (cause B), where the second cause encompasses all non-material or non-identifiable causes. Information from four different panels with the same production and usage specifications were considered. Throughout the observation period, these items failed between 9 and 13 times. The graph depicted in Figure 45 illustrates the failure times (in days) leading to failures for each of these components, where each line corresponds to an individual component and each point represents a specific failure instance, including its cause as indicated by the color and shape of the point.

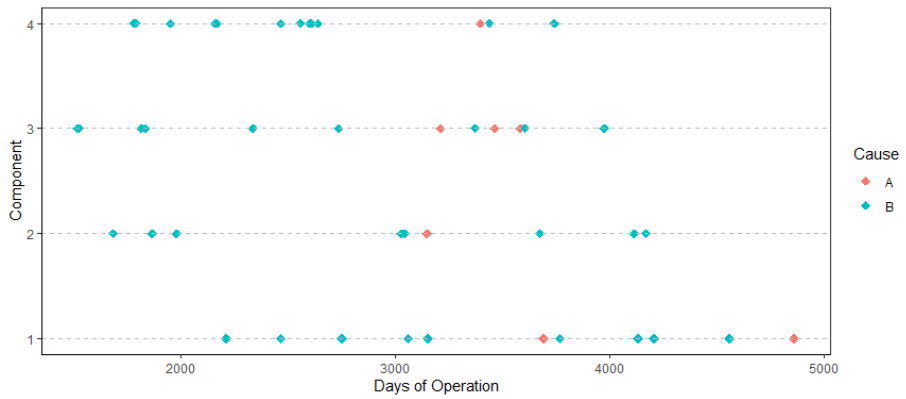

Figure 45 – Failure times, in days, for each locomotive component by cause.

We employed the log-likelihood functions (6.8) and (6.9) corresponding to the ARA and ARI classes, respectively, to derive parameter estimates for each model. These models were associated with different failure memory settings for each cause. The parameters to be estimated are the α of the Gamma$(1/\alpha, 1/\alpha)$ frailty variance assumed in the model, as well as (β_A, β_B) and (η_A, η_B) of the PLPs for each of the two failure causes, and (θ_A, θ_B) referring to the repair effect linked to each cause. As discussed in Section 6.1.2, the approach involved maximizing the log-likelihood functions (6.8) and (6.9) through computational methods to obtain the desired parameter estimates.

The aforementioned process was conducted across all memory combinations, considering all potential memories for each cause. For cause A, the highest number of observed failures within a single system was 3, whereas for cause B, this number was 12. Consequently, the possible memories to establish the model that defines each process of failures referring to these two causes are $m_A = 1, \ldots, 3$ and $m_B = 1, \ldots, 12$, resulting in a total of $m_A \times m_B = 36$ possible combinations between these memory choices.

Out of the 36 possible models, each designed to fit the database, any of the criteria such as AIC, BIC, or the maximum estimated value of the log-likelihood could be employed to identify the optimal model. Our findings led us to determinate that the best parameter combination (evidenced by the lowest AIC and BIC values, along with the highest estimated value for the log-likelihood) for both ARA and ARI classes corresponds to $m_A = 1$ and $m_B = 12$. As discussed in the application in Section 4.2.5, we also assert $m_B = \infty$, as this represents the maximum feasible memory for cause B. The parameters estimates for each best model in the both classes ARA and ARI are presented in Table 16, as well as its respective criteria estimates.

Table 16 – Estimation results for competing risks under frailty ARA and ARI models applied to locomotive components data.

	ARA	ARI
$\hat{\alpha}$ (95% $\text{CI}_{\hat{\alpha}}$)	0.266 (0.092, 0.764)	0.088 (0.043, 0.179)
$\hat{\beta}_A$ (95% $\text{CI}_{\hat{\beta}_A}$)	10.01 (4.84, 20.69)	5.47 (3.15, 9.49)
$\hat{\eta}_A$ (95% $\text{CI}_{\hat{\eta}_A}$)	3388.7 (3012.6, 3811.8)	3569.8 (2934.2, 4343.1)
$\hat{\theta}_A$ (95% $\text{CI}_{\hat{\theta}_A}$)	0.72 (0.55, 0.84)	0.19 (0.06, 0.45)
$\hat{\beta}_B$ (95% $\text{CI}_{\hat{\beta}_B}$)	3.62 (2.22, 5.91)	2.59 (1.91, 3.51)
$\hat{\eta}_B$ (95% $\text{CI}_{\hat{\eta}_B}$)	1537.0 (1200.0, 1968.4)	1146.2 (1057.6, 1977.6)
$\hat{\theta}_B$ (95% $\text{CI}_{\hat{\theta}_B}$)	0.87 (0.79, 0.92)	0.83 (0.49, 0.96)
$\hat{l}$	-311.614	-314.359
AIC	637.228	642.719
BIC	649.874	655.365

By examining Table 16 and applying the same selection criteria as mentioned earlier, we can decide for the optimal model for this dataset, choosing between the ARA and ARI models that exhibited superior performance in their respective analyses. Note that all metrics indicate

the ARA model outperforming the ARI model. Consequently, the ARA model is selected as our final choice for this dataset.

The interpretations on the parameter estimates are similar to those performed in the applications outlined in Sections 4.1.5 and 4.2.5, but, in this case, the evaluations are specific to each failure cause-specific. For both causes A and B, the estimates $\hat{\beta}_A$ and $\hat{\beta}_B$ indicate that the system's condition deteriorates progressively over time. The estimates $\hat{\theta}_A$ and $\hat{\theta}_B$ quantify the impact of repair interventions, and their CIs indicate that, for neither of the causes are repairs close to MR or PR scenarios. Finally, the estimate for the parameter α ($\hat{\alpha} = 0.266$) indicates the existence of unobserved heterogeneity exerting influence on the systems.

In this illustrative case, the estimated variance of the frailty variables is not so close to zero as seen in the examples presented earlier. This discrepancy suggests a notable disparity in the role of unobservable effects on the failure processes of each system. This indicates a significant difference in the action of unobservable effects on the failure processes of each system. This distinction becomes evident when examining Table 17. This table showcases the individual frailties of the four studied systems, derived from the parameter estimates and the historical failure time data linked to each cause, incorporated into equation (6.10). It is evident that systems #3 and #4 are more fragile compared to the other two systems. We can say that these particular systems are significantly impacted by factors that are not fully captured by the model.

Table 17 – Individual frailty for each locomotive component, in the competing risks under shared frailty ARA model.

Frailty	Estimate	Frailty	Estimate
$\hat{z}_1$	0.571	$\hat{z}_3$	1.159
$\hat{z}_2$	0.704	$\hat{z}_4$	1.683

With all the model estimates in hand, we can once again employ graphical techniques to assess goodness-of-fit, which involves comparing the empirical MCF against the MCF estimated by the proposed models. In this instance, we consider both the ARA and ARI models, while taking into account the memories $m_A = 1$ and $m_B = 12$ associated with causes A and B, respectively. The justification for constructing and analyzing these graphs is the same as discussed in previous chapters. The graphical outcomes are shown in Figure 46. Note that both models present a reasonable fit on average, with a slight advantage in favor of the ARA model, as expected given its superior performance as indicated by the selection criteria.

Once again, utilizing the parameter estimates, it is possible to project the system's reliability starting from a specific time or from the last observed failure. In this scenario, equations (6.12) and (6.13) are employed for the ARA and ARI models, respectively. The objective is to calculate the system reliability at a time t after the time t_n of the last observed failure. Figure 47 depicts the reliability prediction curves for the four systems, calculated from their respective last observed failure times. These graphs indicate that the probability of any one of these four systems not failing in 500 days is practically zero.

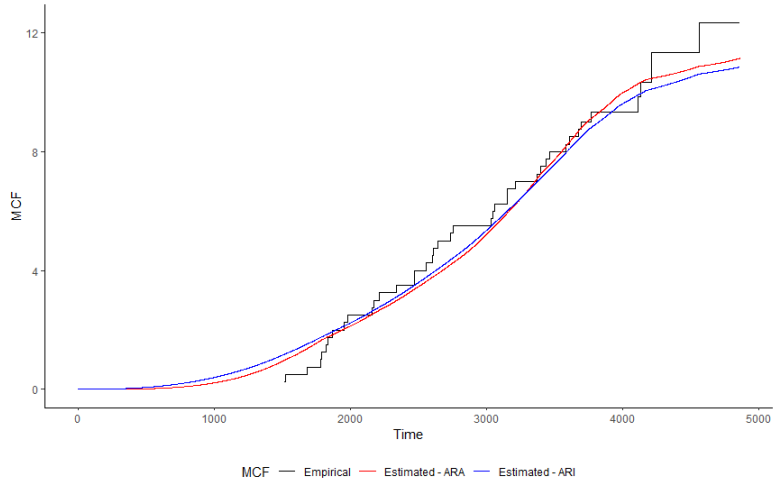

Figure 46 – Empirical and estimated MCFs for the locomotive components times, in the competing risks under shared frailty ARA model.

Figure 47 also shows the MTTF values attributed to the most fitting ARA model, derived using equation (6.14). These estimated mean times until the next failure incorporate the influences of both cause-specifics A and B. Consequently, in this instance, it is not possible to interpret these values by correlating them directly to the estimates of the parameters η_A and η_B, as was done in Section 4.2.5. Nevertheless, this information is relevant in itself, as it helps in the protective maintenance policies of the logistics company responsible for the studied systems.

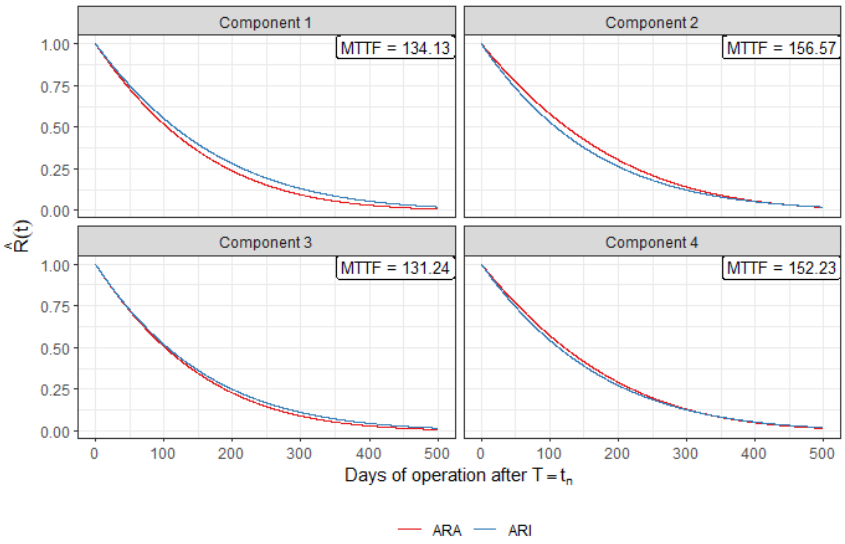

Figure 47 – Estimated reliability functions and MTTFs at last failure time t_n, for each locomotive component in the dataset, under the fitted competing risks under shared frailty ARA model.

6.3.2 Automobile Fleet Data

In this section, we analyze a dataset comprising instances of car failures, introduced by Somboonsavatdee and Sen (2015a). This dataset encompasses recurrent failure information from a fleet of 172 vehicles, including general information about the cars (such as make and model), the mileage at which each failure occurred (relative to "failure time"), and the corresponding labor code linked to each failure event. These data were extracted from a car warranty claim database, so it can be concluded that the profound understanding of the car failure process derived from this dataset holds reaching implications, particularly for insurance companies.

According to Somboonsavatdee and Sen (2015a), these data were observed in a time-truncation scenario, in this case by a mileage of 3,000 miles. Additionally, the failure causes have been categorized into three distinct groups based on the rate of failures, denoted as A, B, and C, each attributed to a specific cause for the failure. The authors also conducted tests to confirm that the initial failure processes related to each cause-specific can be modeled by a PLP.

Figure 48 illustrates the failure mileage (measured in miles) for each car, organized row-wise. Each individual point on the graph corresponds to a specific failure mileage, with differentiation based on the underlying cause of the failure. For each of the causes A, B, and C, the maximum number of failures per car was 2, 4, and 6, respectively.

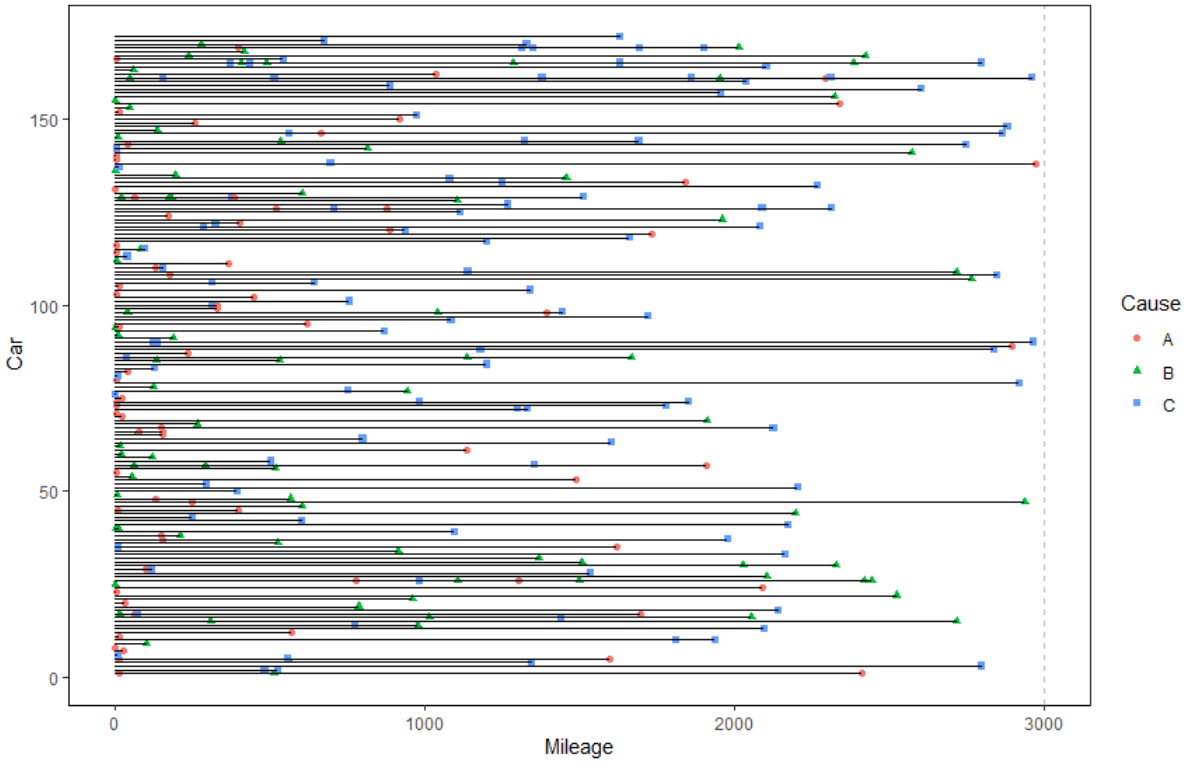

Figure 48 – Failure mileage for each car from warranty claims data, by cause.

Somboonsavatdee and Sen (2015a) used this database to illustrate their frailty models for systems operating under competing risks, along with our proposed model. However, a key

distinction lies in the fact that these authors only considered MR after each failure. Our models, in contrast, extend this investigation to encompass the realm of IR following each failure event, being also able to quantify the effects introduced by the carried out repairs.

The procedures in this example are exactly those outlined in Section 6.3.2 illustration. However, a distinguishing factor is that our systems now involve three distinct failure causes, thus giving rise to the definition of three distinct failure counting processes with particular parameters.

For the estimation of parameters in the proposed competing risk models under shared frailty ARA and ARI models, equations (6.8) and (6.9) were employed, respectively. The estimation was conduced across all the possible memory combinations for both classes. Based on the results obtained, our analysis in this example will focus on the ARA models. This decision stems from the parameter estimates, especially for the β parameter, which does not indicate that the systems are deteriorating over time (as we will see later, $\beta < 1$), and this characteristic causes problems in the graphical goodness-of-fit analysis for the ARI models. In this way, the maximum log-likelihood, the AIC and BIC criteria can be used to choose the best memory for the ARA class of models. Table 18 shows the comparison of the estimates obtained for two ARA models, represented by ARA_1, the model where $m_A = m_B = m_C = 1$, and by ARA_∞, the model where $m_A = 2$, $m_B = 4$ and $m_C = 6$, which corresponds to $m = \infty$ for the three causes since $m_A = 1, 2$, $m_B = 1, \ldots, 4$ and $m_C = 1, \ldots, 6$.

Table 18 – Estimation results for competing risks under frailty ARA_1 and ARA_∞ models applied to car warranty data.

	ARA_1	ARA_∞
$\hat{\alpha}$ (95% $\text{CI}_{\hat{\alpha}}$)	0.072 (0.044, 0.119)	0.013 (0.009, 0.018)
$\hat{\beta}_A$ (95% $\text{CI}_{\hat{\beta}_A}$)	0.31 (0.24, 0.38)	0.30 (0.24, 0.37)
$\hat{\eta}_A$ (95% $\text{CI}_{\hat{\eta}_A}$)	36619 (15005,89368)	51987 (18587, 145405)
$\hat{\theta}_A$ (95% $\text{CI}_{\hat{\theta}_A}$)	0.79 (0.57, 0.92)	0.87 (0.71, 0.95)
$\hat{\beta}_B$ (95% $\text{CI}_{\hat{\beta}_B}$)	0.44 (0.36,0.54)	0.39 (0.31, 0.49)
$\hat{\eta}_B$ (95% $\text{CI}_{\hat{\eta}_B}$)	14813 (7900, 27778)	21865 (10500,45535)
$\hat{\theta}_B$ (95% $\text{CI}_{\hat{\theta}_B}$)	0.31 (0.11, 0.63)	0.10 (0.05, 0.18)
$\hat{\beta}_C$ (95% $\text{CI}_{\hat{\beta}_C}$)	0.64 (0.52, 0.79)	0.68 (0.56, 0.83)
$\hat{\eta}_C$ (95% $\text{CI}_{\hat{\eta}_C}$)	7263 (4881, 10807)	5830 (4221, 8054)
$\hat{\theta}_C$ (95% $\text{CI}_{\hat{\theta}_C}$)	0.09 (0.04, 0.19)	0.37 (0.14, 0.67)
$\hat{l}$	-2499.906	-2497.389
AIC	5019.811	5014.778
BIC	5055.942	5050.909

Based on the results in Table 18 and our established selection criteria, the best model chosen for this dataset is the ARA_∞ model, where $m_A = 2$, $m_B = 4$ and $m_C = 6$. Note that the β values obtained for all three causes of failure are less than 1, indicating that the model does not suggest deterioration of the components responsible for the mileage (intervals between failures are very wide and this impacts the estimation of the β parameter); second, in the IR context the

repair effect contributes to the maintenance of these components. The second point is even more evident for causes C and B (mainly), where the repair effect approaches a PR (θ close to zero). In contrast, the repair effect of cause A leans more toward a MR, although this cause exhibits the highest estimate for the η parameter, specifically related to the time intervals between failures.

Finally, the model also captured the existence of unobserved heterogeneity among the systems ($\alpha > 0$). In this way, utilizing the estimates derived from the ARA$_\infty$ model within the equation (6.10), we obtain estimates of the individual frailties associated with each analyzed vehicle. Due to the extensive nature of the dataset, in Table 19 we present the result for a subset of 10 cars, featuring the 5 lowest and 5 highest estimated frailties z_i, where i represents the car's index in the database.

Table 19 – Individual frailty for ten cars, in the competing risks under shared frailty ARA$_\infty$ model.

Frailty	Estimate	Frailty	Estimate
$\hat{z}_{79}$	1.0046	$\hat{z}_{169}$	1.0594
$\hat{z}_{148}$	1.0047	$\hat{z}_{26}$	1.0703
$\hat{z}_{3}$	1.0048	$\hat{z}_{129}$	1.0757
$\hat{z}_{158}$	1.0052	$\hat{z}_{165}$	1.0807
$\hat{z}_{132}$	1.0059	$\hat{z}_{161}$	1.0897

An interesting observation from Table 19 is that the five cars with the highest estimated frailty are precisely the ones that experienced the most failures among the 172 cars. However, it is worth noting that the car with the highest number of failures (#161) does not necessarily have the highest estimated frailty. This highlights the nuanced relationship between failure frequency and estimated frailty, which is evidently impacted by the cause of the failures. Conversely, the five cars with the lowest estimated frailty all experienced only one failure, and these failures were attributed to the same cause (C). Since these cars failed later in the observation, it follows that their estimated frailty is lower. This illustrates how the timing of failures and the specific cause of failure can influence the estimated frailty values, underscoring the importance of considering both factors in reliability analysis.

For the assessment of goodness-of-fit, the graphical comparison between the empirical MCF and the MCF estimated by the ARA$_\infty$ model was once again employed. In Figure 49, it is possible to verify that the model exhibits a good fit to the dataset (for the same reasons that we have already discussed in similar analyses of the work).

Concluding the analysis, the equations (6.12) and (6.13) were utilized to compute reliability prediction estimates for each vehicle based on the last observed failure mileage. In this sense, using the equation (6.14), the MTTF can also be calculated. In Figure 50, we display the reliability curves for six selected cars, the three with the greatest frailties and the three with the smallest ones. From the reliability graphs shown in Figure 50, it is notable that the three cars with the highest estimated frailties exhibit lower reliability compared to the other three cars. This difference becomes even more apparent when examining the MTTF values: these estimates for

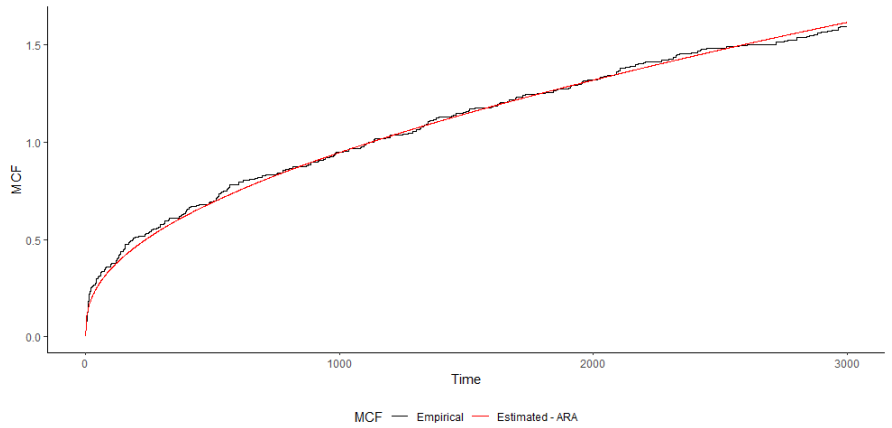

Figure 49 – Empirical and estimated MCFs for the car warranty data in the competing risks under shared frailty ARA model.

the last three cars, which are characterized by higher frailty, are substantially lower than those of the first three cars with lower frailty.

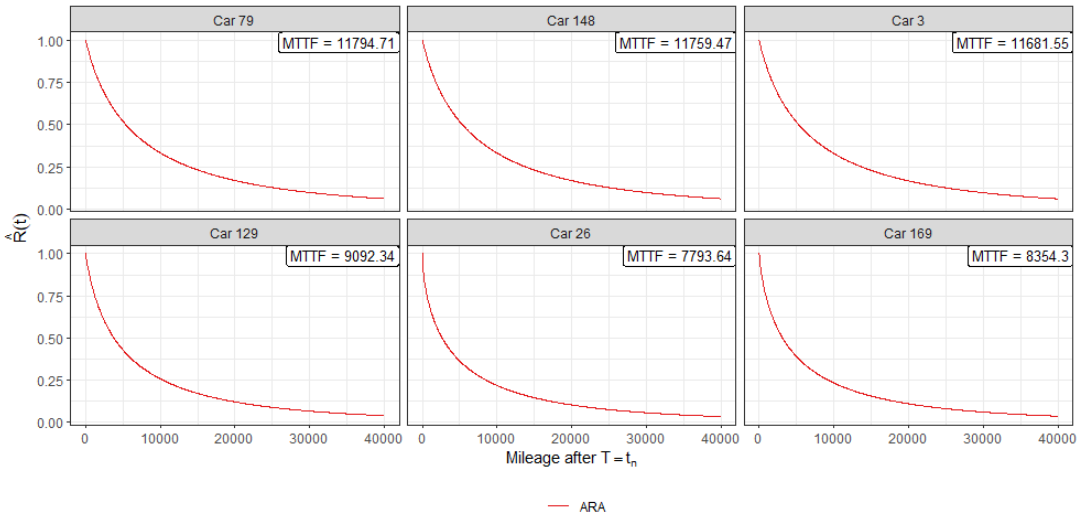

Figure 50 – Estimated reliability functions and MTTFs at last failure mileage t_n, for six cars in the warranty data, under the fitted competing risks under shared frailty ARA model.

These reliability graphs provide valuable insights, particularly in terms of calculating the probability of failure for these cars considering their upcoming mileage of use. This information is of significant relevance, particularly for insurance companies, as it aids in assessing risk and making informed decisions about coverage and premiums. Cars with lower reliability and shorter MTTF values may require more comprehensive insurance coverage or more frequent maintenance to mitigate potential risks.

6.4 Concluding Remarks of the Chapter

In this chapter we proposed new models considering multiple repairable systems subjected to failure due to different causes. These models are generalizations of the frailty models presented earlier in this work and also of models known in the literature, since they admit competing risks and that repairs carried out after failure are imperfect.

By employing these models, we achieve a multi-faceted analysis. They enable us to establish the failure process corresponding to each cause within the system, quantify the impact of repairs executed for each cause, and identify unobservable factors influencing system failure times. In essence, these models extract a comprehensive spectrum of information about system failure occurrences.

The models assumptions are in line with similar works in the reliability field. For each failure cause was associated a PLP as the initial counting process and a repair effect θ that characterizes the IR performed after the failures. In addition, for each system, a frailty term Z with Gamma$(1/\alpha, 1/\alpha)$ distribution shared between the causes and failure times was assumed.

We defined models encompassing both ARA$_m$ and ARI$_m$ classes of IR. We considered all possible failure memories m for each of the causes, which results in an array of model combinations to fit recurrent failure times within repairable systems. Inferential methods were suggested based on maximum likelihood estimation and their respective parameter CIs were constructed using asymptotic theory of Normal distribution. Once again, we computed reliability prediction functions and the MTTF for the proposed models.

Through an extensive simulation study, we verified the asymptotic properties of the proposed MLEs. We evaluated samples generated under various parameter scenarios to analyze the performance. Both the ARA and ARI models showcased favorable outcomes, exhibiting well-behaved estimates across all chosen analysis metrics.

Finally, two real datasets were used to illustrate the procedures presented and validate the applicability of the proposed models. In the first example, we considered failure data from locomotive component failures, caused by two distinct causes. Through the application of our proposed models, it was possible to verify that the repairs executed for each cause have an effect on the lifetime of the systems and, in addition, the analysis revealed the presence of unobserved heterogeneity between the systems, so that two systems are more fragile compared to others. In the second example, we revisited a well-known car failure dataset in the literature. In this case, the failures could be attributed to three distinct causes, allowing us to discern the distinctive impacts of repairs associated with each of these causes. For instance, the analysis identified that one of the repairs is similar to a PR, a logical finding within this context. Additionally, a slight unobserved heterogeneity acting on the failure process of the studied cars has been identified.

From all the theoretical discussion, simulation study and real data applications, we can conclude that these presented models possess both theoretical relevance and strong applicability

within practical scenarios. With current technological advancements, there are many complex repairable systems in large industries and companies subjected to failure due to different causes. In this sense, it is crucial to comprehend the systems' failure process to establish maintenance policies and avoid financial losses. In this pursuit of uncovering insights hidden within failure data, our models offer valuable contributions.

CHAPTER

7

FINAL REMARKS AND FURTHER RESEARCH

7.1 Final Remarks

In this thesis we proposed new parametric frailty models designed for general repairable systems. Our main objective was to expand upon existing frailty models from the literature, which primarily focused on minimal repairs following systems' failures. In this sense, in our models we made the assumption that the systems are subjected to either perfect (Chapter 3) or imperfect (Chapters 4, 5 and 6) repairs. In the case of imperfect repairs, we considered both the ARA_m and ARI_m classes known in the literature, for any possible value m of their memory failure histories. In Chapter 6, in particular, we introduced shared frailty models within the framework of competing risks, with independent risks that lead to failures whose repairs are imperfect (also considering the ARA_m and ARI_m classes). In all of our models, we made the assumption that the initial failure intensity function follows a PLP and the frailty variables are IID with Gamma distribution.

For all proposed models, classical inferential methods were presented to obtain the likelihood function in each. Given the complexity of all expressions found, numerical methods were suggested to obtain the MLEs and their respective asymptotic confidence intervals. Specially for the shared IR frailty models, a hierarchical Bayesian methodology based on MCMC sampling was also proposed (Chapter 5). Furthermore, for each new model, system reliability estimators were proposed based on their failure history.

For the models under a classical approach (Chapters 3, 4 and 6), Monte Carlo simulation studies considering several parameter scenarios were carried out with the purpose of verifying the asymptotic properties of consistency and efficiency of the MLEs and attesting to the suitability of the proposed models. The results obtained in all of these studies behaved as expected since they approached the nominal parameters values with small dispersion as the observed failure samples increased, under different scenarios.

Throughout the work, four different real datasets were used to illustrate our proposed methodologies and validate the applicability of our models. The first two datasets that deal with the failure times of sugarcane harvesters and dump truck engines, are well known in the literature and were employed to adjust the frailty models encompassing all types of repair, including minimal and perfect repairs (Chapter 3), as well as imperfect repair (Chapters 4 and 5). In Chapter 6, we turned our attention to two datasets that not only contained system failure times but also detailed the causes of these failures. The first dataset deals with failure times of locomotive panels, while the second dataset (also known in the literature) deals with the failure mileage of fleet of cars; both of these datasets were used to adjust the frailty models within the context of competing risk scenarios and imperfect repairs. Graphical goodness-of-fit verification methods were used to compare the empirical MCF with the average of the estimated cumulative failure functions for each system and all examples indicated favorable results.

Considering the comprehensive theoretical discussions, thorough simulation studies, and the successful application of our models in real-world examples, we can confidently conclude that our proposed models hold substantial relevance and contribute to the statistics literature, in particular, to the reliability field.

From a theoretical perspective, our models fill some gaps in the realm of reliability literature, especially regarding unobserved heterogeneity in systems undergoing imperfect repairs. Our contribution lies in the fact that our models are extensions and generalizations of other existing models, but now accommodate more general and extremely relevant information about system failure processes or even their causes of failure. From a computational standpoint, a substantial amount of code was generated during the thesis preparation process. We are committed to making this code available to the entire research community, promoting transparency and reproducibility in future studies.

Lastly, from a practical viewpoint, the applications showcased in our work underscore the versatility and utility of our proposed models. They are capable of simultaneously providing information on the effect of repairs carried out on a system, as well as the presence or absence of unobserved heterogeneity related to each failure time or between the observed systems. This information refines knowledge about the failure processes within the observed systems, or even the distinct failure processes attributed to each cause of failure (as seen in Chapter 6 within the competing risk framework). This multi-faceted approach demonstrates the practical value and effectiveness of our models across various domains.

7.2 Future Works

The field of reliability is inherently expansive and continually evolving, especially in light of the rapid technological evolution and the widespread dissemination of knowledge that we are currently experiencing. In this sense, there is still a lot of further contributions to be made

based on the findings of this thesis.

One avenue of future research involves revisiting the models introduced in this study, exploring alternative parameterizations of the initial failure process, or considering different frailty distributions. These investigations are natural extensions and are likely to be central to upcoming research endeavors. Moreover, the scope of research can be broadened by exploring additional characteristics associated with repairable systems. This could include delving into areas such as accelerated test models, degradation models, and repair alert models, which can further generalize and enhance the models presented in this work.

BIBLIOGRAPHY

AALEN, O. Nonparametric inference for a family of counting processes. **The Annals of Statistics**, JSTOR, p. 701–726, 1978. Citation on page 79.

ALMEIDA, M. P.; PAIXAO, R.; RAMOS, P.; TOMAZELLA, V.; LOUZADA, F.; EHLERS, R. Multiple repairable systems under dependent competing risks with nonparametric frailty. **arXiv preprint arXiv:2004.05217**, 2020. Citations on pages 27 and 141.

ANDERSEN, P. K.; BORGAN, O.; GILL, R. D.; KEIDING, N. **Statistical models based on counting processes**. [S.l.]: Springer Science & Business Media, 2012. Citation on page 27.

ASCHER, H.; FEINGOLD, H. **Repairable systems reliability: modeling, inference, misconceptions and their causes**. [S.l.]: M. Dekker New York, 1984. Citation on page 25.

ASFAW, Z. G.; LINDQVIST, B. H. Unobserved heterogeneity in the power law nonhomogeneous poisson process. **Reliability Engineering & System Safety**, Elsevier, v. 134, p. 59–65, 2015. Citation on page 67.

BARLOW, R.; HUNTER, L. Optimum preventive maintenance policies. **Operations research**, Informs, v. 8, n. 1, p. 90–100, 1960. Citation on page 26.

BERNOULLI, D. Essai d'une nouvelle analyse de la mortalité causée par la petite vérole, et des avantages de l'inoculation pour la prévenir. **Histoire de l'Acad., Roy. Sci.(Paris) avec Mem**, Mem. Acad. Roy. Sci.(Paris), p. 1–45, 1760. Citation on page 61.

BRITO, É. S.; TOMAZELLA, V. L.; FERREIRA, P. H. Statistical modeling and reliability analysis of multiple repairable systems with dependent failure times under perfect repair. **Reliability Engineering & System Safety**, Elsevier, v. 222, p. 108375, 2022. Citations on pages 31 and 91.

BURNHAM, K. P.; ANDERSON, D. R. Multimodel inference: understanding aic and bic in model selection. **Sociological methods & research**, Sage Publications Sage CA: Thousand Oaks, CA, v. 33, n. 2, p. 261–304, 2004. Citation on page 77.

CHAN, J.-K.; SHAW, L. Modeling repairable systems with failure rates that depend on age and maintenance. **IEEE Transactions on Reliability**, IEEE, v. 42, n. 4, p. 566–571, 1993. Citation on page 52.

COOK, R. J.; LAWLESS, J. **The statistical analysis of recurrent events**. [S.l.]: Springer Science & Business Media, 2007. Citations on pages 25 and 37.

COX, D. R. Regression models and life-tables. **Journal of the Royal Statistical Society: Series B (Methodological)**, Wiley Online Library, v. 34, n. 2, p. 187–202, 1972. Citation on page 55.

CROW, L. H. **Reliability analysis for complex, repairable systems**. [S.l.], 1975. Citations on pages 25 and 38.

CROWDER, M. J. **Classical competing risks**. [S.l.]: CRC Press, 2001. Citations on pages 27, 61, 62, and 64.

D'ANDREA, A. M. E. Classe de modelos de fragilidade com efeito do acúmulo de reparos em múltiplos sistemas reparáveis. Universidade Federal de São Carlos, 2019. Citations on pages 27 and 28.

DOYEN, L.; GAUDOIN, O. Classes of imperfect repair models based on reduction of failure intensity or virtual age. **Reliability Engineering & System Safety**, Elsevier, v. 84, n. 1, p. 45–56, 2004. Citations on pages 26, 47, 48, 49, 52, 120, and 142.

____. Imperfect maintenance in a generalized competing risks framework. **Journal of Applied probability**, Cambridge University Press, v. 43, n. 3, p. 825–839, 2006. Citation on page 27.

D'ANDREA, A. M. E.; FEITOSA, C. C.; TOMAZELLA, V. L. D.; VIEIRA, A. M. C. Frailty modeling for repairable systems with minimum repair: An application to dump truck data of a brazilian mining company. 2019. Citations on pages 56, 67, 68, and 73.

ELBERS, C.; RIDDER, G. True and spurious duration dependence: The identifiability of the proportional hazard model. **The Review of Economic Studies**, Wiley-Blackwell, v. 49, n. 3, p. 403–409, 1982. Citation on page 56.

ENGELHARDT, M.; BAIN, L. J. On the mean time between failures for repairable systems. **IEEE Transactions on Reliability**, IEEE, v. 35, n. 4, p. 419–422, 1986. Citation on page 26.

GELMAN, A.; CARLIN, J. B.; STERN, H. S.; RUBIN, D. B. **Bayesian data analysis**. [S.l.]: Chapman and Hall/CRC, 1995. Citations on pages 119, 122, 123, 125, 128, and 131.

GELMAN, A.; RUBIN, D. B. Inference from iterative simulation using multiple sequences. **Statistical science**, Institute of Mathematical Statistics, v. 7, n. 4, p. 457–472, 1992. Citation on page 130.

GEWEKE, J. **Evaluating the accuracy of sampling-based approaches to the calculation of posterior moments**. [S.l.], 1991. Citation on page 129.

GILARDONI, G. L.; COLOSIMO, E. A. Optimal maintenance time for repairable systems. **Journal of quality Technology**, Taylor & Francis, v. 39, n. 1, p. 48–53, 2007. Citation on page 26.

HAMADA, M. S.; WILSON, A.; REESE, C. S.; MARTZ, H. **Bayesian reliability**. [S.l.]: Springer Science & Business Media, 2008. Citations on pages 26, 36, 37, and 38.

HEIDELBERGER, P.; WELCH, P. D. Simulation run length control in the presence of an initial transient. **Operations Research**, INFORMS, v. 31, n. 6, p. 1109–1144, 1983. Citation on page 129.

HOUGAARD, P. Life table methods for heterogeneous populations: distributions describing the heterogeneity. **Biometrika**, Oxford University Press, v. 71, n. 1, p. 75–83, 1984. Citation on page 56.

____. **Analysis of multivariate survival data**. [S.l.]: Springer Science & Business Media, 2012. Citation on page 27.

JUNIOR, O. A. G. **Frailty model for multiple repairable systems hierarchically represented in serial/parallel structures under assumption of ARAm imperfect repairs**. Phd Thesis (PhD Thesis) — Universidade Federal de São Carlos, 2021. Citations on pages 27, 28, 29, 55, 56, 85, and 91.

KIJIMA, M. Some results for repairable systems with general repair. **Journal of Applied probability**, JSTOR, p. 89–102, 1989. Citations on pages 26, 41, 44, and 46.

KIJIMA, M.; MORIMURA, H.; SUZUKI, Y. Periodical replacement problem without assuming minimal repair. **European Journal of Operational Research**, Elsevier, v. 37, n. 2, p. 194–203, 1988. Citations on pages 26, 46, and 49.

LANCASTER, T. Econometric methods for the duration of unemployment. **Econometrica: Journal of the Econometric Society**, JSTOR, p. 939–956, 1979. Citation on page 56.

LANGSETH, H.; LINDQVIST, B. H. Competing risks for repairable systems: A data study. **Journal of Statistical Planning and Inference**, Elsevier, v. 136, n. 5, p. 1687–1700, 2006. Citation on page 27.

LINDQVIST, B. H. Competing risks. **Encyclopedia of Statistics in Quality and Reliability. New York: Wiley**, Citeseer, v. 10, p. 9780470061572, 2006. Citations on pages 62 and 141.

LINDQVIST, B. H. *et al.* On the statistical modeling and analysis of repairable systems. **Statistical science**, Institute of Mathematical Statistics, v. 21, n. 4, p. 532–551, 2006. Citations on pages 40 and 47.

LIU, X.; VATN, J.; DIJOUX, Y.; TOFTAKER, H. Unobserved heterogeneity in stable imperfect repair models. **Reliability Engineering & System Safety**, Elsevier, v. 203, p. 107039, 2020. Citations on pages 27, 28, 85, and 101.

NASH, J. C. **optimr: A Replacement and Extension of the 'optim' Function**. [S.l.], 2019. Available: <https://CRAN.R-project.org/package=optimr>. Citation on page 75.

NELSON, W. B. **Recurrent events data analysis for product repairs, disease recurrences, and other applications**. [S.l.]: SIAM, 2003. Citation on page 25.

NIELSEN, G. G.; GILL, R. D.; ANDERSEN, P. K.; SØRENSEN, T. I. A counting process approach to maximum likelihood estimation in frailty models. **Scandinavian journal of Statistics**, JSTOR, p. 25–43, 1992. Citation on page 147.

OLIVEIRA, M. D. D.; COLOSIMO, E. A.; GILARDONI, G. L. Power law selection model for repairable systems. **Communications in Statistics-Theory and Methods**, Taylor & Francis, v. 42, n. 4, p. 570–578, 2013. Citation on page 38.

OLIVEIRA, M. D. de; COLOSIMO, E. A.; GILARDONI, G. L. Bayesian inference for power law processes with applications in repairable systems. **Journal of Statistical Planning and Inference**, Elsevier, v. 142, n. 5, p. 1151–1160, 2012. Citation on page 120.

PAN, R.; RIGDON, S. E. Bayes inference for general repairable systems. **Journal of Quality Technology**, Taylor & Francis, v. 41, n. 1, p. 82–94, 2009. Citations on pages 120, 121, 122, 123, and 129.

PARK, D. H.; JUNG, G. M.; YUM, J. K. Cost minimization for periodic maintenance policy of a system subject to slow degradation. **Reliability Engineering & System Safety**, Elsevier, v. 68, n. 2, p. 105–112, 2000. Citation on page 26.

PIEVATOLO, A.; RUGGERI, F. Bayesian reliability analysis of complex repairable systems. **Applied Stochastic Models in Business and Industry**, Wiley Online Library, v. 20, n. 3, p. 253–264, 2004. Citation on page 120.

PINTILIE, M. **Competing risks: a practical perspective**. [S.l.]: John Wiley & Sons, 2006. Citation on page 62.

PLUMMER, M.; BEST, N.; COWLES, K.; VINES, K. Coda: Convergence diagnosis and output analysis for mcmc. **R News**, v. 6, n. 1, p. 7–11, 2006. Available: <https://journal.r-project.org/archive/>. Citation on page 129.

R Core Team. **R: A Language and Environment for Statistical Computing**. Vienna, Austria, 2021. Available: <https://www.R-project.org/>. Citations on pages 74, 91, and 151.

RIGDON, S. E.; BASU, A. P. The power law process: a model for the reliability of repairable systems. **Journal of Quality Technology**, Taylor & Francis, v. 21, n. 4, p. 251–260, 1989. Citation on page 26.

____. **Statistical methods for the reliability of repairable systems**. [S.l.]: Wiley New York, 2000. Citations on pages 26, 33, 35, 36, 38, 39, and 40.

ROSS, S. M. Stochastic processes. john wiley & sons. **New York**, 1996. Citations on pages 26 and 33.

SLIMACEK, V.; LINDQVIST, B. H. Nonhomogeneous poisson process with nonparametric frailty. **Reliability Engineering & System Safety**, Elsevier, v. 149, p. 14–23, 2016. Citation on page 67.

SOMBOONSAVATDEE, A.; SEN, A. Parametric inference for multiple repairable systems under dependent competing risks. **Applied Stochastic Models in Business and Industry**, Wiley Online Library, v. 31, n. 5, p. 706–720, 2015. Citations on pages 27, 150, and 159.

____. Statistical inference for power-law process with competing risks. **Technometrics**, Taylor & Francis, v. 57, n. 1, p. 112–122, 2015. Citations on pages 62, 121, and 141.

TOLEDO, M. L. G. de. Determination of the optimal periodic maintenance policy under imperfect repair assumption. Universidade Federal de Minas Gerais, 2014. Citation on page 95.

TOLEDO, M. L. G. de; FREITAS, M. A.; COLOSIMO, E. A.; GILARDONI, G. L. Ara and ari imperfect repair models: Estimation, goodness-of-fit and reliability prediction. **Reliability Engineering & System Safety**, Elsevier, v. 140, p. 107–115, 2015. Citations on pages 26, 79, 80, 100, and 112.

TOMAZELLA, V. L. D. **Modelagem de dados de eventos recorrentes via processo de Poisson com termo de fragilidade.** Phd Thesis (PhD Thesis) — Universidade de São Paulo, 2003. Citations on pages 27, 56, and 59.

VAUPEL, J. W.; MANTON, K. G.; STALLARD, E. The impact of heterogeneity in individual frailty on the dynamics of mortality. **Demography**, Springer, v. 16, n. 3, p. 439–454, 1979. Citations on pages 55 and 59.

WIENKE, A. **Frailty models in survival analysis**. [S.l.]: CRC press, 2010. Citations on pages 27, 55, 57, 58, 59, 60, and 61.

APPENDIX

A

PLOTS OF MCMC SAMPLES FROM APPLICATIONS IN SECTION 5.2

A.1 Section 5.2.1 - Sugarcane Harvester Data

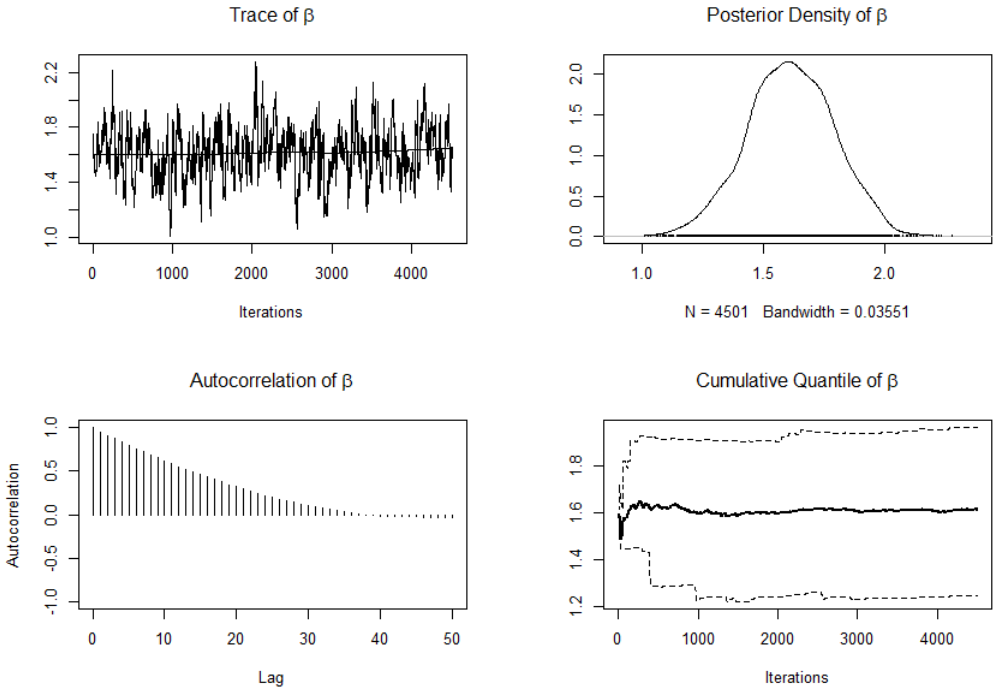

Figure 51 – Plots of MCMC outputs for the parameter β in application of Section 5.2.1

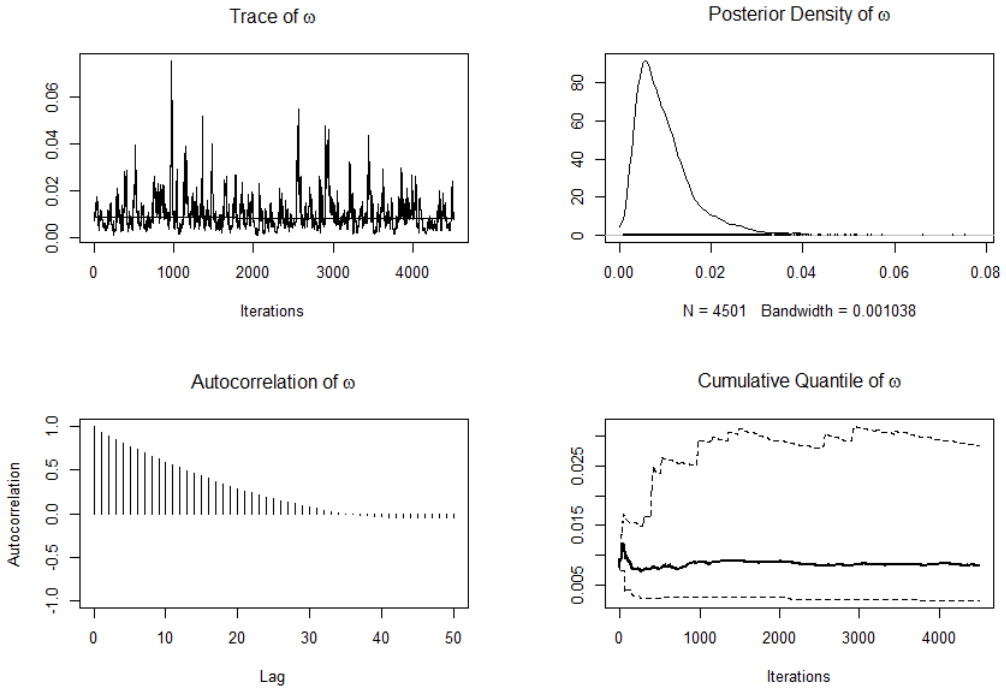

Figure 52 – Plots of MCMC outputs for the parameter ω in application of Section 5.2.1

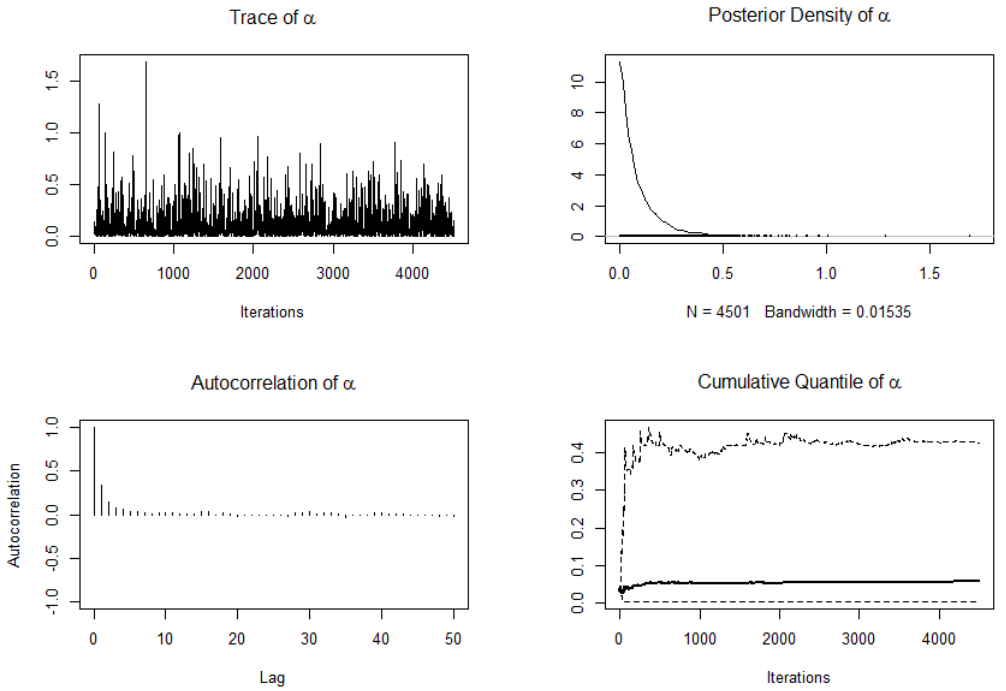

Figure 53 – Plots of MCMC outputs for the parameter α in application of Section 5.2.1

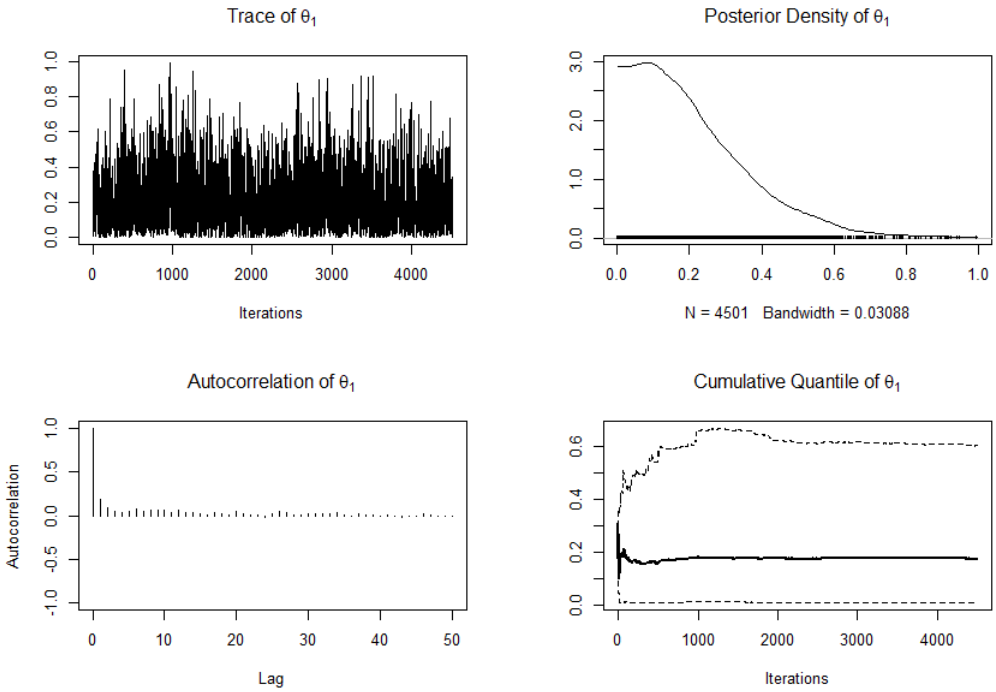

Figure 54 – Plots of MCMC outputs for the parameter θ_1 in application of Section 5.2.1

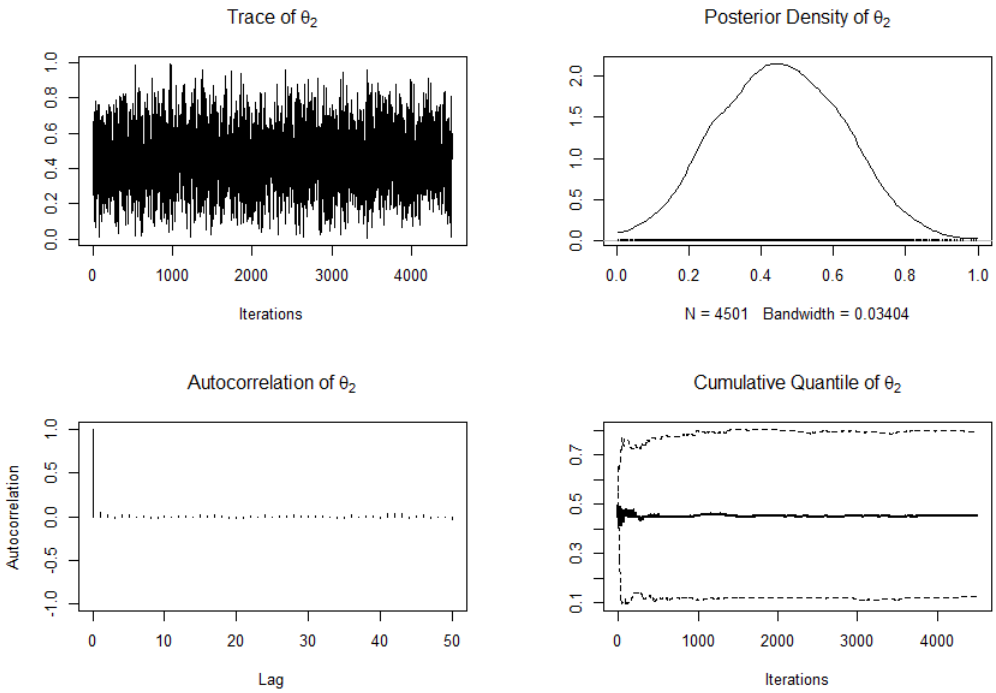

Figure 55 – Plots of MCMC outputs for the parameter θ_2 in application of Section 5.2.1

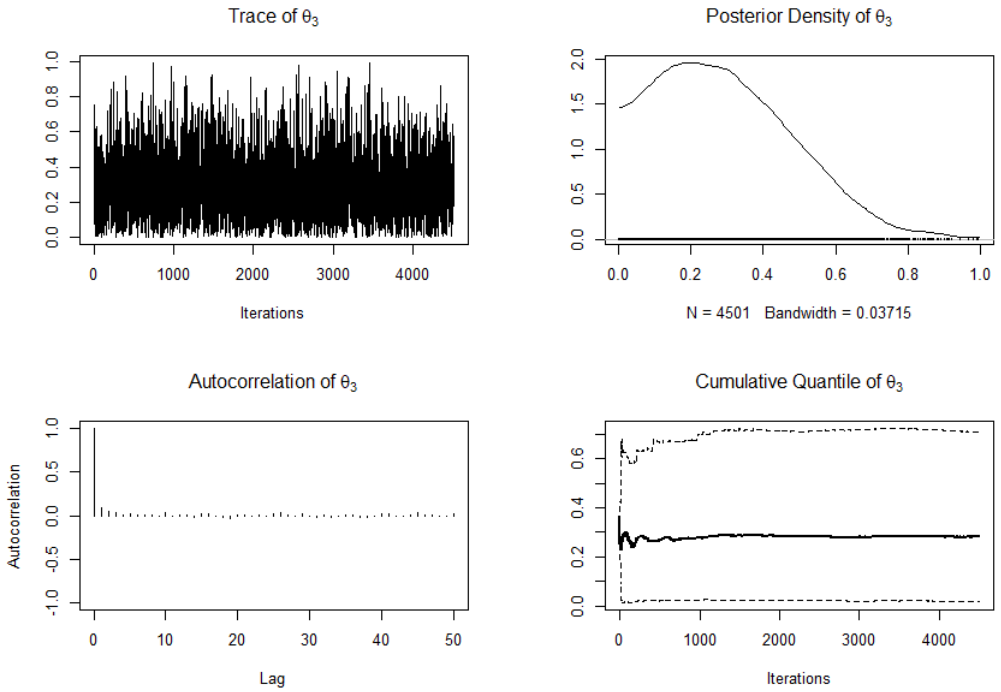

Figure 56 – Plots of MCMC outputs for the parameter θ_3 in application of Section 5.2.1

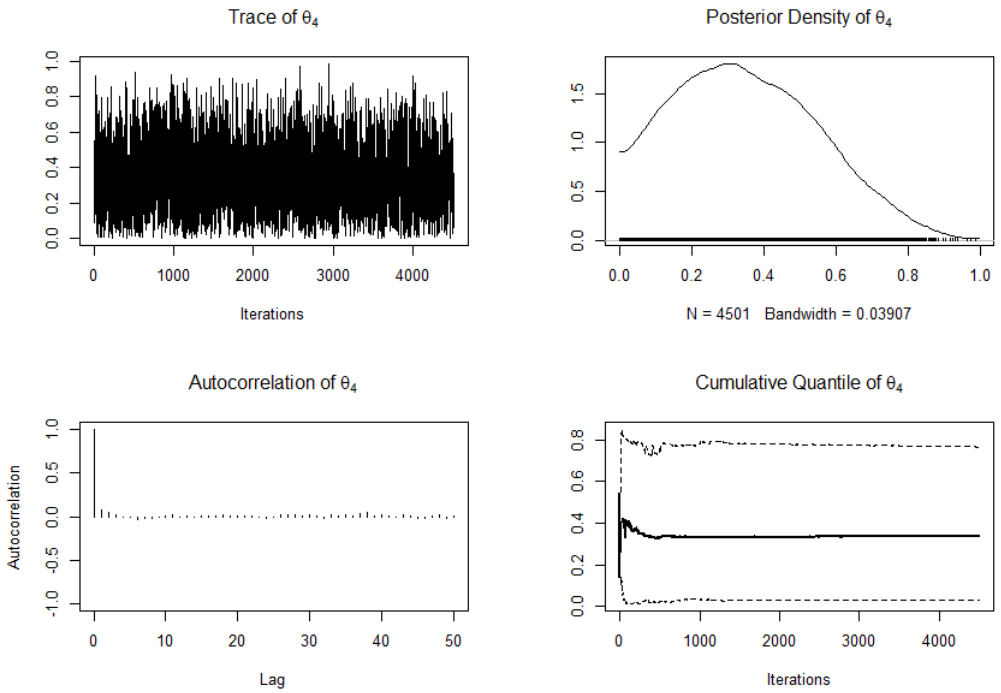

Figure 57 – Plots of MCMC outputs for the parameter θ_4 in application of Section 5.2.1

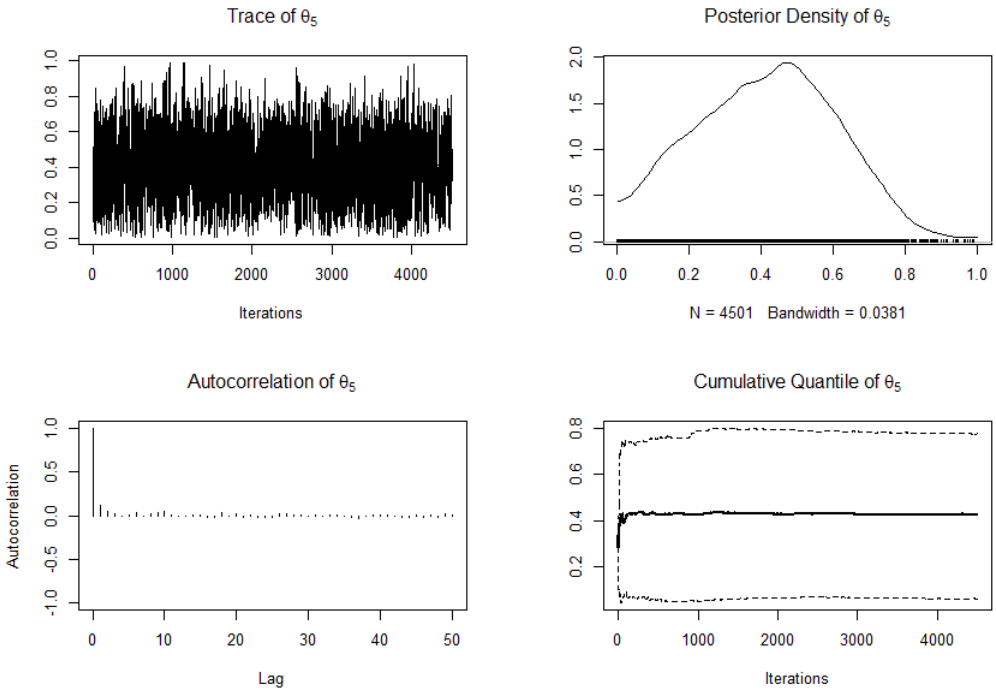

Figure 58 – Plots of MCMC outputs for the parameter θ_5 in application of Section 5.2.1

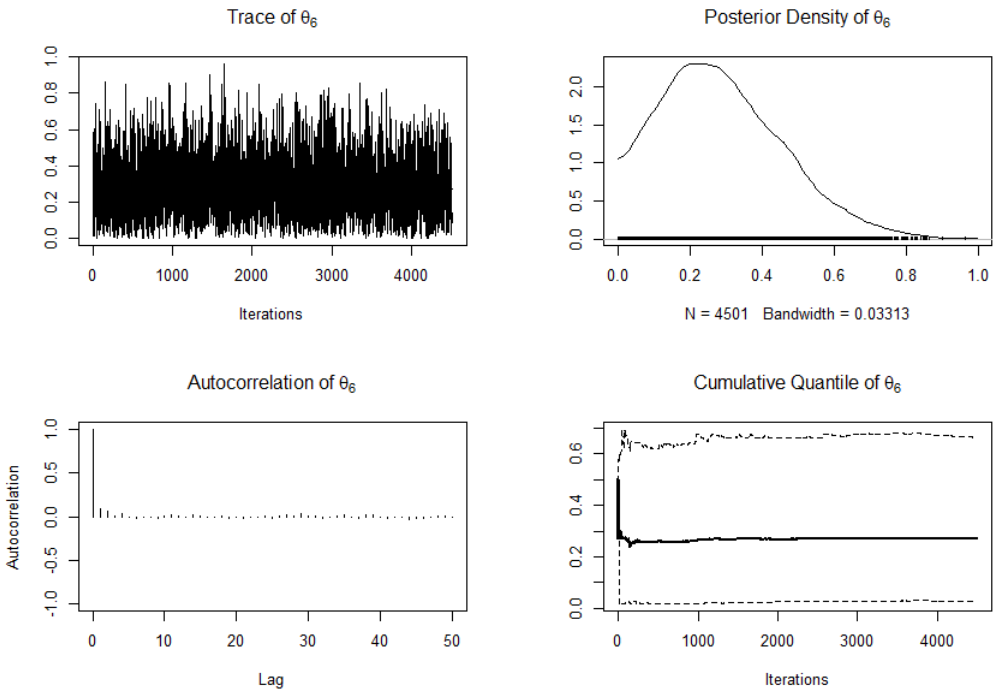

Figure 59 – Plots of MCMC outputs for the parameter θ_6 in application of Section 5.2.1

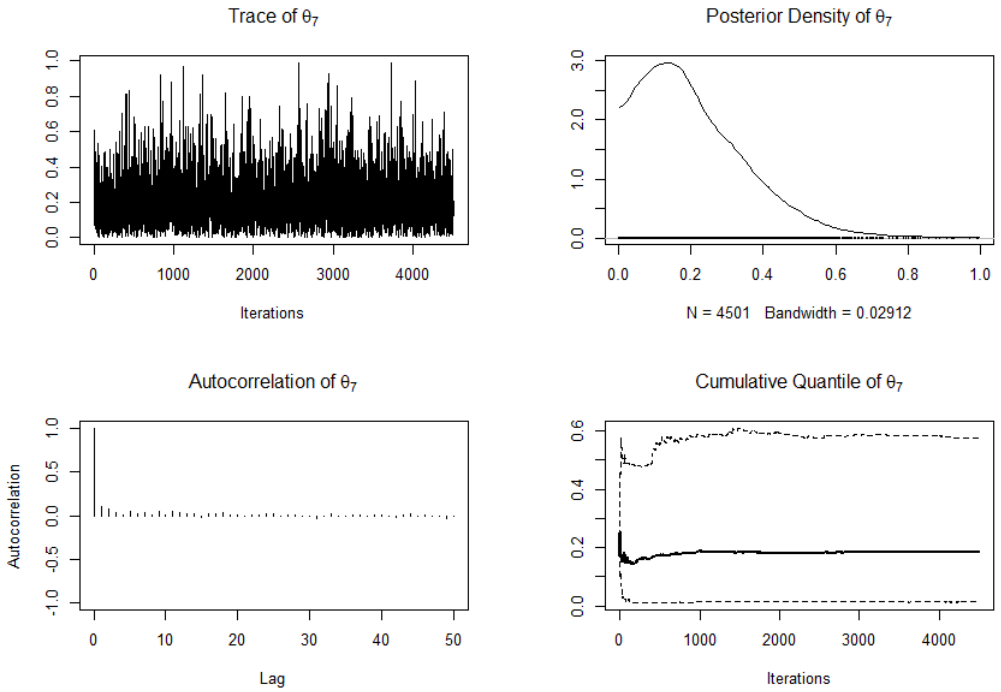

Figure 60 – Plots of MCMC outputs for the parameter θ_7 in application of Section 5.2.1

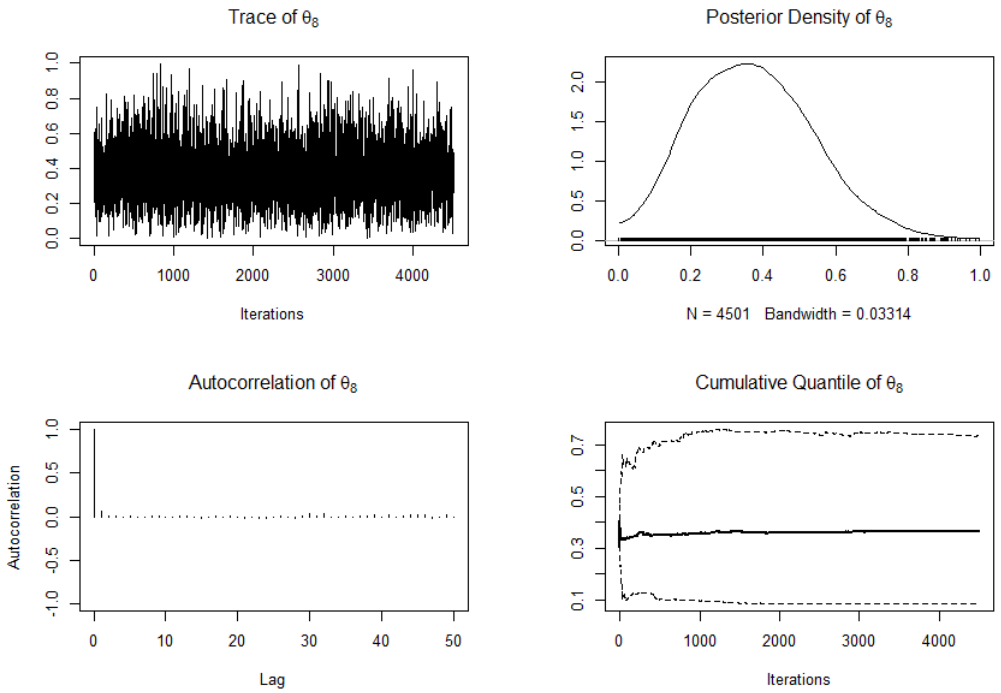

Figure 61 – Plots of MCMC outputs for the parameter θ_8 in application of Section 5.2.1

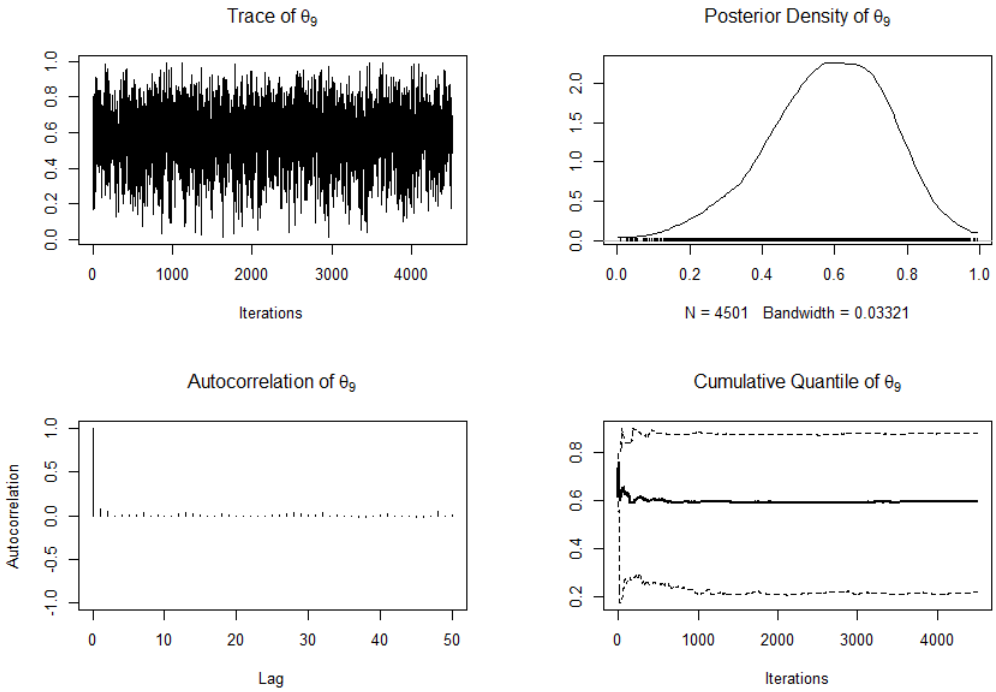

Figure 62 – Plots of MCMC outputs for the parameter θ_9 in application of Section 5.2.1

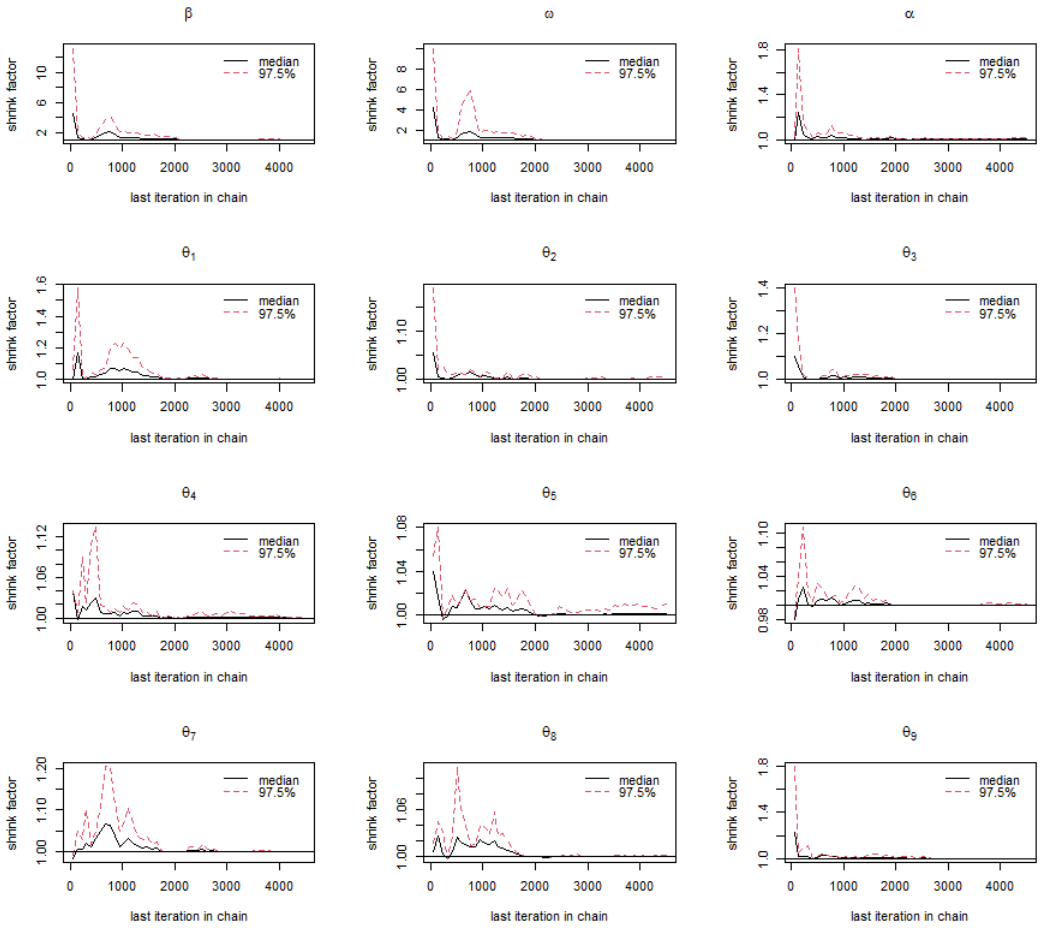

Figure 63 – Plots of Gelman-Rubin's criteria outputs for all the model parameters in application of Section 5.2.1

A.2 Section 5.2.1 - Dump Truck Data

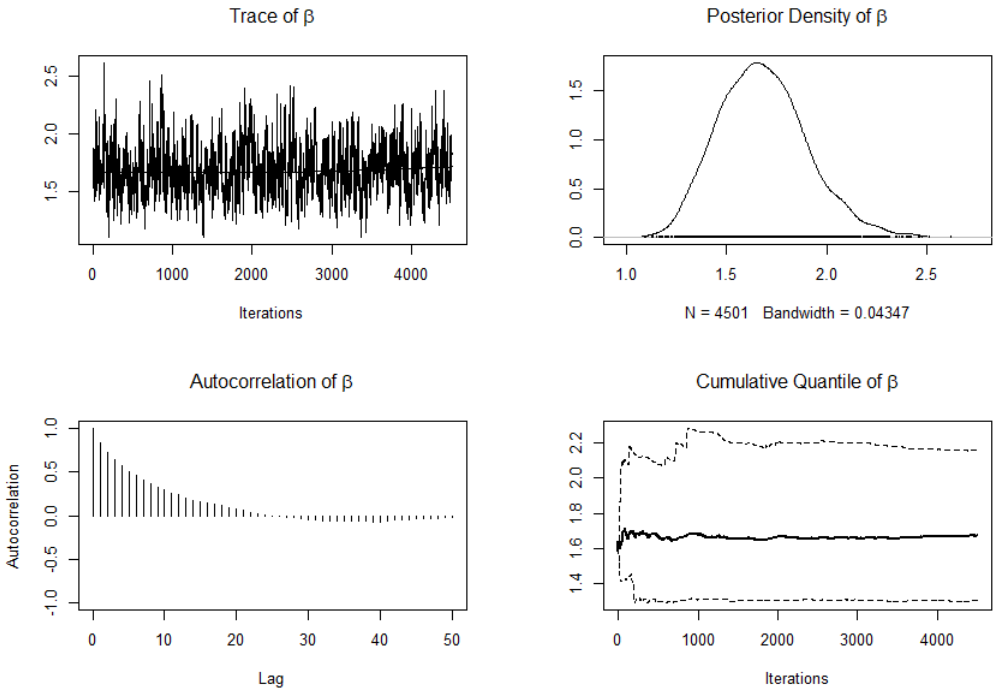

Figure 64 – Plots of MCMC outputs for the parameter β in application of Section 5.2.2

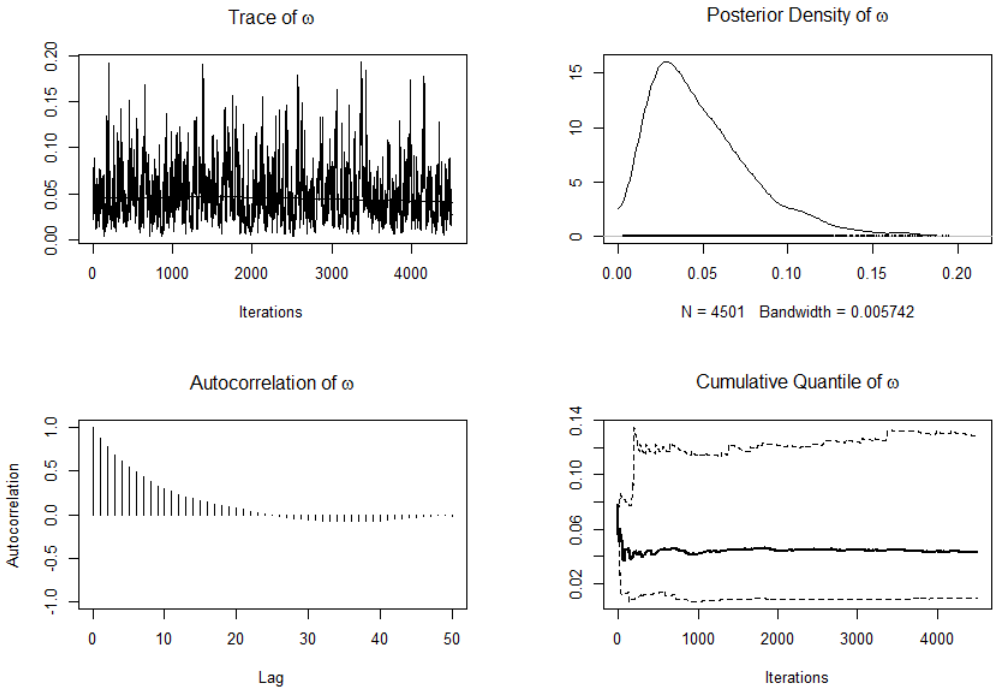

Figure 65 – Plots of MCMC outputs for the parameter ω in application of Section 5.2.2

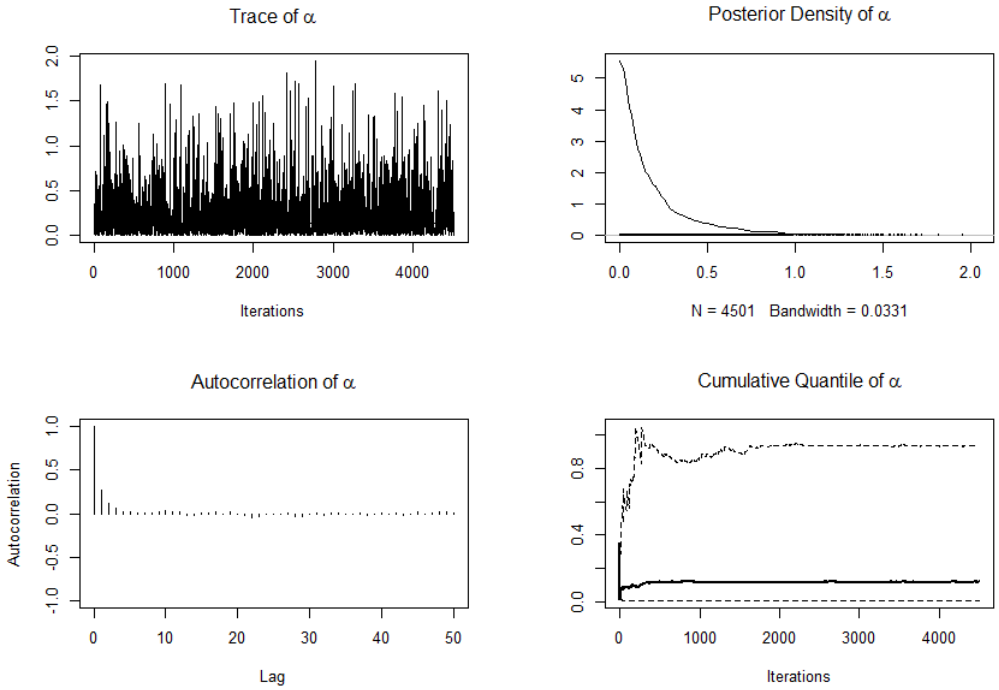

Figure 66 – Plots of MCMC outputs for the parameter α in application of Section 5.2.2

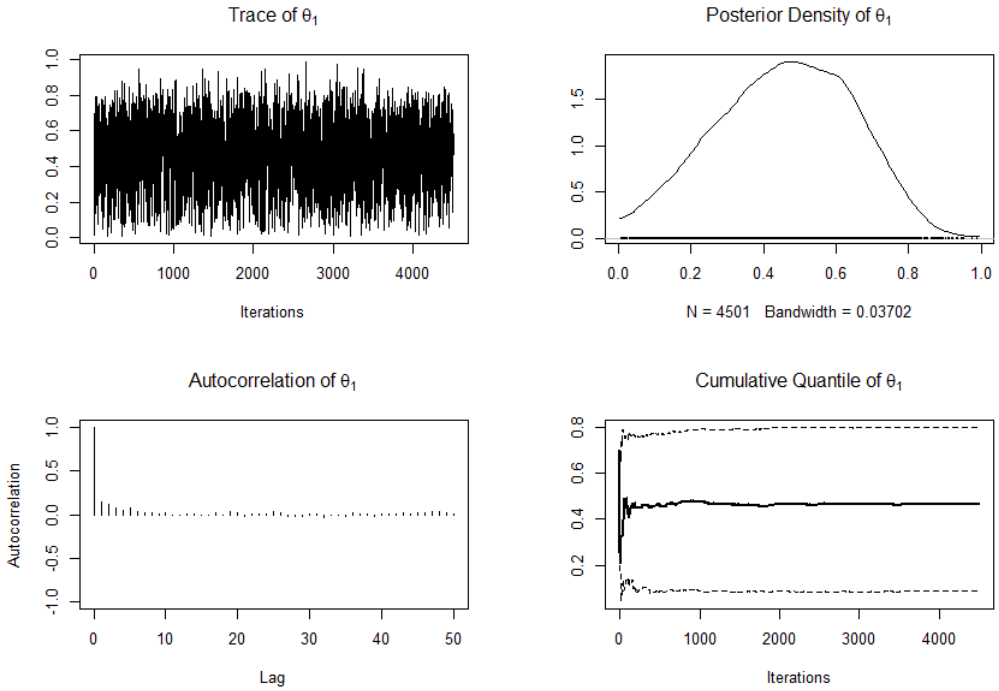

Figure 67 – Plots of MCMC outputs for the parameter θ_1 in application of Section 5.2.2

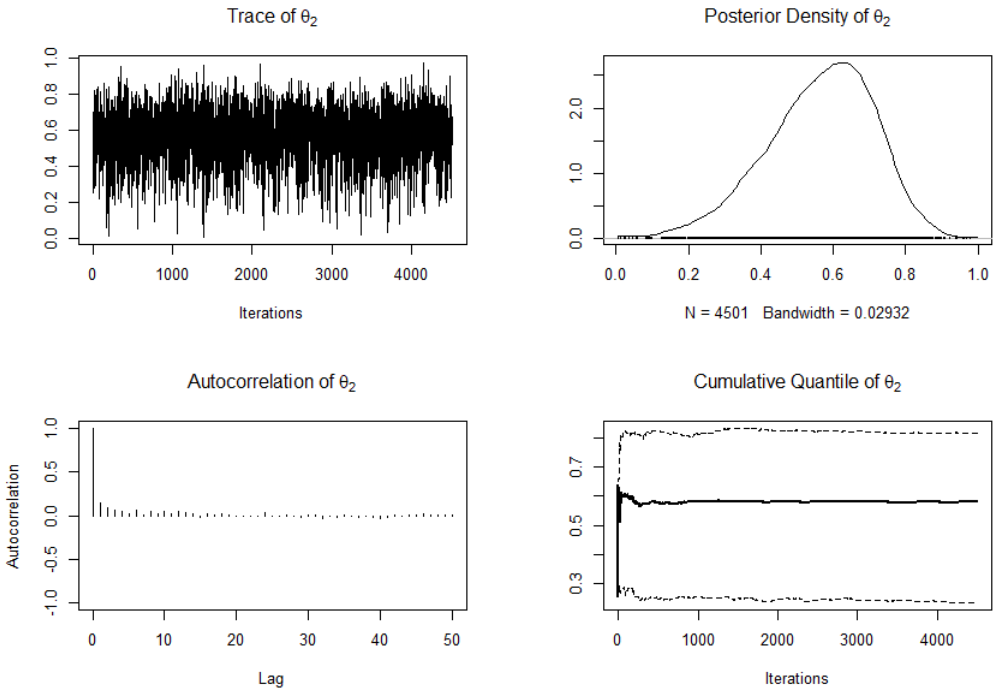

Figure 68 – Plots of MCMC outputs for the parameter θ_2 in application of Section 5.2.2

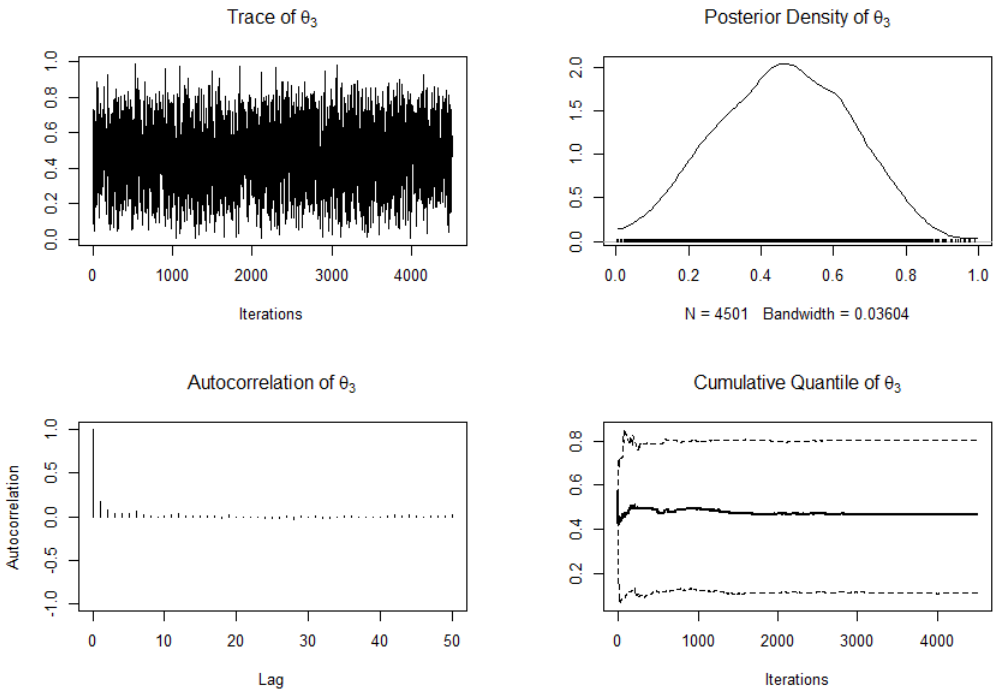

Figure 69 – Plots of MCMC outputs for the parameter θ_3 in application of Section 5.2.2

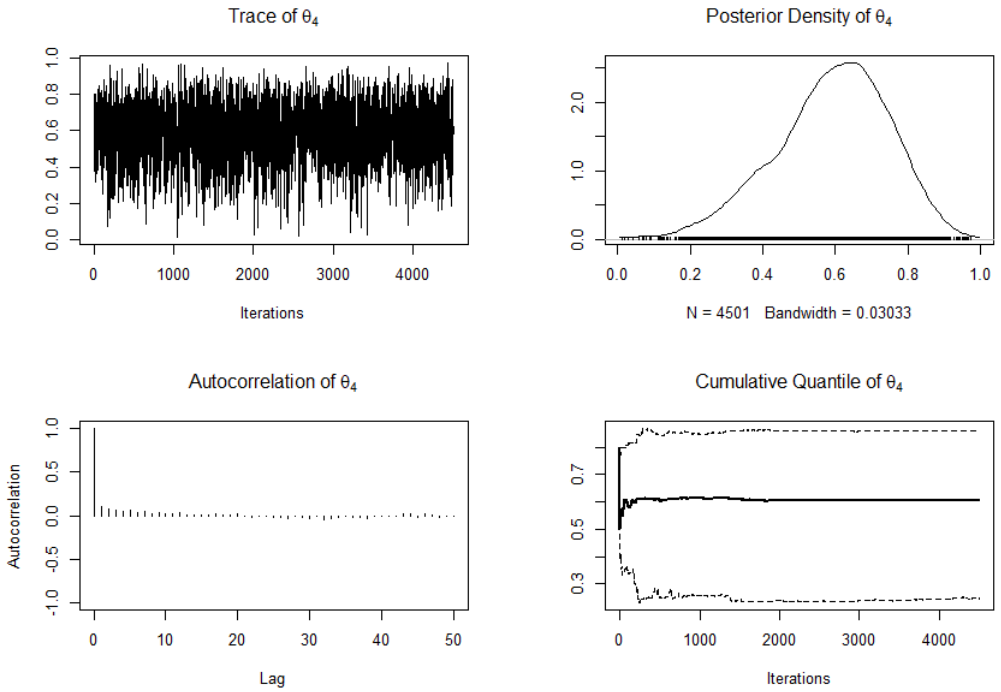

Figure 70 – Plots of MCMC outputs for the parameter θ_4 in application of Section 5.2.2

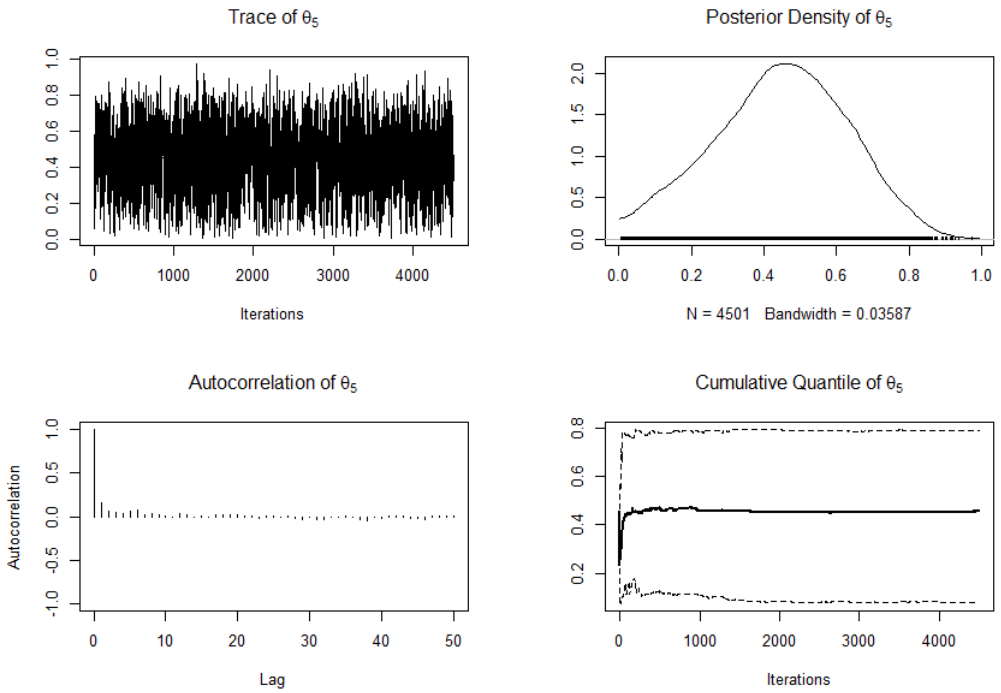

Figure 71 – Plots of MCMC outputs for the parameter θ_5 in application of Section 5.2.2

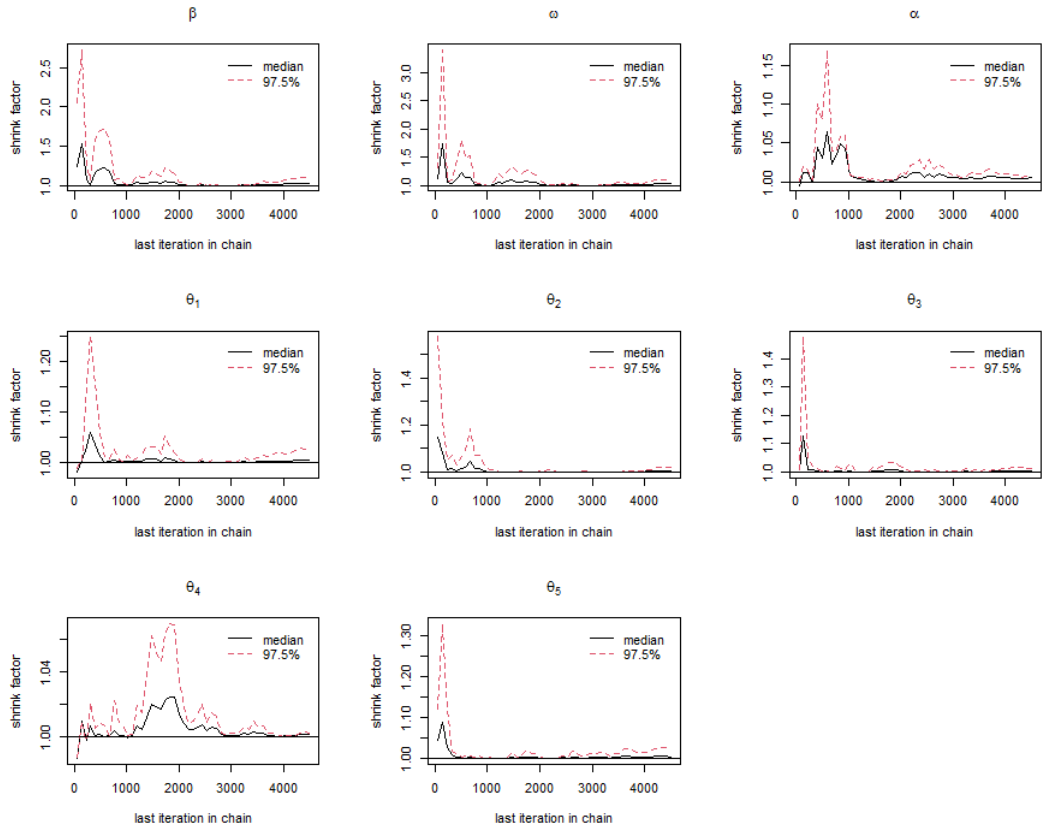

Figure 72 – Plots of Gelman-Rubin's criteria outputs for all the model parameters in application of Section 5.2.2


ICMC
USP
SÃO CARLOS